ICODIA 25'

4th International Conference on Digital Industry and Engineering Applications 2025

BOOK OF PROCEEDINGS

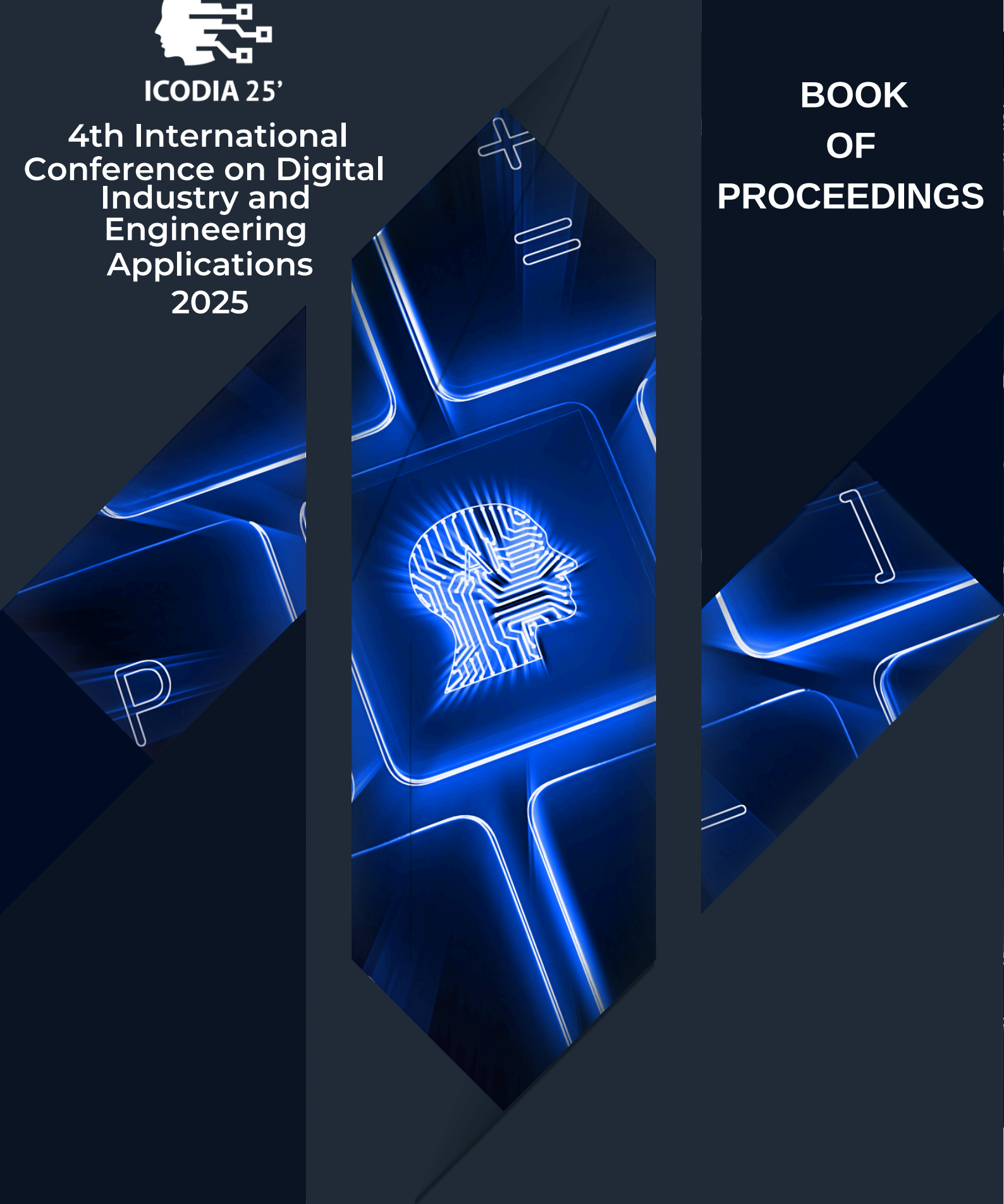

13-14 October 2025

InnoPark
KONYA TECHNOLOGY DEVELOPMENT ZONE

KÜNYE

Basıldığı Yer ve Tarih: Konya, 2025
Yayımcının/Basımcının Adı: InnoPark Konya Teknoloji Geliştirme Bölgesi Yönetici A.Ş.
Yayımcı/Basımcı Adresi: Büyükkayacık Mah 101. Cadde No: 2 Selçuklu/Konya
Web: www.innopark.com.tr,
Tel: +90 332 999 14 88,
E-posta: bilgi@innopark.com.tr
Yayımcı/Basımcı Sertifika Numarası: 47829
Sayfa Sayısı: 167
ISBN Numarası: 978-625-93681-0-8
Eser Adı: ICODIA 2025 Proceedings Book

PREFACE

The opportunities emerging through the rapid advancement of information and communication technologies, the changing expectations of customers, and the necessity for organizations to become more effective and efficient have made Digital Transformation an essential process for all enterprises and institutions.
A common belief shared by both developed and developing countries is that:
“All organizations should sail with the wind of digital transformation rather than resist it.”
Digital Industry can be defined as the development of new products and business processes that create value for organizations and their customers while enhancing competitiveness and sustainability.
Digital Transformation refers to the transition to new ways of conducting business and thinking, where digital, mobile, and emerging technologies are extensively utilized.

Digital Transformation encourages all organizations to make significant changes in the following areas:

- Organizational vision and strategies,
- Organizational structure, governance, and business models,
- Decision-making mechanisms,
- Products and services,
- Processes within the value chain, particularly production,
- Customer experience,
- Technologies and technological infrastructure.

Nowadays, the concepts of digital industry and digital transformation are frequently discussed. However, there are only a few who share practical experiences or implemented projects in these fields. Most speakers merely repeat what they have read or heard. With this conference, our aim is to give a stronger voice to those who present practical implementations, success stories, and best practices in the field of digital industry and digital transformation.
Participants were expected to present success stories and case studies related to the implementation of digital industry and digital transformation.
We hope that all participants will have the opportunity to exchange valuable knowledge and experiences that will significantly contribute to their ongoing efforts in these areas.

ICODIA – International Conference on Digital Industry and Engineering Applications
ICODIA is the first scientific conference in Türkiye organized in the field of digital industry and digital transformation.
It is a biennial event, the first of which was held in 2019 under the title “International Symposium on Implementations of Digital Industry and Management of Digital Transformation.”
The conference is organized by InnoPark, the managing company of the Konya Technology Development Zone.
Unlike most technoparks located on or near university campuses, InnoPark is situated in an industrial zone. As a production-oriented technopark, InnoPark aims to support the digital transformation efforts of industrial enterprises. Accordingly, the aim of this conference is to create an international platform for the interaction, exchange, and discussion of global ideas, success stories, best practices, case studies, experiences, developments, and insights on Digital Industry (Industry 5.0) and Digital Transformation.
I sincerely hope that this conference will serve as a source of inspiration and knowledge for participants in their digital transformation efforts.
The wide range of participation from universities, R&D centers, industrial organizations, and technology providers has greatly enriched our conference.
I would like to express my heartfelt gratitude to all invited speakers, academicians, researchers, and participants who have contributed to this event.
Abstracts of all orally presented papers will be published in the ICODIA Book of Abstracts.
Selected articles will be recommended for publication in reputable scientific journals.
All other presented papers will be included in the ICODIA Proceedings Book, with the approval of their authors.
On behalf of the Organizing Committee, I extend my deepest gratitude to all invited speakers and authors; without their valuable contributions, this event would have no meaning.
I would also like to express our sincere appreciation to all ICODIA partners —
Necmettin Erbakan University, Selçuk University, Konya Technical University, KTO Karatay University, KOP Regional Development Administration, Konya Chamber of Industry, International Balkan University, Artificial Intelligence Application and Research Center, Anadolu EDIH, and all partners of InnoPark — for supporting this meaningful and memorable event.
I would like to thank Konya Technical University and its Rector Prof. Dr. Osman Çelik for hosting this year’s conference. Finally, I would like to sincerely thank the Organizing Committee, Scientific Committee, InnoPark staff, and everyone who has contributed to the success of this conference.
I hope this conference will make a significant contribution to the ongoing digital transformation efforts in Türkiye and around the world.

Prof.Dr.Ali KAHRAMAN
Conferense Chairperson

CONFERENCE SCHEDULE

OCT-2025

13

Thursday

ICODIA 25'

Opening Session / Salon 2

Time (GMT+3)	Participation	Speaker	Presentation Title
09:00 / Registration			
10:00-10:30	In-person	Prof. Dr. Ali KAHRAMAN	Opening
10:30-10:45	In-person	Prof. Dr. Radoslav Dakov YOSHINOV	Opening
10:45-11:00	In-person	Prof. Dr. Daniela BORISSOVA	Opening
11:00 / coffee break			

Time (GMT+3)	Participation	Speaker	Presentation Title
11:20-11:40	In-person	Prof. Dr. Yakup KARA	Opening Speech
11:40-12:00	In-person	Assist. Prof. Sümeyye BAKIM	Opening Speech
12:00-12:20	In-person	İsmail Hakkı KARACA	Opening Speech
12:20 / Lunch Break			

CONFERENCE SCHEDULE

OCT-2025

13

Thursday

ICODIA 25'

Session 1 Invited Speakers / Salon 2

Chair : Assoc. Prof. Mehmet Korkmaz

Time (GMT+3)	Participation	Authors	Presentation Title
13:30-13:45	In-person	Musa KURUÇAY, Onur İlyas YAVUZ and Hakkı SOY	Reducing System Current Consumption by Transitioning to Low Power Mode Using a Power Saving Chip (NanoPower EVK)
13:45-14:00	In-person	Erkan BEKDEMİR, Sinem SELÇUK, Onur İlyas YAVUZ and Hakkı SOY	ERP-Integrated IoT Framework: Real-Time Process Tracking, Quality Assurance, and QR-Based Traceability for Smart Manufacturing
14:00-14:15	In-person	Samet AYDIN, Onur İlyas YAVUZ and Hakkı SOY	Functional IoT Board Design Using Wired and Wireless Communication Infrastructure
14:15-14:30	In-person	Abdurrahman Enes ÜNSAL, Hüseyin Cenk KARATOPÇU and Onur İlyas YAVUZ	Yeni Nesil Kontrol ve Dizgi Sisteminin Geliştirilmesi: Termoelektrik Modüllerin Seri Üretimine Yönelik Akıllı Ara Kontrol ve Dizgi Cihazı
14:30-14:50 / coffe break			

Session 2 Invited Speakers / Salon 2

Chair : Assist. Prof. Sule Eryuruk

Time (GMT+3)	Participation	Authors	Presentation Title
14:50-15:05	In-person	Ali DEMİR and Kadir ERDOĞAN	BASED IMAGE PROCESSING TECHNIQUE FOR ICE DETECTION IN INDUSTRIAL REFRIGERATION CABINETS
15:05-15:20	In-person	Mahmut SAĞLIYAN and Sait Ali UYMAZ	EVALUATION OF YOLO MODELS FOR MILITARY AIRCRAFT DETECTION AND CLASSIFICATION
15:20-15:35	In-person	Ahmet Furkan HAZAR and Fatih Titrek	Hazardous Object Detection and Classification from X-ray Devices using YOLO and Faster R-CNN Models
15:35-15:50	In-person	Onur İlyas YAVUZ and Hakkı SOY	Transformation of Industrial Tracking and Management Infrastructure with Wi-Fi Mesh-Based Wireless Digital Label System
15:50 / coffee break			

CONFERENCE SCHEDULE

OCT-2025

13

Thursday

ICODIA 25'

Session 3 Invited Speakers / Salon 2 - (HYBRID)

Chair : Professor Murat Dilmeç

Time (GMT+3)	Participation	Authors	Presentation Title
16:10-16:25	In-person	Alma LATIFI, Isak SHABANI, Rinesa BISLIMI and Mërgim H. HOTI	A hybrid machine learning framework for real-time network intrusion detection using supervised
16:25-16:40	In-person	Hakan ERDEŞ, Ahmet PEKER and Kemal ALAYKIRAN	PROJECT TEAM FORMATION PROBLEM: A GOAL PROGRAMMING APPROACH
16:40-16:55	Online	Rana Bedir URFALI and Ersin KAYA	Forecasting in the Field of Electromobility Using Univariate and Multivariate Time Series Model
17:30	Bus departure time is 17:45 for the GALA DINNER		

CONFERENCE SCHEDULE

OCT-2025

14

Friday

ICODIA 25'

Opening Session

Time (GMT+3)	Participation	Speaker	Presentation Title
09:00 / Registration			
09:30-09:45	In-person	Assoc. Prof. Zlatogor MINCHEV	Opening Speech
09:45-10:00	In-person	Assist. Prof. Hüseyin Oktay ALTUN	Opening Speech

Session 1 Invited Speakers / Salon 3

Chair : Assoc. Prof. Sercan Dogan

Time (GMT+3)	Participation	Authors	Presentation Title
10:00-10:15	Online	İkbal Işık ORHAN and Caner KESİM	MANAGING DIGITAL TRANSFORMATION IN MAINTENANCE OPERATIONS THROUGH STANDARDIZED AND CONTROLLED SAP PM MASTER DATA PROCESSES
10:15-10:30	Online	Rıdvan Safa HATİPOĞLU, Muhammet Doğukan KUYUMCU, Mevlüt BAŞARAN and Murat CEYLAN	Improving The Performance Of Object Detection Model With Real-Time Extraction On Jetson AGX Orin Edge Device
10:30-10:45	Online	Şeymanur BAŞGÖZE, Esra Odabaş YILDIRIM and Ahmet ÖZCAN	ANALYSIS OF LAND COVER CHANGE IN THE CAPPADOCIA REGION USING REMOTE SENSING
10:45-11:00	Online	Yılmaz Furkan EKMEKÇİBAŞI	A Multi-Purpose Autonomous Agricultural Robot
11:00 / coffee break			

CONFERENCE SCHEDULE

OCT-2025

14

Friday

ICODIA 25'

Session 2 Invited Speakers / Salon 2

Chair : Assist. Prof. Hasan Çınar

Time (GMT+3)	Participation	Authors	Presentation Title
11:20-11:35	Online	Mehmet ARIKAN, İnci SARIÇİÇEK, Sinem Bozkurt KESER, Silvia DELBONO, Ali KAFALI and Ahmet YAZICI	Selection of Battery Cooling System for Electric Vehicles Using Multi Criteria Decision Making
11:35-11:50	Online	Sercan BÜLBÜL, Fuat BAŞÇİFTÇİ and Burhaneddin BİLGEN	APRIL 16, 2024 INVESTIGATING THE DYNAMICS OF THE MODERATE GEOMAGNETIC STORM
11:50-12:05	Online	Atakan BAŞTOSUN and Alper KILIÇ	SLAM-Based Mapping and Localization with Lidar and IMU Sensors in Autonomous Agricultural Robots
12:05-12:20	Online	PInar Atak KAFA, Emine İŞİN and Nurettin ÇETİNKAYA	OPERATIONAL EFFECTS OF ATMOSPHERIC CONDITIONS ON THE HIGH VOLTAGE ELECTRICITY GRID IN COASTAL SETTLEMENTS
12:20 / Lunch Break			
14:00	Tour of Mevlana's Tomb and Çatalhöyük		

4th International Conference on Digital Industry and Engineering Applications 2025

ICODIA 25'

InnoPark
KONYA TECHNOLOGY DEVELOPMENT ZONE

SYMPOSIUM SCIENTIFIC COMMITTEE

- A.A. Altun, Selçuk University, Türkiye
- H. Soy, Necmettin Erbakan University, Türkiye
- M. Kalyoncu, Konya Teknik University, Türkiye
- S.E. Kesen, Konya Teknik University, Türkiye
- H. Erdinç Koçer, Selçuk University, Türkiye
- M.A. Durdu, Konya Teknik University, Türkiye
- M.A. Erişmiş, Necmettin Erbakan University, Türkiye
- S.A. Uymaz, Konya Teknik University, Türkiye
- R, Battaloğlu Niğde Ömer Halisdemir University, Türkiye
- S. Koçer, Necmettin Erbakan University Türkiye
- T. Paksoy, Necmettin Erbakan University, Türkiye
- U. Önen, Necmettin Erbakan University, Türkiye
- M. Mayda, Karamanoğlu Mehmetbey University, Türkiye
- İ. Köse, İstanbul Ticaret University, Türkiye
- M. Dilmeç, Necmettin Erbakan University, Türkiye
- A. Kahraman, Necmettin Erbakan University, Türkiye
- E. Kaya, Konya Teknik University, Türkiye
- K. Tütüncü, Selçuk University, Türkiye
- T. Karaçay, Gazi University, Türkiye
- M. H. HOTI , University of Prishtina, Kosova
- Shabani, University of Prishtina, Kosova
- U. Köklü, Karamanoğlu Mehmetbey University, Türkiye
- Ü. Akdağ, Aksaray University, Türkiye
- M.S.Kıran, Konya Teknik University, Türkiye
- E. Ülker, Konya Teknik University, Türkiye
- İ. Karaoğlan, Konya Teknik University, Türkiye

CONTENTS

MANAGING DIGITAL TRANSFORMATION IN MAINTENANCE OPERATIONS THROUGH STANDARDIZED AND CONTROLLED SAP PM MASTER DATA PROCESSES

İkbal Işık ORHAN [a*], Caner KESİM [b]

[a] *Nagarro + MBIS, Ar-Ge Departmanı: Cevizli Mh. Tugay Yolu Cd. Ofisim İstanbul A Blok 34846 Maltepe/İstanbul*

[b] *Nagarro + MBIS, Ar-Ge Departmanı: Cevizli Mh. Tugay Yolu Cd. Ofisim İstanbul A Blok 34846 Maltepe/İstanbul*

ABSTRACT

Digital transformation requires not only technological updates but also the restructuring of business processes through a data-driven approach. Enterprise Resource Planning (ERP) systems are central to this transformation, enabling business processes and driving digitalization strategies across organizations. The accuracy and governance of master data, which forms the foundation of ERP systems, are essential for successful transformation. In widely used ERP platforms like SAP, master data in the Plant Maintenance (PM) module—such as equipment and maintenance plans—is critical for operational efficiency, proactive maintenance, and sustainability.

In distributed enterprise environments, managing PM master data in a standardized, consistent manner presents major challenges in data integrity, process standardization, and governance. These highlight the need for auditable, centralized data management models at the corporate level to ensure sustainable digital transformation.

This study proposes a centralized data management model to improve the quality and governance of SAP PM master data in response to digital transformation requirements in maintenance operations. The model includes workflow-based approvals, rule-driven validation, and reporting tools to standardize data and ensure consistency. Results show improved data accuracy, reduced inconsistencies, and greater traceability. The study offers practical insights by addressing the intersection of digital maintenance management and data quality.

KEYWORDS

- Data Quality
- Digital Transformation
- Enterprise Resource Planning (ERP)
- Master Data Management (MDM)
- Plant Maintenance (PM)
- Workflow Management

[*] Corresponding author: İkbal Işık Orhan
E-mail: ikbal.orhan@nagarro.com

STANDARTLAŞTIRILMIŞ VE KONTROLLÜ SAP PM ANA VERİ SÜREÇLERİYLE BAKIM OPERASYONLARINDA DİJİTAL DÖNÜŞÜM YÖNETİMİ

İkbal Işık ORHAN [a]*, Caner KESİM [b]

[a] *Nagarro + MBIS, Ar-Ge Departmanı: Cevizli Mh. Tugay Yolu Cd. Ofisim İstanbul A Blok 34846 Maltepe/İstanbul*

[b] *Nagarro + MBIS, Ar-Ge Departmanı: Cevizli Mh. Tugay Yolu Cd. Ofisim İstanbul A Blok 34846 Maltepe/İstanbul*

ÖZET

Dijital dönüşüm yönetimi, yalnızca teknolojik altyapıların yenilenmesini değil, aynı zamanda kurumsal süreçlerin veri odaklı bir yaklaşımla yeniden yapılandırılmasını da gerektirmektedir. Bu dönüşümün merkezinde yer alan Kurumsal Kaynak Planlama (ERP) sistemleri, iş süreçlerinin yürütülmesini sağlayarak organizasyonların dijitalleşme stratejilerinde kritik bir rol üstlenmektedir. ERP sistemlerinde süreçlerin temelini oluşturan ana verilerin doğruluğu ve yönetimi, dijital dönüşümün başarısında belirleyici bir faktördür. Dünyada yaygın olarak kullanılan SAP ERP sisteminin Bakım Yönetimi (PM) modülündeki ekipman ve bakım planı gibi ana veriler; operasyonel verimlilik, bakım planlaması ve sürdürülebilirlikte büyük önem taşımaktadır. Özellikle dağıtık yapıya sahip organizasyonlarda, bu verilerin standart ve tutarlı biçimde yönetilmesi; veri bütünlüğü, süreç standardizasyonu ve yönetişim açısından önemli zorluklar doğurmakta, dijital dönüşüm sürecinin sürdürülebilirliğini sağlamak için kurumsal düzeyde standartlaştırılmış, denetlenebilir ve merkezi veri yönetimi modellerine gereksinimi ortaya koymaktadır.

Bu çalışma, bakım operasyonlarında dijital dönüşüm gereksinimlerine yanıt olarak, SAP PM ana verilerinin kalite ve yönetişim süreçlerini iyileştirmeyi önermektedir. Model, iş akışı tabanlı onay mekanizmaları, kural bazlı doğrulama sistemleri ve raporlama araçları ile veri süreçlerinin standartlaştırılmasını ve veri bütünlüğünün sağlanmasını hedeflemektedir. Uygulama sonuçları, veri doğruluğunda artış, tutarsızlıklarda azalma ve süreç izlenebilirliğinde iyileşme sağlamış; çalışmayla dijital bakım yönetimi ve ana veri kalitesi etkileşimine dair literatürdeki önemli bir boşluk doldurularak uygulamaya yönelik somut katkılar sunulmuştur.

ANAHTAR KELİMELER

- Ana Veri Yönetimi
- Bakım Yönetimi
- Dijital Dönüşüm
- ERP (Kurumsal Kaynak Planlaması- Enterprise Resource Planning)
- Veri Kalitesi (Data Quality)
- İş Akışı Yönetimi

* Corresponding author: İkbal Işık Orhan
E-mail: ikbal.orhan@nagarro.com

1. Giriş

Günümüzde dijital dönüşüm yönetimi, kurumların sadece teknolojik sistemlerinin yenilenmesiyle sınırlı kalmayıp, kurumsal işleyişin veriye dayalı olarak yeniden tasarlanmasını da zorunlu kılan stratejik bir süreç haline gelmiştir. Literatürde dijital dönüşümün çoğu zaman yalnızca teknolojik bir yenileme olarak algılandığı, ancak aslında organizasyonel kültür, süreç ve stratejilerin bütüncül bir dönüşümünü gerektirdiği vurgulanmaktadır. Bu nedenle dijital dönüşümün başarılı olması, yalnızca teknolojik altyapı yatırımlarına değil, aynı zamanda bu sürecin planlanma, yönetişim ve sürdürülebilirlik stratejilerine de bağlıdır [1]. Dijital dönüşümün yönetilmesinde Kurumsal Kaynak Planlama (ERP) sistemleri, işletmelerin dijitalleşme stratejilerinde kritik bir rol üstlenerek merkezde yer alır. ERP sistemleri; finans, üretim, tedarik zinciri, insan kaynakları ve bakım gibi iş fonksiyonlarını entegre biçimde yönetmeye olanak tanır. Bu bağlamda, dünya genelinde yaygın olarak kullanılan ERP sistemlerinden biri olan SAP, işletmelerin dijital dönüşüm süreçlerinde stratejik bir altyapı unsuru olarak öne çıkmaktadır. SAP sistemi içerisinde yer alan Plant Maintenance (PM) modülü ise fiziksel varlıkların bakım planlaması, arıza takibi ve bakım geçmişi gibi operasyonel süreçlerin yönetilmesine olanak sağlar.

Endüstri 4.0 ile birlikte üretim ortamları giderek daha fazla dijitalleşmekte; makineler, sistemler ve insanlar arasında sürekli veri alışverişi gerçekleşmektedir. Bu veri odaklı yapı, karar alma süreçlerinin hızını ve doğruluğunu artırmakla birlikte, sürdürülebilir bir dijital dönüşüm için kurumsal veri yönetişiminin de etkin biçimde planlanmasını gerektirmektedir. Bu bağlamda veri yönetimi, kurumsal süreçlerin sürdürülebilirliği açısından yalnızca teknik bir gereklilik değil; karar alma, risk yönetimi, performans izleme ve dijital stratejilerin uygulanması gibi yönetsel işlevlerin merkezinde yer alan stratejik bir unsur olarak değerlendirilmektedir [2].

ERP sistemlerinin başarısı, özellikle ana verilerin (master data) doğruluğu, kalitesi ve standardizasyonu ile ilişkilidir. Eksik tanımlanmış, tutarsız veya mükerrer ana veriler; süreç bütünlüğünü bozmakta, karar kalitesini düşürmekte ve sistemin genel işlevselliğini olumsuz etkileyerek dijital dönüşümün sürdürülebilirliğini tehdit etmektedir. Literatürde, malzeme ana verilerindeki düşük kalite seviyesinin, ERP sistemlerinin sağladığı faydayı ciddi biçimde azalttığı ortaya konmuştur [3]. Bu bağlamda, veri kalitesi sorunlarının yalnızca teknik eksikliklerden değil, yetersiz yönetişim uygulamalarından da kaynaklandığı görülmektedir. Ana veri yönetimi (MDM) çözümleri; veri standardizasyonu, merkezi onay süreçleri ve bütünsel denetim mekanizmaları sunarak bu yönetişim ihtiyacına yanıt vermektedir [4].

Bu çalışma, dijital dönüşüm süreçlerinde sürdürülebilir veri yönetişimi sağlamak amacıyla, SAP PM modülündeki ana veri yönetimini kurumsal düzeyde standartlaştırmayı amaçlamaktadır. Geliştirilen model; iş akışı tabanlı onay mekanizmaları, kural bazlı veri doğrulama sistemleri ve raporlama araçları aracılığıyla bakım süreçlerine ait ana verilerin kalite ve bütünlüğünü artırmayı, bakım süreçlerinin dijital dönüşümünü yönetilebilir, denetlenebilir ve izlenebilir bir yapıya kavuşturmayı hedeflemektedir. Uygulama sonuçları; veri doğruluğunda artış, tutarsızlıklarda azalma ve süreç izlenebilirliğinde iyileşme sağlamıştır. Bu yönüyle çalışma,

dijital dönüşümün teknik değil yönetsel boyutuna da katkı sunmakta; veri yönetişimi perspektifinden dijital bakım süreçlerinin stratejik yönetimine dair literatürdeki boşluğu doldurmaktadır.

2. Bakım Operasyonlarında Dijital Dönüşüm Gereksinimleri

2.1 Dijital Bakım Süreçlerinin Yükselişi ve Veri İhtiyacı

Endüstri 4.0 ile birlikte bakım operasyonları, geleneksel yaklaşımlardan dijital ve veri odaklı sistemlere evrilmiştir. Nesnelerin İnterneti (IoT) cihazları, sensör tabanlı izleme sistemleri ve yapay zeka destekli analiz araçları, bakım süreçlerinde sürekli veri akışını mümkün kılmaktadır. Bu durum, bakım kararlarının daha hızlı ve veri odaklı alınmasına olanak sağlamaktadır. Dijital bakım süreçlerinde toplanan veriler, ekipman performansının değerlendirilmesinden bakım planlamasına ve kaynak tahsisine kadar geniş bir yelpazede kullanılmaktadır. Ancak bu süreçlerin etkin yönetimi, yalnızca verinin miktarına değil; aynı zamanda kalitesi, doğruluğu ve bütünlüğüne bağlıdır. Dolayısıyla, bakım süreçlerinin dijital dönüşümü, teknik kapasitenin yanı sıra güçlü bir veri yönetişimi modelini de gerektirmektedir [2].

2.2 SAP PM Nesnelerinde Veri Yönetim Zorlukları

SAP PM modülünde yer alan temel nesneler; ekipman, teknik birim, iş planı, bakım planları gibi ana verileri kapsamaktadır. Bu nesneler, bakım operasyonlarının doğru ve verimli bir şekilde yürütülmesi için kritik öneme sahiptir. Ancak veri girişinde standart eksikliği, hatalı veya eksik tanımlamalar ve kullanıcıların farklı yöntemlerle veri kaydetmesi; veri kalitesini olumsuz etkileyerek bakım süreçlerinin verimliliğini azaltmaktadır. Düşük kaliteli ana veriler ERP sistemlerinden elde edilen faydayı azaltarak süreç bütünlüğünü ve kurumsal düzeyde operasyonel karar alma süreçlerini olumsuz etkiler [3]. Bu durum, bakım faaliyetlerinde yanlış planlamalara, operasyonel aksamalara ve maliyet artışlarına yol açabilmektedir.

2.3 Dağıtık Organizasyonlarda Veri Bütünlüğü ve Standardizasyon İhtiyacı

Çoklu iş birimi ve dağıtık organizasyon yapısına sahip işletmelerde, farklı lokasyonlar standart bir düzen ve yöntem olmaksızın kendi SAP PM veri girişlerini bağımsız şekilde yaptığında, veri tutarsızlığı kaçınılmaz hale gelmektedir. Literatürde, özellikle veri sahipliğinin net tanımlanmadığı büyük ölçekli organizasyonlarda, veri kalitesinin düşmesi ve süreçler arası kopuklukların ortaya çıkması yaygın bir sorun olarak belirtilmiştir. Bu durum, verilerin oluşturulması, kullanımı ve bakımı için ortak standartların bulunmamasından kaynaklanmakta; sonuç olarak işletme genelinde veri yönetimi faaliyetleri dağınık bir yapıya bürünmektedir [5]. Böyle bir yapı, hatalı, eksik veya tekrarlı verilerin oluşmasına yol açarak veri bütünlüğünü zayıflatmakta ve raporlama ile karar verme süreçlerinin güvenilirliğini düşürmektedir. Veri bütünlüğünün sağlanamaması, sistemler arası uyumsuzluklara, hatalı bakım emirlerine, planlamada gecikmelere, bakım maliyetlerinin yükselmesine ve operasyonel risklerin artmasına neden olmaktadır. Bu bağlamda merkezi veri yönetimi modelleri, veri girişinin standardizasyonunu, kural tabanlı doğrulamaları ve onay süreçlerini birleştirerek, tüm organizasyon genelinde veri kalitesini güvence altına almayı amaçlamaktadır [4]. Böylece,

dijital bakım süreçlerinde kurumsal düzeyde standart veri giriş süreçlerinin ve merkezi kontrol mekanizmalarının oluşturulması, bakım operasyonlarının dijital dönüşümünde kaçınılmaz hale gelmektedir [6].

2.4 Dijital Projelerde Kaliteli Ana Verinin Önemi

Dijital dönüşüm projelerinde kaliteli ana veri, yalnızca operasyonel süreçlerin verimliliğini artırmakla kalmaz, aynı zamanda iş süreçlerinin bütünlüğünü ve etkinliğini doğrudan etkiler. SAP PM modülünde ekipman, teknik birim ve bakım planı gibi nesnelerin doğru ve tutarlı tanımlanması, bakım taleplerinin oluşturulmasından kaynak planlamasına, iş emirlerinin yürütülmesinden bakım raporlamasına kadar tüm süreçlerin kesintisiz ve hatasız işlemesini sağlar. Örneğin, hatalı ekipman ana veri kayıtları, yanlış iş emirleri oluşturulmasına ve bakım kaynaklarının yanlış kullanılmasına yol açabilir; eksik bakım planları ise bakım stratejilerinin başarısız olmasına sebep olabilir. Bu tür sorunlar, iş gücü verimliliğini düşürmekle kalmaz, aynı zamanda maliyetleri artırır ve operasyonel riskleri büyütür. Nitelikli ana veriler ise süreçlerin bütüncül olarak izlenebilmesini, raporlamaların güvenilirliğini ve doğru karar almayı destekler [4].

Kaliteli ana veri, iş süreçlerinin otomasyonu ve dijital izlenebilirliğini mümkün kılar. İş akışı tabanlı onay mekanizmaları, kural bazlı doğrulama sistemleri ve gelişmiş raporlama araçları ile veri süreçleri standartlaştırılıp, veri bütünlüğü güvence altına alınır. Böylece süreçlerin izlenebilirliği artar ve hataların erken tespitine olanak tanınır. Bu nedenle, dijital projelerde veri kalitesinin sağlanması, yalnızca teknik bir gereklilik değil, bakım süreçlerinde sürdürülebilir performansın temel bileşeni haline gelir.

Bu bağlamda, dijital bakım operasyonlarının başarısı, yüksek kaliteli ana verilerin sağlandığı, standartlaştırılmış ve denetlenebilir bir veri yönetimi modelinin uygulanmasına bağlıdır.

3. SAP PM Ana Verileri için Merkezi Veri Yönetim Modeli

Bakım operasyonlarındaki dijital dönüşüm sürecinde, veri kalitesi, bütünlüğü ve yönetimi, sürecin başarısının temel kriterleri olarak öne çıkmaktadır. Bu gereksinimler doğrultusunda, SAP PM modülünde ana verilerin etkin biçimde yönetilmesini, standardizasyonunu ve denetlenebilirliğini sağlayacak merkezi bir veri yönetimi yaklaşımı geliştirilmiştir.

Aşağıdaki alt bölümlerde önerilen modelin genel yapısı, işleyiş prensipleri ve bileşenleri detaylı bir biçimde ele alınarak modelin dijital bakım yönetimi süreçlerine sağladığı katkılar açıklanmaktadır.

3.1 Genel Yapı ve İşleyiş Prensipleri

SAP PM modülünde ana verilerin etkin yönetimi, bakım operasyonlarının verimliliği ve sürdürülebilirliği açısından kritik bir rol oynar. Kurumsal bilgi sistemlerinde ana verilerin farklı uygulamalarda çoğaltılmasıyla, senkronizasyon karmaşıklığının arttığı ve tutarlılık sorunlarının

derinleştiği gözlemlenmiştir. Bu nedenle merkezi yönetim yaklaşımı, yalnızca verimlilik değil, sürdürülebilir veri bütünlüğü için de zorunluluk haline gelmektedir [7].

Önerilen merkezi veri yönetim modeli, tüm bakım süreçlerinin temelini oluşturan ana verileri tek bir merkezden kontrol etmeyi ve dağıtmayı amaçlar [8]. Bu model, veri girişlerinin standartlaştırılması, iş akışı tabanlı onay mekanizmalarının uygulanması ve kural tabanlı doğrulama süreçleri ile desteklenir. Model, yalnızca teknik doğruluk değil, aynı zamanda veri yönetişimi ilkeleri doğrultusunda süreçlerin denetlenebilirliği, rol bazlı sorumluluk paylaşımı ve kurum genelinde hesap verebilirliğin güçlendirilmesini hedeflemektedir. Merkezi yönetim yaklaşımı, dağıtık organizasyonlarda veri tutarsızlıklarını azaltarak SAP PM nesnelerinin doğru ve tutarlı şekilde tanımlanmasını sağlar. Veri kalitesinin sürekli izlenmesi ve raporlanması, bakım süreçlerinin izlenebilirliğini artırır ve karar alma doğruluğunu güçlendirir. Merkezi veri yönetimi çözümü ekipman ve bakım planı gibi ana veriler üzerinde etkin bir şekilde uygulandığı durumda, dijital bakım süreçlerinde veri bütünlüğü ve operasyonel verimlilik güvence altına alınır.

3.2 Veri Giriş Süreçleri ve Standardizasyon

Farklı departmanların kendi veri giriş kurallarını uygulaması, ERP sistemlerinde tutarsız kayıtların oluşmasına yol açan en temel nedenlerden biridir. Bu durum, hatalı veya tekrar eden kayıtların oluşmasına neden olur. Önerilen model, bu sorunu önlemek için veri giriş sürecinde belirlenen iş akışlarını kullanır. Alanlar, iş akışındaki yetkili departmanlar ve kullanıcılar için doldurulması zorunlu, yetkisi olmayanlar için ise değiştirilemez şekilde tanımlanır. Böylece, sisteme girilen verilerin standart bir düzende olması ve kaydedilen ana verilerin doğruluğu garanti altına alınır.

Ana verilerin ve ana veri ilişkili süreçlerin standardizasyonu, doğruluğu ve yönetimi, SAP PM modülünde bakım operasyonlarının verimliliği ve veri bütünlüğü açısından kritik bir öneme sahiptir. Ekipman, bakım planı gibi PM ana verilerinin yaratılması ve güncellenmesi sırasında, masraf yeri, üretim yeri gibi gerekli alanların kullanıcılar tarafından zorunlu olarak doldurulması ya da girilen verilere bağlı olarak bazı verilerin otomatik olarak dolması, veri girişinde tutarlılığı sağlar. Benzer şekilde, gerekli verilerin değiştirilemez olarak ayarlanması veya görüntüleme modunda sunulmasıyla hatalı veri girişleri ve değişikliklerinin önüne geçilir. Veri giriş süreçlerinin standartlaştırılması, veri kalitesini artırarak işletmelerin dijital dönüşüm süreçlerinde etkin rolünün devamlılığını sağlar [9]. Bu standartlaşma, SAP PM nesnelerinin doğru ve tutarlı şekilde tanımlanmasına olanak tanır ve merkezi veri yönetimi çözümlerinin etkinliğini güçlendirir. Böylece veri giriş süreçleri, merkezi veri yönetimi yaklaşımının temelini oluşturan sağlam ve tutarlı bir yapı kazanır.

3.3 Kural Tabanlı Doğrulama ve Onay Süreçleri

Kural tabanlı doğrulama, merkezi veri yönetiminde ana verinin tutarlılığını ve güvenilirliğini sağlamak için kritik bir mekanizmadır. Modelin sahip olduğu bu doğrulama mekanizmaları, SAP PM modülünde ana veri yaratma, güncelleme süreçlerinde verilerin belirlenen kriterlere uygunluğunu kontrol eder ve hatalı girişlerin önüne geçer. Bununla beraber ana veri yaratılırken

girilen koşul ve seçimler ile kural tabanlı doğrulama mekanizması entegre çalışır. Bu yöntem, ekipman gibi ana verilerin yaratılma sürecinden kayıt sürecine kadar veri girişlerinde doğruluk ve kolaylık sağlamaktadır. Örneğin, bir ekipman ana verisi oluşturulurken tanımlanan ekipman tipine bağlı olarak yalnızca belirli alanların doldurulmasına izin verilir. Bu koşullu doğrulama yapısı, hatalı veri girişlerini engellediği gibi, kullanıcıların yalnızca ilgili veriler üzerinde işlem yapmasını sağlayarak süreci hem hız hem de doğruluk açısından optimize eder. Modelin sunduğu iş akışına bağlı onay süreçleri ile PM ana verilerinin yaratılması ve güncellenmesi, belirlenen kontrol noktalarından geçerek yalnızca yetkili onay mercilerinin onayı sonrasında tamamlanmakta, bu da veri kalitesinin sürekliliğini ve süreç şeffaflığını sağlamaktadır. Ayrıca modelin veri yönetişimini belirli ve yönetilebilir iş akışları etrafında kurgulaması, kurum genelinde hesap verebilirlik ve karar haklarının net biçimde tanımlanmasını desteklemektedir [10]. İş akışları sayesinde kalite güvencesi ve standartlara uyumluluğun sağlanmasına katkı sunmakta, en iyi uygulamaların sistematik biçimde hayata geçirilmesini kolaylaştırmaktadır [11].

3.4. Süreç İzleme ve Veri Yönetişimi Araçları

Süreç izleme ve veri yönetişimi, merkezi veri yönetimi modelinin sürdürülebilirliğini sağlayan temel bileşenlerdir. Veri yönetimi statik bir faaliyet değil; sürekli denetim, kontrol ve iyileştirme gerektiren dinamik bir süreçtir. Bu nedenle, SAP PM modülünde ana verilerin yalnızca doğru biçimde oluşturulması değil, bu verilerin yaşam döngüsü boyunca izlenmesi ve yönetilmesi de önemlidir.

Merkezi ana veri yönetiminde, SAP PM kapsamında ekipman veya teknik birim gibi ana verilerin yaratılması ve güncellenmesi süreçlerinde, denetim kayıtlarıyla değişikliğin ve ana veri kaydının kim tarafından, ne zaman yapıldığıyla birlikte sürecin izlenmesi kritik öneme sahiptir. Modelin bir bileşeni olan iş akışlarına dayalı izleme araçları, merkezileştirilmiş rapor ve veri kaydı görüntüleme ekranları ile veri girişlerinin standartlara uygunluğunu kontrol etmeye ve hatalı veya eksik kayıtları erken aşamada tespit etmeye olanak tanır. Bu durum, veri süreçlerinde şeffaflığı artırmakta ve bakım operasyonlarında kullanılan verilerin güvenilirliğini sürdürülebilir kılmaktadır [12]. Ayrıca merkezi raporlama araçları sayesinde organizasyonel sorumluluk paylaşımı ve veri yönetişimi mekanizmaları güçlenmektedir.

3.5. MDM Çözümü Tanıtımı

SAP PM ana verileri için önerilen modelin kurumsal düzeyde uygulanabilirliği, geliştirilen MDM (Master Data Management) çözümü üzerinden somutlaştırılmıştır. Çözüm, SAP S/4HANA sistemlerinde ana veri yaratma ve güncelleme ihtiyaçlarının; talep bazlı, iş akışına dayanan ve ön tanımlı kurallarla desteklenen bir altyapıyla karşılanmasını sağlamıştır [13].

SAP PM ana veri faaliyetleri açısından MDM çözümü kapsamı aşağıdaki bileşenlerle açıklanabilir.

a. Talep Yönetimi

Ana veri yaratma, değiştirme veya silme taleplerinin merkezi bir ekran üzerinden iş akışına bağlanarak ilgili birimlere yönlendirilmesini ve süreç boyunca izlenmesini sağlar.

b. Kural Yönetimi

Veri girişlerinde doğruluk, bütünlük ve tutarlılığı sağlamak amacıyla zorunlu alanlar, varsayılan değerler ve koşullu kontroller gibi iş kurallarının sistematik biçimde uygulanmasını mümkün kılar.

c. İş Akışları Yönetimi

Ana veri taleplerinin veri girişi, kontrol, onay ve geri bildirim adımlarının belirli bir akış sırasına göre yürütülmesini sağlayarak, süreçlerin şeffaf ve denetlenebilir olmasını sağlar.

d. Alan ve Görünüm Yönetimi

Farklı ana veri tipleri için bakımı yapılacak tüm alanların görünürlüklerinin ve varyant yapılandırmalarının yönetilmesini sağlar, esnek ama standart bir veri giriş yapısı oluşturur.

e. Yetki Yönetimi

Kullanıcı rollerine ve sorumluluk alanlarına göre sistemde erişim ve işlem yetkilerini tanımlar.

f. Vekalet Yönetimi

Herhangi bir nedenle (izin vb.) ana veri bakımını belirli bir periyot için gerçekleştiremeyecek kullanıcıların, yetkilerini ilgili periyot için başka bir kullanıcıya tayin etmesini sağlar.

g. Bildirimler

Talep durum değişiklikleri, onay gereksinimleri veya hata mesajları gibi süreçlerle ilgili bilgilendirmeleri otomatik olarak ilgili kullanıcılara iletir.

SAP PM modülündeki ana verilerin standartlaştırılıp kontrollü, güvenilir ve tutarlı biçimde yönetilmesine olanak tanıyan MDM çözümünün, ana veri işleme sürecine ilişkin akış şeması aşağıda gösterilmektedir.

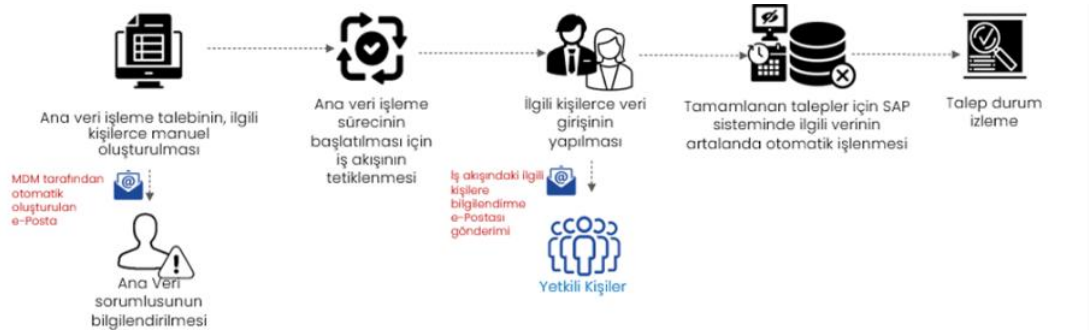

Fig. 1. MDM süreç akışı

Talep yönetimi ile tek bir ekrandan ana veri yaratma, değiştirme ve silme talepleri oluşturabilir. Oluşturulan talebe istinaden ön tanımlı iş akışı başlatılır ve talep farklı birimlerce yapılması gereken veri girişleri için ilgili sorumlulara gönderilir. İlgili sorumlu, talep içerisinde yalnızca veri girişi yapmaktan yetkili olduğu alanlar için belirlenen kurallara göre işlem yapabilir. MDM çözümü bu aşamada hata, uyarı ve bilgi mesajlarıyla sorumlu kullanıcıyı yönlendirir. İş akışı boyunca ilgili sorumlulara talep durumu bildirilir ve aynı zamanda raporlar aracılığıyla süreç izlenebilir. İş akışı tamamlanan talep sonucu, ilgili ana veri işlemi sistemde otomatik olarak kayıt altına alınmış olur.

4. Sonuçlar ve Bulgular

Geliştirilen MDM çözümü, SAP S/4HANA sistemlerinde ana verilerin yönetimini merkezi, standart, denetlenebilir hale getiren bütünleşik bir veri yönetimi modelidir. SAP ERP sistemini kullanan firmaların, operasyonel süreçlerin temeli olan ana verilerini kontrollü, doğru ve tutarlı biçimde yönetebilmesine olanak tanıyan bu model, dijital dönüşümün sürdürülebilirliğine yönelik stratejik bir örnek uygulama niteliğindedir [13].

Bu model, standartlaştırılmış veri giriş süreçleri ve kural tabanlı doğrulama mekanizmaları aracılığıyla hataları en aza indirirken, iş akışı tabanlı onay süreçleriyle yalnızca yetkili kullanıcıların değişiklik yapmasına izin vererek veri bütünlüğünü güvence altına alır. Ana verilerin doğru ve tutarlı hale gelmesi, bakım planlaması, iş emirleri ve performans raporlaması gibi kritik süreçlerde güvenilir veri kullanımını sağlar. Böylece karar alma süreçlerinin doğruluğu yükselir, karar alma süreleri kısalır ve dijital dönüşüm için sağlam bir temel oluşturulur. Bu yapı, özellikle dağıtık organizasyonlarda veri standardizasyonunu ve merkezi kontrol mekanizmalarını güçlendirmiştir.

Merkezi veri yönetimi yaklaşımı ile yinelenen ve eksik kayıtların önüne geçilmesi hedeflenmiştir. Zorunlu alanların doldurulması, otomatik tamamlama ve veri kısıtlamaları sayesinde SAP PM nesneleri tekil ve tutarlı şekilde tanımlanır; tekrarlar ve boşluklar en aza indirilir. Böylece planlama hataları, gecikmeler ve kaynak israfı azalırken; operasyonel riskler ve bakım maliyetleri düşürülmüş olur.

Model, yalnızca veri doğruluğunu artırmakla kalmamış, aynı zamanda süreçlerin izlenebilirliğini de artırmıştır. İş akışı tabanlı raporlama araçları, veri girişlerinin hangi aşamalardan geçtiğini ve kimler tarafından onaylandığını şeffaf bir biçimde gösterir. Bu sayede hatalar erken tespit edilir, hızlı müdahale imkânı doğar ve operasyonların sürekliliği güvence altına alınır.

Bakım ve onarım süreçlerinin dijital dönüşümü söz konusu olduğunda önceden doğrulanmış veriler; planlama, raporlama ve analiz süreçlerinin güvenilirliğini artırır. Bu sayede bakım planları ve iş emirleri zamanında oluşturulur, ilişkili faaliyetler daha kısa sürede ve daha verimli uygulanabilir hale gelir ve maliyetler azalır. Güncel ve doğru veriye dayalı planlama, arızaların öngörülmesini kolaylaştırır ve önleyici bakım faaliyetlerinin doğru zamanlamayla

yürütülmesini sağlar. Böylece kritik ekipmanlarda risk azalırken performans raporlamaları daha anlamlı ve hızlı gerçekleşir.

Sonuç olarak, önerilen merkezi veri yönetimi modeli; dağıtık organizasyonlarda koordinasyonu kolaylaştırarak farklı lokasyonlardan gelen veri taleplerinin uyumlu ve kontrollü biçimde yönetilmesini sağlamaktadır. Modelin uygulanması sonucu ana verilerin kalitesindeki artış, bakım kararlarını destekleyerek organizasyonel verimliliği güçlendirir. Genel olarak, SAP PM modülünde merkezi veri yönetimine dayalı bu yaklaşım, dijital dönüşüm hedefleriyle uyumlu, veri temelli, sürdürülebilir bir bakım yönetim yapısı oluşturmuştur. Ölçeklenebilir ve çevik olan bu yapı işletmelere maliyet avantajı, operasyonel verimlilik ve yüksek süreç görünürlüğü kazandırmaktadır [14].

Referanslar

[1] Vial, G. (2019). Understanding digital transformation: A review and a research agenda. *The Journal of Strategic Information Systems*, *28*(2), 118–144. https://doi.org/10.1016/j.jsis.2019.01.003
[2] Raptis, T. P., Passarella, A., & Conti, M. (2019). Data management in Industry 4.0: State of the art and open challenges. *IEEE Access*, *7*, 97052–97093. https://doi.org/10.1109/ACCESS.2019.2929296
[3] Knolmayer, G. F., & Röthlin, M. (2006). Quality of material master data and its effect on the usefulness of distributed ERP systems. *ACM SIGMIS Database: The DATABASE for Advances in Information Systems*, *37*(1), 40–54. https://doi.org/10.1145/1120501.1120506
[4] Hikmawati, S., Santosa, P. I., & Hidayah, I. (2021). Improving data quality and data governance using master data management: A review. *International Journal of Information Technology and Electrical Engineering (IJITEE), 5*(2), 90–96. https://doi.org/10.22146/ijitee.66307
[5] Otto, B. (2011). Organizing data governance: Findings from the telecommunications industry and consequences for large service providers. *Communications of the Association for Information Systems, 29*(3), 45–66. https://doi.org/10.17705/1CAIS.02903
[6] Mahmood, F., Khan, A. Z., & Bokhari, R. H. (2020). ERP Issues and Challenges: A Research Synthesis. *Kybernetes*, 49, 629-659. https://doi.org/10.1108/k-12-2018-0699
[7] Dreibelbis, A., Hechler, E., Milman, I., Oberhofer, M., van Run, P., & Wolfson, D. (2008). *Enterprise Master Data Management: An SOA Approach to Managing Core Information.* IBM Press.
[8] Adapa, Chandra Sekhara Reddy. (2025). Enterprise Master Data Management: Trends and Solutions. *European Journal of Computer Science and Information Technology.* 13. 96-105. https://doi.org/10.37745/ejcsit.2013/vol13n1296105
[9] Hong, D., Zhang, Y., Luo, J., Liu, C., Xu, M., & Suo, Z. (2017). *Research on centralized data-sharing model based on master data management.* MATEC Web of Conferences, 139, 00195. https://doi.org/10.1051/matecconf/201713900195
[10] Weill, P., & Ross, J. W. (2004). *IT Governance: How Top Performers Manage IT Decision Rights for Superior Results.* Harvard Business School Press.
[11] Osinachi, Deborah & Segun-Falade, & Osundare, Olajide & Adeleke, Adams & Abioye, Kehinde & Efunniyi, Christianah & Agu, Edith. (2024). Operationalizing Data Governance: A Workflow-Based Model for Managing Data Quality and Compliance, *International Journal of Engineering Inventions* 13(9). 142 -150.
[12] Redman, T. C. (2008). *Data driven: Profiting from your most important business asset.* Harvard Business Press.
[13] Bakır, B., & Ekici, K. (2023). Kurumsal Kaynak Planlama Sistemlerinde Ana Veri Yönetimine İlişkin Örnek Uygulama Yaklaşımı. *Başkent Uluslararası Multidisipliner Çalışmalar Kongresi Bildiriler Kitabı,* pp. 45–58.
[14] Pansara, R. R. (2024). *Strategies for master data management integration and their benefits*. *Scholars Journal of Engineering and Technology (SJET)*, 12(2), 40–47 https://doi.org/10.36347/sjet.2024.v12i02.002

TRANSFORMATION OF INDUSTRIAL TRACKING AND MANAGEMENT INFRASTRUCTURE WITH WI-FI MESH-BASED WIRELESS DIGITAL LABEL SYSTEM

Onur İlyas YAVUZ[a*], Hakkı SOY[b]

[a] *Demsay Elektronik A.Ş. R&D Center, 34520, Beylikdüzü, İstanbul*

[b] *Necmettin Erbakan University, Engineering Faculty, 42090, Meram, Konya*

A B S T R A C T

In today's manufacturing and logistics sectors, the need for real-time information access, traceability, and operational flexibility is rapidly increasing. To address these demands, this study presented the electronic shelf labeling system operating on a Wi-Fi Mesh architecture, designed for use on production lines and warehouse shelves. The designed system consists of OLED-display digital labels with dynamic QR code support, a master control unit, and centralized management software. Labels communicate with each other via MAC address-based connections, establishing a self-organizing wireless network without requiring an external internet infrastructure. Each label automatically updates its displayed information in real time, while dual-color LED indicators provide visual notifications for data updates and location identification. The implementation of developed system has minimized human-dependent data entry errors, reduced manual operational workload, and eliminated paper usage, thereby contributing to environmental sustainability. The solution has been successfully deployed within printed circuit board production and warehouse facilities of DEMSAY Electronics. This study presents the system architecture, wireless communication protocol, ERP integration, dynamic content management, and field application results, while discussing its role within the IoT ecosystem and its scalability across industrial domains.

K E Y W O R D S

- Wi-Fi Mesh
- Digital Label
- Industrial IoT
- Digital Warehouse

* Corresponding author: Onur İlyas YAVUZ
E-mail: o.yavuz@demsay.com

1. Introduction

With the rapid advancement of Industry 4.0 and the Internet of Things (IoT), the need for data-driven management, real-time traceability, and operational flexibility in manufacturing and logistics sectors has significantly increased [1]. Traditional barcode or paper-based labeling methods have become inadequate for handling continuously changing information, often resulting in inefficiencies in both time and resource utilization [2].

In response to these challenges, the electronic shelf labeling systems has been developed to automate data exchange within industrial processes and to establish a smart tracking and management infrastructure across production lines, warehouses, and logistics operations [3,4]. These systems operate in full integration with centralized software, enabling dynamic updates of field devices while ensuring data accuracy without requiring manual intervention [5].

This paper presents the architecture, wireless communication protocol, ERP integration, and field implementation results of the developed system, and discusses its contribution to industrial digital transformation within the IoT ecosystem [6,7].

2. Material and Metod

The developed electronic shelf labeling system is based on an ESP32 Wi-Fi Mesh architecture. Within the system, devices communicate with each other using the ESP-NOW protocol, forming a self-organizing mesh network without the need for any external Wi-Fi access point. Each digital label is uniquely identified by its MAC address, and data transmitted from the master device is propagated sequentially across all connected nodes within the network.

Figure 1: Digital Shelf Label Board

Each label module incorporates an OLED display to present dynamic product and stock information such as company name, material name, box number, and item code. Additionally, status LEDs on the devices visually indicate communication, update, and alert states. The system operates through wired power lines integrated into the shelves, eliminating the need for batteries and enabling uninterrupted, maintenance-free operation.

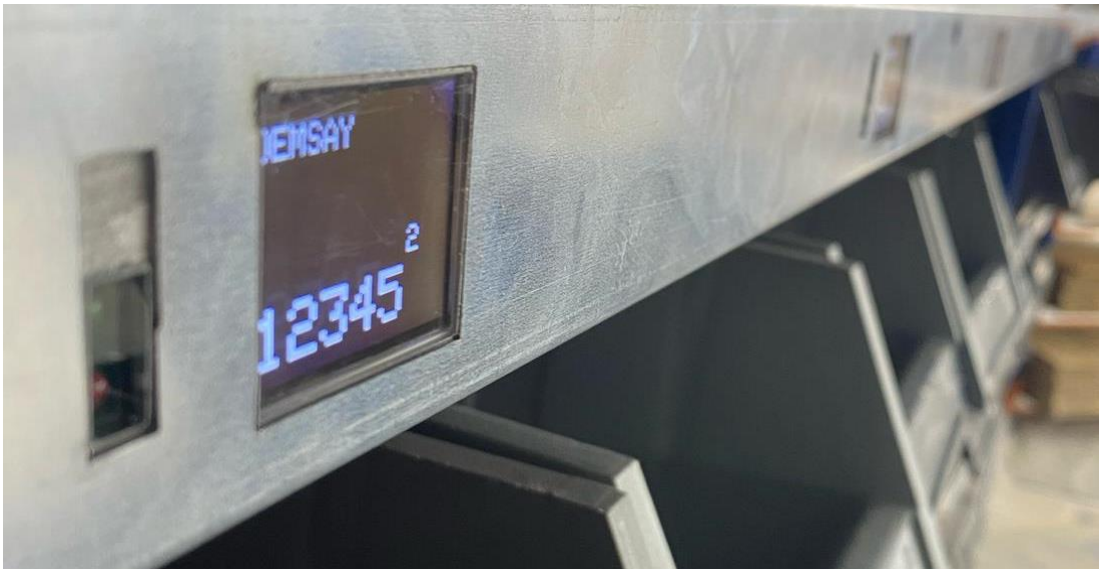

Figure 2: Display of company name, product ID, and bin number on the Digital Label

The master device manages all digital labels and distributes data updates throughout the mesh network. It communicates with the ERP system via a Python-based script, processing incoming data to determine which label should receive which information. Following the defined update sequence, the master device connects to each label sequentially and at high speed via their MAC addresses, ensuring fast and synchronized data delivery across the entire network.

Figure 3: Display of dynamic QR code on the digital label

This design provides a fully automated, high-speed, and real-time data update infrastructure, minimizing manual intervention while enhancing traceability and operational efficiency in industrial environments.

Figure 4: General shelf view of digital label

3. Results and Discussion

The developed Wi-Fi Mesh-based digital labeling system was implemented and tested within the production and warehouse facilities of DEMSAY Electronics R&D Center. Field tests demonstrated that the system provides stable communication up to 200 meters between nodes, and that the mesh routing structure effectively extends the coverage area through multi-hop data transmission. During data update experiments, it was observed that the master device connects sequentially and rapidly to all labels using their MAC addresses, completing the network-wide update process within a few seconds. The ESP-NOW-based communication ensured high reliability and low latency, allowing all labels to remain synchronized in real time. The OLED displays updated instantaneously during data transmission, while the dual-color LED indicators successfully reflected device states such as “updating,” “active,” or “disconnected.” Integration with the ERP system enabled automatic synchronization between the production database and the field devices, eliminating manual data entry errors and increasing update efficiency by over 80% compared to traditional barcode-based labeling methods. Furthermore, the removal of paper labels reduced material waste and maintenance needs, contributing to environmental sustainability. The obtained results confirm that the developed system offers a reliable, scalable, and sustainable solution for industrial data visualization, traceability, and real-time asset management, positioning it as a key component in the advancement of industrial digital transformation.

4. Conclusion

This study presented the design and implementation of a Wi-Fi Mesh-based wireless digital labeling system aimed at improving traceability, flexibility, and automation in industrial environments. The developed system enables seamless and reliable wireless communication through the ESP-NOW protocol, allowing the master device to update all labels sequentially and efficiently using their MAC addresses without requiring any external network infrastructure. Integration with the ERP system enables automatic data synchronization between the production database and on-field digital labels, thereby eliminating human errors and enhancing operational efficiency. The shelf-powered design ensures continuous operation without battery maintenance, supporting sustainability and long-term reliability. The experimental results confirm that the proposed system provides a scalable, high-speed, and eco-friendly infrastructure for industrial digital transformation. Future studies will focus on energy optimization, cloud-based data analytics, and AI-assisted process monitoring to further expand the system's capabilities and industrial applicability.

Acknowledgment

The authors would like to express their sincere gratitude to the DEMSAY Electronics R&D Center for supporting the execution of this study, to the management of DEMSAY Electronics for their continuous encouragement, and to the R&D personnel for their valuable contributions during the system design, testing, and validation phases.

References

[1] IBM Institute for Business Value. (2022, May 25). *Manufacturing 4.0: From data to decisions.* IBM. Retrieved from https://www.ibm.com/thought-leadership/institute-business-value/en-us/report/manufacturing-4-0

[2] The Manufacturer. (n.d.). *Industry 4.0 and the traceability revolution: What smart manufacturing really means.* Retrieved from https://www.themanufacturer.com/press-releases/industry-4-0-and-the-traceability-revolution-what-smart-manufacturing-really-means

[3] Automation Magazine. (2024). *Smart manufacturing: How data-driven decisions are shaping Industry 4.0.* Retrieved from https://www.automationmag.com/smart-manufacturing-data-industry-4-0

[4] Beliatis, M. J., Jensen, K., Ellegaard, L., Aagaard, A., & Presser, M. (2021). *Next Generation Industrial IoT Digitalization for Traceability in Metal Manufacturing Industry: A Case Study of Industry 4.0. Electronics*, 10(5), 628. https://doi.org/10.3390/electronics10050628

[5] MDPI. (2023). *Wireless communications for smart manufacturing and industrial IoT. Sensors*, 23(1), 73. https://doi.org/10.3390/s23010073

[6] WIOT Group. (2023). *Challenges in industrial labeling and identification.* Retrieved from https://wiot-group.com/think/en/resources/labeling-and-identification

Hazardous Object Detection and Classification from X-ray Devices using YOLO and Faster R-CNN Models

Ahmet Furkan HAZAR*, Fatih TİTREK

Department of Computer Engineering, Faculty of Computer and Information Science, Konya Technical University, 42250, Konya/TÜRKİYE

A B S T R A C T

In recent years, significant advances in technology is led to significant research in the fields of computer vision and artificial intelligence. In the critically important field of security, the development of artificial intelligence technology has accelerated research and led to significant advances. Security protection to counter potential threats to critical infrastructures is taken by their own Institutions. X-ray machines play a crucial role in these security measures, allowing users to check the contents of their luggage upon entering a building. The X-ray machine allows high-density items in luggage to be monitorized using X-rays, and these images are used to identify potentially threatening objects by the experts. Therefore, the security of an institution is directly related to the expertise, physical, and mental state of the relevant personnel. In this study, we analyzed the classification results of dangerous objects by examining the results, which are obtained from the Yolov11, Yolov12, Faster R-CNN Resnet50, and Faster R-CNN MobileNetV3-Large models to eliminate personnel dependency and minimize errors in detecting hazardous objects. According to the Precision, Recall, F1 Score, mAP@50 metric values, the best result is obtained by using YOLOv12 model.

K E Y W O R D S

- Artificial Intelligence
- Deep Learning
- Faster R-CNN
- X-ray images
- YOLO

* Corresponding author: Ahmet Furkan HAZAR
E-mail: f211220068@ktun.edu.tr

1. Introduction

X-ray machines allow us to see some materials within objects with the help of X-rays. For instance, in the field of medical technology, we can see the organs behind the muscle and skin tissue or in some security points, it is used for detecting items that it in some baggage, bags, or fabric. The X-rays sent by X-ray devices cause reflection in atoms depending on the density of the substances. For example, high-density substances such as metals reflect X-rays in a way that corresponds to darker colors, while substances of lower density, such as clothing and foods, reflect them in a way that corresponds to lighter colors. With the help of this technology, the detection of various items at security checkpoints that could cause an attack threat, which are typically made of metal (e.g., firearms, knives, scissors), will be improved. X-ray devices, which are usually located at the entrances of facilities, serve a detection function that prevents various attack attempts and ensures the security of people and valuable assets [1, 2]. These devices are utilized by professionals. The effectiveness may vary depending on the training and mood of the staff. This may result in ways of possibilities of security vulnerabilities. Prevention of these vulnerabilities is aimed through the use of improved image processing and artificial intelligence technologies. Digital image processing assists in tasks such as clarifying image contents, analyzing data, transforming color planes, resizing images, and segmenting objects.

The technology known as Artificial Intelligence is the general name for model systems that have been trained on large amounts of data, using mathematical and statistical methods, to perform various tasks such as making inferences, decision-making, content generation, and data analysis. Today, artificial intelligence technology continues to accelerate its development in parallel with advancements in hardware and software [3]. In today's world, the advancement of artificial intelligence plays a significant role in minimizing errors that is caused by human frailties among personnel working in critical roles. As an example, AI programs that analyze results from medical imaging devices can detect details that might be overlooked by a doctor. This allows the AI to accurately guide physicians on vital issues related to patient care. Furthermore, by using the hardware and programs located at checkpoints, it can perceive various threats and assist personnel in executing their jobs to perfection. Deep learning technology, a subfield of artificial intelligence that simplifies and contributes to the improvement of human life in many areas, is actively used to perform specialized tasks. Deep learning tools are used to perform tasks such as image processing, object detection, natural language processing, and audio analysis etc. [4].

In the literature review, studies about the detection of objects that could pose a threat from X-ray devices at security checkpoints were examined. In the study conducted by İ. Karakaya and his colleagues, a Faster R-CNN model was trained by using a dataset created by them for the detection of weapons known as handguns [5]. According to the AP (IoU=O.50:0.95) [24] metric, they have gotten a result of 0.712. In another study conducted by S. Özcan Faster R-CNN model trained by the SIXRAY [6] dataset was used [7]. S. Özcan has gotten the result of 0.906 according to the mAP@50 [24] metric [7]. In a final study, Tao and his colleagues used

the OPIXray [8] dataset to train an SSD model [9]. According to mAP metric, the model achieved a result of 0.70.

In this study, models were trained to detect and classify objects that could be considered dangerous, to assist personnel at security checkpoints, and enhance institutional security. Various methods were used for image processing, and the results were analyzed. Faster-RCNN, YOLOv11, and YOLOv12 deep learning methods were used, and their performances were compared. Models were trained on a combination of SIXRAY and OPIXray datasets. Some evaluation metrics like Precision, Recall, F1 Score, and mAP@50 were chosen, and the results were analyzed.

2. Materials and Methods

2.1. Deep Learning

The structure of the human brain and its system of thought have long been subjects of curiosity. With the rapid development of science and technology over the past two centuries, the functioning of the human brain can now be largely explained biologically. The rise of computer science brought interest in whether machines with similar capabilities could be created by modeling this system. Efforts to model the human brain in computer-based systems, beginning in the 20th century, led to the emergence of Artificial Neural Networks (ANNs) and Genetic Algorithms (GAs). Initially designed to mimic human neurons, ANNs have advanced rapidly in the past two decades, giving rise to the concept of Deep Learning [10]. Deep learning is a subsystem that forms one of the foundations of the artificial intelligence field. Unlike artificial intelligence models, which have broad functionalities, deep learning models are trained for a specific task. Deep learning consists of an Input Layer, Hidden Layers, and an Output Layer. Deep learning models process the input data given to them in the hidden layers and pass it to the output layer. The system operates by sending the output layer back to the input layer. Through the transfer between these layers, the model trains itself and specializes in a specific subject [4]. The connection and communication between the layers are shown in Figure 1.

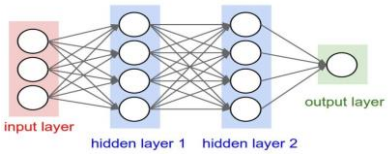

Figure 1. Deep learning layer structure [13]

2.2. Deep Learning for Object Classification and Detection

In this study, the field of deep learning is emphasized for object detection and classification tasks. One of the first architectures used for object classification is the Convolutional Neural Network (CNN) architecture. It is based on the principle of feeding a large number of images into the input layers, applying convolutional operations to the images, and forwarding the results through the layers to the output layer [10]. Methods such as GoogleLeNet, AlexNet, VGG, and ZF Net, which were developed according to this system, can be given as examples [4]. For single or multiple object detection and identification, CNN-based methods such as R-CNN, Fast R-CNN, Faster R-CNN, and YOLO have been developed. The R-CNN method

divides the image into approximately 2000 segments and sends these segments one by one to the CNN layer to find regions with a high probability of containing objects. After the feature extraction process occurs within the CNN, classification is performed. In this way, the location and class of the object are determined within the image by the R-CNN model. However, the R-CNN model has a very slow operational performance because the divided segments are fed into the CNN model one at a time. To overcome this problem, the Fast R-CNN and Faster R-CNN models were developed. The Fast R-CNN model operates on the principle of sending the entire image for detection and classification at once, rather than sending 2000 segmented regions to the CNN network one by one. The optimized version of this model, with the addition of a Region Proposal Network (RPN), is called Faster R-CNN [10]. Today, the Faster R-CNN model is widely used for many object detection and classification tasks.

Another object recognition method developed with the convolution technique is the YOLO model. This model is widely used because its testing and training times are quite short, and it achieves high-performance results. The primary reason for its short processing time is that the image input is fed into YOLO models in a single pass, and the object's location and class information can be obtained as the output. For this reason, the sizes of the models are also quite small. It is frequently preferred for object detection in streaming images [11]. Furthermore, advanced YOLO models can perform image segmentation tasks. In this study, YOLOv11 [12] and YOLOv12 [23], which are among the most current YOLO models, were used.

2.3. Datasets

In this study, different deep learning models were trained by combining the SIXRAY and OPIXray datasets. The literature review revealed that studies have been conducted on the SIXRAY and OPIXray datasets separately. Information about the datasets is described below.

a. SIXRAY Dataset:

SIXRAY is a dataset consisting of 5 classes with 8929 positive and 1050302 negative image data points. The dataset is composed of dangerous objects collected from X-ray devices shown in Figure 2. The images have a resolution of 640x640 and are in the RGB color format. The dataset includes the following classes: ‘Gun’, ‘Knife’, ‘Pliers’, ‘Scissors’, and ‘Wrench’.

Figure 2. SIXRAY data examples.

In the study conducted within the source document for the SIXRAY dataset, it was observed that the SIXray10, SIXray100, and SIXray1000 subsets were created to examine the effect of negative data distribution on model performance. The SIXray10 and SIXray100 datasets were formed by combining 8929 positive images with 10 and 100 times the number of negative images, respectively. The SIXray1000 dataset, on the other hand, was created by randomly selecting 1000 positive images from each class and combining them with 1050302 negative images. The datasets were split into training and test data at a 4:1 ratio. The results of the study conducted with these datasets can be examined in Table 1.

Table 1. SIXray subsets mAP values (From left to right SIXray10, SIXray100, SIXray1000) [6].

Method	*Gun*			*Knife*			*Wrench*			*Pliers*			*Scissors*			*Mean*		
ResNet34[14]	*89.71*	*83.06*	*72.05*	*85.46*	*78.75*	*56.42*	*62.48*	*30.49*	*16.47*	*83.50*	*55.24*	*14.24*	*52.99*	*16.14*	*7.12*	*74.83*	*52.74*	*33.26*
ResNet34+CHR[6]	*87.16*	*81.96*	*73.35*	*87.17*	*77.70*	*60.46*	*64.31*	*36.85*	*23.72*	*85.79*	*64.56*	*17.98*	*61.58*	*14.49*	*18.19*	*77.20*	*55.11*	*38.74*
ResNet50[14]	*90.64*	*84.75*	*74.19*	*87.82*	*77.92*	*59.82*	*63.62*	*28.49*	*16.03*	*84.80*	*50.53*	*16.59*	*57.35*	*19.39*	*2.87*	*76.85*	*52.22*	*33.90*
ResNet50+CHR[6]	*87.55*	*82.64*	*73.43*	*86.38*	*79.60*	*61.32*	*69.12*	*41.19*	*18.88*	*85.72*	*58.02*	*12.32*	*60.91*	*27.89*	*19.03*	*77.94*	*57.87*	*37.00*
ResNet101 [14]	*87.65*	*82.83*	*76.04*	*84.26*	*76.16*	*63.53*	*69.33*	*35.59*	*13.65*	*85.29*	*54.82*	*15.57*	*60.39*	*20.63*	*11.28*	*77.38*	*54.01*	*36.01*
ResNet101+CHR[6]	*85.45*	*83.25*	*75.38*	*87.21*	*77.53*	*64.80*	*71.23*	*42.02*	*15.27*	*88.28*	*68.01*	*19.02*	*64.68*	*32.33*	*16.21*	*79.37*	*60.63*	*38.14*
Inception-v3[15]	*90.05*	*81.18*	*75.52*	*83.80*	*77.28*	*56.33*	*68.11*	*32.47*	*24.01*	*84.45*	*66.89*	*16.75*	*58.66*	*22.63*	*20.72*	*77.01*	*56.09*	*38.67*
Inception-v3+CHR[6]	*88.90*	*79.22*	*76.91*	*87.23*	*73.48*	*61.29*	*69.47*	*37.20*	*29.60*	*86.37*	*69.01*	*19.11*	*65.50*	*31.81*	*47.56*	*79.49*	*58.15*	*46.89*
DenseNet[16]	*87.36*	*83.23*	*75.00*	*87.71*	*77.24*	*65.55*	*64.15*	*37.72*	*23.57*	*87.63*	*62.69*	*18.09*	*59.95*	*24.89*	*14.18*	*77.36*	*57.15*	*39.28*
DenseNet+CHR[6]	*87.05*	*82.06*	*74.87*	*85.89*	*78.75*	*71.23*	*70.47*	*43.22*	*29.79*	*88.34*	*66.75*	*21.57*	*66.07*	*28.80*	*44.27*	*79.56*	*59.92*	*48.36*

In this study, the dataset was split into 5806 Training, 1660 Validation, and 829 Test positive images. Because there can be more than one instance within a single image, the number of instances is not equal to the number of images. There are 4386 instances belonging to the ‘Gun’ class, 2084 instances to the ‘Knife’ class, 5314 instances to the ‘Pliers’ class, 1105 instances to the ‘Scissors’ class, and 2779 instances to the ‘Wrench’ class.

b. OPIXray Dataset:

The OPIXray dataset consists of 5 classes and 8885 image data points. The data were collected from X-ray devices in airports. The images have a resolution of 1225x954 and are in the RGB color format. The classes are named ‘Folding Knife’, ‘Straight Knife’, ‘Scissors’, ‘Utility Knife’, and ‘Multi-tool Knife’. There are 1993 instances belonging to the ‘FoldingKnife’ class, 1044 instances to the ‘Straight Knife’ class, 1978 instances to the ‘Utility Knife’ class, 1863 instances to the ‘Scissors’ class, and 2042 instances to the ‘Multi-tool Knife’ class.

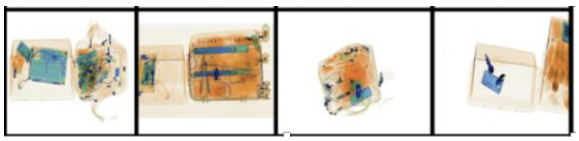

Figure 3. OPIXray data examples.

Due to the presence of multiple instances within a single image shown in Figure 3, the number of instances is greater than the number of images. The data were split into 6715 Training, 1590 Validation, and 1088 Test data points. Upon examining the documentation prepared for the OPIXray dataset, the results of study using the SSD method are shared in Table 2 [8].

Table 2. Performance comparisons of models trained using the OPIXray dataset.

Metot	*mAP*	*Folding Knife*	*Straight Knife*	*Scissors*	*Utility Knife*	*Multi-tool Knife*
SSD[17]	*70.89*	*76.91*	*35.02*	*93.41*	*65.87*	*83.27*
SSD+SE[18]	*71.85*	*77.17*	*38.39*	*92.03*	*66.10*	*85.67*
SSD+Non-local [19]	*71.41*	*77.55*	*36.38*	*95.26*	*64.86*	*82.98*
SSD+DA [20]	*71.96*	*79.68*	*37.69*	*93.38*	*64.14*	*84.90*
SSd+DOAM[8]	*74.01*	*81.37*	*41.50*	*95.12*	*68.21*	*83.83*

3. Proposed Study

3.1. Studies on the Datasets

The YOLOv11 model was trained and its results were shared. The model training processes were carried out using a CUDA-supported GTX 1650 TI graphics card with 4GB of VRAM and the PyTorch library [25]. An Intel i5-10300H was used as the processor. After the initial training processes, the SIXRAY and OPIXray datasets were combined to increase the number of class and instance data points, and a model was then trained on this merged dataset.

a. YOLOv11 Model Training Process with the SIXRAY Dataset:

The SIXRAY dataset was used to train the YOLOv11 model without being subjected to any preprocessing, with the epoch value set to 30. Information regarding the training results can be accessed in Table 3 below. The results of the prediction process of the Yolov11 model trained with the SIXRAY dataset are shown in Figure 4.

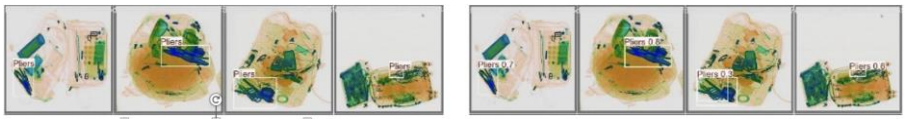

Original Data Prediction Results

Figure 4. Labeled original data and prediction results of trained Yolov11 model

Table 3. Class-based accuracy metrics of the Yolov11 model trained with SIXRAY data

Class	*Images*	*Instances*	*Precision*	*Recall*	*mAP50*
Gun	551	888	0.936	0.936	0.973
Knife	291	442	0.85	0.756	0.833
Pliers	794	1110	0.865	0.74	0.854
Scissors	178	206	0.784	0.743	0.819
Wrench	392	530	0.811	0.647	0.758
All	1660	3176	0.849	0.764	0.847

b. YOLOv11 Model Training Process with the OPIXray Dataset:

The OPIXray dataset was subjected to some preprocessing steps to work properly with the YOLO model. First, the resolution values were changed from 1225x954 to 640x640. The coordinate values within the annotations folder were updated according to the new resolution and then normalized. Following these procedures, the training data was fed into the YOLOv11 model with an epoch value of 30. The training results are shared in Table 4.

Table 4. Class-based accuracy metrics of the Yolov11 model trained with OPIXray data

Class	*Images*	*Instances*	*Precision*	*Recall*	*mAP50*
Folding Knife	*1227*	*1233*	*0.903*	*0.856*	*0.931*
Multi-tool Knife	*1258*	*1259*	*0.832*	*0.943*	*0.952*
Scissor	*1850*	*1852*	*0.983*	*0.98*	*0.989*
Straight Knife	*1043*	*1043*	*0.856*	*0.713*	*0.848*
Utility Knife	*1353*	*1355*	*0.896*	*0.788*	*0.894*
All	*6715*	*6742*	*0.894*	*0.856*	*0.923*

The results of the prediction process of the Yolov11 model trained with the OPIXray dataset are shown in Figure 5.

Original Data Prediction Results

Figure 5. Labeled original data and prediction results of trained Yolov11 model

3.2. Combination of the OPIXray and SIXRAY Datasets

The OPIXray and SIXRAY datasets were merged with the aim of training a model with an increased number of classes and instances. During the merging process, all images were standardized to a 640x640 resolution. The 'Scissors' and 'Knife' classes, common to both datasets, were combined. Afterward, the data was split into Train, Test, and Validation sets.

As a result of the merging process, a dataset with 8 classes, totaling 17144 images and 24546 instances, was obtained. The data was partitioned into 72% Training, 19% Validation, and 9% Test data. Information about the classes and instances in the dataset can be found in Table 5.

Table 5. Classes, sample numbers and distributions of the data set created as a result of merging

Class	*Train*	*Valid*	*Test*	*Total*
Pliers	*3680*	*1110*	*524*	*5314*
Gun	*3024*	*888*	*474*	*4386*
Straight_Knife	*2516*	*442*	*169*	*3127*
Scissor	*2631*	*206*	*120*	*2957*
Wrench	*1943*	*530*	*306*	*2779*
Multi-tool_Knife	*1225*	*560*	*246*	*2031*
Folding_Knife	*1202*	*557*	*226*	*1985*
Utility_Knife	*1326*	*443*	*198*	*1967*
Total Sample	*17547*	*4736*	*2263*	*24546*

3.3. YOLOv11 Train

The combined dataset was trained on the YOLOv11 and results are shown in Table 6.

Table 6. Evaluation results of the Yolov11 model trained with the combined dataset

Class	*Precision*	*Recall*	*mAP50*	*F1 Score*
all	*0.84*	*0.771*	*0.843*	*0.803*
Folding_Knife	*0.881*	*0.824*	*0.888*	*0.851*
Gun	*0.945*	*0.941*	*0.976*	*0.942*
Multi-tool_Knife	*0.851*	*0.846*	*0.895*	*0.869*
Pliers	*0.861*	*0.759*	*0.865*	*0.806*
Scissor	*0.76*	*0.729*	*0.791*	*0.744*
Straight_Knife	*0.745*	*0.764*	*0.806*	*0.754*
Utility_Knife	*0.868*	*0.623*	*0.737*	*0.725*
Wrench	*0.813*	*0.682*	*0.782*	*0.741*

Some examples of prediction results from the training of the YOLOv11 model are shown in Figure 6.

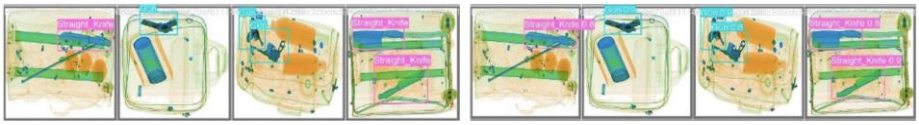

Original Data Prediction Results

Figure 6. Labeled original data of the merged dataset and prediction results of the trained Yolov11 model

3.4 Applied Image Processing Methods

As seen in Figures 2 and 3, the X-ray images from security checkpoints do not have any noise, variable brightness values, or mosaics. For this reason, separate datasets were created using image processing methods on the color planes of the images, subsequently subjected to model training, and the results have been shared.

a. Applying a Threshold to RED Values on the RGB Channel:

The reason for applying this process is that, as seen in the examples, the majority of objects considered dangerous are composed of metal. Since metals have a dominant BLUE channel in the RGB images produced by X-ray devices, a process was implemented to separate the pixels where the RED value is predominant. The threshold for the RED channel was set to 150, and all pixels satisfying the condition RED >= 150 were assigned the color white. Sample images from the dataset created as a result of this process are shown in Figure 7.

Figure 7. Sample data pre-processed through Red Threshold

As an advantage, this process allowed the objects within the images to appear more distinctly; however, it also caused the formation of noise on the objects. The YOLOv11 model was trained with the resulting dataset. The training results are shown in Table 7.

Table 7. Evaluation results of the Yolov11 model trained with Red Threshold applied data

Class	*Precision*	*Recall*	*mAP50*	*F1 Score*
all	*0.816*	*0.741*	*0.818*	*0.776*
Folding_Knife	*0.846*	*0.757*	*0.845*	*0.799*
Gun	*0.915*	*0.935*	*0.971*	*0.924*
Multi-tool_Knife	*0.839*	*0.803*	*0.862*	*0.820*
Pliers	*0.840*	*0.741*	*0.844*	*0.787*
Scissor	*0.758*	*0.714*	*0.779*	*0.735*
Straight_Knife	*0.734*	*0.767*	*0.808*	*0.750*
Utility_Knife	*0.834*	*0.555*	*0.689*	*0.666*
Wrench	*0.759*	*0.656*	*0.744*	*0.703*

Prediction results for training the YOLOv11 model are shown in Figure 8.

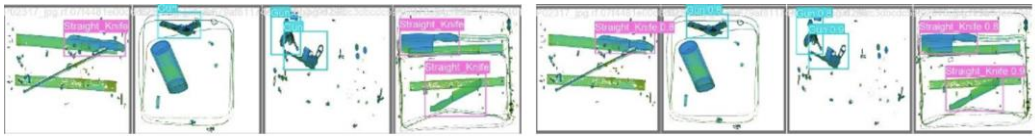

Original Data Prediction Results

Figure 8. Labeled original data and prediction results of trained Yolov11 model after preprocessing

b. Preprocessing with Red Threshold, Grayscale, and Gaussian Blur

First, the regions where the RED channel was dominant were eliminated using a threshold value, and then the images were converted to the grayscale channel. An attempt was made to remove the noise, caused by the operations on the RED channel, using the Gaussian Blur [21] method. Sample images are shared in Figure 9.

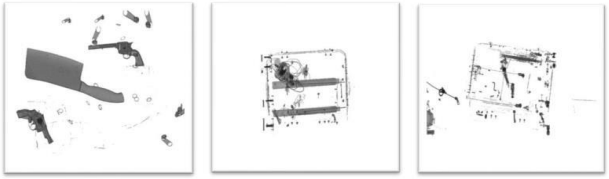

Figure 9. Sample data that has undergone red Threshold – Gray Scale – Gaussian Blur preprocessing

With this method, objects are made more prominent. It was also aimed to minimize the resulting noise and information loss. The created dataset was used to train the YOLOv11 model. The training results are shown in Table 8.

Table 8. Model training result of data applied with Red Threshold – Gray Scale – Gaussian Blur

Class	*Precision*	*Recall*	*mAP50*	*F1 Score*
all	0.838	0.735	0.819	0.783
Folding_Knife	0.885	0.808	0.884	0.844
Gun	0.934	0.932	0.972	0.932
Multi-tool_Knife	0.865	0.804	0.878	0.833
Pliers	0.840	0.748	0.860	0.791
Scissor	0.791	0.659	0.776	0.718
Straight_Knife	0.771	0.741	0.795	0.755
Utility_Knife	0.830	0.533	0.643	0.649
Wrench	0.782	0.657	0.744	0.714

The prediction results of the training of the YOLOv11 model are shown in Figure 10.

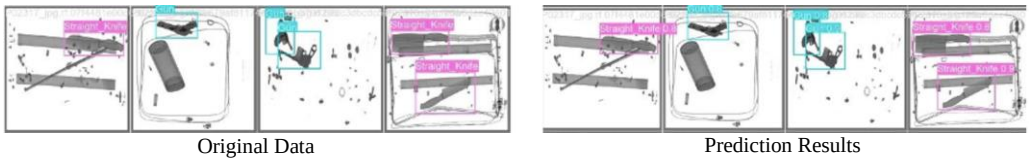

Original Data Prediction Results

Figure 10. Labeled original data and prediction results of trained Yolov11 model after preprocessing

3.5 Training Process

Following the merge of the SIXRAY and OPIXray datasets, the YOLO and Faster R-CNN models were trained on this combined dataset. In the training process, models with different weights were used, and the results were recorded.

a. YOLOv12 Train:

An object detection model was trained using the YOLOv12 Small model with the merged versions of the datasets. The training results of this model are shown in Table 9.

Table 9. Evaluation results of the Yolov12 model trained with the combined datase

Class	*Precision*	*Recall*	*mAP50*
all	0.884	0.801	0.869
Folding_Knife	0.900	0.823	0.886
Gun	0.970	0.939	0.979
Multi-tool_Knife	0.908	0.844	0.914
Pliers	0.904	0.794	0.894
Scissor	0.841	0.814	0.860
Straight_Knife	0.820	0.773	0.832
Utility_Knife	0.867	0.704	0.767
Wrench	0.864	0.720	0.820

When the performance metrics were compared with the YOLOv11n model, it was observed that the metric values of the YOLOv12s model were higher.

b. Faster R-CNN Train:

For the Faster R-CNN training process, two different models were trained with two different backbones. ResNet50 and MobileNetV3-Large were used as the backbones [22]. The results obtained from the MobileNetV3-Large training are shown in Table 10.

Table 10. General evaluation results of the Faster R-CNN MobileNetV3-Large model

Metric	*Value*
Precision	*0.83*
Recall	*0.73*
F1-Score	*0.77*
mAP@50	*0.71*

Class-based results obtained from Faster R-CNN MobileNet V3-Large training are shown in Table 11.

The training results with ResNet50 backbone are shown in Table 12 and the class-based results of the training with ResNet50 backbone are shown in Table 13.

Table 11. Class-based evaluation results of the Faster R-CNN MobileNetV3-Large model

Class_Name	*Precision*	*Recall*	*F1_Score*
Folding_Knife	*0.89*	*0.74*	*0.81*
Gun	*0.91*	*0.92*	*0.92*
Multi-tool_Knife	*0.89*	*0.78*	*0.83*
Pliers	*0.84*	*0.74*	*0.79*
Scissor	*0.76*	*0.70*	*0.73*
Straight_Knife	*0.71*	*0.73*	*0.72*
Utility_Knife	*0.85*	*0.58*	*0.69*
Wrench	*0.75*	*0.66*	*0.70*

Table 12. General evaluation results of the Faster R-CNN ResNet50 model

Metric	*Value*
Precision	*0.76*
Recall	*0.78*
F1-Score	*0.76*
mAP@50	*0.74*

Table 13. Class-based evaluation results of the Faster R-CNN ResNet50 model

Class_Name	*Precision*	*Recall*	*F1_Score*
Folding_Knife	*0.91*	*0.81*	*0.86*
Gun	*0.87*	*0.92*	*0.90*
Multi-tool_Knife	*0.91*	*0.84*	*0.87*
Pliers	*0.72*	*0.81*	*0.76*
Scissor	*0.73*	*0.74*	*0.73*
Straight_Knife	*0.58*	*0.75*	*0.65*
Utility_Knife	*0.82*	*0.66*	*0.73*
Wrench	*0.52*	*0.72*	*0.61*

4. Conclusion

In this study, research was conducted on image processing, artificial intelligence, deep learning, and X-ray devices. Based on these studies, deep learning models were trained using image processing and deep learning techniques to detect objects that may pose a threat to institutions within images obtained from X-ray devices. Results of the models are presented in Table 14.

Table 14. Evaluation results of models trained using the combined dataset

Model	*Precision*	*Recall*	*F1 Score*	*mAP@50*
YOLOv11n	*0.84*	*0.77*	*0.80*	*0.84*
YOLOv12s	*0.88*	*0.80*	*0.84*	*0.86*
Faster R-CNN MobileNetV3-Large	*0.83*	*0.73*	*0.77*	*0.71*
Faster R-CNN ResNet50	*0.76*	*0.78*	*0.76*	*0.74*

References

[1] Kaya, A., & Kartal, M. (2021). Havalimanı güvenlik yönetiminde teknoloji ve insan. *Journal of Aviation, 5*(2), 298–309.

[2] Seyfi, G., Yilmaz, M., Esme, E., & Kiran, M. S. (2024). X-ray image analysis for explosive circuit detection using deep learning algorithms. *Applied Soft Computing, 151*, 111133. https://doi.org/10.1016/j.asoc.2023.111133

[3] Fathima Anjila, P. K. (1984). What is artificial intelligence? Success is no accident: It is hard work, perseverance, learning, studying, sacrifice and most of all, love of what you are doing or learning to do, *International Journal of information and management sciences, 65*, 85–108.

[4] Tan, F. G., Yüksel, A. S., Aydemir, E., & Ersoy, M. (2021). Derin öğrenme teknikleri ile nesne tespiti ve takibi üzerine bir inceleme. *Avrupa Bilim ve Teknoloji Dergisi, (25)*, 159–171.

[5] Karakaya, İ., Şafak, I., Öztürk, O., Bal, M., & Esin, Y. E. (2020, October). Gun detection with Faster R-CNN in X-ray images. *In 2020 28th Signal Processing and Communications Applications Conference (SIU)* (pp. 1–4). IEEE. https://doi.org/10.1109/SIU49456.2020.9302156

[6] Miao, C., Xie, L., Wan, F., Su, S., Liu, Y., Jiao, J., & Ye, Q. (2019). SIXray: A large-scale security inspection X-ray benchmark for prohibited item discovery in overlapping images. *In Proceedings of the IEEE/CVF Conference on Computer Vision and Pattern Recognition (CVPR)* (pp. 2119–2128). IEEE. https://doi.org/10.1109/CVPR.2019.00219

[7] Sorgun, Ö. (2022). X-ray görüntülerinde Faster R-CNN kullanılarak yasaklı nesne tespiti (Yüksek lisans tezi). *Sakarya Uygulamalı Bilimler Üniversitesi, Lisansüstü Eğitim Enstitüsü*, Sakarya.

[8] Wei, Y., Tao, R., Wu, Z., Ma, Y., Zhang, L., & Liu, X. (2020). Occluded prohibited items detection: An X-ray security inspection benchmark and de-occlusion attention module. *In Proceedings of the 28th ACM International Conference on Multimedia* (pp. 138–146). ACM.

[9] Tao, R., Wei, Y., Li, H., Liu, A., Ding, Y., Qin, H., & Liu, X. (2021). Over-sampling de-occlusion attention network for prohibited items detection in noisy X-ray images. *arXiv preprint arXiv*:2103.00809.

[10] İnik, Ö., & Ülker, E. (2017). Derin öğrenme ve görüntü analizinde kullanılan derin öğrenme modelleri. *Gaziosmanpaşa Bilimsel Araştırma Dergisi, 6*(3), 85–104.

[11] Jiang, P., Ergu, D., Liu, F., Cai, Y., & Ma, B. (2022). A review of YOLO algorithm developments. *Procedia Computer Science, 199*, 1066–1073.

[12] Khanam, R., & Hussain, M. (2024). YOLOv11: An overview of the key architectural enhancements. *arXiv preprint*arXiv:2410.17725.

[13] Deep Learning. (2025, June 12). CS231n: Convolutional Neural Networks for Visual Recognition. Retrieved from https://cs231n.github.io/neural-networks-1/.

[14] He, K., Zhang, X., Ren, S., & Sun, J. (2016). Deep residual learning for image recognition. *Proceedings of the IEEE Conference on Computer Vision and Pattern Recognition (CVPR)*, 770–778.

[15] Szegedy, C., Vanhoucke, V., Ioffe, S., Shlens, J., & Wojna, Z. (2016). Rethinking the inception architecture for computer vision. *Proceedings of the IEEE Conference on Computer Vision and Pattern Recognition (CVPR)*, 2818–2826.

[16] Huang, G., Liu, Z., Van Der Maaten, L., & Weinberger, K. Q. (2017). Densely connected convolutional networks. *Proceedings of the IEEE Conference on Computer Vision and Pattern Recognition (CVPR)*, 2, 3.

[17] Liu, W., Anguelov, D., Erhan, D., Szegedy, C., Reed, S., Fu, C.-Y., & Berg, A. C. (2016). SSD: Single shot multibox detector. *In European Conference on Computer Vision (ECCV)* (pp. 21–37). Springer..

[18] Hu, J., Shen, L., & Sun, G. (2018). Squeeze-and-excitation networks. *In Proceedings of the IEEE Conference on Computer Vision and Pattern Recognition (CVPR)* (pp. 7132–7141).

[19] Wang, X., Girshick, R., Gupta, A., & He, K. (2018). Non-local neural networks. *In Proceedings of the IEEE Conference on Computer Vision and Pattern Recognition (CVPR)* (pp. 7794–7803).

[20] Wang, P., Li, Z., Hou, Y., & Li, W. (2016). Action recognition based on joint trajectory maps using convolutional neural networks. *In Proceedings of the 24th ACM International Conference on Multimedia* (pp. 102–106).

[21] Gedraite, E. S., & Hadad, M. (2011). Investigation on the effect of a Gaussian blur in image filtering and segmentation. *In Proceedings of ELMAR 2011* (pp. 393–396). IEEE.

[22] Hakim, L., Hendrawan, A., & Khoiriyah, R. (2024). Traffic vehicle detection using Faster R-CNN: A comparative analysis of backbone architectures. *International Journal of Artificial Intelligence and Science*, *1*(1), 50–62.

[23] Tian, Y., Ye, Q., & Doermann, D. (2025). Yolov12: Attention-centric real-time object detectors. *arXiv preprint arXiv*:2502.12524..

[24] Rainio, O., Teuho, J., & Klén, R. (2024). Evaluation metrics and statistical tests for machine learning. *Scientific Reports, 14*, 6086. https://doi.org/10.1038/s41598-024-56706-x

[25] Jha, R. G., & Samlodia, A. (2024). GPU-acceleration of tensor renormalization with PyTorch using CUDA. *Computer Physics Communications, 294*, 108941.

ANALYSIS OF LAND COVER CHANGE IN THE CAPPADOCIA REGION USING REMOTE SENSING

Şeymanur BAŞGÖZE[a*], Esra ODABAŞ YILDIRIM[b], Ahmet ÖZCAN[c]

[a] *Kapadokya University, Faculty of Computer and Information Technologies, Department of Information Systems and Technologies, Ürgüp / Nevşehir, Türkiye*

[b] *Atatürk University, Faculty of Engineering, Department of Software Engineering, Erzurum, Türkiye*

[c] *Kapadokya University, Faculty of Computer and Information Technologies, Department of Artificial Intelligence and Machine Learning, Ürgüp / Nevşehir, Türkiye*

ABSTRACT

This study analyzes land use/land cover (LULC) dynamics in the Cappadocia region, a culturally and ecologically significant UNESCO World Heritage site, over the period of 2015–2024. The research utilizes the Google Earth Engine (GEE) platform and Landsat 8 satellite imagery combined with supervised machine learning classification. The landscape was categorized into three main classes: agricultural land, natural land, and urban/built-up areas. To ensure reliable classification, four machine learning algorithms were compared: Random Forest (RF), Classification and Regression Trees (CART), Support Vector Machines (SVM), and Naive Bayes. Among these, RF demonstrated the highest performance, achieving a Kappa coefficient of 0.6327 and an overall accuracy of 75.82%, and was therefore selected for the final spatio-temporal assessment. The analysis indicates a notable expansion of agricultural land, increasing from 25.3% to 31.8% of the total area during the study period, predominantly at the expense of natural landscapes. These findings highlight both the dynamic nature of land transformation in Cappadocia and the effectiveness of integrating GEE with machine learning techniques. Additionally, the study emphasizes the importance of model comparison in ensuring the accuracy and reliability of LULC classification in sensitive environments.

KEYWORDS

- Remote Sensing
- Land Cover Change
- Image Classification
- Cappadocia
- Landsat 8

[*] Corresponding author: Şeymanur BAŞGÖZE
E-mail: seymanur.basgoze@kapadokya.edu.tr

1. Introduction

Land cover and land use (LCLU) represent the most concrete and observable manifestations of the complex interactions between the Earth's biophysical systems and the socio-economic dynamics that shape them. Monitoring changes in LCLU, which play a fundamental role in understanding the human–nature relationship, is of critical importance for sustainable land management, natural resource planning, and environmental policy development [1]. Anthropogenic factors such as agricultural expansion, rapid urbanization, deforestation, and infrastructure development are transforming natural landscapes at an unprecedented rate. These transformations have resulted in severe and often irreversible ecological consequences, including the degradation of ecosystem services, biodiversity loss, alteration of hydrological cycles, and soil degradation [2]. Therefore, accurate, consistent, and periodic mapping and analysis of LCLU dynamics are indispensable for understanding environmental change and formulating informed policies to mitigate adverse impacts.

Remote sensing technologies have become the primary means for monitoring LCLU changes due to their ability to provide periodic, large-scale, and objective information about the Earth's surface. Unlike traditional land survey methods, satellite-based observations offer cost-effective time-series data that enable the analysis of the rate, direction, and spatial patterns of processes such as agricultural expansion, rangeland degradation, and urban sprawl. Among these, the Landsat satellite program—providing continuous, freely accessible data since 1972—constitutes an invaluable resource for long-term change detection and trend analysis [3].

Historically, the technical and financial challenges associated with downloading, storing, and processing large datasets have limited the application of such analyses. However, the advent of cloud-based geospatial computing platforms, particularly Google Earth Engine (GEE), has led to a paradigm shift in the field. GEE enables instant access to petabytes of satellite imagery archives (e.g., Landsat, Sentinel, MODIS) and facilitates large-scale analyses using Google's extensive computational infrastructure and high-performance parallel processing capabilities [4]. Furthermore, it allows for the effective integration of advanced machine learning algorithms, such as Random Forest (RF), in computationally intensive tasks like LCLU classification [5].

This study focuses on the Cappadocia region, one of Turkey's and the world's most significant cultural and natural heritage sites. Characterized by volcanic tuffs and erosion-sculpted geomorphology ("fairy chimneys"), along with rock-carved churches and underground cities, the region is inscribed on the UNESCO World Heritage List. Nevertheless, Cappadocia is currently subject to competing land-use pressures arising from intensive tourism activities and traditional agricultural practices. While tourism serves as a major economic driver, it simultaneously exerts pressure on the natural and cultural landscape through unplanned construction and infrastructure development [6]. Agricultural land-use changes, on the other hand, significantly affect the region's fragile soil and water resources within its semi-arid

ecosystem. These complex and interdependent dynamics pose substantial threats to Cappadocia's ecological integrity and unique cultural identity.

Accordingly, the main objectives of this study are as follows:

1. To map land cover and land use changes in the Cappadocia region between 2015 and 2024 using Landsat 8 imagery within the Google Earth Engine (GEE) platform.
2. To comparatively evaluate the classification performance of four machine learning algorithms—Random Forest (RF), Classification and Regression Trees (CART), Support Vector Machines (SVM), and Naive Bayes—and identify the most effective model.
3. To quantitatively analyze the spatial and areal variations of major land cover classes (agricultural, natural, and urban) in the study area using the best-performing model.

2. Material and Methods

The methodology of this study comprises several sequential stages, including the definition of the study area, acquisition and preprocessing of satellite and ground-truth data, implementation of comparative machine learning models, accuracy assessment, and temporal change analysis. All geospatial data processing and analysis procedures were conducted on Google Earth Engine (GEE), a cloud-based geospatial computing platform.

2.1 Study Area

The study area covers the Cappadocia region and its surroundings, located at the intersection of the Nevşehir, Kayseri, and Aksaray provinces in the Central Anatolia Region of Türkiye, centered approximately at 38.6° N latitude and 34.8° E longitude. The region, characterized by a continental climate, exhibits a heterogeneous landscape where unique geomorphological formations developed on volcanic tuff terrains coexist with steppe vegetation and agricultural lands. The area's economy is primarily driven by intensive tourism activities and agricultural production, which together shape the region's land-use dynamics.

2.2 Dataset and Preprocessing

a. Satellite Imagery and Atmospheric Correction

This study utilized Landsat 8 OLI (Operational Land Imager) imagery provided by the United States Geological Survey (USGS). The dataset consists of Collection 2 Level-2 Surface Reflectance products with a 30-meter spatial resolution. These products, derived from sensor-recorded radiance data, are corrected for atmospheric scattering and absorption effects, thereby enhancing spectral consistency and reliability in time-series analyses.

For the analysis period (2015, 2018, 2020, and 2024), all available images acquired between May 1 and September 30—the period characterized by peak vegetation activity and minimal cloud coverage—were used. Six spectral bands were selected for classification: Band 2 (Blue),

Band 3 (Green), Band 4 (Red), Band 5 (Near-Infrared, NIR), Band 6 (Shortwave Infrared 1, SWIR1), and Band 7 (Shortwave Infrared 2, SWIR2).

To remove atmospheric artifacts such as clouds and cloud shadows, the QA_PIXEL quality assurance band of each image was utilized for masking. Subsequently, a median composite method was applied to generate a single cloud-free and seasonally normalized composite image for each year. This method effectively eliminates outliers and residual noise by computing the median value of all valid observations for each pixel location, thereby providing a robust dataset for classification and temporal change detection.

b. Ground Truth Data and Preparation

To train and validate the models, a ground truth dataset representing the classes of Agricultural Land, Natural Land, and Built-up Area was generated using high-resolution Google Earth imagery as a reference. The accuracy of this dataset is critically important to ensure the reliability of the accuracy assessment process. Initially digitized in GeoJSON format as LineString geometries, the polygon boundaries were programmatically converted into Polygon geometries within the Google Earth Engine (GEE) environment. Erroneous labels outside the three defined classes (e.g., class 0 or null) were filtered and removed from the dataset. The final dataset consisted of 169 valid polygons, which were randomly split into two subsets on GEE: 70% for training and 30% for testing. This partitioning is a standard practice designed to prevent overfitting by evaluating model performance on previously unseen data, thereby ensuring an unbiased assessment of model accuracy.

2.3 Land Cover Classification Methodology

a. Comparative Classification Algorithms

In this study, four machine learning algorithms—commonly used in the literature and based on different theoretical foundations—were tested for LCLU classification:

- Random Forest (RF): An ensemble learning method that constructs multiple decision trees and aggregates their results to produce the final classification. By using random subsampling (bootstrap aggregating) of the training set and randomly selecting a subset of features at each node, it ensures diversity among trees, enhances generalization ability, and mitigates overfitting [7].
- CART: A decision tree model that recursively partitions the dataset based on feature values using impurity measures such as the Gini index, forming a hierarchical structure for classification [8].
- Support Vector Machines (SVM): A classification model that identifies an optimal hyperplane maximizing the margin between data points belonging to different classes, thereby improving classification robustness [9].
- Naive Bayes: A probabilistic classifier based on Bayes' theorem that assumes strong independence among features, allowing efficient computation and effective classification performance even with limited training data [10].

b. Model Training and Accuracy Assessment

All defined models were trained on the 2024 composite image and the corresponding training dataset within the Google Earth Engine (GEE) environment. The performance of the models was evaluated using the test data, which were not included in the training phase, by constructing a Confusion Matrix (Error Matrix). This matrix enables comparison between the classified data and the reference (ground truth) data, where rows typically represent reference classes and columns correspond to classified outputs. From this matrix, two key accuracy metrics were derived: Overall Accuracy and the Kappa Coefficient. The Kappa Coefficient (κ) measures the agreement between the observed and expected accuracies (by chance) and is considered a more robust indicator of classification performance, particularly when class distributions are imbalanced.

c. Temporal Change Analysis

The model yielding the highest Kappa value was selected as the most reliable classifier and was subsequently employed to produce the land cover and land use (LCLU) maps of the Cappadocia region for the years 2015, 2018, 2020, and 2024. Using the post-classification comparison technique, the number of pixels corresponding to each land cover class in every map was calculated and multiplied by the pixel area (30 m × 30 m) to determine the total area (in hectares) occupied by each class. This approach allowed the quantitative assessment of land cover and land use changes over the ten-year study period.

3. Results and Discussion

3.1 Comparative Performance of Classification Models and Model Selection

In this study, the performance of four different machine learning algorithms for land cover and land use (LCLU) classification was evaluated using identical training and test datasets. The results obtained from the models, based on Overall Accuracy and Kappa Coefficient metrics, are summarized in Table 1.

Table 1. Performance Evaluation of All Classification Models

Model	*Accuracy*	*Kappa*
Random Forest	0.76	0.63
SVM	0.73	0.59
Navie Bayes	0.33	0.00
CART	0.67	0.50

An examination of Table 1 clearly indicates that the Random Forest (RF) model achieved the highest performance, with a Kappa coefficient of 0.6327 and an overall accuracy of 75.82%. Since the Kappa statistic is a robust measure that quantifies how much better the classification performs compared to random chance, it was adopted as the primary criterion for model selection. The superior performance of the RF model can be attributed to its ensemble learning structure, which combines multiple decision trees to produce more stable and generalizable results compared to a single decision tree model such as CART. Furthermore, the random selection of feature subsets during the training of each tree enhances model generalization and helps prevent overfitting, thereby improving overall accuracy.

Support Vector Machines (SVM) also demonstrated competitive performance, achieving 73% overall accuracy and a Kappa coefficient of 0.59, although slightly lower than that of the RF model. On the other hand, the Naive Bayes model yielded a Kappa value of 0.00, indicating its inadequacy for this type of geospatial data analysis. This poor performance can be attributed to the violation of the model's strong independence assumption among features, as spectral bands in multispectral imagery often exhibit high autocorrelation.

Overall, this comparative analysis highlights the critical influence of methodological choice on the reliability of classification outcomes and provides a scientific rationale for selecting the Random Forest model as the most suitable approach for this study.

3.2 Comparative Evaluation of the Spatial Outputs of Classification Models

Although the accuracy metrics presented in Table 1 provide a quantitative framework for evaluating the performance of the classification models, visual examination of the resulting maps is crucial for understanding the spatial behavior of the models and their consistency with geographical reality. In this section, the classification maps produced by the four tested models are comparatively evaluated. To facilitate a clearer comparison, the classification outputs for the year 2024—corresponding to the dataset employed during the model training phase—are presented in Figures 1, 2, 3, and 4.

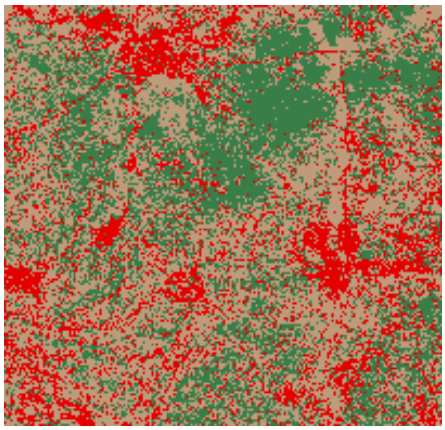

Fig. 1. CART Model Output (2024)

Fig. 2. Naive Bayes Model Output (2024)

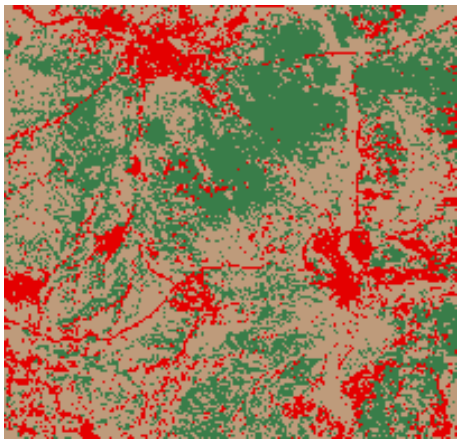

Fig. 3. Random Forest Model Output (2024)

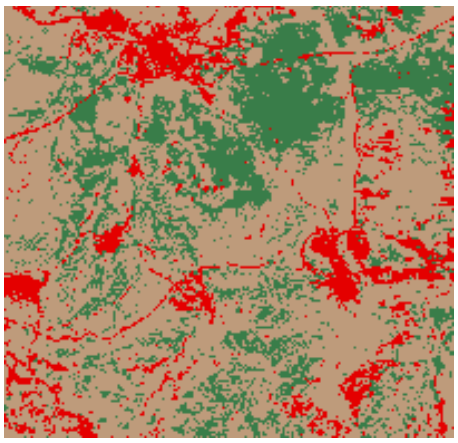

Fig. 4. SVM Model Output (2024)

- **Random Forest (RF) and SVM Models:** These two models, which achieved the highest Kappa scores, produced highly similar and spatially consistent results. In both maps, homogeneous agricultural parcels, extensive and cohesive natural areas, and the main outlines of built-up zones are clearly distinguishable. The RF map exhibits slightly sharper boundary delineations and a less "noisy" appearance compared to the SVM output. These two maps can therefore be considered the most accurate representations of the region's overall land structure.

- **CART Model:** The output of the CART model, which is based on a single decision tree, performed less successfully than RF and SVM, as reflected by its Kappa score (0.50). The map is characterized by a noticeable "salt-and-pepper" noise effect and a more blocky spatial appearance. This reflects the inherent limitation of single decision trees, which tend to have lower generalization capacity and higher sensitivity to noise compared to ensemble models such as RF. Misclassifications are particularly evident in areas with fragmented and heterogeneous land patterns.

- **Naive Bayes Model:** As indicated by its Kappa value of 0.00, the Naive Bayes model demonstrated the weakest performance, and its map visually confirms this outcome. The classification shows random and unrealistic spatial patterns, with large areas incorrectly assigned to a single class (e.g., extensive regions misclassified as agricultural land). This

result vividly illustrates the significance of appropriate model selection and highlights how an unsuitable algorithm can produce misleading spatial representations.

This visual comparison demonstrates that the Random Forest model outperformed the others not only in numerical accuracy but also in terms of spatial consistency and agreement with geographical reality. Consequently, the RF model was selected for generating the temporal land cover and land use change maps used in the subsequent analysis of the Cappadocia region.

3.3 Temporal and Spatial Changes in Land Cover (2015–2024)

The maps presented in Figures 5, 6, 7, and 8 reveal that the region has undergone a significant transformation in land use and land cover over the ten-year period.

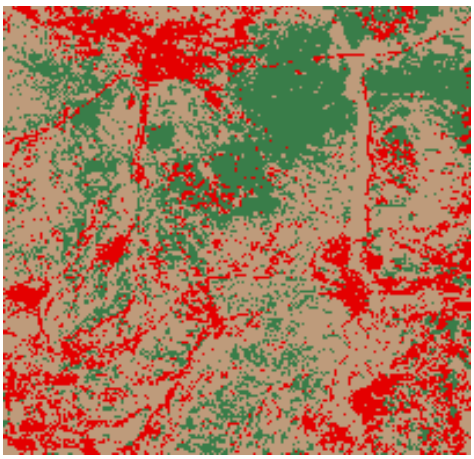

Fig. 5. 2015 Image Analysis

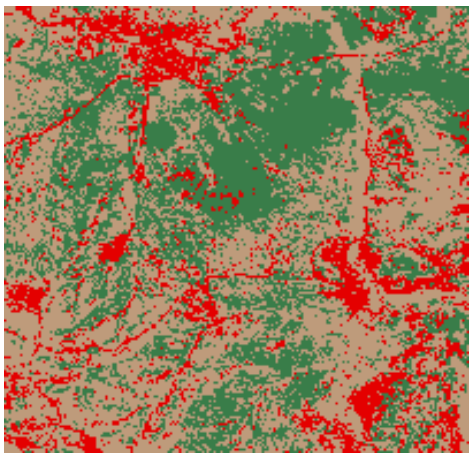

Fig. 6. 2018 Image Analysis

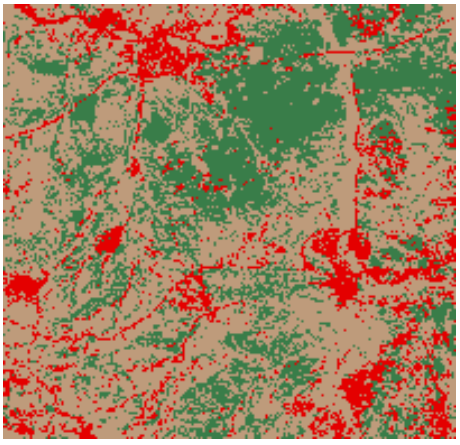

Fig. 7. 2020 Image Analysis

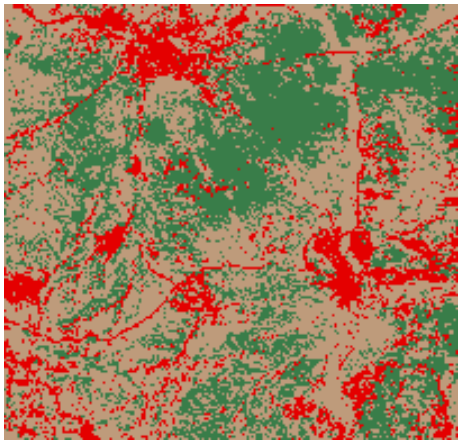

Fig. 8. 2024 Image Analysis

- **Expansion of Agricultural Areas**
  One of the most striking findings of the study is the steady and significant increase in agricultural areas. Covering 25.33% of the region in 2015, agricultural lands expanded to 31.82% by 2024, corresponding to a net increase of approximately 1,600 hectares. The sharpest growth occurred between 2015 and 2018, during which the share of agricultural land rose to 34.27%. This trend may reflect the influence of socio-economic

policies or favorable economic conditions that promoted agricultural production during that period.

- **Decline in Natural Areas**
  Parallel to the expansion of agricultural land, the region's dominant land cover type—natural areas—exhibited a decreasing trend. The notable 4.5% decline observed between 2015 and 2018 suggests that much of the new agricultural land was converted from natural steppe and pasture ecosystems. This shift indicates increasing fragmentation pressure on the region's natural landscape integrity and habitats.
- **Fluctuations in Built-up Areas**
  Contrary to expectations for a region under urbanization pressure, the model results indicate a decline in built-up areas between 2015 and 2020, followed by a slight increase afterward. Rather than representing an actual structural shrinkage, this fluctuation may be attributed to the model's reclassification of low-density or undeveloped rural zones surrounding settlements as agricultural land, as previously noted.

4.Conclusion

This study aimed to quantitatively analyze land cover and land use (LCLU) changes in the Cappadocia region—a UNESCO World Heritage Site—between 2015 and 2024 using the Google Earth Engine (GEE) platform and machine learning techniques, and to identify the most suitable classification model for this process. The findings revealed both methodological and thematic insights of significant importance.

From a methodological perspective, the results demonstrated that among the four tested machine learning algorithms (Random Forest, CART, SVM, and Naive Bayes), the Random Forest (RF) model exhibited the highest performance, achieving an overall accuracy of 75.82% and a Kappa coefficient of 0.6327. This outcome confirms the methodological superiority and reliability of ensemble learning-based models, particularly for classifying spectrally complex and heterogeneous landscapes such as those found in Cappadocia. The comparison clearly illustrates the critical role of model selection in determining classification accuracy and, consequently, the reliability of subsequent spatial analyses.

The primary analytical finding of the study is that the temporal analysis performed using the optimal RF model quantitatively revealed a significant expansion of agricultural areas at the expense of natural landscapes over the ten-year study period. The proportion of agricultural land increased from 25.3% in 2015 to 31.8% in 2024, with the most rapid change occurring between 2015 and 2018. These results quantitatively highlight the growing anthropogenic pressure on Cappadocia's unique natural and cultural landscape, providing an essential scientific basis for regional land management policies, agricultural planning, and sustainable conservation strategies.

The main limitation of this study lies in the 30-meter spatial resolution of the Landsat data used. This resolution may lead to spectral mixing and misclassification in highly heterogeneous and fragmented landscapes, particularly in rural settlement zones. Future research should focus on incorporating higher spatial and temporal resolution imagery—such as Sentinel-2 data (10 m

resolution)—to enhance classification accuracy, especially for complex land cover classes. Furthermore, integrating socio-economic driving factors (e.g., agricultural incentives, tourism investments, population dynamics) into the analysis would allow a more comprehensive understanding of human–environment interactions in the region.

In conclusion, this research not only provides up-to-date and valuable insights into land use trends in the Cappadocia region but also demonstrates that modern cloud-based platforms such as GEE, combined with comparative machine learning approaches, offer a powerful, efficient, and replicable methodological framework for monitoring and managing valuable heritage landscapes.

References

[1] Rawat, J. S. ve Kumar, M. (2015). Monitoring land use/cover change using remote sensing and GIS techniques: A case study of Hawalbagh block, district Almora, Uttarakhand, India. *The Egyptian Journal of Remote Sensing and Space Science, 18*(1), 77-84.

[2] Butt, A., Shabbir, R., Ahmad, S. S. ve Aziz, N. (2015). Land 7 use change mapping and analysis using Remote Sensing and GIS: A case study of Simly watershed, Islamabad, Pakistan. *The Egyptian Journal of Remote Sensing and Space Science, 18*(2), 251-259.

[3] Wulder, M. A., Masek, J. G., Cohen, W. B., Loveland, T. R. ve Woodcock, C. E. (2012). Opening the archive: How free data has enabled remote sensing science. *Remote Sensing of Environment, 122*, 2-10.

[4] Gorelick, N., Hancher, M., Dixon, M., Ilyushchenko, S., Thau, D. ve Moore, R. (2017). Google Earth Engine: Planetary-scale geospatial analysis for everyone. *Remote Sensing of Environment, 202*, 18-27.

[5] Phiri, D. ve Morgenroth, J. (2017). Developments in Landsat Land Cover Classification Methods: A Review. *Remote Sensing, 9*(9), 967.

[6] Akan, Z. ve Arici, Y. (2013). Tourism and its effects on the land use in a tourism-driven town: a case study of Goreme. *DetURO - The Journal of the Department of Urban and Regional Planning, 5*(2).

[7] Breiman, L. (2001). Random Forests. *Machine Learning, 45*(1), 5-32.

[8] Breiman, L., Friedman, J. H., Olshen, R. A. ve Stone, C. J. (1984). *Classification and Regression Trees*. Wadsworth & Brooks/Cole Advanced Books & Software.

[9] Cortes, C. ve Vapnik, V. (1995). Support-vector networks. *Machine Learning, 20*(3), 273-297.

[10] Rish, I. (2001). An empirical study of the naive Bayes classifier. *IJCAI 2001 Workshop on Empirical Methods in Artificial Intelligence, 3*(22), 41-46.

IMPROVING THE PERFORMANCE OF OBJECT DETECTION MODEL WITH REAL-TIME EXTRACTION ON JETSON AGX

Rıdvan Safa HATİPOĞLU[a*], Muhammet Doğukan KUYUMCU[a], Mevlüt BAŞARAN[b], Murat CEYLAN[c]

[a] *Aselsan Konya Co. Inc., Konya, Türkiye*

[b] *Kapsül Technology Platform, EngineHub, Konya, Türkiye*

[c] *Faculty of Engineering and Natural Sciences, Department of Electrical and Electronics Engineering, Konya Technical University, Konya, Türkiye*

ABSTRACT

Nowadays, technological advances have led to significant increases in the processing capacity of edge devices, and it is becoming increasingly important to run AI-based object detection algorithms on such hardware. In this context, using the Jetson AGX Orin platform developed by NVIDIA, this study evaluates various optimizations to improve the performance of convolutional neural network (CNN) based object detection models. In particular, the preprocessing and postprocessing steps required for the model to make decisions during object detection were converted to ONNX and TensorRT formats and tested in different working formats. In these analyses based on the YOLOv9-c and YOLOv11-m models, these steps were run on both CPU and GPU and the performance metrics obtained are presented comparatively. As a result of the tests, an extraction speed of 88.45 FPS was obtained for the YOLOv9-c model when the preprocessing and postprocessing layers were run in TensorRT format, while this value reached 108.32 FPS for the YOLOv11-m model. When the preprocessing and postprocessing layers of the same models were run with CPU-based ONNX, 26.28 and 27.64 FPS values were achieved, respectively. Accordingly, TensorRT optimization results in a performance improvement of approximately 236.5% for the YOLOv9-c model and 291.8% for the YOLOv11-m model. These results show that optimizing the pre- and post-processing layers and converting them to TensorRT format offers a significant advantage for real-time object detection applications in embedded systems.

KEYWORDS

- Edge Device
- Object Detection
- Real-Time Image Processing

[*] Corresponding author: Rıdvan Safa HATİPOĞLU
E-mail: rshatipoglu@aselsankonya.com.tr

1. Introduction

When examining current technological advancements, the increase in processing capabilities of hardware and the optimization of power consumption have enabled the deployment of computer vision applications on edge devices. Consequently, fundamental tasks such as object detection, classification, and localization can now be performed directly on these devices.

Edge devices are characterized by limited resources, including energy consumption, computational power, and memory capacity. These constraints are critical for machine learning and image processing algorithms that demand high computational efficiency. Real-time and energy-efficient detection of objects within images on edge devices has become feasible through the implementation of AI-based object detection models. Such models are specifically designed and optimized to align with the architectural and performance characteristics of edge hardware. In this context, the present study aims to optimize and deploy state-of-the-art object detection models on the NVIDIA Jetson Orin AGX edge platform to achieve high-speed, real-time inference performance.

2. Related Works

When examining recent advancements in edge computing hardware, Nikouei et al. introduced a lightweight version of the SSD model, termed Lightweight Convolutional Neural Network (L-CNN), for real-time object detection applications. The proposed model operated on a Raspberry Pi 3 development board at an average of 1.79 FPS, with a maximum of 2.06 FPS achieved during inference [1].

In the study conducted by Kang and Somtham, the performance of various edge devices was comparatively analyzed. Performance benchmarks were carried out using Jetson Nano, Xavier NX, and Google Coral Dev Board platforms. For the Jetson Nano, the FPS/Watt value was reported as 8.13 for the YOLOv4-Tiny object detection model, and 7.92 for the SSD MobileNet V2 model [2].

In 2022, Jiang et al. proposed a framework called Remix for high-resolution object detection on edge devices. Remix allocates different amounts of computational resources to different regions of an image, thereby maximizing overall performance and improving detection accuracy. The method achieved up to a 120% improvement in detection accuracy and an 8.1-fold increase in detection speed [3].

In another study, Jiang et al. selected the Jetson TX2 as the target edge platform and proposed a method based on the YOLOv4 model, termed YOLOv4-Dense. This approach reduced the number of model parameters from 162 million to 20.3 million, while the inference speed increased from 3.1 FPS to 22.6 FPS [4].

Implementing object detection on edge devices such as Raspberry Pi and NVIDIA Jetson boards presents significant challenges due to limited resources. Key limitations include power consumption, GPU performance and capacity, CPU core count and frequency, and the restricted RAM size available on these devices [5].

Li and Ye developed an edge application using the Rockchip 3588 processor, modifying the YOLOv5m architecture for improved performance on thermal imagery. The optimized model, named Edge-YOLO, achieved 0.75 mAP at 80 FPS [6].

You et al. proposed the TIP-YOLO model for pedestrian detection in thermal camera images, achieving 0.85 mAP with an inference speed of 70 FPS [7].

In a recent study by Hatipoğlu and Ceylan, multiple edge platforms — including Jetson Nano, Jetson NX, Jetson Orin Nano, Jetson Orin NX, and Rockchip 3588 — were evaluated using YOLOX, YOLOv8, Gold-YOLO, and YOLOv10 models. Performance comparisons incorporated both power consumption and FPS to derive an efficiency metric termed RSH-AY. Among the tested combinations, the YOLOv8–Jetson Orin Nano pair demonstrated the highest efficiency [8].

3. Methods

In this study, investigations were conducted on optimizing contemporary object detection models to achieve high-speed inference on the NVIDIA Jetson Orin AGX edge device. As object detection models, YOLOv11-m and YOLOv9-c, both trained on the COCO dataset, were employed. The YOLOv11-m model comprises approximately 20.1 million parameters, whereas YOLOv9-c contains around 25.3 million parameters.

3.1. Object Detection Models

Among real-time object detection frameworks, the YOLO (You Only Look Once) model family remains one of the most widely used and continuously evolving architectures. The YOLO machine learning model is a deep learning algorithm developed using Convolutional Neural Networks (CNNs) [9].

YOLOv9 introduces the concept of Programmable Gradient Information (PGI) to address the information bottleneck problem observed in deep networks. Through this approach, auxiliary reversible structures are employed to compensate for lost information in the network flow, thereby ensuring a more stable gradient propagation. Additionally, the architecture integrates the Generalized Efficient Layer Aggregation Network (GELAN), which generalizes the ELAN architecture by incorporating various computational blocks, thereby enhancing parameter efficiency, particularly in lightweight models [10].

YOLOv9 provides multiple variants — v9-S, v9-M, v9-C, and v9-E — differentiated by parameter size and computational demand, all optimized to maintain high accuracy even in compact configurations [11]. Experiments conducted on the COCO dataset have demonstrated that YOLOv9 achieves superior efficiency in terms of parameter utilization, computational cost, and detection accuracy compared to earlier versions [10]. In practical applications, YOLOv9 has been further improved through the integration of attention mechanisms, multi-scale dilated attention, and deformable kernels [12]. Furthermore, fine-tuned YOLOv9 models are increasingly utilized in large-scale infrastructure and industrial monitoring projects [13].

YOLOv11, one of the latest iterations developed by Ultralytics, incorporates several architectural enhancements, including C3k2, SPPF (Spatial Pyramid Pooling – Fast), and C2PSA (Parallel Spatial Attention) modules. These components significantly improve the detection of small objects and enhance multi-scale feature extraction efficiency [14]. The model is available in multiple configurations — Nano (n), Small (s), Medium (m), Large (l), and X-Large (xl) — making it adaptable for both embedded edge devices and high-performance computing servers [15].

Beyond object detection, YOLOv11 supports a wide range of tasks, including segmentation, pose estimation, image classification, and oriented bounding box (OBB) detection [16]. Benchmark evaluations have shown that YOLOv11 achieves higher mean Average Precision (mAP) and faster inference speeds than previous versions, even with fewer parameters [17]. These characteristics position YOLOv11 as a leading architecture for real-time computer vision applications.

3.2. Object Detection Pipeline

Object detection models take an input image and generate an output containing the bounding box coordinates of the detected objects along with their corresponding class labels. This process is executed through a sequence of computational stages, typically organized as Preprocess, Inference (Model), and Postprocess.

a. Preprocess

YOLO The deep learning architectures of the YOLO family are designed to accept input data in specific dimensions and formats to preserve network learning consistency and ensure compatibility with convolutional operations. Consequently, these models typically utilize a fixed input size structured as a four-dimensional tensor: [B, C, H, W], where B represents the batch size, C denotes the number of channels, H the height, and W the width. This configuration is crucial for maintaining consistent kernel sliding across deep convolutional layers and preventing dimensional mismatches during the mathematical operations on activation maps [9]. If the input data is presented in a different arrangement (e.g., [B, H, W, C]), channel–spatial axis inconsistencies may occur during convolution operations, potentially leading to computational errors or meaningless outputs [18]. Therefore, the preprocessing (Preprocess) stage is implemented to bridge the gap between the model's input format requirements and the raw image data. The preprocess step typically consists of three main components: resizing, normalization, and channel order transformation.

- Resizing: The input image is scaled to match the resolution expected by the model (e.g., 640×640 pixels). This process optimizes the network's ability to learn spatial features and prevents geometric distortions that may arise from varying image resolutions [19].
- Normalization: Pixel values, generally ranging from 0–255, are converted to a normalized scale (0–1 or –1–1). This normalization stabilizes weight updates during training and mitigates issues such as gradient explosion, ensuring smoother convergence [20].
- Channel Order Transformation: Deep learning frameworks (e.g., PyTorch, TensorFlow) often differ in their expected channel arrangements. While PyTorch models typically expect input in the [C, H, W] format, image processing libraries such as OpenCV provide data in [H, W, C] format. Consequently, the preprocess stage includes conversion to the appropriate channel ordering for the model [21]

In YOLO models, the preprocess stage is not limited to format conversion; it also serves as a crucial step in data standardization. This ensures that the model can generate consistent and reliable outputs across images from various sources, resolutions, color profiles, or camera types. Hence, the preprocessing process directly influences the model's generalization ability and output consistency [22].

b. Inference

Object detection models generally consist of three fundamental components: Backbone, Neck, and Head [23]. The Backbone is responsible for extracting hierarchical features from the input image, ranging from low-level to high-level representations, and typically employs CNN-based architectures such as ResNet or CSPDarknet for this purpose [24]. The Neck module fuses multi-scale features to generate richer and more robust representations; commonly used structures in this stage include the Feature Pyramid Network (FPN) and Path Aggregation Network (PANet) [25,26]. The final component, the Head, predicts both class scores and bounding box coordinates for the detected objects. In YOLO-like architectures, this prediction process is single-stage (dense prediction), whereas in models such as Faster R-CNN, it is performed in two stages [27].

The coordinated operation of these three components determines the model's overall performance in terms of both accuracy and inference speed. Notably, the YOLO family has achieved significant advancements in real-time object detection by optimizing the interaction and efficiency of these architectural elements [28].

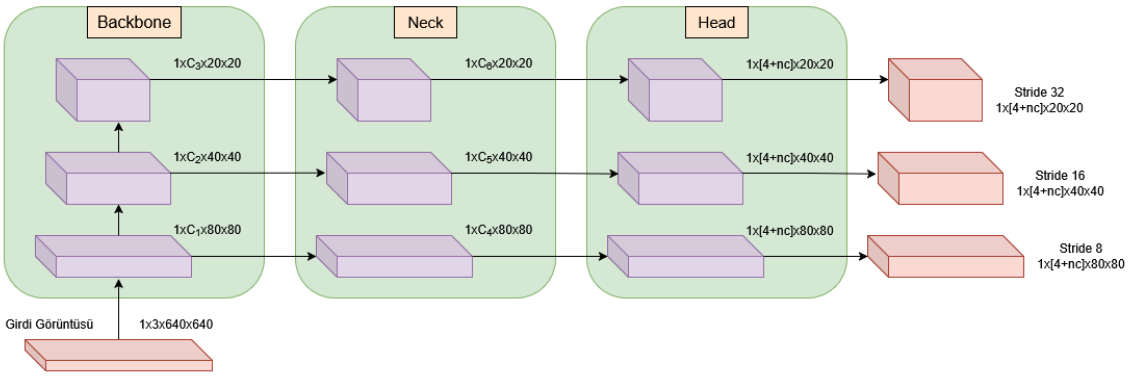

Fig. 1. Schematic block diagram representing the inference process

Figure 1 illustrates the flow between the stages of the inference process. Feature maps extracted from different depths of the Backbone, each with distinct resolutions, are transferred to the Neck. The Neck processes each incoming feature map through convolutional layers that preserve spatial resolution while enriching the semantic relationships among features. As a result, the feature maps with enhanced contextual representation are passed to the Head. The Head then generates pixel-level bounding box coordinates and class scores for object detection.

c. Postprocess

After the inference stage, the model produces feature representations of the input image at multiple spatial scales. Figure 2 presents grid representations of the input image at 40×40, 20×20, and 10×10 resolutions. These grids enable the model to detect objects of varying sizes

across different scales. The stride value defines how many pixels each grid cell corresponds to in the original image.

Each cell predicts the Left, Top, Right, and Bottom (LTRB) offsets of the bounding box relative to its position, along with the class scores for the detected object. In YOLO models, grid resolutions of 80×80, 40×40, and 20×20 are commonly employed. Consequently, the model performs approximately 8,400 predictions in total — 6,400, 1,600, and 400 from each feature map, respectively.

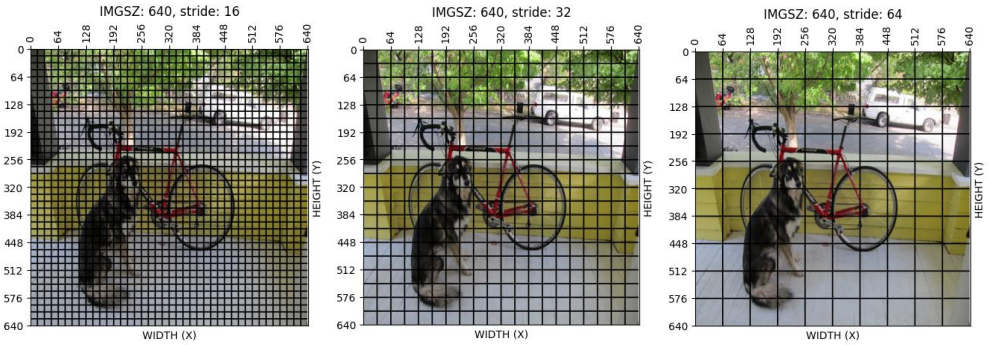

Fig. 2. Schematic representation of the input image using 40×40, 20×20, and 10×10 grid cells, respectively

At this stage, overlapping bounding boxes corresponding to the same detected object are filtered out. The elimination process consists of two main steps: Coordinate Transformation and Non-Maximum Suppression (NMS).

During Coordinate Transformation, the LTRB (Left, Top, Right, Bottom) offsets predicted for each grid cell are converted into XYXY (Xmin, Ymin, Xmax, Ymax) coordinates by incorporating the center position of each cell. This transformation enables the bounding boxes to be properly processed by the Non-Maximum Suppression function (see Figure 3).

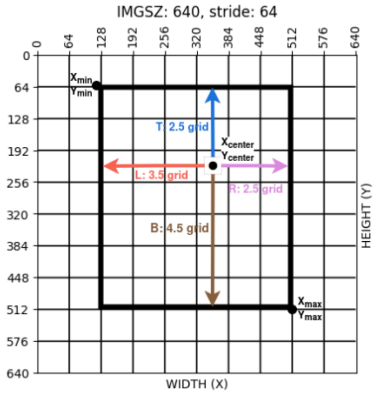

Fig. 3. LTRB-to-XYXY transformation

Non-Maximum Suppression (NMS) is applied because multiple grid cells within the feature maps may represent the same object, leading to redundant detections. In grid-based object detection models (e.g., YOLO, SSD, RetinaNet), this issue is mitigated by employing the NMS algorithm.

In this step, a predefined Intersection over Union (IoU) threshold is used. The IoU represents the ratio of the intersection area to the union area of two bounding boxes. When multiple bounding boxes overlap, only those with an IoU value below the specified threshold are retained, while boxes with higher IoU values (indicating redundancy) are suppressed or discarded.

4. Experiments And Results

This study was conducted on the NVIDIA Jetson AGX Orin, a platform distinguished by its high parallel processing capability. For object detection, the models YOLOv9-c and YOLOv11-m were selected, operating at computational costs of approximately 68 GFLOPs and 102.8 GFLOPs, respectively. The GPU unit was utilized for inference, as GPUs can parallelize operations and deliver faster computation compared to CPUs.

The models were evaluated under three different execution configurations:

- CPU (ONNX): In this configuration, functions are executed in the Open Neural Network Exchange (ONNX) format, and all computations are performed on the CPU. ONNX is a standardized format that contains the necessary information for visualizing deep learning models and executing their computational graphs [29].
- GPU (ONNX): This mode also employs the ONNX format, but the computations are executed on the GPU, leveraging its parallel processing capability for faster inference.
- GPU (TRT): In this configuration, the model functions are converted into the TensorRT format, utilizing kernel fusion, reduced-precision computation (FP16/INT8), and layer-level optimizations. TensorRT, developed by NVIDIA, is a high-performance deep learning inference optimization and runtime platform that maximizes performance in real-time applications by optimizing neural networks on GPUs for speed, memory efficiency, and low latency [30].

These three configurations were tested in various combinations across both preprocessing and postprocessing stages to analyze the performance impact of CPU, GPU, and TensorRT under different workloads.

Through TensorRT optimization, computationally intensive operations are effectively shortened by generating a hardware-specific optimized execution graph, resulting in significantly faster inference. Because of the high computational cost of this optimization process, it is applied only to the core model itself, excluding the preprocessing and postprocessing stages.

By implementing the preprocessing and postprocessing steps within the model using PyTorch and ONNX implementations, and by executing the model in three modes — GPU (TRT) (TensorRT-optimized GPU inference), GPU (ONNX) (non-optimized GPU inference), and CPU (ONNX) (CPU-only inference) — a total of nine experimental scenarios were evaluated for both YOLOv11-m and YOLOv9-c models

For each scenario, the total latency and frames per second (FPS) were measured and recorded on the NVIDIA Jetson AGX Orin (64 GB) platform.

Table 1. Performance and model comparison table

Preprocess Unit	*Model Unit*	*Postprocess Unit*	*YOLOv9-c (FPS)*	*YOLOv11-m (FPS)*
CPU (ONNX)	GPU (TRT)	CPU (ONNX)	**26.28**	**27.64**
CPU (ONNX)	GPU (TRT)	GPU (ONNX)	**20.52**	**20.51**
CPU (ONNX)	GPU (TRT)	GPU (TRT)	**25.56**	**26.92**
GPU (ONNX)	GPU (TRT)	CPU (ONNX)	**56.72**	**62.64**
GPU (ONNX)	GPU (TRT)	GPU (ONNX)	**35.42**	**38.13**
GPU (ONNX)	GPU (TRT)	GPU (TRT)	**58.02**	**64.68**
GPU (TRT)	GPU (TRT)	CPU (ONNX)	**86.14**	**101.72**
GPU (TRT)	GPU (TRT)	GPU (ONNX)	**45.14**	**48.47**
GPU (TRT)	GPU (TRT)	GPU (TRT)	**88.45**	**108.32**

In the tests where the Preprocess stage was executed on the CPU (ONNX), as shown in Table 1, both YOLOv9-c and YOLOv11-m exhibited parallel performance trends. Since the preprocessing unit operated entirely on the CPU, a significant pipeline bottleneck occurred at the initial stage. Even though the model itself ran at high speed on the GPU (TRT), the overall FPS values remained low due to this limitation.

For YOLOv9-c, the combination of Preprocess (CPU ONNX) + Model (GPU TRT) + Postprocess (CPU ONNX) yielded 26.28 FPS. When the Postprocess was moved to GPU (ONNX), performance dropped sharply to 20.52 FPS, primarily due to the inefficiency and lack of kernel optimization in the ONNX-based GPU postprocessing. However, when postprocessing was executed on GPU (TRT), performance improved again, reaching 25.56 FPS. Thus, for YOLOv9-c, the least efficient configuration was with GPU (ONNX) postprocessing, while CPU (ONNX) and GPU (TRT) postprocess modes produced relatively similar and balanced results.

A similar pattern was observed for YOLOv11-m. Under the Preprocess (CPU ONNX) + Model (GPU TRT) + Postprocess (CPU ONNX) configuration, the model achieved 27.64 FPS, slightly higher than YOLOv9-c. When Postprocess was executed on GPU (ONNX), FPS dropped substantially to 20.51, eliminating the benefits of GPU–TRT acceleration. When switched to GPU (TRT), performance recovered, reaching 26.92 FPS.

Both models demonstrated consistent behavior under identical hardware conditions: GPU (ONNX) postprocessing caused a considerable performance degradation, whereas CPU (ONNX) and GPU (TRT) postprocessing provided more stable results. Although YOLOv11-m outperformed YOLOv9-c by roughly 1–1.5 FPS across all combinations, this difference remained limited due to the CPU-bound preprocessing and postprocessing stages. The observed slowdown is attributed to the Non-Maximum Suppression (NMS) operations within the postprocessing phase, which depend more on memory access and parallel indexing efficiency rather than pure computational throughput. Additionally, during GPU (ONNX) postprocessing,

model outputs had to be copied from GPU memory to CPU memory and then back to GPU, further reducing FPS.

In tests where Preprocess was executed on the GPU (ONNX), the Model ran on GPU (TRT) while the Postprocess stage was distributed across different hardware configurations. This setup highlighted the benefits of GPU-based preprocessing acceleration and particularly the influence of the postprocessing stage on final inference performance

For YOLOv9-c, when Postprocess ran on CPU (ONNX), the FPS reached 56.72, a significant improvement compared to CPU-preprocess scenarios due to GPU acceleration. However, moving Postprocess to GPU (ONNX) caused a drastic FPS drop to 35.42, confirming the inefficiency of ONNX Runtime's GPU-based postprocessing implementation. Conversely, Postprocess (GPU TRT) achieved the highest value, 58.02 FPS, making it the optimal setup for YOLOv9-c.

A comparable trend was observed for YOLOv11-m. When Postprocess was on CPU (ONNX), FPS reached 62.64; on GPU (ONNX), performance dropped to 38.13; and on GPU (TRT), FPS increased to 64.68. YOLOv11-m consistently outperformed YOLOv9-c under all configurations, with an average advantage of 6 FPS in CPU and GPU (TRT) postprocess setups. However, under GPU (ONNX) postprocess conditions, both models suffered severe performance degradation, and YOLOv11-m's lead was reduced to only 2–3 FPS.

When Preprocess was executed on the GPU (TRT), with postprocessing distributed across different hardware units, the results revealed the full advantages of end-to-end GPU acceleration, emphasizing the postprocessing stage as the key determinant of final FPS.

For YOLOv9-c, with Postprocess (CPU ONNX), FPS reached 86.14, indicating that although CPU-based postprocessing introduced a slight bottleneck, GPU (TRT) acceleration maintained high overall performance. When Postprocess (GPU ONNX) was used, FPS sharply dropped to 45.14, once again confirming ONNX Runtime's inefficiency in GPU-based postprocessing. With Postprocess (GPU TRT), FPS peaked at 88.45, marking the best performance configuration. Therefore, the optimal setup for YOLOv9-c involved running all three stages—Preprocess, Model, and Postprocess—on GPU (TRT).

A similar pattern was found in YOLOv11-m. With Postprocess (CPU ONNX), the model achieved 101.72 FPS; with GPU (ONNX), FPS dropped to 48.47; and with GPU (TRT), the highest value of 108.32 FPS was recorded. These findings demonstrate that YOLOv11-m maintained high performance even with CPU-based postprocessing, but experienced significant slowdowns under GPU (ONNX) postprocessing. The maximum performance was attained with GPU (TRT) postprocessing, where the model achieved 108 FPS.

In summary, YOLOv11-m consistently outperformed YOLOv9-c across all configurations. The FPS advantage was approximately 15 FPS in CPU (ONNX) postprocess scenarios, 3 FPS in GPU (ONNX) postprocess cases, and over 20 FPS in GPU (TRT) configurations. These results indicate that YOLOv11-m is better optimized for GPU–TRT execution, demonstrating a clear performance superiority in a fully GPU-accelerated inference pipeline.

5. Conclusion And Future Work

Under CPU-based ONNX conditions, both models exhibited comparable performance, with the FPS difference remaining within the 2–6% range. This suggests that the bottleneck in CPU execution primarily stems from hardware limitations and the ONNX runtime environment, rather than the model architecture itself. However, as the level of GPU acceleration increased, the performance advantage of YOLOv11-m became more evident. In particular, under the fully GPU (TRT) pipeline, YOLOv11-m achieved approximately 22% higher FPS compared to YOLOv9-c. This difference is of critical importance for applications requiring high computational throughput, such as high-resolution video streams and multi-camera systems.

Furthermore, in scenarios where both models were tested with the same preprocessing method, CPU (ONNX) and GPU (TRT) postprocessing results were found to be similar, whereas GPU (ONNX) consistently underperformed. In the final evaluation, the YOLOv11-m model running on a fully TensorRT-optimized pipeline achieved the highest inference speed of 108.32 FPS.

In the continuation of this research, it is planned to comprehensively evaluate the inference performance of the TensorRT-optimized Preprocess–Model–Postprocess pipeline on embedded systems with limited computational capacity, such as Jetson Orin Nano and Jetson Orin NX. This evaluation will analyze the impact of various optimization strategies—including layer fusion, half-precision (FP16), and integer (INT8) inference—on execution time, energy efficiency, and memory utilization.

Additionally, investigating the performance characteristics of the YOLOv10 architecture—which operates independently of the traditional Non-Maximum Suppression (NMS) algorithm—will constitute another key extension of this study. This comparison aims to reveal the inference speed improvements, detection accuracy, and latency behavior of architectures that are less dependent on NMS, thereby assessing their suitability for next-generation hardware

Moreover, based on the findings obtained, the study aims to identify optimal distributed computation strategies among different hardware–software configurations, such as TensorRT, ONNX Runtime, and hybrid PyTorch–TensorRT environments. Defining the most efficient model pipeline for real-time object detection on low-power embedded systems will guide future system optimization and deployment efforts in this research domain.

References

[1] Nikouei, S. Y., Chen, Y., Song, S., Xu, R., Choi, B.-Y., & Faughnan, T. R. (2018). Real-Time Human Detection as an Edge Service Enabled by a Lightweight CNN. 2018 IEEE International Conference on Edge Computing (EDGE). doi:10.1109/edge.2018.00025

[2] Kang P, Somtham A. An Evaluation of Modern Accelerator-Based Edge Devices for Object Detection Applications. Mathematics. 2022; 10(22):4299. https://doi.org/10.3390/math10224299

[3] Jiang, S., Lin, Z., Li, Y., Shu, Y. , Liu, L., 2022, Flexible High-resolution Object Detection on Edge Devices with Tunable Latency ,ACM MobiCom '21, January 31-February 4, 2022, New Orleans, LA, USA

[4] Jiang, Y., Li, W., Zhang, J., Li,F., Wu Z., 2022, YOLOv4-dense: A smaller and faster YOLOv4 for real-time edge-device based object detection in traffic scene, IET Image ProcessingVolume 17, Issue 2 p. 570-580

[5] Subedi, P., Hao, J., Kim, I. K., and Ramaswamy, L., ''AI multi-tenancy on edge: Concurrent deep learning model executions and dynamic model placements on edge devices,'' in Proc. IEEE 14th Int. Conf. Cloud Comput. (CLOUD), Chicago, IL, USA, Sep. 2021, pp. 31–42, doi: 10.1109/CLOUD53861.2021.00016.

[6] Li, J.; Ye, J. Edge-YOLO: Lightweight Infrared Object Detection Method Deployed on Edge Devices. Appl. Sci. 2023, 13, 4402. https://doi.org/10.3390/ app13074402

[7] You, S.; Ji, Y.; Liu, S.; Mei, C.; Yao, X.; Feng, Y. A Thermal Infrared Pedestrian-Detection Method for Edge Computing Devices. Sensors 2022, 22, 6710. https:// doi.org/10.3390/s22176710

[8] Hatipoğlu, R. S. (2025). Hassas Güdümlü Ateşli Silahların Grup Halinde Kullanımlarında Taktiksel Etkinliklerinin Artırılması.

[9] Redmon, J., Divvala, S., Girshick, R., & Farhadi, A. (2016). You Only Look Once: Unified, Real-Time Object Detection. 2016 IEEE Conference on Computer Vision and Pattern Recognition (CVPR). doi:10.1109/cvpr.2016.91

[10] Wang, C.-Y., Yeh, I.-H., & Liao, H.-Y. M. (2024). YOLOv9: Learning What You Want to Learn Using Programmable Gradient Information. arXiv. https://arxiv.org/abs/2402.13616

[11] Ultralytics. (2024). YOLOv9 models documentation. Retrieved from https://docs.ultralytics.com/models/yolov9/

[12] Huang, G., Huang, Y., Li, H. et al. An Improved YOLOv9 and Its Applications for Detecting Flexible Circuit Boards Connectors. Int J Comput Intell Syst 17, 261 (2024). https://doi.org/10.1007/s44196-024-00669-4

[13] Fahim, S. A. (2024). Finetuning YOLOv9 for Vehicle Detection: Deep Learning for Intelligent Transportation Systems in Dhaka, Bangladesh. arXiv. https://arxiv.org/abs/2410.08230

[14] Lin, H., Zhang, Y., & Li, P. (2024). An improved YOLOv11 architecture with multi-scale attention and spatial fusion. SSRN. https://doi.org/10.2139/ssrn.5263718

[15] Ultralytics. (2024). YOLO11 models documentation. Retrieved from https://docs.ultralytics.com/models/yolo11/

[16] Buildings. (2024). Research and application of YOLOv11-based object segmentation in intelligent recognition at construction sites. Buildings, 14(12), 3777. https://doi.org/10.3390/buildings14123777

[17] Zhao, R., Chen, L., & Wu, Q. (2024). YOLOv11 for vehicle detection: Advancements, performance, and applications in intelligent transportation systems. arXiv. https://arxiv.org/abs/2410.22898

[18] Goodfellow, I., Bengio, Y., & Courville, A. (2016). Deep Learning. MIT Press.

[19] Bochkovskiy, A., Wang, C. Y., & Liao, H. Y. M. (2020). YOLOv4: Optimal Speed and Accuracy of Object Detection. arXiv:2004.10934

[20] Ioffe, S., & Szegedy, C. (2015). Batch Normalization: Accelerating Deep Network Training by Reducing Internal Covariate Shift. Proceedings of the 32nd International Conference on Machine Learning (ICML), 448–456.

[21] Paszke, A., et al. (2019). PyTorch: An Imperative Style, High-Performance Deep Learning Library. Advances in Neural Information Processing Systems (NeurIPS), 8026–8037.

[22] Jocher, G., Chaurasia, A., Qiu, J., & Stoken, A. (2023). YOLOv8: Next-Generation Real-Time Object Detector. Ultralytics Documentation.

[23] Bochkovskiy, A., Wang, C. Y., & Liao, H. Y. M. (2020). YOLOv4: Optimal speed and accuracy of object detection. arXiv. https://arxiv.org/abs/2004.10934

[24] Redmon, J., & Farhadi, A. (2018). YOLOv3: An incremental improvement. arXiv. https://arxiv.org/abs/1804.02767

[25] Lin, T. Y., Dollár, P., Girshick, R., He, K., Hariharan, B., & Belongie, S. (2017). Feature pyramid networks for object detection. Proceedings of the IEEE Conference on Computer Vision and Pattern Recognition (CVPR), 2117–2125. https://doi.org/10.1109/CVPR.2017.106

[26] Liu, S., Qi, L., Qin, H., Shi, J., & Jia, J. (2018). Path aggregation network for instance segmentation. Proceedings of the IEEE Conference on Computer Vision and Pattern Recognition (CVPR), 8759–8768. https://doi.org/10.1109/CVPR.2018.00913

[27] Ren, S., He, K., Girshick, R., & Sun, J. (2015). Faster R-CNN: Towards real-time object detection with region proposal networks. Advances in Neural Information Processing Systems (NeurIPS), 28. https://arxiv.org/abs/1506.01497

[28] Jocher, G., Chaurasia, A., Stoken, A., Borovec, J., NanoCode012, Kwon, Y., … & Ultralytics. (2022). YOLOv5 by Ultralytics. Zenodo. https://doi.org/10.5281/zenodo.3908559

[29] Bai, J., Lu, F., Zhang, K., & ONNX Community. (2019). ONNX: Open Neural Network Exchange. GitHub Repository. https://github.com/onnx/onnx

[30] NVIDIA Corporation. (2021). TensorRT: High-Performance Deep Learning Inference Optimizer and Runtime. NVIDIA Technical Report TR-2021-001. Santa Clara, CA: NVIDIA.

April 16, 2024 Investigating The Dynamics of The Moderate Geomagnetic Storm

Sercan BULBUL[a*], Fuat BASCIFTCI[b] and Burhaneddin BILGEN[c]

[a]*Department of Geomatic Engineering, Faculty of Engineering and Natural Sciences, Konya Technical University, Türkiye*

[b]*Map and Cadastre Programme, Vocational School of Technical Sciences, Karamanoglu Mehmetbey University, Türkiye*

[c]*Academy of Land Registry and Cadastre, Ankara Hacı Bayram Veli University, Türkiye*

A B S T R A C T

This study investigates the dynamics of the moderate geomagnetic storm that occurred on April 16, 2024. Magnetic storms are formed when high-energy particles from the Sun interact with the Earth's magnetosphere. These storms were evaluated using geomagnetic indices such as Dst, Ap, Bz_GSE, Bz_GSM and F10.7. The analysis showed that during the storm, the Dst index decreased to -65 nT, the Bz component reached -84 nT, the Ap index increased to 56, and the F10.7 index remained stable at 200.2. According to the correlation analysis, there is a strong negative correlation between Ap and Dst (r = -0.72), a negative correlation between Bz and Ap (r = -0.64) and a positive correlation between Bz and Dst (r = 0.47). The results reveal that the main determinants of magnetic storms are a decrease in Bz to negative values, an increase in Ap and sudden drops in Dst. Modeling with artificial neural networks provided highly accurate predictions for the Dst and Ap indices. The study emphasizes the importance of using more advanced machine learning models in future space weather forecasts.

K E Y W O R D S

- Artificial Neural Network
- Geomagnetic Storm
- Solar Wind Parameters
- Zonal Geomagnetic Indexes

1. Introduction

Magnetic storms are large magnetic disturbances caused by high-energy particles from the Sun interacting with the Earth's magnetic field. These storms are often associated with events such as coronal mass ejections (CMEs) and solar flares [1-2]. When particles emitted from the Sun are directed towards the Earth's magnetic field, they cause the magnetic field to change abnormally. This causes auroras (aurora borealis), especially in the polar regions [3]. But the impact of magnetic storms is not only visual; powerful storms can severely affect satellite

systems, communication networks, navigation systems and power grids [4]. In addition, the high energy density in the upper layers of the atmosphere can disrupt electrical systems, leading to major economic and security problems [2].

Magnetic storms are often monitored by measurements of geomagnetic activity, such as the Kp index. The Kp value is a parameter that indicates how much the Earth's magnetic field is disturbed and the severity of a storm. Other indicators, such as the Dst index and the Ap index, also provide information on the extent and impact of magnetic storms [1,5]. The severity of magnetic storms varies in parallel with the cycle of solar activity, with the peak of the solar cycle increasing the likelihood of more and more severe magnetic storms [6]. For this reason, scientists are constantly conducting research to understand the relationship between solar activity and magnetic storms, and strive to develop technology and forecasting systems to minimize the impact of these events [7].

2. Geomagnetic Storm Indices

2.1. Bz_GSE (Geocentric Solar Ecliptic Coordinate System)

Bz_GSE is a parameter used to measure the north-south component in the Earth's magnetic field and is expressed in the Geocentric Solar Ecliptic (GSE) coordinate system. The GSE coordinate system is a reference frame set from the center of the Earth parallel to the ecliptic plane of the Sun [8]. Bz_GSE is used to understand whether solar winds interact with the Earth's magnetic field to trigger geomagnetic storms. The Bz component reflects the magnetic field direction of the solar wind, revealing north-south effects. Negative values of Bz_GSE indicate an orientation that weakens the Earth's magnetic field and can trigger geomagnetic storms [1].

2.2.Bz_GSM (Geocentric Solar Magnetospheric Coordinate System)

Bz_GSM refers to the north-south component of the Earth's magnetic field in the Geocentric Solar Magnetospheric (GSM) coordinate system. The GSM coordinate system is used to study magnetic field interactions and space weather phenomena in more detail [9]. In this system, the Bz_GSM value indicates the component of the magnetic field on the Z axis and provides information about the influence of the solar wind on the Earth's magnetic field. Negative Bz_GSM values are directly related to the orientation and intensity of the solar wind and can signal the possible onset of geomagnetic storms. These values play a critical role in space weather forecasting and modeling of geomagnetic phenomena [2].

2.3.Dst Index (Disturbance Storm Time)

Dst stands for "Disturbance Storm Time" and is an index that measures the severity of geomagnetic storms. This index shows the impact of disturbances in the Earth's magnetic field, especially at low latitudes [10]. As the Dst index falls in the negative direction, the severity of geomagnetic storms increases, which can have serious impacts, especially on power grids and communication systems. When the value of Dst falls below -50 nT, it is generally considered that the Earth's magnetic field has been significantly disturbed and a strong geomagnetic storm is taking place [1]. Dst is an important parameter in space weather forecasting and protection of technological infrastructures [5].

2.4.F107 Index (Solar Flux at 10.7 cm)

F10.7 is an index that measures the intensity of radio waves from the Sun at a wavelength of 10.7 cm. This index is used to monitor the Sun's overall activity and in particular the effects of coronal holes or solar flares [11]. The F10.7 value is an indicator of the Sun's level of energy emission, and higher F10.7 values generally mean that the Sun is more active and therefore stronger solar winds can reach Earth. F10.7 is a critical parameter, especially for studying solar cycles and predicting the effects of solar activity. High F10.7 values provide important information for predicting space weather events [2].

2.5.Ap Index (Average planetary index)

Ap is an index that measures the overall activity in the Earth's magnetic field and is a kind of average of the Kp index. Ap averages the Kp index over a 24-hour period and this reflects the variation of geomagnetic activity over time [12]. Ap has a value ranging from 0 to 400; high values can herald large geomagnetic storms or high solar activity. The Ap index is used to determine the severity of geomagnetic events over a large geographical area and is often one of the key parameters included in space weather forecasts. High values of Ap indicate that space weather events can spread their effects over a wider area, which can affect technological infrastructures such as communication and navigation systems [7].

3. Artificial Neural Networks

Artificial neural networks (ANNs) have been used as an effective tool for analyzing geomagnetic data due to their ability to learn complex and non-linear relationships [13, 14]. In particular, one of the strengths of ANNs is to understand and predict the time evolution of geomagnetic parameters such as Bz_GSE, Bz_GSM, Dst, F107, and Ap. These parameters are critical for determining the effects of solar winds on the Earth's magnetic field and the severity of potential geomagnetic storms [1]. By learning the complex interactions between these parameters, ANNs can predict future space weather events. For example, a change in the negative values of the Bz components can be an indication that a storm is approaching, and such information can be accurately and quickly analyzed by ANNs to predict potential impacts [15].

In recent years, the combination of geomagnetic indices and artificial neural networks has been an important tool in improving the accuracy of space weather forecasts[16, 17]. Especially when indicators of solar activity such as the F107 value are combined with geomagnetic parameters such as Ap and Dst, ANNs can learn the relationships between these data and make more accurate forecasts [18,19]. This integration plays a major role not only in space weather forecasting, but also in predicting the effects of solar winds on Earth's electrical and communication infrastructures. Because ANNs have the capacity to process large data sets, they can more accurately model the potential impacts of geomagnetic storms over time, providing advance warnings to protect technological infrastructures [20].

4. Application

In this study, the dynamics of the moderate geomagnetic storm that occurred on April 16, 2024 was investigated by considering Ap, Dst, F10.7, Bz_GSE and Bz_GSM indices. To examine the April 16, 2024 storm, 2 days before and 2 days after the storm were taken (April 14-18, 2024). Changes of 5-day geomagnetic indices are shown in Fig 1.

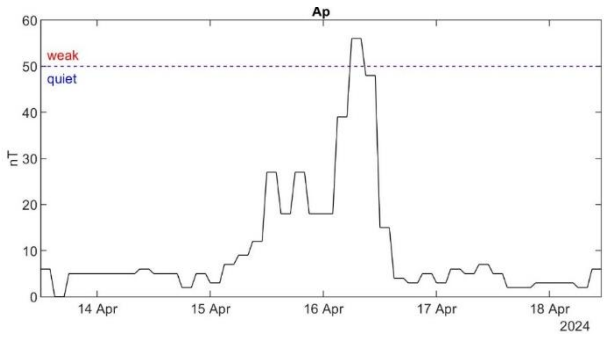

Fig 1. Temporal variation of Ap index

Fig 1 shows the change in the Ap index over time. It can be seen that the Ap index rises sharply in the selected date range and then falls back to low levels. The Ap index indicates interplanetary magnetic activity and high values indicate strong geomagnetic storms: Ap < 10 → Magnetic activity is low, 10 ≤ Ap < 30 → Moderate activity, Ap ≥ 30 → High magnetic activity (storm indicator).

As an indicator of geomagnetic activity, the Ap index reflects the interactions between the interplanetary magnetic field and the magnetosphere. When the data for April 2024 were analyzed, it was determined that the Ap index showed a significant increase between 15:00 and 23:00 on April 16, 2024. In this time period, the Ap index increased up to 56 levels.

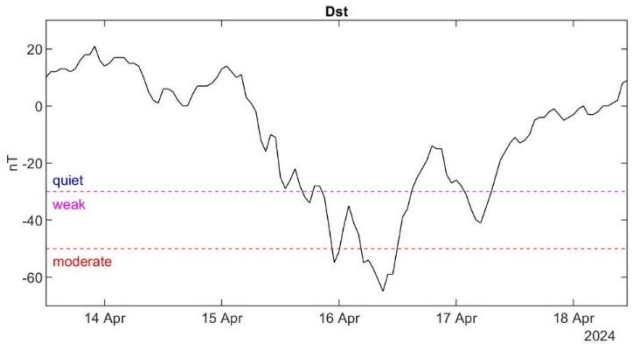

Fig 2. Temporal variation of Dst (nT) index

Fig 2 shows the change in the Dst index over time. When Dst falls below -50 nT, it is generally considered a geomagnetic storm. If the Dst value varies between -50 nT and -100 nT, it is considered a moderate storm, and if it falls below -100 nT, it is considered a severe storm. The Dst (Disturbance Storm Time) index is a critical parameter that determines the severity of geomagnetic storms. Negative Dst values reveal the impact of magnetic storms by showing the suppression and energy input in the magnetosphere. When the April 2024 data is analyzed, a significant decrease in the Dst index was observed between 11:00 and 23:00 on April 16, 2024.

In this time period, the Dst index decreased to -65 nT, indicating a moderate geomagnetic storm. If the Ap values show a positive increase and the Dst index a negative decrease, this could indicate a strong geomagnetic storm.

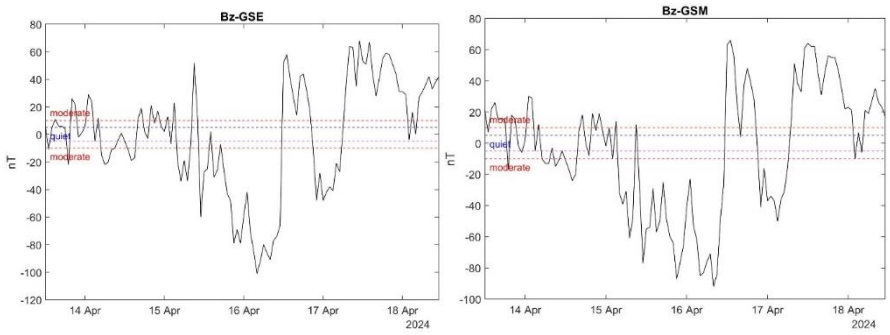

Fig 3. Variation of Bz (GSM/GSE) component over time

Fig 3 shows the variation of the Bz (GSM/GSE) component over time. A decrease in Bz to negative values increases the interaction between the magnetosphere and the solar wind and can increase geomagnetic activity. If Bz is negative (especially when it falls below -10 nT), magnetic reconnection increases and the risk of storms increases. If Bz is positive, the magnetosphere remains more stable and large storms are not expected.

The Bz component is a critical parameter that determines the interaction of the interplanetary magnetic field (IMF) with the magnetosphere. The difference between Bz_GSE (Bz component in GSE coordinate system) and Bz_GSM (Bz component in GSM coordinate system) is important for understanding the dynamic response of the magnetosphere. When the April 2024 data is analyzed, a significant negative deviation is observed in the Bz components starting from 11:00 on April 16, 2024. During this period Bz_GSE declined to -92 nT. Bz_GSM, on the other hand, decreased to lower levels with -101 nT.

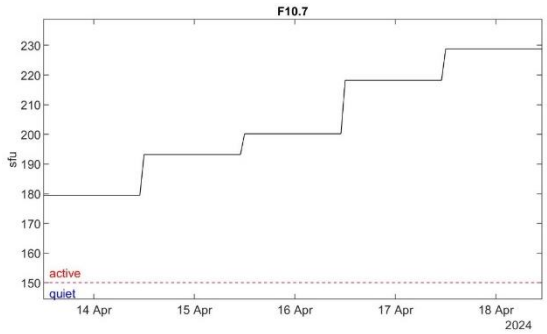

Fig 4. Temporal variation of F10.7 index

The F10.7 index is a parameter that measures the sun's radio flux at 10.7 cm wavelength and is an important indicator of solar activity. High F10.7 values indicate increased solar activity and the influence of solar winds on the magnetosphere. The F10.7 index is used as an important indicator of solar activity by measuring the sun's radio flux at 10.7 cm wavelength. High F10.7 values indicate increased solar activity and the potential for the magnetosphere to be affected by this activity. When the April 2024 data were analyzed, it was found that the F10.7 index

remained constant at 200.2 on April 16, 2024 (Fig 4). On April 16, 2024, the Ap index reached 56, indicating an increase in geomagnetic activity. The Dst index decreased to -65 nT, indicating a moderate geomagnetic storm. The Bz component decreased to negative values (-101 nT), indicating that the magnetosphere is heavily energized by solar winds. These findings confirm that geomagnetic activity also increases during periods of high levels of the F10.7 index. During periods of high solar radiation, the severity of geomagnetic storms and magnetic field disturbances increases.

Correlation analysis was performed to reveal the relationship between Bz, Dst, Ap and F10.7 indices during the storm.

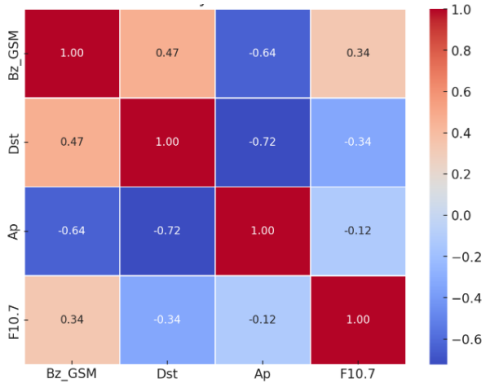

Fig 5. Correlation analysis

In Fig 5;

- Bz_GSM with Dst (+0.47): Moderate positive correlation. This means that when Bz value increases (is positive), Dst also increases. This leads to a decrease in storm intensity. This is expected because a negative Bz index triggers magnetic storms.

- Ap with Dst (-0.72): Strong negative correlation. In other words, as the Ap index increases, Dst decreases to more negative values. This shows that strong storms are associated with Ap.

- Bz_GSM with Ap (-0.64): Strong negative correlation. Negative Bz causes more interaction between the magnetosphere and the solar wind and increases the Ap index.

- F10.7 (Solar Activity) with other variables: There is a weak negative correlation between F10.7 and Dst (-0.33), but the relationship with Ap is quite low (-0.11). This suggests that the April 16, 2024 Moderate storm is largely driven by short-term magnetic interactions.

This analysis shows that Ap and Bz are the main determinants of storms and Dst decreases depending on these variables.

In the study, the April 16 Moderate Storm was modeled with the Artificial Neural Networks theorem using geomagnetic storm indices (Dst and ap).

The neural network prototypes employ a 5-day (120 hours) data set for the modeling of the Dst and ap zonal geomagnetic indices. In all our education models, 70% of the data for training (84

data), 15% of the data for validation (18 data), and 15% of the data for testing (18 data) are used.

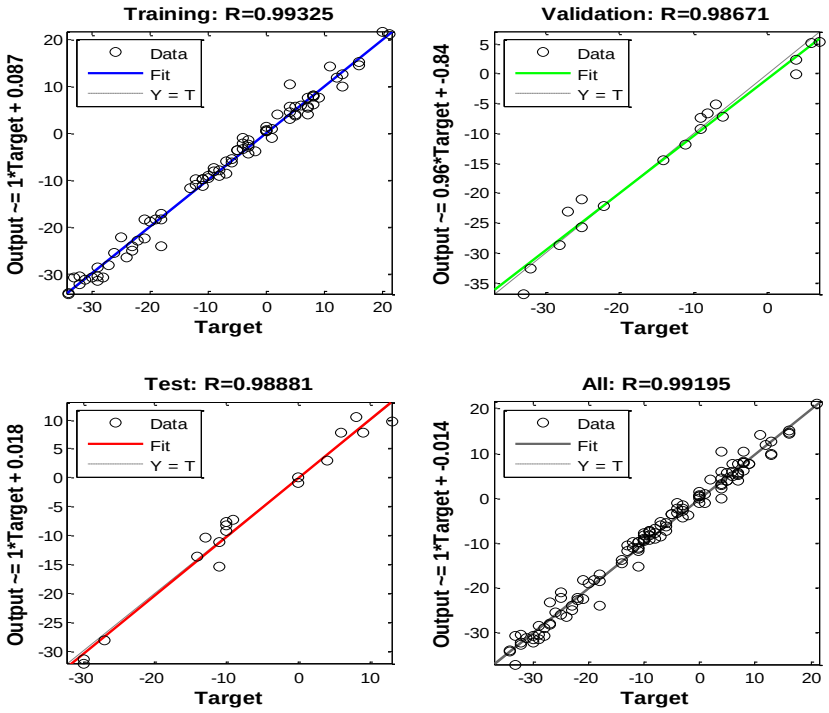

Fig 6. Correlation scores for the Dst modeling

Fig6 shows R correlation constants for the Dst index modeling. The procedure used for the Dst index modeling accomplishes a 99.20% correlation rate and 2.2847 nT MSE score after 53 epochs with the aid of *25* neurons.

Fig 7 exhibits the MSE rate and average R correlation score.

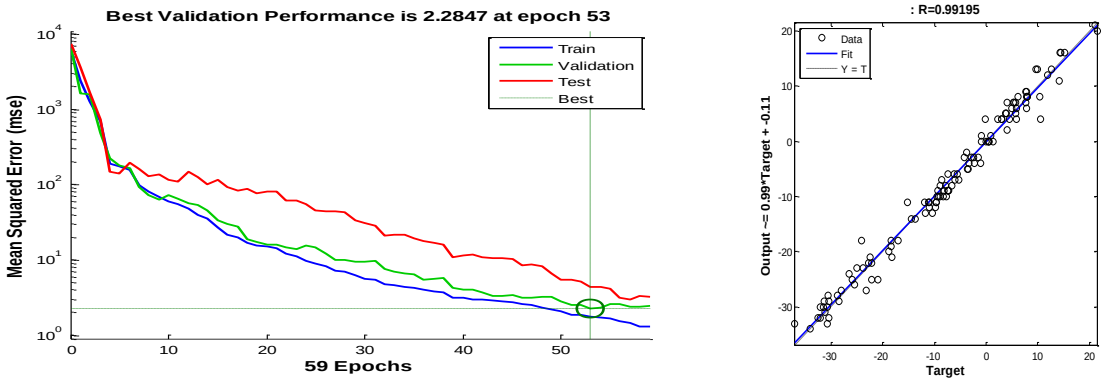

Fig 7. MSE rate and the model average correlation score for the Dst modeling.

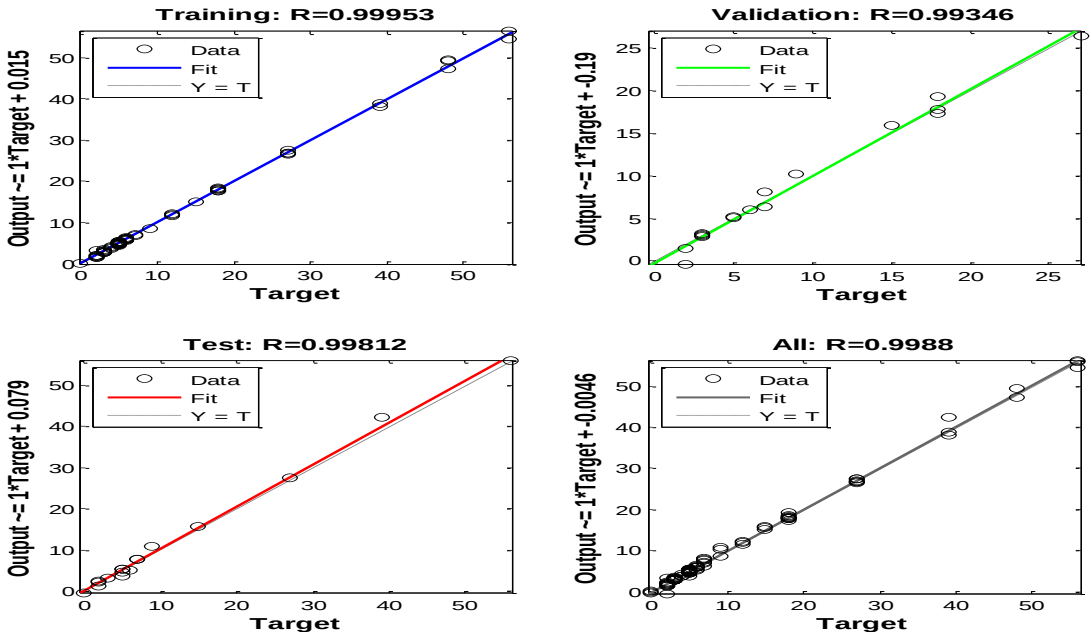

Fig 8. Correlation scores for the Ap modeling

Fig 8 shows R correlation constants for the ap zonal geomagnetic index modeling.

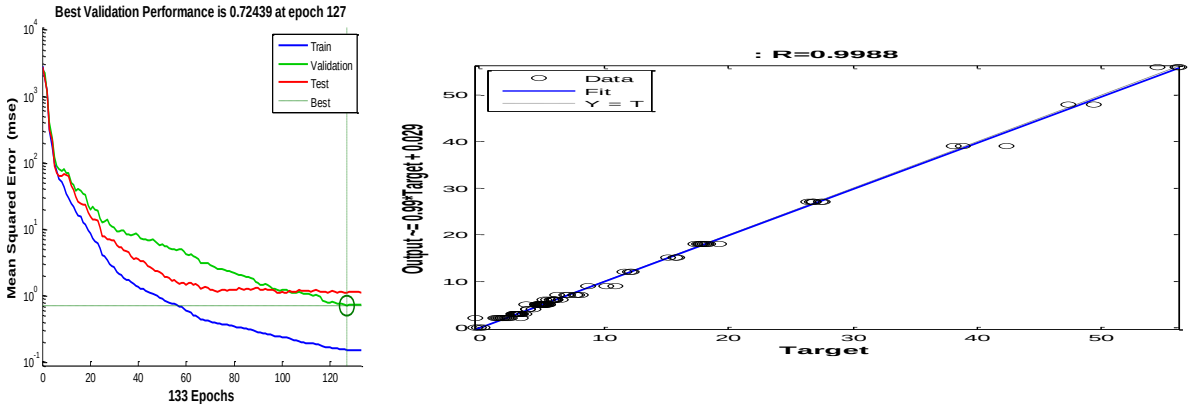

Fig 9. MSE rate and the model average correlation score for the ap modeling.

Fig. 9 exhibits the MSE rate and average R correlation score. The process used for the ap index modeling gains a 99.88% correlation rate and 0.72439 nT MSE score after 127 epochs with the aid of *25* neurons.

5. Conclusion

This study was carried out to investigate the dynamics of the moderate geomagnetic storm that occurred in April 2024. As a result of the analysis, the main determinants of the storm formation were determined by the decrease in the Bz component to negative values, the Ap index reaching high levels, the increase in the F10.7 index and the sudden decreases in the Dst index.

As a result of the data analysis, it was found that the Dst index decreased to -65 nT at 21:00 on April 16, 2024. At the same time, the Bz component reached -84 nT, the Ap index increased to

48 levels and the F10.7 index showed a strong increase, indicating an increase in the strength of the storm. The relationship between these variables was supported by correlation analysis.

According to the correlation analysis, the Bz component has a positive correlation with Dst (r=0.47), the Ap index has a negative correlation with Dst (r=-0.72), and the F10.7 index has a weak but significant negative correlation with Dst. These findings support the critical role of the interplanetary magnetic field, solar activity and interaction in the magnetosphere on the severity of geomagnetic storms.

This study reveals that monitoring variables such as Ap, Bz, F10.7 and Dst is critical to improve the predictability of geomagnetic storms. Future work could be directed towards making these predictions more accurate, especially with machine learning and advanced time series analysis.

References

[1]. Gonzalez, W. D., Joselyn, J. A., Kamide, Y., Kroehl, H. W., Rostoker, G., Tsurutani, B. T., & Vasyliunas, V. M. (1994). What is a geomagnetic storm? *Journal of Geophysical Research: Space Physics*, 99(A4), 5771–5792. https://doi.org/10.1029/93JA02867

[2]. Bothmer, V., & Daglis, I. A. (Eds.). (2007). *Space Weather: Physics and Effects. Springer*.

[3]. Kivelson, M. G., & Russell, C. T. (Eds.). (1995*). Introduction to Space Physic*s. Cambridge University Press.

[4]. Borovsky, J. E., & Denton, M. H. (2006). Differences between CME-driven storms and CIR-driven storms. *Journal of Geophysical Research: Space Physics*, 111(A7). https://doi.org/10.1029/2005JA011447

[5]. Kamide, Y., & Chian, A. C. L. (2007). *Magnetospheric Current Systems*. American Geophysical Union.

[6]. Richardson, I. G., & Cane, H. V. (2012). Near-Earth interplanetary coronal mass ejections during solar cycle 23 (1996–2009): Catalog and summary of properties. *Solar Physics*, 281, 187–222. https://doi.org/10.1007/s11207-012-9972-x

[7]. NOAA Space Weather Prediction Center (SWPC). (2025, August 01). Space Weather Scales and Indices. https://www.swpc.noaa.gov

[8]. Russell, C. T. (1971). Geophysical coordinate transformations. *Cosmic Electrodynamics*, 2, 184–196.

[9]. Hapgood, M. A. (1992). Space physics coordinate transformations: A user guide. *Planetary and Space Science*, 40(5), 711–717. https://doi.org/10.1016/0032-0633(92)90012-D

[10]. Sugiura, M. (1964). Hourly values of the equatorial Dst for the IGY. *Annals of the International Geophysical Year*, 35, 9–45.

[11]. Tapping, K. F. (2013). The 10.7 cm solar radio flux (F10.7). *Space Weather*, 11(7), 394–406. https://doi.org/10.1002/swe.20064

[12]. Mayaud, P. N. (1980). Derivation, Meaning, and Use of Geomagnetic Indices. *American Geophysical Union*.

[13]. Rumelhart, D. E., Hinton, G. E., & Williams, R. J. (1986). Learning representations by back-propagating errors. *Nature*, 323(6088), 533–536. https://doi.org/10.1038/323533a0

[14]. Haykin, S. (1999). *Neural Networks: A Comprehensive Foundation* (2nd ed.). Prentice Hall.

[15]. Lundstedt, H., Gleisner, H., & Wintoft, P. (2002). Operational forecasts of the geomagnetic Dst index. *Geophysical Research Letters*, 29(24), 34-1–34-4. https://doi.org/10.1029/2002GL016151

[16]. Pallocchia, G., Amata, E., Consolini, G., Bertello, I., & Marchetti, E. (2006). Geomagnetic Dst index forecast based on IMF data only. *Annales Geophysicae*, 24, 989–999. https://doi.org/10.5194/angeo-24-989-2006

[17]. Bala, R., & Reiff, P. H. (2012). Improvements in short-term forecasting of geomagnetic activity. *Space Weather*, 10(6). https://doi.org/10.1029/2012SW000779

[18]. Wu, J. G., & Lundstedt, H. (1997). Neural network modeling of solar wind–magnetosphere interaction. *Journal of Geophysical Research: Space Physics*, 102(A7), 14257–14266. https://doi.org/10.1029/97JA00996

[19]. Revallo, M., Valach, F., Hejda, P., & Bochníček, J. (2014). Artificial neural network-based nonlinear prediction of the geomagnetic activity. *Journal of Atmospheric and Solar-Terrestrial Physics*, 110–111, 9–15. https://doi.org/10.1016/j.jastp.2014.01.018

[20]. Gonzalez, W. D., Echer, E., Tsurutani, B. T., & Vieira, L. E. A. (2018). Interplanetary origin of intense, superintense and extreme geomagnetic storms. *Space Science Reviews*, 214, 5. https://doi.org/10.1007/s11214-017-0433-5

OPERATIONAL EFFECTS OF ATMOSPHERIC CONDITIONS ON THE HIGH VOLTAGE ELECTRICITY GRID IN COASTAL SETTLEMENTS

Pınar ATAK KAFA[a*], Emine İŞIN[b], Nurettin ÇETİNKAYA[c]

[a] *Electricity Program, Vocational School of Technical Sciences, Konya Technical University*

No:351, 42250, Selçuklu/KONYA TURKEY

[b-c] *Department of Electrical and Electronics Engineering, Faculty of Engineering, Konya Technical University,*

Rauf Orbay Cad. 42250, Selçuklu/KONYA TURKEY

Organization, Address: Büyükkayacık Mah. 101. Cad. 42250 Selçuklu/KONYA TURKEY

ABSTRACT

Electricity transmission lines are one of the most critical parts of the power grid. Power outages caused by high voltage power grid failures; It is important in terms of energy supply security, economic losses and social impacts.

In this study; the effects of atmospheric conditions on the high voltage electricity network in coastal settlements in terms of operation depend on the changing temperature; using the data of the main insulation limit in the conductors (corona discharge), and other High Voltage (HV) power grid fault situations in terms of humidity and dew point; classification study was carried out. The importance of predictive maintenance methods and the increasing role of weather data used in these methods are explained.

KEYWORDS

- Energy Efficiency
- Corona losses
- Leakage current
- High voltage isolator
- Superficial discharges
- Surface leakage currents

[*] Corresponding author:
E-mail: patak@ktun.edu.tr

1. Introduction

1.1 Effects of Meteorological Conditions on HV Electricity Network Fault Types and General Information

Today, the need for electrical energy is constantly increasing with industrialization and developing technology due to the increase in population. Thus, while human beings include new energy sources in the system in one way; They work to reduce the loss-leakage rates in the generation, transmission, distribution and facility systems of electrical energy and to minimize power outages.

The need to meet the increasing energy demand due to the difficulties in the immediate commissioning of New Energy sources has led field workers and researchers to work for the most efficient use of existing energy resources. Transmission, distribution and operation of electrical energy produced in existing electricity generation plants; It is known that it causes some problems.

The main problems of the HV/LV Electricity network are; leakage-losses of the network, short circuit problems caused by various reasons, old and inadequate infrastructure, maintenance and repair deficiencies, material quality, interruptions and malfunctions caused by various reasons, voltage fluctuations, reactive power problems, lack of digitalization, work accidents, etc. Considering all these problems, uninterrupted energy, that is, energy efficiency, should be ensured.

Energy losses; When describing technical losses and non-technical losses, the difference between the energy produced and the energy consumed defines this phenomenon. Electrical technical losses; Transformer and line losses are directly related to the current flowing from the network. Line losses; interconductor copper loss occurs from radiation, induction, dielectric losses. Transformer losses; core losses and copper losses caused by the inner windings of the transformer (1).

Technical losses; It consists of incorrect grounding operations, harmonic distortions, unbalanced, continuous overloading with long-distance single-phase lines belonging to the consumer, low voltage levels and the use of equipment with poor standards or substandard equipment (2). Non-technical losses; It consists of reasons such as incorrect meter reading, measurement errors, illegal line connection detected in electricity transmission and electricity distribution networks (1).

Metals or alloys cause corrosion, which is an electrochemical phenomenon, due to their unstable structure and tendency to return to the ore state in nature. Corrosion causes indirect costs due to damages such as material loss and environmental damage caused by transported materials, damages due to the failure of electricity transmission and distribution facilities, labor losses, etc. (3). One of the events that cause corrosion is atmospheric events.

Another situation affected by atmospheric events on electricity transmission and distribution networks is; It is an electrical jump event that is frequently encountered in isolators. The jumping phenomenon depends on environmental problems such as moisture in the air, ice on transmission lines and connection points, ice density, accumulated dirt, temperature of ice, etc.

Leakage currents, on the other hand, are directly related to the surface properties of ice-covered insulators, which are also caused by icing, which is an atmospheric phenomenon. By

measuring the leakage current, the icing status of the insulators and the jumps can be analyzed. Icing affects the electrical field on the insulator surface and causes partial discharges and electrical jumps due to loss of insulation feature (4).

In high voltage insulators, electrical jumping occurs as a result of the combination of moisture and dirt provided by the atmosphere. Pollutants accumulated on the insulator surface in dry air are dissolved by the humidification of the insulator surface as a result of atmospheric events, thus making the surface electrically conductive. The large arc current generated by electrical jumping can damage insulators and arc horns. If the tripping speeds of the breakers are slow and there are no protection rings in the insulator chain; The arc short-circuits the HV line with the ground and can cause voltage spikes in other phases, melting both the overhead and underground conductors of the power transmission line.

HV Insulators where electrical network overhead line connections are made, we see various types of natural pollution;

a) Desert Pollution: According to the results of chemical analysis, the majority of desert dirt consists of sulfate and chlorine, 18% soluble salt, 3% NaCl, 0.5% KCl, 10% CaSO4 mixture.
b) Industrial Pollution: It consists of the dirt layer formed in the insulators, harmful gases and fumes of the factories, chemical components and cement dust (5).
c) Marine Pollution: Wind causes evaporated seawater droplets to be carried to the insulator surface.

Salt water droplets with high electrical conductivity completely cover the insulator surface and the insulator surface is covered with a thin film as a result of drying within a few hours. Contamination; It depends on the direction of the wind blowing from the sea to the land, and still conditions supported by land-to-sea winds or sunlight cause drying on the insulator surface and a partial recovery of 8 to 12 hours (6).

In power transmission and energy distribution systems, superficial jumps of high voltage insulators contaminated as a result of atmospheric events;

1. As a result of the coating of the insulator surface with a conductive dirt film, ignition of pre-discharges can be seen in dry dirt areas due to the arc created by the heat energy released by the leakage currents flowing along the surface.
2. Pre-discharge ignition can be seen propagating along the dirty insulator surface (7), (8).

In the operating conditions of the jump voltage in electricity transmission networks; polarity of tension (9), particle size of the contaminant (10), (11) uneven wetting and moisture surface conductivity, length, distance, profile of the insulator, diameter (12), dirt layer thickness, etc.

Superficial contamination in insulators disrupts the distribution of space by allowing a capacitive-resistive leakage current to flow from the surface and causes frequent short circuit events in high voltage insulators, causing economic losses and unwanted power outages (13).

The thin, wet, conductive dirt film layer formed on the insulator surface due to fog, rain, dew, moisture and dust carried by winds, which are atmospheric phenomena, is one of the most important events to be considered in the operation and design of high voltage insulation devices against leakage current. The interruption of the aforementioned infiltration current creates dry bands that cause arcs on the surface. In addition, the arcs jump along the wet layer surface by extending instantaneously (14),(15).

The significant loss in electrical energy transmission lines is corona losses (16). In order to reduce the electrical losses that occur in the lines, the voltage level on the transmission lines is high; The current is desired to be low. However, it increases corona losses with excessive increase in voltage. Electrical energy losses caused by corona divorces are important for the design and design of transmission lines (17).

In the world, the transmission of energy with HV values in electricity networks is mostly carried out by overhead lines. In overhead lines, after a certain level of tension value; significant insulation problems are seen in lines and joints. Insulation process in energy transmission systems; The insulation between the line and the pole, between the line and the line and the ground is created by air. Compared to other gas types used during insulation, the small electric field strength that provides the puncture resistance of the air causes ionization around the conductors, which paves the way for electrical discharges. Thus, electrical discharges occur in the form of partial discharges as they cannot flow from the conductor to the ground and from one conductor to another conductor. Electrical partial discharges that do not fully occur but constantly feed themselves are called corona discharges (18).

Ionization occurs when electrical energy strikes the conductors of the electrical transmission line when the voltage between the concentric cylinders gradually increases (19). Although the necessary conditions for discharge are met at certain voltage values, no light is seen at the beginning (20). However, as the voltage level increases a little more, a crown-shaped layer of purple light begins to appear surrounding the conductors and a hissing sound is heard. This event is called the corona event and the voltage value of the discharge at this moment is called the corona initial voltage (19). After this voltage value, the line is self-feeding. An example Voltage-Current graph of corona discharge is given in Figure 1 (20).

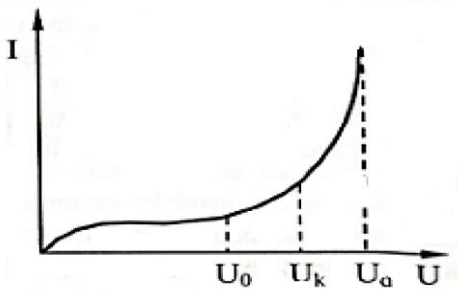

Figure 1. An example Voltage-Current graph of corona discharges

- Uo: The voltage at which ionization occurs by impact,
- Uk: Corona tension,
- Oud: Puncture Tension

refers to. According to the World Meteorological Organization's State of the Climate statement, the global average temperature in 2025 (January-March) is shown in Figure 2 to be 1.1 degrees higher than before the industrialization period. This situation in global warming, its effects on dew point, wind characteristics and air humidity, and the effect of HV overhead conductors on failures as a result of insulation failure due to Corona were examined.

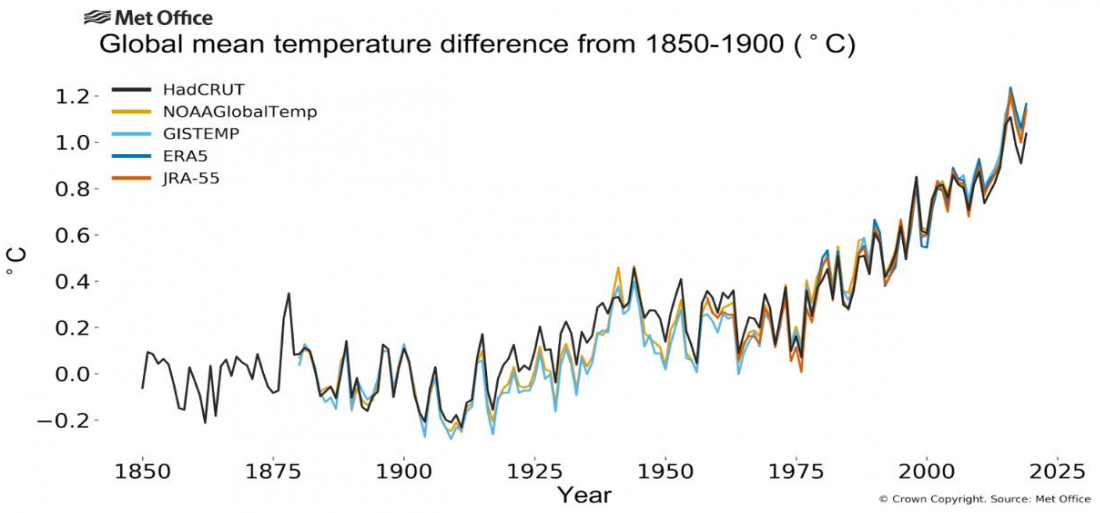

Figure 2 Global mean temperature curve in 2025 (January-March) (21)

In this study; The effects of atmospheric conditions on the high voltage electricity network in coastal settlements in terms of operation are due to changing temperature. It is aimed to compare the fault situations that occur as a result of exceeding the insulation limit (corona discharge) in the conductors in terms of humidity and dew point.

It is emphasized that electricity transmission lines are one of the most critical parts of the grid. Energy supply security, economic losses and social effects of interruptions caused by failures are explained. The importance of predictive maintenance methods and the increasing role of weather data in these methods are explained.

2. HV ELECTRICITY NETWORK FAILURE TYPES AND CAUSES IN METEOROLOGICAL CONDITIONS

Common types of faults in transmission lines; line breakage, isolator failures, pole overturning, overheating / loading, short circuit, electrical impulse currents that occur during power cut-off-on-maneuvering of step-down centers.

The relationship of these failures with meteorological conditions; pole collapse caused by excessive winds, contact with tree branches, conductor release. Thermal expansion caused by excessive temperature, conductor sagging. Excessive weight increase on masts and lines due to heavy snow/ice load. Direct damage or temporary failures caused by lightning. Caused by humidity and rain; insulation resistance decrease, spark splashes.

2.1. Meteorological Data Used

Parameters that can be used via MGM, NASA, OpenWeatherMap API as data sources; temperature, wind speed/direction, precipitation amount, humidity, snow thickness, sunshine duration, storm and lightning frequency.

2.2.Ar Iza Estimation Methods

2.2.1 Traditional Methods:

Statistical Modeling: While the methods used in this type of modeling vary according to the types and purpose of the variables used in the research; issues such as the outcome variable, the variables and variables that may have an effect on the variables, the signs and magnitudes of

their effects on the outcome variable, and how much of the explained and unexplained change in the outcome variable are explained can be investigated (22).

Regression Analysis: It is an analysis method used to measure the existence of a relationship between two or more measurable variables and the strength of the relationship between these variables. Analysis using a single variable is called univariate regression, and if more than one variable is used, it is called multivariate regression analysis (23).

Failure Frequency – Weather Correlation: Correlation, one of the statistical methods, describes the direction and strength of the relationship between two or more variables and helps to understand how one variable affects the other (24).

2.2.2. Artificial Intelligence Methods

- Artificial Neural Networks (ANNs)
- Decision Trees / Random Forest
- Support Vector Machines (SVM)
- LSTM and GRU Time Series Models

3. DATA REQUIRED FOR MODEL TRAINING

ANN (Artificial Neural Networks) makes it possible to solve problems that are impossible to solve with normal programming techniques. General features of ANN; It performs machine learning, stores information and can learn with examples, and can also produce information about unseen examples thanks to the information given in the training. ANN has an input and an output set. The information to be taught is given to the ANN to be trained by turning it into a vector. The system parameters are adjusted to produce the correct output.

Learning in ANN is done in 2 stages. In the first stage, the output values to be produced while training the system are given. The weights of the network's connections are changed according to the accuracy of the output value. After the training of the network is completed, the test data is presented to the system to measure the performance of the system. During the test phase, no changes are made to the weight values, the weights used in the training are used, and this produces outputs for the test data it does not encounter. The performance of the system is evaluated according to the accuracy values of the outputs obtained.

Input data: Hourly/Daily Weather Data for the years 2012-2025; felt temperature, humidity, visibility, pressure, dew point, daytime temperature, nighttime temperature, weather (sunny, showery, cloudy... etc.), wind data and fog information were used as input data (25), (26)

Output data: Fault type/fault (labeled data), MV (Medium Voltage) feeder trip, MV fuse blow, network maintenance work, MV isolator failure, contractor work, MV jumper failure, MV disconnector failure, MV terminal failure, TEİAŞ transformer failure, MV line tree cutting, MV conductor breakage, MV disconnector failure, MV transformer failure, network maintenance work, wild animal contact, HV maneuver, fire and damages caused by third parties constitute the output data (27).

The block of input-output data is shown in Figure 3.

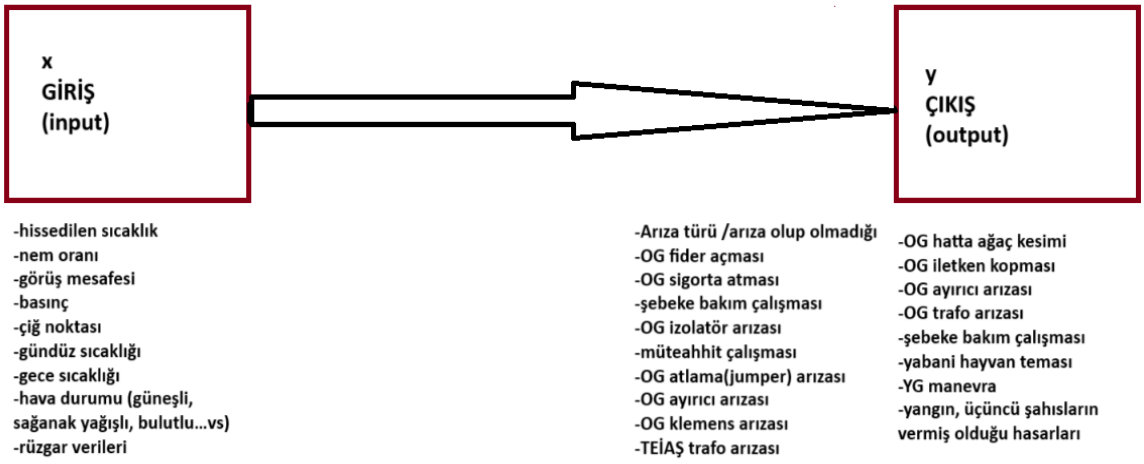

Figure 3 Block diagram with input-output data

4. SAMPLE APPLICATION AND PROGRAM RESULTS

- Model used (ANN)
- Training and test data rate
- Metrics such as accuracy, error rate
- Monthly/weekly forecast performance
- Potential for integration into decision support systems

4.1. Evaluate the performance of the model with classification using Confusion Matrix. At the same time, different quantitative values can be found by using the Confusion matrix and the success of the model can be evaluated in detail according to the operation performed (28).

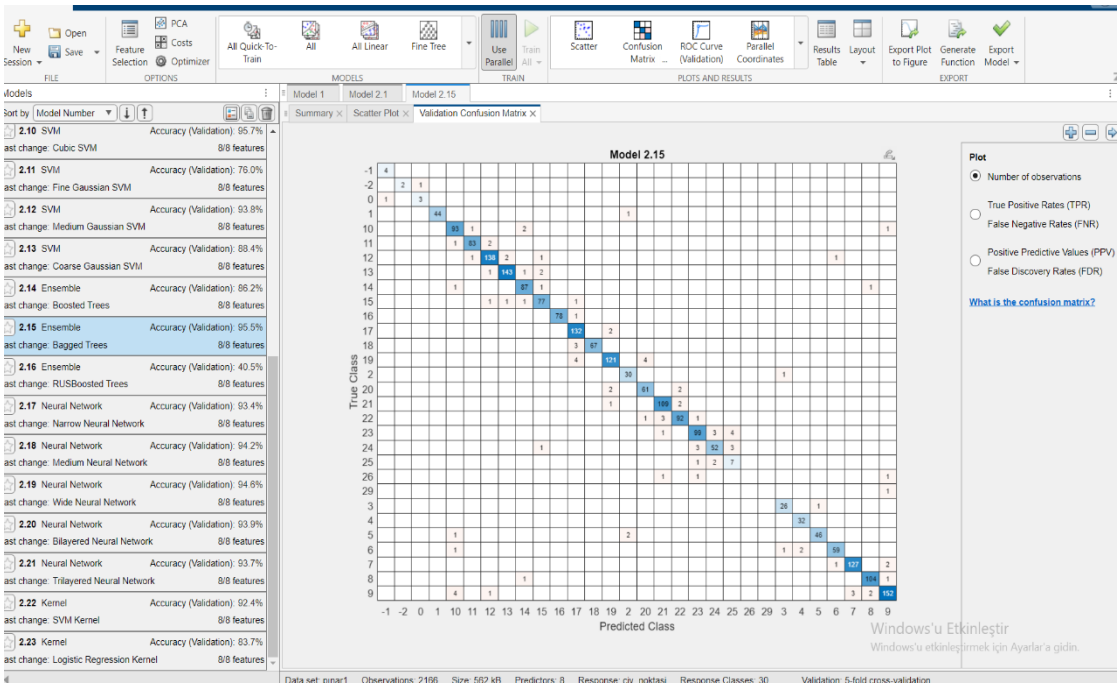

Figure 4. Classification model we made using Confusion Matrix

4.2. Scatter Plot: Scatter plot is used to determine the relationship between two different variables and to determine the relationship with the cause and to understand how strong the relationship is. One of the purposes of statistics is to organize and display data. Most of the time, a graph, chart, or table is used. When working with paired data, a useful type of graph is the scatter plot. This type of graph examines the distribution of points in the plane, allowing for easy and effective evaluation of the data used. Matched data; A scatter plot is a type of chart used for paired data. This is a type of dataset in which each of the data points has two numbers associated with it (29).

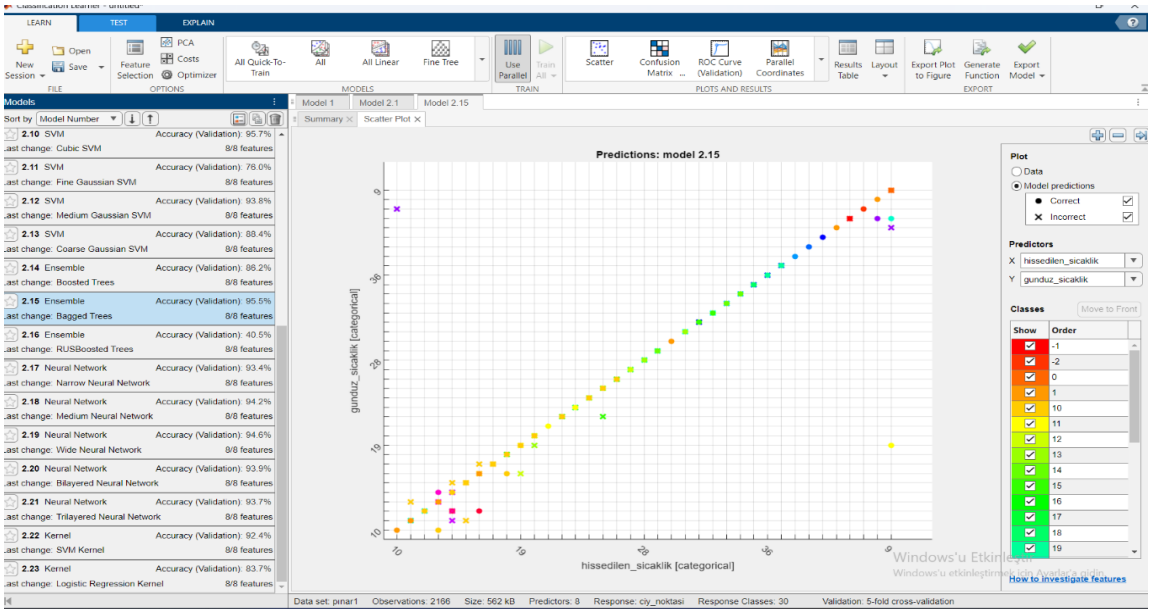

Figure 5. Scatter Plot: Classification model using Scatter Diagram

4.3. Parallel coordinates plot:

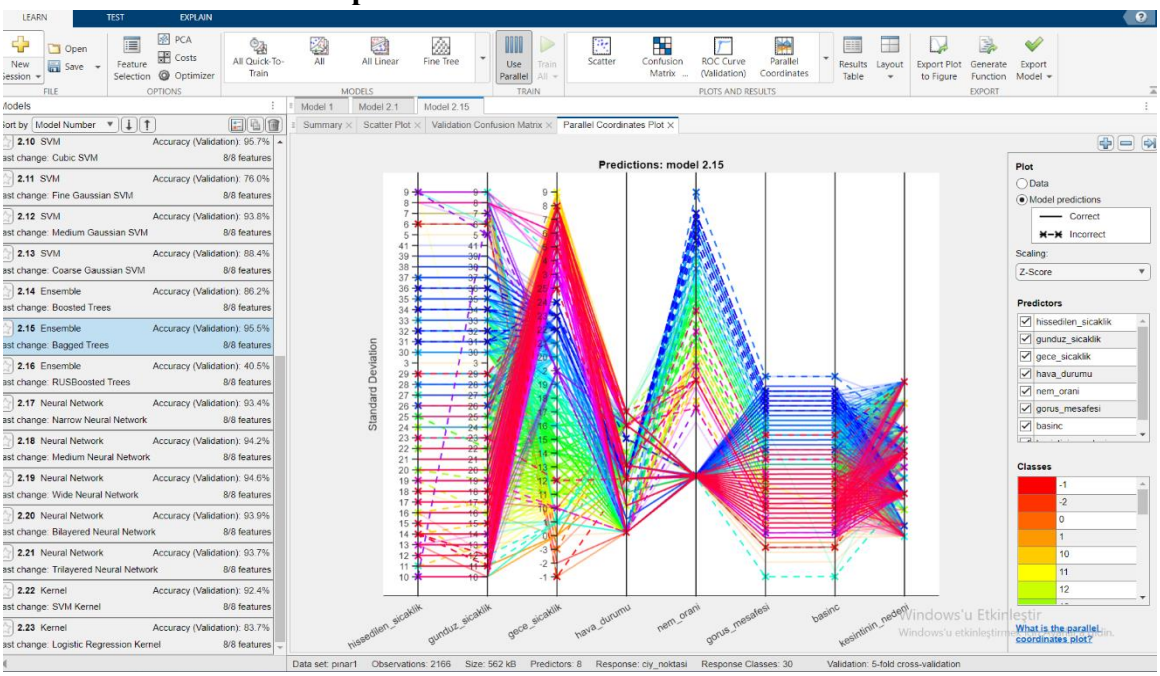

Figure 6. Classification model using parallel coordinates plot diagram

4.4. ROC Curve: is an important tool often used in the medical and data analysis fields. This curve is used to evaluate the performance of a classification model, visualizing the trade-off between the model's sensitivity and specificity. The ROC curve can be defined as a graph that shows the specificity and sensitivity values under different breakpoints. These values can be used to determine the performance of the classification model and are also used to adjust the accuracy rate of the model (30).

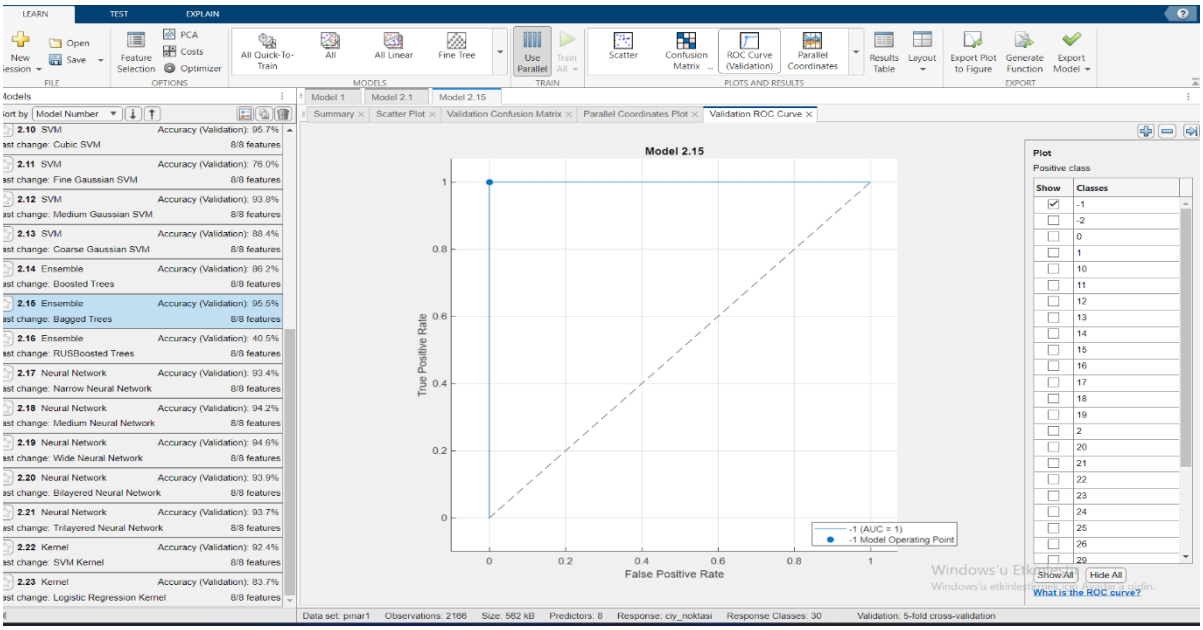

Figure 7. Classification model we made using the ROC curve diagram

Predictive maintenance operates on the premise of leveraging historical and real-time data from various operational aspects to anticipate potential issues. This multifaceted approach involves real-time monitoring of asset status and performance, analyzing work order data, and comparing MRO (Maintenance, Repair, and Operations) inventory usage. Predictive Maintenance, also known as predictive maintenance, has an important place among modern industrial applications and is used in the equipment maintenance approach. This proactive maintenance strategy leverages data analytics to predict operational anomalies and potential failures, allowing for timely interventions before failures occur (31).

5. CONCLUSIONS AND RECOMMENDATIONS

With this study, the effect of global warming on the climate, its effects on dew point, wind characteristics and air humidity over the years, and the increase in failures of HV overhead conductors as a result of insulation failure due to corona were estimated.

Study; By using machine learning and artificial intelligence methods, weather data is a powerful predictor of transmission line failures and is also seen to provide high accuracy in such predictive analysis.

In future application areas; real-time risk warning, planned maintenance resource saving, reducing downtime, increasing energy supply security, detection of risky areas in transmission

line designs, safer energy systems can be built with more holistic (weather + aging + maintenance data) models in the future.

In the light of this study; It can be further improved by organizing irregular data records, adding geographical differences (e.g. microclimate effect in mountainous regions), increasing the generalization capability of the model, and eliminating real-time application difficulties.

RESOURCES

[1] Davidson, E., Odubiyi, A., Kachienga, M. O. and Manhire. B., 2002. Technical Loss Computation and Economic Dispatch Model for T & D Systems in a Deregulated ESI." Power Engineering Journal, 16(2), 55–60.

[2] Navani, J. P., Sharma, N. K. and Sapra, S., 2012. Technical and Non-Technical Losses in Power System and Its Economic Consequence in Indian Economy, International Journal of Electronics and Computer Science Engineering, 1(2), 757–761

[3] Karataş*, Emre Levent Seyfi, Measurement of AC Interference Levels on the Natural Gas Pipeline in Afyon Region and Evaluation of AC Corrosion Possibility, MASTER'S THESIS Department of Electrical and Electronics Engineering May- 2019 KONYA

[4] ÖZKÜÇÜK* Muhammed Buğracan, Muhsin Tunay GENÇOĞLU, "Investigation of the Effect of Icing on Surface Leakage Currents in Isolators", Fırat University Eng. Bil. Research Article 35(2), 713-723, 2023

[5] Gouda, O.E., Influence of Pollution on H.V. Insulators, Conference Record of the 1990. IEEE International Symposium on Electrical Insulation, Toronto, Canada. 195-198, 1990.

[6] Gubanski, S.M., Vlastos, A.E., Wettability of Naturally Aged Silicone and EPDM Composite Insulators, IEEE Transaction on Power Delivery, 3: 1527-1535, 1990.

[7] Sundararajan R. and Gorur R.S., Dynamic arc modeling of pollution flashover of insulators under dc voltage, IEEE Transactions on Electrical Insulation, 28(2), 209-218, 1993

[8] Rumeli, A., Calculation of Fouling Jump Voltages of High Voltage Insulators, Tübitak Engineering Research Group, Project No: Mag-294, Ankara, 1973.

[9] Jolly D.C. and Poole C.D., Flashover of contaminated insulators with cylindrical symmetry under dc conditions, IEEE Trans. EI, 14 (2), 77-84, 1979.

[10] Rizk F., Mathematical models for pollution flashover, Electra 78:71-103, 1981.

[11] Astorga O.A.M. and Do Prado A.J., The flashover phenomenon:An analysis with influence of the thickness of the layer pollution of the high voltage polluted insulators, Conference Record of the 1994 IEEE Int. Symposium on Electrical Insulation, Pittsburgh, PA USA, 546-549, 1994

[12] Williams D.L., Haddad A., Rowlands A.R., Young H.M. and Waters R.T., Formation and characterization of dry bands in clean fog on polluted insulators, IEEE Transactions on Dielectrics and Electrical Insulation 6(5), October, 1999.

[13] Rumeli, A., Propagation of Discharges and Lapse on Dirty Isolated Surfaces, Electrical Engineering, 199:419427,1973.

[14] Dhahbi-Megriche, N., Beroual, A., Flashover Dynamic Model of Polluted Insulators Under AC Voltage, IEEE, Transactions on Dielectrics and Electrical Insulation, 7 (2): 283-289, 2000.

[15] Gençoğlu, M. T., M. Cebeci / Journal of Erciyes University Institute of Natural and Applied Sciences 22(1-2) 37-49 (2006)

[16] Kumar, A., 2013. Corona Effect on Transmission Lines, International Journal of Electrical and Electronics Engineering Research (IJEEER), 3(5), 133–136.

[17] Phan-Cong J. L., Pirotte P., Brunelle R., Trinh N.G., 1974. A Study of Corona Discharges at Water Drops over the Freezing Temperature Range, IEEE Transactions on Power Apparatus and System, 93(2), 727–734.

[18] Yıldırım H., 2003. Numerical Analysis of Electrical Discharges by Charge Simulation Method, PhD Thesis, Istanbul University Institute of Natural and Applied Sciences, 2-5.

[19] Peek, W.F., 1915. Dielectric Phenomena in High Voltage Engineering, First Edition, McGRAW-HILL BOOK COMPANY, Inc, London, 38

[20] Özkaya, M., 2008. High Voltage Technique 'static electric field and discharge phenomena' volume 1, Birsen Publishing House, 2008, 233-284.
[21] https://www.iklimhaber.org/yeni-rapor-2019-kaydedilen-en-sicak-ikinci-veya-ucuncu-yil-olarak-tarihe-gececek/ [Date of Visit: May 6, 2025]
[22] http://www.isum.yildiz.edu.tr/sayfa/H%C4%B0ZMETLER%C4%B0M%C4%B0Z/%C4%B0STAT%C4%B0ST%C4%B0KSEL-MODELLEME/63 [Date of Visit: May 6, 2025]
[23] https://tr.wikipedia.org/wiki/Regresyon_analizi [Date of Visit: May 6, 2025]
[24] https://www.getmidas.com/blog/korelasyon-nedir/ [Date of Visit: May 6, 2025]
[25] https://www.mgm.gov.tr/ [Date of Visit: May 6, 2025]
[26] https://tr.weatherspark.com/h/y/94264/2024/2024-y%C4%B1l%C4%B1-i%C3%A7in-Dat%C3%A7a-T%C3%BCrkiye-Tarihi-Hava-Durumu [Date of Visit: May 6, 2025]
[27] https://www.admelektrik.com.tr/bilgi-merkezi/yasal-bildirimler/hizmet-kalitesi-gostergeleri/tedarik-surekliligi-kalitesi-tablolari [Date of Visit: May 6, 2025]
[28] https://iremkomurcu.medium.com/confusion-matrix-nedir-ve-nedenkullan%C4%B1l%C4%B1r-cd686a7fc993 [Date of Visit: May 6, 2025]
[29] https://www.dayibilir.com/soru/38865/scatter-plot-ne-icin-kullanilir [Date of Visit: May 6, 2025]
[30] https://www.spss-yardimi.com/roc-curve-roc-egrisi-nedir [Date of Visit: May 6, 2025]
[31] https://sensemore.io/tr/kestirimci-bakim-nedir/ [Date of Visit: May 6, 2025]

PROJECT TEAM FORMATION PROBLEM: A GOAL PROGRAMMING APPROACH

Hakan ERDEŞ[a*], Ahmet PEKER[a], Kemal ALAYKIRAN[b]

[a] *Department of Industrial Engineering, Faculty of Engineering and Natural Sciences, Konya Technical University, 42280 Selçuklu/Konya, Turkey*

[b] *Department of Industrial Engineering, Faculty of Engineering, Necmettin Erbakan University, 42140 Meram/Konya, Turkey*

ABSTRACT

As project-based work continues to gain popularity in organizations for its ability to enhance teamwork, flexibility, and resource optimization, assigning individuals and tasks becomes more critical which is widely addressed in literature. This paper tackles a problem of assigning individuals—each characterized by multiple attributes such as skills, experience etc.— and tasks — each characterized by required skills and durations— to teams, while ensuring balanced teams and workload. We propose a Mixed-Integer Linear Programming (MILP) model, developed using the goal programming technique which includes three phases and, in each phase, one of the deviations (related to balancing) is minimized. In this way, the model can respond to varying priorities of organizations. To validate the effectiveness of our proposed model, computational experiments on problem instances of varying sizes, including up to 24-36 individuals and tasks are conducted—a scale commonly encountered in practice. Results demonstrate that our model can provide optimal or near-optimal solutions within a reasonable computational time. We also conduct experiments using single objective function (no priority defined). Results indicate that, compared to model with single objective function, our approach achieved better solutions in more than one-third of the experiments with respect to the prioritized components.

KEYWORDS

- Equitable Partitioning
- Goal Programming
- Project-Based Work
- Project Team
- Team Formation

[*] Corresponding author: Hakan ERDEŞ
E-mail: herdes@ktun.edu.tr

1. Introduction

Formation of a project team for a project-based work where individuals—each defined by a range of attributes such as skills, experience, qualifications etc.— and tasks —each with skill requirements and completion times— is a challenging problem (Rahmanniyay & Yu, 2019). We can define project-based work as a structure in which individuals and tasks are organized into specific projects, often carried out on a periodic basis and adopted by many organizations. This type of work involves individuals from a variety of backgrounds which places a strong emphasis on teamwork so that productivity, participation, creativity and commitment can be increased (Adams, 2003; van de Water et al., 2007). While individuals/workers have the opportunity to lead their own careers by being part of these works considering their skills, organizations have the opportunity to reduce the cost by employing certain workers for a certain period of time (Erdeş, 2021). Given all these benefits along with the significant impact of the pandemic on remote work, it is becoming increasingly clear that the future work model will inevitably be project-based, so, organizations are increasingly shifting from role-based to project-based work (Reuters, 2021; Forbes, 2021). However, there several key factors which are crucial for a successful implementation for this work model such as assigning individuals and tasks to the appropriate teams and ensuring workload balance (Forbes, 2021; Sankaran et al., 2020; Džamić et al., 2019). Given the growing importance of project team formation in project-based works, both its practical applications have expanded and the problems related to this topic, particularly the team formation problem, have been extensively studied in the operations research literature (Campêlo & Figueiredo, 2021; Çavdur et al., 2019).

In this study, we apply the Equitable Partitioning Problem (EPP) approach to form balanced teams, considering both individuals and tasks (O'brien & Mingers, 1997; Mingers & O'Brien, 1995). The EPP refers to the assignment of individuals who have certain skills to the teams in such a way that the resulting teams are as balanced as possible with respect to these skills. This approach contrasts with the standard classification problem (Mingers & O'Brien, 1995), where teams are formed based on grouping similar individuals. Beyond the assignment of individuals to teams, we extend the EPP approach to include the assignment of tasks to teams as well, aiming to achieve balance in task assignments. According to definition of the problem at hand, we have individuals with specific skills and experience, as well as tasks that have required skill levels and completion time. In this context, the aim is to create balanced teams in terms of both individuals and tasks for which reason, we consider three components in the balanced assignments as follows: (i) For each attribute (e.g. programming skill, foreign language skill etc.), the minimization of the total deviation between the total attribute scores of individuals in the teams and the average attribute score per team, (ii) For each team, the minimization of the total deviation between the total task duration and average task duration per team, (iii) For each attribute and team, the minimization of the total deviation between the average score of individuals and the average required skill levels. Additionally, we assign the most experienced individuals to different teams in order to maximize the benefits derived from their expertise (Mingers & O'Brien, 1995). Considering that organizations may prioritize different components, the three components addressed in this paper are treated as separate objective functions. To this end, a three-phase approach is employed. In the first phase, the first deviation is minimized and treated as a constraint in the second phase in which the second deviation is minimized. Finally, the result obtained in the second phase is treated as a constraint in the third

phase in which the third deviation is minimized. In accordance with this purpose, we formulated the problem as a Mixed Integer Linear Programming (MILP) model based on goal programming technique. In what follows, we list the scientific contributions of our study: (i) To the best of the authors' knowledge, individuals with skills and expertise, tasks with required skill levels and completion times and EPP approach are considered simultaneously for the first time, (ii) A mathematical model with three-phases is presented which is designed to address the varying needs and priorities of organizations operating in the project-based work sector, (iii) A comprehensive dataset specifically designed to address the problem at hand is generated.
The remainder of this paper is organized as follows. Section 2 reviews the studies regarding EPP approach as well as creating balanced teams. In section 3, we provide the definition of the problem at hand and present the MILP model. Experimental results of the problem are given in Section 4. Finally, Section 5 concludes the paper with a summary and future research directions.

2. Literature Review

There are several factors critical to the creation and successful execution of project-based work teams, including: skills of individuals, the capabilities of teams to effectively fulfill the assigned tasks and workload balance (Rahmanniyay & Yu, 2019; Li & Shan, 2010; Wei et al., 2013). Regarding these issues, Askin and Huang (2001) proposed a mixed-integer goal programming model for the team formation problem, considering individual-task compatibility with the objective of minimizing training costs. Baykasoglu et al. (2007) addressed the time and budget constraints in project team formation, proposing a fuzzy optimization model and a simulated annealing algorithm. Related to the Team Formation Problem, Fathian et al. (2017) studied the formation of teams with individuals having specific skills, while introducing a novel optimization model aimed at minimizing the probability of team members leaving the project. Rahmanniyay et al. (2019) addressed the project team formation problem by proposing a general and multi-objective stochastic model that simultaneously considers the competencies of team members and associated costs. Holmberg (2019) explored the team formation problem for student groups, which shares similarities with project team formation in terms of problem inputs, outputs, and solution approaches. Regarding students, Cavdur et al. (2019) proposed a two-stage approach based on goal programming for the student team formation problem in which assignment of students and academic advisors are conducted in the first and second stages, respectively. For a similar problem, Çavdur et al. (2020) developed a decision support system. Similarly, Tabansız et al. (2023) examined the student-project allocation problem in which students and projects are assigned to multiple teams using the goal programming as in this paper. In another similar approach, Daş et al. (2022) proposed a goal programming model based on multi-objective set partitioning for the team formation problem where they ensured that teams include individuals with required skills. There are also extensions of team formation problems, such as Multiple Team Formation Problem which is studied by Gutiérrez et al. (2016) where individuals, categorized based on specific skills, are assigned to teams and projects and they employed variable neighborhood search and local search algorithms to enhance the efficiency of multidisciplinary teams. Another extension, Quality Team Formation Problem was addressed by Huang et al. (2017) in which the maximization of the team score is considered by taking individual skills and working hours into account.

Regarding another crucial factor in project-based work teams, i.e., creating balanced teams, Desrosiers et al. (2005) employed a variable neighborhood search algorithm to create balanced team designs so that the teams provide good representation of the population, whereas van de Water and Bukman (2010) first defined team roles and then executed the team formation considering different role types for individuals. Rubin and Bai (2015) aimed to form teams which are as similar as possible in terms of both quantitative and qualitative characteristics, proposing a MILP model and developing a genetic algorithm. Similarly, Solow et al. (2020) introduced the Team Balancing Problem where groups are balanced across a variety of attributes and presented heuristic methods. Another crucial factor in the balanced formation of teams is the task assignment phase. Regarding this factor, Shen et al. (2003) considered the relationship among tasks, skill requirements for the relevant task, capabilities of the individuals and social relationships among the workers. Wei et al. (2013) proposed an approach to assess the imbalance between project teams prior to project initiation, thereby enhancing the likelihood of project success. Similarly, Hosseini and Akhavan (2017) focused on maximizing information sharing among individuals, minimizing project costs, and optimizing workload balance for project team selection, introducing a non-dominated sorting genetic algorithm II (NSGA-II) to achieve these objectives.

Although there are several studies focusing on the assignment of individuals to project teams based on skills and task allocation to ensure workload balance, the problem addressed in this study is unique in that it simultaneously incorporates three key elements: assigning individuals to teams based on their skills and experiences, balancing task allocation in terms of durations, and consideration of the required skill levels for tasks. To this end, the Equitable Partitioning Problem approach, based on the goal programming technique, is employed, and a novel MILP model is introduced which can address the needs of organizations with varying priorities.

3. Problem Definition

The Equitable Partitioning Problem which is the basis of our mathematical model was introduced as a variant of assignment problems (O'brien & Mingers, 1997; Mingers & O'Brien, 1995) and it focuses on allocating individuals into teams considering specific attributes of individual so that the teams are formed as equal as possible. Mingers and O'Brien (1995) noted that the EPP can also be implemented for the equitable allocation of tasks among teams who also developed the mathematical model for the EPP utilizing the goal programming technique (Charnes et al., 1955; Charnes & Cooper, 1957; Lee, 1972; Ignizio, 1976). According to their problem definition, a set of individuals who are defined by a set of attributes are assigned to teams and for each team and attribute, sum of the deviations is minimized.

The problem under study can be formally defined as follows. There exists n individuals—each individual i is characterized by attribute j and attribute score s'_{ij}— and k attributes. Parameter e_i is 1 if individual i is one of the most experienced ones, 0 otherwise. While each individual is assigned to a team t—each consists of s individuals—, each of the most experienced individuals is assigned to different teams to enhance the advantages gained from their expertise (Mingers & O'Brien, 1995) ensuring that their total number equals the number of teams i.e., m. While another parameter m'_i is 1 if individual i is male, 0 otherwise, there is another constraint concerns maintaining the female-to-male ratio within the teams. To preserve this ratio as closely as possible in each team, the minimum and maximum number of males per team are determined

through a pre-processing step (denoted as $l'$and u', respectively) and the corresponding constraint is incorporated into the mathematical model. Regarding the tasks, a total of d tasks exist each of which is assigned to team where each team consists of t' tasks. For each task g, there is an associated completion time c'_g and score requirement s^*_{gj} for each attribute j. The last parameters is a' which is the average task duration per team.

Decision variables x_{it} take value 1 if individual i is assigned to team t and 0 otherwise. In addition, decision variables z_{gt} take value 1 if task g is allocated to team t and 0 otherwise. As stated before, there are three types of deviations. First, for each attribute, the deviation between the total attribute scores of individuals in the teams and the average attribute score per team. Positive and negative deviation values are traced by decision variables d_{tj}^{+1} and d_{tj}^{-1}, respectively. Second, for each team, the deviation between the total task duration and average task duration per team. These deviations are traced by decision variables d_t^{+2} and d_t^{-2}. Third and the last, both for each attribute and for each team, the deviation between the average score of individuals and the average required skill levels. To this end, decision variables d_{tj}^{+3} and d_{tj}^{-3} are utilized to trace the third type of deviation. Finally, the total of first, second and third types of deviations are traced by decision variables c_1, c_2 and c_3, respectively. To this end the MILP model developed for the problem at hand is as follows.

$$Min\ Z_1 = c_1 \quad (1)$$
$$Min\ Z_2 = c_2 \quad (2)$$
$$Min\ Z_3 = c_3 \quad (3)$$
$$\sum_{i=1}^{n}(x_{it}s'_{ij}) - d_{tj}^{+1} + d_{tj}^{-1} = \frac{\sum_{i=1}^{n} s'_{ij}}{m} \quad \begin{matrix}(j=1,\dots.,k)\\(t=1,\dots.,m)\end{matrix} \quad (4)$$
$$\sum_{t=1}^{m} x_{it} = 1 \quad (i=1,\dots.n) \quad (5)$$
$$\sum_{i=1}^{n} x_{it} = s \quad (t=1,\dots.m) \quad (6)$$
$$\sum_{i=1}^{n} x_{it}e_i = 1 \quad (t=1,\dots.m) \quad (7)$$
$$\sum_{i=1}^{n} x_{it}m'_i \geq l' \quad (t=1,\dots.m) \quad (8)$$
$$\sum_{i=1}^{n} x_{it}m'_i \leq u' \quad (t=1,\dots.m) \quad (9)$$
$$\sum_{t=1}^{m} z_{gt} = 1 \quad (g=1,\dots.d) \quad (10)$$
$$\sum_{g=1}^{d} z_{gt} = t' \quad (t=1,\dots.m) \quad (11)$$
$$\sum_{g=1}^{d}(z_{gt}c'_g) - d_t^{+2} + d_t^{-2} = a' \quad (t=1,\dots.,m) \quad (12)$$
$$\frac{\sum_{i=1}^{n}(x_{it}s'_{ij})}{s} - \frac{\sum_{g=1}^{d}(z_{gt}s^*_{gj})}{t'} - d_{tj}^{+3} + d_{tj}^{-3} = 0 \quad \begin{matrix}(j=1,\dots.,k)\\(t=1,\dots.,m)\end{matrix} \quad (13)$$
$$\sum_{t=1}^{m}\sum_{j=1}^{k}(d_{tj}^{+1} + d_{tj}^{-1}) \leq c_1 \quad (14)$$
$$\sum_{t=1}^{m}(d_t^{+2} + d_t^{-2}) \leq c_2 \quad (15)$$
$$\sum_{t=1}^{m}\sum_{j=1}^{k}(d_{tj}^{+3} + d_{tj}^{-3}) \leq c_3 \quad (16)$$
$$\sum_{t=1}^{m}\sum_{j=1}^{k}(dp_{tj} + dn_{tj}) \leq Z_1 \quad \begin{matrix}(j=1,\dots.,k)\\(t=1,\dots.,m)\end{matrix} \quad (17)$$
$$\sum_{t=1}^{m}(dp2_t + dn2_t) \leq Z_2 \quad (t=1,\dots.,m) \quad (18)$$
$$x_{it} \in \{0,1\} \quad \begin{matrix}(i=1,\dots.,n)\\(t=1,\dots.,m)\end{matrix} \quad (19)$$
$$z_{gt} \in \{0,1\} \quad \begin{matrix}(g=1,\dots.,d)\\(t=1,\dots.,m)\end{matrix} \quad (20)$$
$$d_{tj}^{+1}, d_{tj}^{-1}, d_t^{+2}, d_t^{-2}, d_{tj}^{+3}, d_{tj}^{-3}, c_1, c_2, c_3 \geq 0 \quad \begin{matrix}(j=1,\dots.,k)\\(t=1,\dots.,m)\end{matrix} \quad (21)$$

Eq.s (1-3) represent the objective functions as the minimization of the first, second and third type of deviations, respectively. Eq. (4) is used to calculate the decision variables related to the first type of deviation. Assignment of each individual to exactly one team is guaranteed by Eq. (5). Eq. (6) ensures that each team consists of s individuals. Assignment of each of the most experienced individuals to different teams is guaranteed by Eq. (7). Eq.s (8-9) ensure that the minimum and maximum number of males in each team are met, respectively. Assignment of each task to exactly one team is ensured by Eq. (10). Eq. (11) guarantees that each team consists of t' tasks. Eq.s (12-13) are used to calculate the decision variables related to second and third type of deviations, respectively. The total of the first type of deviations i.e., c_1, the total of the second type of deviations i.e., c_2 and the total of the third type of deviations i.e., c_3 are determined by Eq.s (14-16), respectively. While Eq. (17) is used in the second and in the third phases to preserve the solution of the first phase, Eq. (18) is used in the third phase of the

solution procedure to preserve the solution of the second phase. Eq.s (19-21) ensures the binary constraint and nonnegativity of the decision variables.

Since the solution procedure consists of three phases, the objective function and the constraints addressed in each phase change accordingly. As stated before, the first phase is related to balancing the attribute scores of individuals. So, Eq. (1) is used as the objective function and Eq.s (4-9, 14, 19, 21) are used as constraints in the first phase. After solving the first phase and finding the value of first objective function, it is included in the second phase as a constraint via Eq. (17). In addition, since the second phase is related to balancing the workload in terms of task duration, Eq. (2) is used as objective function and Eq.s (10-12, 15, 20) are added as constraints into the model, and the second phase is solved. Finally, the value of the second objective function is added into third phase as a constraint via Eq. (18). Finally, since the third phase is related to balancing the required skill levels, Eq. (3) is used as objective function and Eq.s (13, 16) are added as constraints into the model, and the third phase of the model is solved.

To provide an illustrative example, let us consider a scenario in which 9 individuals and 9 tasks are to be assigned to 3 teams. Each individual has three attributes (e.g., programming, foreign language, and mathematics skills). Supposing that while the individuals' attribute scores and the required skill levels for completing the tasks range between 5 and 10 units, task durations range between 10 and 15 units. (i) According to the first type of deviation: Assume that the total score of the 9 individuals for the third attribute is 63 units which is 21 units per team. If the total score of individuals in the first team for the third attribute is 24 units, then considering equality $24 - d_{13}^{+1} + d_{13}^{-1} = 21$, we can conclude that $d_{13}^{+1} = 3$. (ii) According to the second type of deviation: Assume that the total duration required to complete all tasks is 108 units which is 36 units per team. If the total duration of tasks assigned to the third team is 32 units, then considering equality $32 - d_3^{+2} + d_3^{-2} = 36$, we can conclude that $d_3^{-2} = 4$. (iii) According to the third type of deviation: Assume that the total score of individuals in the second team for the second attribute is 27, resulting in an average of 9. If the sum of the score of required skill levels for the tasks assigned to the second team is 24 which is 8 on average, then considering equality $9 - 8 - d_{22}^{+3} + d_{22}^{-3} = 0$, we can conclude that $d_{22}^{+3} = 1$.

4. Experimental Results

This section presents the experimental results concerning the problem at hand. Experiments are conducted using the dataset specifically generated for the problem. Dataset is comprised of instances with 24-36 individuals and tasks and 4-6 teams and attributes. In this case, the number of individuals in the teams varies between 4 and 9 which is consistent with common practices in the literature (Cavdur et al., 2019; van de Water & Bukman, 2010). Experiments were performed on a computer equipped with an Intel(R) Core(TM) i5-5200U 2.20GHz, 8 GB of RAM, and the CPLEX solver within the GAMS package with the time total limit of 7200 seconds with each phase having a time limit of 2400 seconds. We first solved the problem 24b-24g-4t-4o in which “24b”, “24g”, “4t” and “4o” represent the 24 individuals, 24 tasks, 4 teams and 4 attributes, respectively, and then, we conduct additional experiments by increasing the number of individuals, tasks, teams and attributes. In each instance, the number of the most experienced individuals is equal to the number of teams. Regarding the problem 24b-24g-4t-4o, we solved 10 instances and presented the results in Table 1 which includes the values of c_1, c_2 and c_3 as well as solution time (in second) of each phase with columns CPU_1, CPU_2 and CPU_3, respectively. An analysis of Table 1 shows that optimality is guaranteed in 9 out of 10 instances and the time limit is reached only in the second phase of instance 4.

Table 1. Experimental results of problem 24b-24g-4t-4o

Instances	c_1	c_2	c_3	CPU_1	CPU_2	CPU_3
1	20.50	0.00	16.33	3.36	2.70	13.27
2	18.00	2.00	13.83	4.61	1.42	7.05
3	20.50	2.00	13.50	6.31	1.95	29.92
4	21.00	2.00	14.67	4.64	2400.00	8.64
5	21.00	1.50	20.00	3.33	58.00	5.09
6	24.00	0.00	13.33	7.08	3.80	13.80
7	21.50	2.00	29.00	6.27	3.50	8.59
8	21.50	1.50	25.50	6.58	7.59	6.23
9	18.00	0.00	26.33	4.97	0.48	5.41
10	19.00	2.00	25.67	2.08	636.50	3.81

To explore the limitation of the mathematical model, additional problems 36b-24g-4t-4o, 24b-36g-4t-4o, 24b-24g-6t-4o, and 24b-24g-4t-6o are generated by increasing the number of individuals, tasks, teams, and attributes, respectively, by a factor of 1.5. A total of 40 instances were solved, with 10 instances per problem, and the average results are presented in Table 2 which includes c_1, c_2, c_3 values and total CPU time (in seconds). According to the results, the number of experiments in which the optimality is guaranteed for the problems provided in Table 2 are 1, 5, 9, and 5, respectively which corresponds to half of all the experiments. Based on the results, it is observed that increasing the number of individuals raises the problem's complexity more significantly compared to others.

Table 2. Average results for the related problems

Problems	c_1	c_2	c_3	*CPU*
36b-24g-4t-4o	29.70	1.75	96.67	3518.04
24b-36g-4t-4o	104.40	0.80	91.08	1232.63
24b-24g-6t-4o	247.87	1.74	203.28	1152.65
24b-24g-4t-6o	265.45	1.35	165.65	1886.65

In addition, to observe the effect of prioritizing deviations, we also solved the problems given in Table 2 using a model where all deviations are combined into a single objective function which means there is no priority of any deviation over another one, i.e., $Min\ Z = c_1 + c_2 + c_3$. Constraints are determined as the Eq.s (4-21) given in Section 3, except for Eq.s (17-18). The results are presented in Table 3. According to the results, the number of experiments in which the optimality is guaranteed for the problems provided in Table 3 are 9, 5, 10, and 10, respectively. Upon examining all the results, it is observed that when the model presented in Section 3 (results of which are provided in Table 2), which prioritizes deviations, is used, improvements in either c_1, c_2 or both are achieved in 14 out of 40 experiments, compared to the single-objective model where no priority is assigned among deviations. This indicates that in more than one-third of the experiments, better results can be obtained for the relevant deviations when the prioritization among them is considered.

Table 3. Average results of the model with the single objective function for the related problems

Problems	c_1	c_2	c_3	*CPU*
36b-24g-4t-4o	29.75	2.45	95.05	3177.11
24b-36g-4t-4o	104.40	0.80	91.08	3666.75
24b-24g-6t-4o	247.97	4.23	178.53	1904.04
24b-24g-4t-6o	265.45	2.30	163.88	296.57

5. Conclusions

In this study, a problem based on Equitable Partitioning Problem which is addressing the assignment of individuals and tasks to project-based teams is examined, with the aim of achieving balance within these teams across various factors. The balancing criteria considered in the problem include, first, the balanced assignment of individuals based on their attribute scores (such as programming skill, language skills etc.); second, the balanced assignment of task durations; and third, the balanced assignment of required skill levels for tasks. To this end, a three-stage Mixed Integer Linear Programming model based on the goal programming technique is developed, aiming to minimize the deviations with respect to the aforementioned factors. In the first stage, the first type of deviation is minimized; the result is then added to the model as a constraint in the second stage, where the second type of deviation is minimized. Finally, the outcome of the second phase is added to the model again as a constraint for the minimization of the third type of deviation. Here, the purpose is to construct a framework that can meet the needs of organizations with varying priorities and requirements.

We conducted computational experiments depending on the randomly generated instances. We first solved the 10 instances of problem 24b-24g-4t-4o (24 individuals, 24 tasks, 4 teams and 4 attributes). Later, to investigate the limitations of the model, we generated four additional problems by increasing the number of individuals, tasks, teams and attributes by 1.5 times, respectively and solved 10 instances for each. While an optimal solution was obtained for 90% of the instances of problem 24b-24g-4t-4o, an optimal solution was obtained for 50% of the instances of problems where the number of individuals, tasks, teams and attributes are increased. It was observed that the problem complexity increases more significantly, particularly when the number of individuals increases. We also solved the related problems with a model in which deviations are not prioritized and observed that in more than one-third of the experiments, better results can be obtained for the first two deviations when the deviations are prioritized compared to the model with single objective function. This demonstrates that the proposed three-stage problem formulation provides a flexible structure and is capable of addressing the varying needs and priority preferences of organizations.

Although the size of the addressed problems appears to correspond to those encountered in many real-world sectors (software development, education, marketing etc.), it is evident that for more complex and larger-scale organizational settings, the development of heuristic or metaheuristic algorithms, is necessary. To this end, while the mathematical models and experimental studies presented in this paper can provide contribution both theoretically and practically, we can list some of the future directions as follows: (i) Teams can vary in size and task allocation, given that neither team balance nor workload distribution is adversely affected, (ii) Mathematical models tailored to organizations prioritizing different types of deviations can be proposed, (iii) The models can be extended to include cost optimization by considering costs related to projects or personnel.

References

[1] Rahmanniyay, F., & Yu, A. J. (2019). A multi-objective stochastic programming model for project-oriented human-resource management optimization. *International Journal of Management Science and Engineering Management*, *14*(4), 231-239. https://doi.org/10.1080/17509653.2018.1534220

[2] Adams, S. G. (2003). Building successful student teams in the engineering classroom. *Journal of STEM Education: Innovations and Research*, *4*(3).

[3] van de Water, T., van de Water, H., & Bukman, C. (2007). A balanced team generating model. *European Journal of Operational Research*, *180*(2), 885-906. https://doi.org/10.1016/j.ejor.2006.04.017

[4] Erdeş, H. (2021). *Eşit bölümleme (EP) problemi yaklaşımı ile proje bazlı çalışma kapsamında görev ve bireylerin gruplandırılması (Yüksek Lisans Tezi)* Konya Teknik Üniversitesi].

[5] Reuters. (2021). *The Future is Project-Based – Is Your Organization Ready?* Retrieved 20.07.2025 from https://www.reuters.com/brandfeature/the-future-is-project-based-is-your-organization-ready

[6] Forbes. (2021). *How Organizations Can Become Project-Based In The Future Of Work*. Retrieved 20.07.2025 from https://www.forbes.com/sites/forbeshumanresourcescouncil/2021/06/02/how-organizations-can-become-project-based-in-the-future-of-work

[7] Sankaran, S., Vaagaasar, A. L., & Bekker, M. C. (2020). Assignment of project team members to projects: Project managers' influence strategies in practice. *International Journal of Managing Projects in Business*, *13*(6), 1381-1402. https://doi.org/10.1108/IJMPB-12-2018-0285

[8] Džamić, D., Ćendić, B., Marić, M., & Đenić, A. (2019). Solving balanced multi-weighted attribute set partitioning problem with variable neighborhood search. *Filomat*, *33*(9), 2875-2891. https://doi.org/10.2298/FIL1909875D

[9] Campêlo, M., & Figueiredo, T. F. (2021). Integer programming approaches to the multiple team formation problem. *Computers & Operations Research*, *133*, 105354.

[10] Çavdur, F., Sebatlı, A., & Küçük, M. K. (2019). Öğrenci-proje takımı oluşturma problemi için grup-karar verme ve hedef programlama temelli çözüm yaklaşımı. *Gazi Üniversitesi Mühendislik Mimarlık Fakültesi Dergisi*, *34*(1), 505-522.

[11] O'brien, F., & Mingers, J. (1997). A heuristic algorithm for the equitable partitioning problem. *Omega*, *25*(2), 215-223. https://doi.org/10.1016/S0305-0483(96)00046-1

[12] Mingers, J., & O'Brien, F. A. (1995). Creating student groups with similar characteristics: a heuristic approach. *Omega*, *23*(3), 313-321. https://doi.org/10.1016/0305-0483(95)00014-F

[13] Li, C.-T., & Shan, M.-K. (2010). Team formation for generalized tasks in expertise social networks. 2010 IEEE second international conference on social computing, Washington, DC, USA.

[14] Wei, C.-C., Lai, M.-C., Wei, C.-S., & Peng, L.-H. (2013). Assignment of project members considering capability and personality balance. *Kybernetes*. https://doi.org/10.1108/K-10-2012-0096

[15] Askin, R. G., & Huang, Y. (2001). Forming effective worker teams for cellular manufacturing. *International Journal of Production Research*, *39*(11), 2431-2451. https://doi.org/10.1080/00207540110040466

[16] Baykasoglu, A., Dereli, T., & Das, S. (2007). Project team selection using fuzzy optimization approach. *Cybernetics and Systems: An International Journal*, *38*(2), 155-185. https://doi.org/10.1080/01969720601139041

[17] Fathian, M., Saei-Shahi, M., & Makui, A. (2017). A new optimization model for reliable team formation problem considering experts' collaboration network. *IEEE Transactions on Engineering management*, *64*(4), 586-593. https://doi.org/10.1109/TEM.2017.2715825

[18] Rahmanniyay, F., Yu, A. J., & Seif, J. (2019). A multi-objective multi-stage stochastic model for project team formation under uncertainty in time requirements. *Computers & Industrial Engineering*, *132*, 153-165. https://doi.org/10.1016/j.cie.2019.04.015

[19] Holmberg, K. (2019). Formation of student groups with the help of optimisation. *Journal of the Operational Research Society*, *70*(9), 1538-1553. https://doi.org/10.1080/01605682.2018.1500429

[20] Cavdur, F., Sebatli, A., Kose-Kucuk, M., & Rodoplu, C. (2019). A two-phase binary-goal programming-based approach for optimal project-team formation. *Journal of the Operational Research Society*, *70*(4), 689-706. https://doi.org/10.1080/01605682.2018.1457480

[21] Çavdur, F., Bağlarbaşı-Mutlu, M., & Sebatlı-Sağlam, A. (2020). Öğrenci-proje takımı oluşturma problemi için bir karar destek sistemi uygulaması. *Uludağ Üniversitesi Mühendislik Fakültesi Dergisi*, *25*(1), 485-500.
[22] Tabansız, G., Sağlam, A. S., & Çavdur, F. (2023). ÖĞRENCİ-PROJE ATAMA PROBLEMİNDE FARKLI GRUP KARARLARININ DEĞERLENDİRİLMESİ. *Eskişehir Osmangazi Üniversitesi Mühendislik ve Mimarlık Fakültesi Dergisi*, *31*(1), 544-557.
[23] Daş, G. S., Altınkaynak, B., Göçken, T., & Türker, A. K. (2022). A set partitioning based goal programming model for the team formation problem. *International Transactions in Operational Research*, *29*(1), 301-322. https://doi.org/10.1111/itor.13022
[24] Gutiérrez, J. H., Astudillo, C. A., Ballesteros-Pérez, P., Mora-Melià, D., & Candia-Véjar, A. (2016). The multiple team formation problem using sociometry. *Computers & Operations Research*, *75*, 150-162. https://doi.org/10.1016/j.cor.2016.05.012
[25] Huang, J., Sun, X., Zhou, Y., & Sun, H. (2017). A team formation model with personnel work hours and project workload quantified. *The Computer Journal*, *60*(9), 1382-1394. https://doi.org/10.1093/comjnl/bxx009
[26] Desrosiers, J., Mladenović, N., & Villeneuve, D. (2005). Design of balanced MBA student teams. *Journal of the Operational Research Society*, *56*(1), 60-66. https://doi.org/10.1057/palgrave.jors.2601775
[27] van de Water, H., & Bukman, C. (2010). A balanced team-generating model for teams with less than nine persons. *IMA Journal of Management Mathematics*, *21*(3), 281-302. https://doi.org/10.1093/imaman/dpp020
[28] Rubin, P. A., & Bai, L. (2015). Forming competitively balanced teams. *IIE Transactions*, *47*(6), 620-633. https://doi.org/10.1080/0740817X.2014.953643
[29] Solow, D., Ning, J., Zhu, J., & Cai, Y. (2020). Improved heuristics for finding balanced teams. *IISE Transactions*, *52*(12), 1312-1323. https://doi.org/10.1080/24725854.2020.1732506
[30] Shen, M., Tzeng, G.-H., & Liu, D.-R. (2003). Multi-criteria task assignment in workflow management systems. Proceedings of The 36th Annual Hawaii International Conference on System Sciences, 2003.,
[31] Hosseini, S. M., & Akhavan, P. (2017). A model for project team formation in complex engineering projects under uncertainty: a knowledge-sharing approach. *Kybernetes*. https://doi.org/10.1108/K-06-2015-0150
[32] Charnes, A., Cooper, W. W., & Ferguson, R. O. (1955). Optimal estimation of executive compensation by linear programming. *Management science*, *1*(2), 138-151. https://doi.org/10.1287/mnsc.1.2.138
[33] Charnes, A., & Cooper, W. W. (1957). Management models and industrial applications of linear programming. *Management science*, *4*(1), 38-91. https://doi.org/10.1287/mnsc.4.1.38
[34] Lee, S. M. (1972). Goal programming for decision analysis.
[35] Ignizio, J. P. (1976). *Goal programming and extensions*. Lexington Books.

A HYBRID MACHINE LEARNING FRAMEWORK FOR REAL-TIME NETWORK INTRUSION DETECTION USING SUPERVISED

Alma LATIFI[a], Isak SHABANI[a] Rinesa BISLIMI[a] Mërgim H. HOTI[a*]

[a] *Computer and software engineering, Faculty of Electrical and Computer Engineering, University of Prishtina, Address: Rr. George Bush", No.31, 10000 Prishtinë, Republic of Kosova*

ABSTRACT

In this study, a novel machine learning-based framework for intrusion detection is proposed by merging two real-world network datasets to simulate diverse cybersecurity threat scenarios. The methodology combines supervised, unsupervised, and deep learning approaches to classify and detect network anomalies effectively. Supervised models such as LightGBM, Random Forest, and Gradient Boosting were trained and evaluated using standard classification metrics, while unsupervised methods including Isolation Forest, K-Means, and DBSCAN were applied for anomaly detection without labelled data. Also, ML models just like SVM and DL models such as CNN and LSTM were used to further enhance detection capabilities. The results show that LightGBM achieved the highest overall accuracy (92.5%), while Isolation Forest performed best in detecting attack patterns (53.9% recall). A visual analytics dashboard was developed using Power BI to provide deeper insights into user behaviour, protocol usage, and model predictions. The study highlights the trade-offs between model sensitivity and false positive rates and provides a comprehensive comparison of techniques suitable for real-time intrusion detection applications

KEYWORDS

- Anomaly detection
- Deep Learning
- Intrusion Detection System (IDS)
- Machine learning
- Supervised and Unsupervised algorithms.

* Corresponding author: Mërgim H. HOTI
E-mail: mergim.hoti@uni-pr.edu

1. **Introduction**

According to recent data on internet usage (Ani Petrosyan - Statista, 2025), cyberattacks are becoming increasingly aggressive and targeted. This trend is further amplified by the integration of artificial intelligence, which automates complex processes and enhances the sophistication of attacks (S. A. Repalle, V. R. Kolluru, 2017). Conversely, the human element - often considered the weakest link in cybersecurity—tends to delegate less responsibility to automated systems. This results in more intricate workflows, where certain decisions are

intentionally routed for human approval, reinforcing a system-to-system interaction model. Systems are designed to monitor and analyze user activity and behavior in order to make informed decisions based on the collected data.

These actions, while offering valuable insights into user patterns and characteristics, can also pose significant security and privacy risks if not properly managed. By applying both standard algorithms (Yasmeen S. Almutairi et al., 2022), and advanced machine learning techniques (Othman et al., 2018), the internal functioning of the system can be better understood. Such analysis enables the identification of system strengths and vulnerabilities, facilitating targeted improvements. Consequently, this process contributes to enhancing the system's overall effectiveness beyond its initial state. This paper presents a coherent and effective approach by leveraging a combination of supervised and unsupervised learning algorithms. The proposed methodology is designed to be suitable not only for systems with pre-existing behavioral data, but also for those requiring real-time detection of anomalous behavior (P. Sangkatsanee et al., 2011). The core idea lies in leveraging specific machine learning algorithms (Kaushik, S., Bhardwaj, A., Almogren, A. et al., 2025), to analyze available data in a manner that effectively distinguishes abnormal system behavior, such as potential intrusions from legitimate user activities that reflect normal system usage. The model is further designed to identify such behaviors in real time, aiming to minimize operational errors as much as possible.

This paper is structured as follows: Section 2 outlines the methodology, beginning with data collection, followed by preprocessing, and concluding with the application of relevant algorithms. Section 3 examines the connection between existing theoretical frameworks and the current study, identifying key research gaps. Section 4 presents the experimental results, accompanied by analysis and discussion. Finally, Section 5 offers a summary of the study, highlighting the main conclusions and outlining directions for future research.

2. Methodology

The paper follow a strict line up of combining two datasets from Kaggle which are not preprocessed and are not tested as one dataset before of our case, so this is the first time. The datasets we used are "Intrusion Detection Dataset" [https://www.kaggle.com/datasets/dnkumars/cybersecurity-intrusion-detection-dataset/data], and "Network Traffic Dataset" [https://www.kaggle.com/datasets/mohdzia356/network-traffic-data-for-intrusion-detection], where the aim of this merging of datasets is if selected machine learning algorithms will be able to detect cyber threats and attacks, even in real time cases, after we train this model. This means that it could be used in real world scenario to differ in any case if it is a threat for the company and the system, they provide their services, or it is a normal activity of their clients.

To achieve the objective of this study, we selected several machine learning algorithms based on the nature of the data contained in the dataset. We applied both supervised and unsupervised learning techniques to enable performance comparison and determine which algorithms deliver better results. For supervised learning, we used Random Forest, Gradient Boosting, and LightGBM. For each algorithm, we presented results using a confusion matrix and quantitative

metrics such as Accuracy, F1-Score, ROC AUC, Precision, and Recall. These results helped assess each model's ability to identify between "normal" and "attack" data. These algorithms were chosen because they perform well on high-dimensional tabular data, naturally handle both numerical and categorical features, and capture non-linear patterns. Some key reasons for choosing them include ***Random Forest*** is robust to overfitting and provides insight into feature importance. ***Gradient Boosting*** offers high accuracy and can focus on hard-to-classify instances. ***LightGBM*** is fast on large datasets and supports categorical features natively. For unsupervised learning, we implemented Isolation Forest, K-Means Clustering, and DBSCAN. We evaluated these using the same metrics: confusion matrix, accuracy, F1-score, ROC AUC, precision, and recall. These methods are useful for anomaly detection without relying on labeled data. Meanwhile these algorithms we have selected are ***Isolation Forest*** efficiently detects outliers using a tree-based method. ***K-Means*** helps by creating binary groupings of traffic behavior.

DBSCAN identifies dense clusters and considers sparse data points as anomalies. All of them are fit and we have judged that it may give us good results for our proposed model and generate information when and how to identify unusual patterns in the network traffic independently. To improve accuracy and explore more advanced results, we also applied machine learning models like SVM and deep learning models such as CNN and LSTM. Their results were presented using metrics like Accuracy, Precision, Recall and F1-Score. For Autoencoders, results were based on training and validation loss, since they detect anomalies by measuring reconstruction error rather than using standard classification metrics.

By combining supervised, unsupervised, and deep learning approaches, we conducted a comprehensive evaluation of intrusion detection methods. This allowed us to compare strengths and weaknesses across different techniques, ensuring a robust analysis of cybersecurity threats. Initially, we worked with two separate datasets: the intrusion detection dataset (11 columns, 9,537 rows) and the network traffic dataset (9 columns, 2,000 rows). To obtain a larger and more balanced training set, we applied several preprocessing and augmentation steps. First, categorical attributes such as protocol type and traffic labels were encoded numerically, while numerical attributes (e.g., session duration, byte count, failed logins) were normalized using scaling techniques (StandardScaler and RobustScaler). Missing values were handled through imputation, and duplicate records were removed.

Since the original datasets contained relatively few rows, we applied data augmentation to synthetically expand the training set. In particular, oversampling methods such as SMOTE were applied to generate new minority-class attack records, ensuring class balance. Additionally, controlled bootstrapping and resampling were used to create varied network traffic patterns while preserving statistical distributions of key features. After merging both datasets and applying these augmentation techniques, we obtained a balanced dataset with approximately 90,000 rows and 20 columns, capturing a wide range of attack behaviors and normal traffic flows (as shown in Table 1).

Table 1. Dataset size for training part.

Total Entries	*90000*

Total Columns	*20*
Memory Usage	*13.7+ MB*

Table 2 below describes the attributes of the dataset selected for training. The dataset includes various parameters related to the network and user behavior during a communication session. Attributes such as Duration, session_duration, and PacketCount provide information about the duration and volume of traffic, while Protocol, protocol_type, SourceIP, and DestinationIP identify the type of protocol and offer details about the communication. Features that help identify questionable behavior are also included, such as login_attempts, ip_reputation_score, and encryption_used. The Label and attack_detected columns serve to classify sessions as either normal or attcak, which has supported the application of machine learning models to achieve the main objective of this work – detecting attacks and activities within the dataset.

Table 2. Attribute descriptions of the combined network traffic dataset.

Column Name	***Description***
Duration	*Total duration of the session in seconds.*
Protocol	*Network protocol used (e.g., TCP, UDP, ICMP).*
SourceIP	*IP address of the sender.*
DestinationIP	*IP address of the receiver.*
SourcePort	*Port number of the sender.*
DestinationPort	*Port number of the receiver.*
PacketCount	*Number of packets exchanged in the session.*
ByteCount	*Total number of bytes exchanged.*
Label	*Classification label indicating normal or attack activity.*
session_id	*Unique identifier for each session (e.g., SID_00001).*
network_packet_size	*Size of network packets in bytes.*
protocol_type	*Communication protocol used (e.g., TCP, UDP, ICMP).*
login_attempts	*Number of login attempts during the session.*
session_duration	*Length of the session in seconds.*
encryption_used	*Type of encryption used (AES, DES, or None).*
ip_reputation_score	*Score between 0 and 1 indicating how suspicious the IP is.*
failed_logins	*Number of failed login attempts.*
browser_type	*Browser used for the session (e.g., Edge, Firefox).*
unusual_time_access	*Binary flag (0 or 1) indicates unusual access time.*
attack_detected	*Target variable: 1 means an attack was detected, 0 means normal activity.*

Before training the machine learning models, data preprocessing was performed to ensure quality of data. Data preprocessing included handling missing values (none were found), identifying and removing outliers, and normalizing skewed numerical features such as session_duration, failed_logins, and ip_reputation_score. After confirming that no missing values were present, we took a further step to detect outliers, as previously mentioned. Based on the figures, no outliers were found in some columns. However, for the columns where outliers were detected, we applied skewness analysis. Several features get right-skewed distributions, particularly session_duration and failed_logins. To address this, we used data transformation techniques to reduce skewness and bring the data distribution closer to normal.

Table 3. Identified outliers per feature from the dataset.

Feature	***Outliers Detected***
Duration	*0*
SourcePort	*0*
DestinationPort	*0*
PacketCount	*0*
ByteCount	*0*

Network_packet_size	*390*
Login_attempts	*1,907*
Session_duration	*4,071*
IP_reputation_score	*198*
Failed_logins	*3,076*
Unusual_time_access	*13,558*
Attack_detected	*0*

As we mentioned above, the goal of this training dataset is to detect attacks and activities within the dataset. If there is not approximately equal representation of each class in a dataset, it is considered imbalanced. Predictive accuracy is commonly used to assess the effectiveness of machine learning algorithms. When the data is imbalanced and the costs of various errors differ significantly, this is inappropriate, as the same method is applied by (Nitesh V Chawla et al., 2002). The Synthetic Minority Over-sampling Technique (SMOTE) is used to perform classification on imbalanced datasets. This classification technique creates new instances of the minority class to balance a dataset by re-sampling the instances of the minority class (Qiong Gu et al., 2016). After examining the dataset, we decided to focus on the Label column, which indicates whether each data entry is an “Attack” or “Normal” activity. This column is important for achieving our main goal - detecting attacks. Although the raw dataset initially contained approximately 90,000 rows, not all of these were usable. During preprocessing, rows with missing values, duplicates, and strong outliers were removed to improve data quality. After this cleaning phase, the usable dataset contained 59,877 rows, with 31,803 attack entries and 28,074 normal entries. To address this class imbalance, SMOTE oversampling was applied, increasing the minority (normal) class to 31,803. This yielded a balanced dataset of 63,606 rows for training and evaluation as has been shown in Table. 4.

Table 4. Results after SMOTE algorithm application.

Label	***Count_Before***	***Count_After***
Attack	*31803*	*31803*
Normal	*28074*	*31803*

The dataset was first preprocessed and then split into training and testing subsets, ensuring that the same split was used consistently across all models for a fair comparison. This means every model was trained on the same training data and evaluated on the same testing data, eliminating randomness in dataset partitioning as a potential source of variation. Techniques such as SMOTE were applied only on the training data to balance the distribution of attack and normal instances, while the testing data remained untouched to preserve real-world conditions. As a summary of the methodology, we focused on preparing the dataset, including detecting outliers and fixing imbalanced data. This approach resulted in a dataset that performs well with machine learning models, and we achieved good results. These results will be described below in more detail, explaining the performance of each machine learning algorithm used.

3. Related work

This research (T.Saranya et al., 2020), examines various ML algorithms—such as Linear Discriminant Analysis (LDA), Classification and Regression Trees (CART), and Random Forest—used in IDS across a range of environments, including IoT, fog computing, big data, smart cities, and 5G networks. Experiments conducted using the KDD-CUP (KDD’99) dataset demonstrate that detection accuracy, false positive rates, and overall performance depend not only on the choice of algorithm but also on the specific context in which IDS is applied. The

study emphasizes the importance of tailoring IDS approaches to different environments and suggests that future work will focus on applying ML algorithms to real-time datasets for more adaptive and robust intrusion detection solutions.

Network intrusion has become a critical concern due to the rise in cyberattacks threatening service availability and data privacy declare authors (M. N. Chowdhury and K. Ferens, M. Ferens, 2016). This study proposes a hybrid machine learning approach to detect anomalies in network traffic, combining two algorithms to improve accuracy and efficiency. The method was evaluated using key metrics such as detection accuracy, false positive rate, false negative rate, and response time. Results show a significant improvement, achieving a 98.76% detection rate with minimal false positives (0.09%) and false negatives (1.15%), outperforming standard SVM-based methods. The findings highlight the potential of intelligent models in enhancing modern intrusion detection systems. Meanwhile, in research of (Çavuşoğlu, 2019), they introduce a hybrid, layered Intrusion Detection System (IDS) that leverages tailored machine learning techniques and two novel feature selection methods to enhance detection performance across various attack types. Using the NSL-KDD dataset, the system significantly reduces feature dimensions while maintaining high accuracy and low false positive rates. Each layer is optimized with specific algorithms based on attack type, leading to strong results across metrics like DR, TPR, F-Measure, and MCC. Notably, the system outperforms many existing approaches in literature, particularly in challenging attack categories such as R2L and U2R. Overall, it demonstrates a scalable and effective approach for intelligent network intrusion detection.

Moreover, in this study (G. Logeswari, S. Bose and T. Anitha, 2023), it is presented a novel Intrusion Detection System (HFS-LGBM IDS) tailored for Software Defined Networking (SDN), addressing its increased vulnerability due to centralized control. The system integrates a two-phase Hybrid Feature Selection method—combining Correlation-Based Feature Selection and Random Forest Recursive Feature Elimination—to optimize the dataset. A LightGBM classifier is then employed for accurate and efficient attack detection. Evaluated using the NSL-KDD dataset and tested in a simulated SDN environment (Mininet), the proposed model outperforms existing techniques in accuracy, precision, recall, and F-measure, demonstrating its effectiveness for real-time network security. Authors in this paper (Naveen Saran, Nishtha Kesswani, 2023), addresses the growing security challenges in IoT networks, where traditional defenses fall short against sophisticated and multi-class intrusion attacks. To tackle this, a multi-class Intrusion Detection System (IDS) just like the paper of authors (Hongyu Liu and Bo Lang, 2019), is developed using various supervised Machine Learning classifiers on the MQTT-IoT-IDS2020 dataset. The system is tested with algorithms like k-NN, SVM, Naive Bayes, Random Forest, Decision Tree, and SGD, achieving accuracy rates as high as 99.98%. Results show strong performance across all classifiers in detecting diverse attack types. The study not only identifies effective models for IoT security but also opens pathways for future enhancement using Swarm Optimization techniques.

According to authors (O. Faker, E. Dogdu, 2019), the study enhances intrusion detection systems by integrating Big Data processing with Deep Learning techniques, using Apache Spark for scalable computation. Three classifiers Deep Neural Networks (DNN), Random

Forest, and Gradient Boosted Trees, were applied to the UNSW-NB15 and CICIDS2017 datasets, with feature selection guided by a homogeneity metric. DNN achieved top accuracy for multiclass detection (up to 99.57%), while GBT reached 99.99% accuracy in binary classification. All experiments used 5-fold cross-validation to ensure robust evaluation. Future work will focus on improving feature selection methods and analyzing system performance across different distributed cluster configurations.

Also, the authors (S. A. Repalle, V. R. Kolluru, 2017), in this work proposes a secure, AI-driven automated threat detection system that reduces analyst workload by continuously monitoring network activity and responding dynamically to threats. It integrates a Virtual Analyst using machine learning as well as (Biswas, 2018), and active learning mechanisms, allowing the system to evolve over time with analyst feedback. The thesis also highlights the critical role of high-quality, labeled datasets for effective intrusion detection. While K-Nearest Neighbors showed strong performance, unsupervised algorithms required significant manual tuning. Ultimately, the study emphasizes the importance of adaptive, data-driven models for building efficient intrusion detection systems. While (M. Asif, S. Abbas, M.A. Khan et al., 2022) on the other hand research introduces MR-IMID, a MapReduce-based intelligent intrusion detection model that integrates machine learning, specifically Artificial Neural Networks (ANN), to efficiently analyze large-scale network data. Designed for real-time intrusion detection in IoT and expanding network environments, MR-IMID leverages parallel clustering and automated feature tagging to detect and predict anomalies. It also stores intrusion patterns for future reference, improving consistency. Experimental results on real datasets show strong performance, with detection accuracy of 97.6% during training and 95.7% in validation - surpassing prior models.

4. Results and discussions

As mentioned previously, the datasets we used for training and testing were unprocessed and had not been used earlier. Based on the methodology we applied, our main focus was to determine which of the algorithms best predicted the most common outcomes in our main dataset. The results are not only focused on how these algorithms performed on our dataset in the final evaluation, but also on how well our data adapted to each algorithm. We aimed to present also which of category of algorithms supervised or unsupervised performed better.

4.1 Random Forest

As first supervised algorithm to train our data is selected Random Forest (T. Arora, M. Sharma and S. K. Khatri, 2019), (A. H. Hoti et al., 2022), (Y. Y. Aung and M. M. Min, 2017), which was trained using all 18 network traffic features. It was configured with 100 trees, Gini impurity as the split criterion and a random state of 42 to ensure reproducibility. Getting to know more about the algorithm is an ensemble learning method that constructs multiple decision trees during training and outputs the class that is the mode of the classes(classification) or mean predication of the individual trees. Due to its ability to reduce overfitting and provide high accuracy even on complex datasets, it is ideal for network intrusion detection scenarios where multiple input variables contribute to classification.

Table 5: Performance of Random Forest.

Actual \ Predicted	*Normal*	*Attack*
Normal Traffic	*9,507*	*0*
Attack Traffic	*371*	*7,230*

The model demonstrates exceptional performance for network intrusion detection. It shows a perfect ability to identify normal network connections, correctly classifying all 9,507 benign events with zero false alarms. More importantly, it exhibits a strong capability to detect malicious attacks, successfully identifying 7,230 attacks (True Positives) while missing only 371 (False Negatives). This results in a very high sensitivity, indicating the model is highly effective at identifying true threats.

Table 6: Performance metrics of Random Forest.

Metric	*Score*
Accuracy	*97.8%*
Precision	*100%*
Recall	*95.1%*
F1-Score	*97.5%*
Specificity	*100%*

Table 6 shows good results across all key performance metrics. The model achieves accepted overall accuracy of 97.8%. Crucially, it maintains perfect precision and specificity of 100%, meaning it never mistakenly labels normal traffic as an attack. The recall of 95.1% indicates it detects the vast majority of actual attacks, and this is reflected in the strong F1-Score of 97.5%. This balanced performance confirms the model is both reliable and effective for this task.

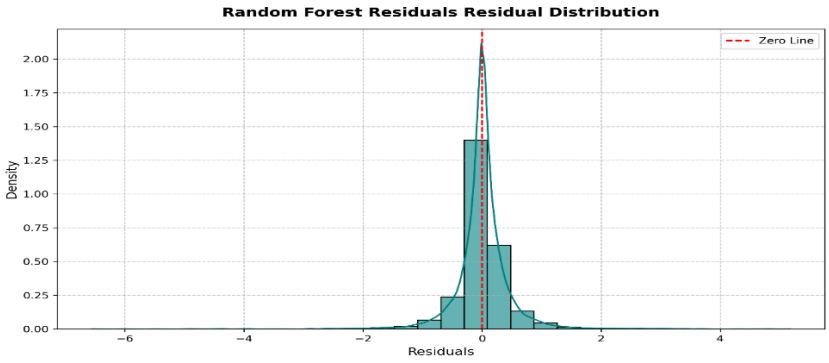

Figure 1: Error distribution (actual vs predicted values) for Random Forest predictions.

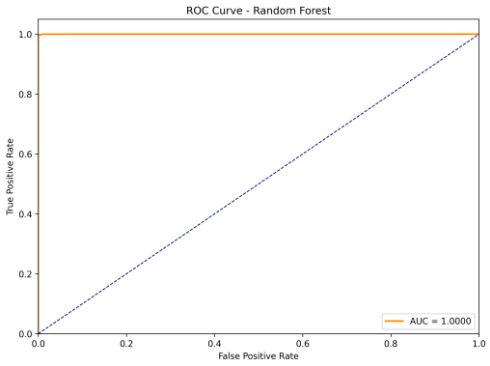

Figure 2: ROC Curve – Random Forest.

Error distribution (actual vs predicted values) for Random Forest predictions helps to identify if the model systematically over or/and underestimates attack probabilities as shown in Figure 1, meanwhile for ROC Curve figure is shown in Figure 2.

4.2 Gradient Boosting Classifier

This model use the same features and was fine-tuned with 100 boosting stages, a learning rate of 0.1, early stopping after 10 rounds to avoid overfitting, and class weighting to address imbalanced attack data. Gradient Boosting (Q. H. Vu, D. Ruta and L. Cen, 2019), (Reham Amin et al., 2023) builds models sequentially attempts to correct the errors made by the previous one. It is especially effective for imbalanced datasets as it can place more focus on harder-to-classify samples. However, it tends to be more sensitive to parameter tuning and overfitting compared to Random Forest.

Table 7: Performance of Gradient Boosting.

Actual \ Predicted	*Normal Traffic*	*Attack Traffic*
Normal Traffic	*9,507*	*0*
Attack Traffic	*1,737*	*5,864*

Table 8 : Performance metrics of Gradient Boosting Classifier

Metric	*Score*	*Interpretation*
Accuracy	*90%*	*Better balanced performance*
Precision	*100%*	*All predicted anomalies were correct*
Recall	*77.1%*	*Detected a large majority of all attacks*
F1-Score	*87.1%*	*Strong balance between precision and recall*
Specificity	*100%*	*Perfect at identifying normal traffic*

As shown in Table 7, this model shows very good performance. It demonstrates perfect precision and specificity by correctly identifying all 9,507 normal traffic instances without any false alarms. The model also shows strong attack detection capability, correctly identifying 5,864 attacks for a high recall of 77.1%. While it misses 1,737 attacks, the Gradient Boosting method effectively balanced the learning process to significantly reduce bias toward the majority class. The result is a powerful model with an excellent trade-off that maximizes threat detection while completely avoiding false alarms.

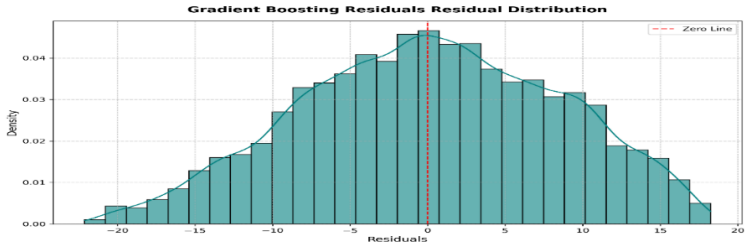

Figure 3: Residual plot for Gradient Boosting.

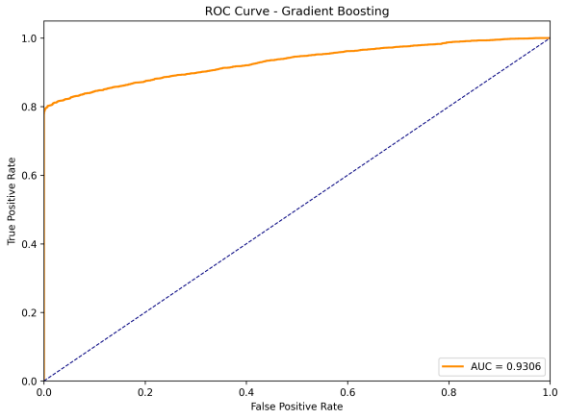

Figure 4: ROC Curve – Gradient Boosting.

The residual plot for the Gradient Boosting model, shown in Figure 3, with prediction errors concentrated around zero, indicates good performance in classifying network intrusions. Meanwhile, Figure 4 shows the ROC Curve for the GB algorithm.

4.3 LightGBM Classifier

Optimized for both speed and efficiency, this model use histogram-based learning with a maximum depth of 5, L2 regularization ($\lambda = 0.1$), and native categorical feature handling via binning. It is known for faster training speed and lower memory usage, making it a strong candidate for real-time or large-scale applications. Its ability to handle categorical variables directly improves both performance and interpretability.

Table 8: Performance of LightGBM.

Actual \ Predicted	***Normal Traffic***	***Attack Traffic***
Normal Traffic	*9,507*	*0*
Attack Traffic	*1,242*	*6,359*

This model, powered by LightGBM [23], offers good performance among the tested models. It achieves perfect precision and specificity (100%) by correctly identifying all 9,507 normal traffic instances without a single false alarm. Furthermore, it demonstrates the highest sensitivity (recall) of 83.7%, successfully detecting 6,359 out of 7,601 attacks. With only 1,242 attacks missed (false negatives), it strikes a superior balance between detecting threats and maintaining operational efficiency by avoiding false alarms. This confirms its strong learning capability from network data and its high suitability for real-time analysis.

Table 9: Metrics of LightGBM performance.

Metric	***Score***	***Significance***
Accuracy	*92.6%*	*Highest overall correctness*
F1-Score	*91.2%*	*Excellent balance precision/recall*
Precision	*100%*	*All identified anomalies were correct*
Recall	*83.7%*	*Some anomalies were missed*

This model shows excellent overall performance, with an accuracy of 92.6% and a near-perfect F1-score of 91.2%. It achieves a perfect precision of 100%, meaning every instance it flagged

as an attack was indeed malicious, resulting in zero false alarms. The recall of 83.7% is high, indicating it successfully detects most true attacks. The combination of perfect precision and high recall makes this the most effective model for this task.

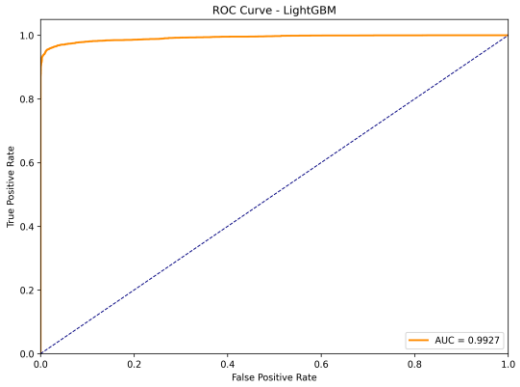

Figure 5 : ROC Curve - LightGBM

4.4 Isolation Forest

Trained only on normal traffic (y = 0), this model isolates anomalies based on a contamination ratio of 29.6% (matching the real-world attack ratio), 100 trees, and automatic subsampling for scalability. An anomaly threshold was set at -1 to classify outliers. Anomalies are more susceptible to isolation and hence require fewer splits. This model is highly scalable and effective in scenarios where labeled attack data is unavailable or incomplete.

Table 10: Performance of Isolation Forest.

Actual \ Predicted	***Normal***	***Attack***
Normal Traffic	*5,381*	*4,126*
Attack Traffic	*3,742*	*3,859*

This unsupervised model demonstrates a solid detection capability, identifying 50.8% of attacks and correctly classifying 56.6% of normal traffic. While it outperforms supervised models in detecting threats, it also produces a high false alarm rate (4,126 false positives) and misses nearly half of the attacks as it is shown in Table 10. Despite these drawbacks, it highlights the potential of anomaly-based detection in uncovering previously unseen threats.

Table 11: Metrics performance of Isolation Forest.

Metric	***Score***	***Interpretation***
Accuracy	*54.1%*	*Baseline performance*
F1-Score	*49.6%*	*Balance between precision/recall*
ROC AUC	*53.6%*	*Moderate separation ability*
Precision	*48.3%*	*Many false positives present*
Recall	*50.8%*	*Half of actual anomalies detected*

Model delivers baseline performance, with low accuracy 54.01% and a moderate F1-score 49.52%, indicating limited effectiveness in distinguishing anomalies. The ROC AUC of 53.69% shows only slight separation between classes. Precision 48.33% suggests a high

number of false positives and recall 50.07% means only half of the actual anomalies were detected, highlighting the need for significant improvement as it is shown in Table 11.

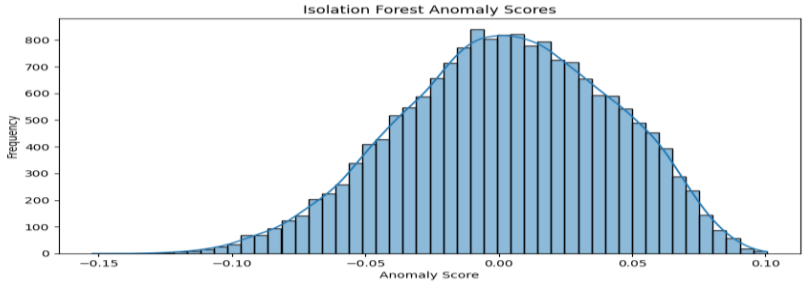

Figure 6: Residual plot for Isolation Forest.

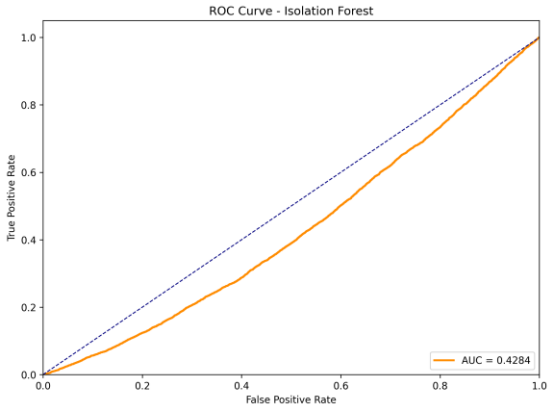

Figure 7: ROC Curve – Isolation Forest

The anomaly score distribution shows most samples clustered near zero (normal traffic), with clear outliers below -0.05 (potential attacks) and above 0.05 (suspicious activity) as it has been shown in Figure 6. The bimodal distribution confirms effective separation between normal and anomalous patterns shown in Figure 7 for ROC Curve for IF.

4.5 K-Means Clustering

Clustering was performed on 11 selected, scaled features. We used 2 clusters (normal vs anomaly), and cluster labels were matched to true labels via majority voting. The Silhouette Score was 0.162, indicating moderate separation. K-Means (N. A. Putri et al., 2017) is a classic unsupervised clustering algorithm that assigns data into k groups by minimizing intra-cluster variance. While basic, it serves as a quick baseline for unsupervised anomaly detection. Its lower performance in this context highlights the complex nature of network traffic data and the benefit of more sophisticated approaches.

Table 12: Performance of K-Means Clustering.

Actual \ Predicted	***Normal***	***Attack***
Normal Traffic	*8,504*	*539*
Attack Traffic	*5,900*	*2,085*

This model demonstrates strong performance in identifying normal traffic, with 94% specificity, but struggles with detecting attacks, achieving only a 26.1% recall. It flagged 539

normal events incorrectly and missed 5,900 actual attacks as it is shown in Table 9. This reflects the common trade-off in unsupervised clustering, where minimizing false positives often comes at the expense of effective threat detection.

Table 13: Metrics performance of K-Means Clustering.

Metric	*Score*	*Interpretation*
Accuracy	*62.2%*	*Moderate overall performance*
F1-Score	*39.2%*	*Low precision-recall balance*
ROC AUC	*60.0%*	*Marginal separation ability*
Precision	*79.4%*	*Few false positives*
Recall	*26.1%*	*Most actual anomalies missed*

This model show in Table 10 moderate overall performance with 62.2% accuracy, but a low F1-score 39.2% highlights poor balance between precision and recall. While it achieves high precision 79.46%, indicating few false positives, its low recall 26.11% reveals it misses most actual anomalies. The ROC AUC of 60% suggests only limited ability to separate normal from malicious activity.

4.6 DBSCAN algorithm

DBSCAN (G. Dong et al., 2019) is a density-based clustering algorithm that groups together closely packed points and marks points in low-density regions as outliers. It's particularly useful for detecting clusters of varying shapes and sizes and is less sensitive to noise. In this analysis, DBSCAN was evaluated for its ability to identify anomalies in network traffic data.

Table 14 : Performance of DBSCAN

Actually \ Predicted	*Normal*	*Attack*
Normal Traffic	*302*	*9,205*
Attack Traffic	*115*	*7,486*

Table 15: Metrics performance of DBSCAN.

Metric	*Score*	*Interpretation*
Accuracy	*45.8%*	*Below baseline performance*
F1-Score	*61.6%*	*Moderate precision-recall balance*
ROC AUC	*50.8%*	*Minimal separation ability*
Precision	*44.9%*	*High false positive rate*
Recall	*98.5%*	*Nearly all actual anomalies found*

The model shown in Table 15 highlights overall accuracy at 45.8%, indicating limited general performance. Its F1-score of 61.63% reflects a moderate balance between precision and recall. The ROC AUC of 50.83%, suggests the model barely distinguishes between classes. While precision is low at 44.9%, indicating a high false positive rate, the recall is very high at 98.5%, meaning the model successfully detects nearly all actual anomalies. This trade-off highlights a tendency to favor detecting anomalies at the cost of many false alarms. The trade-off lies in the availability of labelled data: supervised models require labelled attack data, while unsupervised models can operate without labels, identifying outliers based on normal behaviour.

Table 16: Comparing best performed algorithms.

Metric	*Supervised (LightGBM)*	*Unsupervised (Isolation Forest)*	*Difference*
Accuracy	*92.6%*	*54.1%*	*+38.5%*
Recall	*83.7%*	*50.8%*	*+32.9%*
Specificity	*100%*	*56.6%*	*+43.4%*
False Positive Rate	*0%*	*43.4%*	*-43.4%*

As shown in Table 16, the supervised LightGBM model outperforms the unsupervised Isolation Forest in overall accuracy (92.6% vs. 54.1%) and demonstrates perfect specificity for normal traffic (100%), resulting in a false positive rate of 0%. However, the Isolation Forest detects a lower proportion of attacks, achieving a recall of 50.8% compared to 83.7% for LightGBM. This indicates that the supervised model is significantly better at identifying both normal traffic and true attacks, while also completely avoiding false alarms. This contrast highlights the superior effectiveness and reliability of the supervised approach for this specific network intrusion detection task.

4.7 Discussing and analysis of machine learning algorithms

The chosen models span both supervised ensemble classifiers and unsupervised anomaly detectors, reflecting the dual needs of intrusion detection. For supervised learning, Random Forest, Gradient Boosting, and LightGBM were selected due to their strong performance on high-dimensional tabular data and flexibility. They naturally handle mixed numeric/categorical features and non-linear patterns. These supervised models suit the classification task (attack vs. normal) and can be extended to regression (session duration prediction) by changing the objective. Table 13 summarizes four machine learning models used for anomaly detection. It includes SVM optimized via GridSearch; CNN, a Convolutional Neural Network designed for feature extraction; LSTM, a Long Short-Term Memory network suited for sequential data.

Table 17: Performance of each algorithms.

Model	Accuracy	Precision (Class 1)	Recall (Class 1)	F1-Score (Class 1)	Specificity	NPV
SVM	0.854	0.830	0.932	0.878	0.9320	0.830
CNN	0.9017	0.9619	0.75	0.8057	0.917	0.866
LSTM	0.900	0.99	0.78	0.87	0.987	0.843

The dataset consists of two classes: Class 0 for normal traffic and Class 1 for intrusion or malicious activity. The table compares three models—SVM, CNN, and LSTM—in detecting malicious activity (Class 1). LSTM achieves the highest overall accuracy at 90%, with strong precision (0.99) and recall (0.78), indicating the best balance between detecting intrusions and minimizing false alarms. CNN also performs well, with very high precision (0.9619) but slightly lower recall (0.75). SVM shows balanced metrics, though its lower recall (0.932) suggests it misses more attacks. These results highlight the relative strengths and limitations of each model in intrusion detection.

4.8 Visual Analytics of Intrusion Detection with Power BI

This section provides a collection of insightful visualizations generated with Power BI, aimed at analyzing attack detection patterns across multiple dimensions including protocol traffic, browser usage, login behavior, and prediction probabilities. These charts and summaries help evaluate the model's performance, highlight potential detection gaps, and reveal behavioral trends that support a more robust cybersecurity strategy.

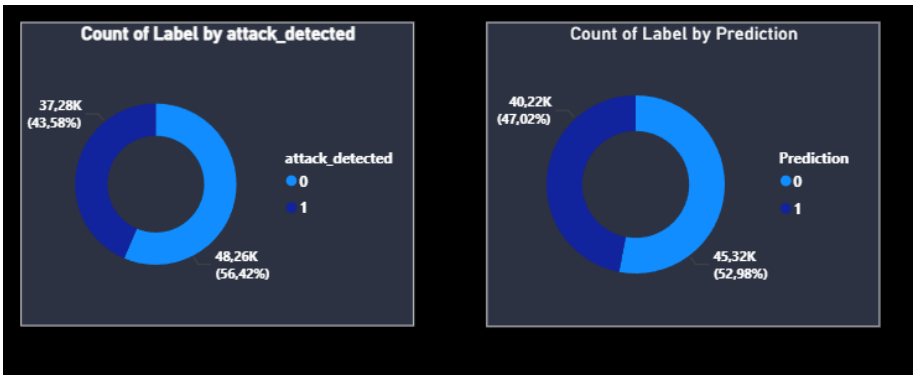

Figure 8: Model vs Reality.

Plots shown in Figure 8 visualizes actual attack detection results (left) vs. model prediction (right) during training. The left plot shows 43.58% (37.28K) of traffic as malicious (attack_detected=1) and 56.42% (48.26K) as normal. The right plot shows the prediction made by the model: 47.02% (40.22K) as attacks (Prediction=1) and 52.98% (45.32K) as normal. The negligible difference (3.44% more predicted attacks than captured) shows the model might be over-flagging risks or spotting patterns the initial detection platform has not noticed.

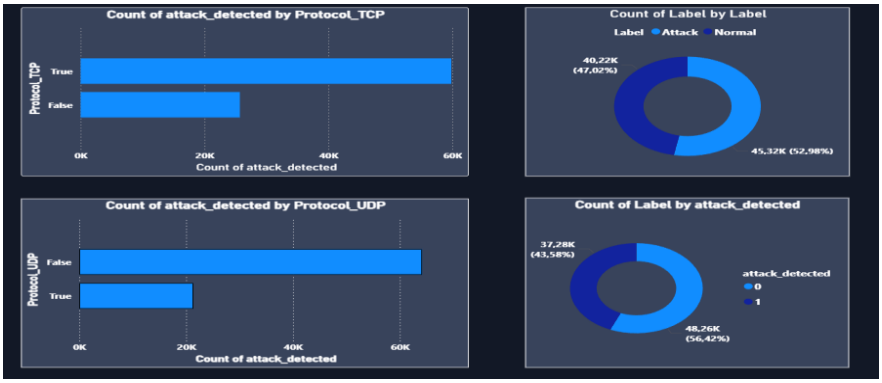

Figure 9: Network Protocol Insights.

Our top protocol shows over 60,000 safe connections, with minimal threats detected, suggesting strong protection shown in Figure 8. Surprisingly, UDP traffic mirrors this safe pattern, despite its known vulnerabilities, indicating either excellent defense or potential blind spots. The dataset has a nearly balanced 47% attack vs. 53% normal split—ideal for training ML models. However, detection lags slightly: only 43.6% of attacks are flagged, leaving a 3.4% gap that may indicate false negatives or mislabeling. On the other hand, the visualization shown in Figure 9 explores user login behavior and its link to attack detection, using login attempts and failed logins, split into Attack and Normal labels for comparison. Session Duration by Login Attempts where the top chart shows that most sessions cluster around 3–5 login attempts for both labels. However, attack sessions are more frequent with higher login attempts (6+), while normal sessions decline, indicating a potential sign of brute-force or scripted activity.

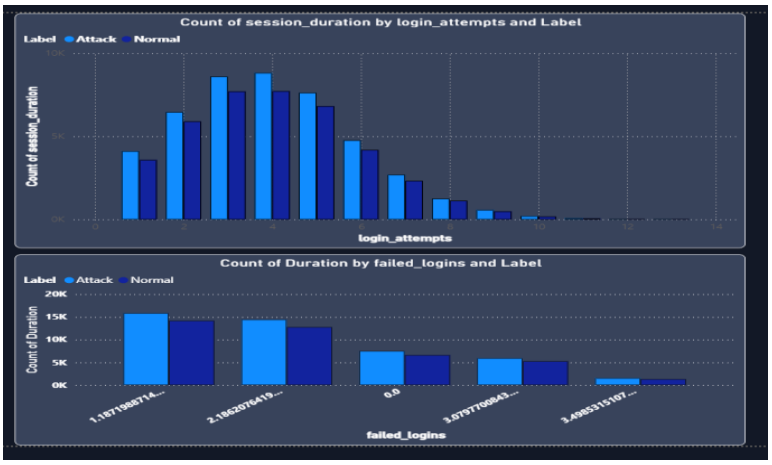

Figure 10: Login Analysis by Session Duration and Failed Logins.

Duration Count by Failed Logins - The bottom chart groups session durations by failed login values. Most sessions occur at low failed login counts, but attack sessions are slightly higher even at 0.0, suggesting that not all malicious actions involve failed logins. Higher failed login values are rare but more often seen in attacks.

5. Conclusions

This research presents a comprehensive evaluation of various machine learning algorithms for network intrusion detection using a unique, combined dataset. The results clearly demonstrate that supervised learning models, particularly LightGBM, offer high accuracy and reliable classification of normal network activity, making them highly effective for systems where labeled data is available. However, unsupervised models such as Isolation Forest proved valuable in detecting unknown or novel attack patterns, albeit at the cost of higher false positives. Deep learning models like LSTM and CNN further contributed to offering balanced performance, especially in capturing sequential patterns in data. The study underscores the importance of data preprocessing, class balancing, and feature engineering in improving model performance. Furthermore, the integration of Power BI visualizations added a practical dimension by enabling interpretability and pattern discovery in real-time network environments. By comparing multiple techniques across consistent metrics, this work lays a strong foundation for developing hybrid intrusion detection systems that can adapt to both labeled and unlabeled threat scenarios.

Future research will aim to expand on this work by incorporating real-time data streams to test the models' capabilities in live environments. Another area of focus will be enhancing the model’s sensitivity without compromising precision by integrating adaptive learning mechanisms and continual training. The use of federated learning across decentralized data sources is also a promising direction to maintain user privacy while strengthening detection performance across distributed systems.

References

[1] A. H. Hoti et al. (2022). Identifying Fake News written on Albanian language in social media using Naïve Bayes, SVM, Logistic Regression, Decision Tree and Random

Forest algorithms. *2022 11th Mediterranean Conference on Embedded Computing (MECO), doi: 10.1109/MECO55406.2022.9797147* (pp. 1-6). Budva, Montenegro: IEEE.

[2] Ani Petrosyan - Statista. (2025, 10 20). *Number of internet and social media users worldwide as of February 2025*. (Statista) Retrieved 08 15, 2025, from Statista: https://www.statista.com/statistics/617136/digital-population-worldwide/

[3] Biswas, S. K. (2018). Intrusion Detection Using Machine Learning: A Comparison Study. *International Journal of Pure and Applied Mathematics, 118*(19), 101-114.

[4] Çavuşoğlu, U. (2019). A new hybrid approach for intrusion detection using machine learning. *Applied Intelligence, https://doi.org/10.1007/s10489-018-01408-x, 49*, 1-27.

[5] G. Dong et al. (2019). DB-Kmeans:An Intrusion Detection Algorithm Based on DBSCAN and K-means. *2019 20th Asia-Pacific Network Operations and Management Symposium (APNOMS), DOI: 10.23919/APNOMS.2019.8892910* (pp. 1-4). Matsue, Japan: IEEE.

[6] G. Logeswari, S. Bose and T. Anitha. (2023). An Intrusion Detection System for SDN Using Machine Learning. *Intelligent Automation & Soft Computing, DOI: 10.32604/iasc.2023.026769, 35*(1), 867-880.

[7] Hongyu Liu and Bo Lang. (2019). Machine Learning and Deep Learning Methods for Intrusion Detection Systems: A Survey. *Appl. Sci., Doi:10.3390/app9204396, 9*(4396), 1-28.

[8] Kaushik, S., Bhardwaj, A., Almogren, A. et al. (2025). Robust machine learning based Intrusion detection system using simple statistical techniques in feature selection. *Sci Rep, DOI: https://doi.org/10.1038/s41598-025-88286-9, 15*(3970), 1-10.

[9] M. Asif, S. Abbas, M.A. Khan et al. (2022). MapReduce based intelligent model for intrusion detection using machine learning technique. *Journal of King Saud University - Computer and Information Sciences, https://doi.org/10.1016/j.jksuci.2021.12.008, 34*(10), 9723–9731.

[10] M. N. Chowdhury and K. Ferens, M. Ferens. (2016). Network Intrusion Detection Using Machine Learning. *Int'l Conf. Security and Management, Proceedings of The 2016 World Congress in Computer Science, Computer Engineering,* (pp. 30-36). WorldComp 2016 Proceedings.

[11] N. A. Putri et al. (2017). Denial of service attack visualization with clustering using K-means algorithm. *2017 International Conference on Electrical Engineering and Computer Science (ICECOS), DOI: 10.1109/ICECOS.2017.8167129* (pp. 177-183). Palembang, Indonesia: IEEE.

[12] Naveen Saran, Nishtha Kesswani. (2023). A comparative study of supervised Machine Learning classifiers for Intrusion Detection in Internet of Things. *Procedia Computer Science, https://doi.org/10.1016/j.procs.2023.01.181, 218*, 2049–2057.

[13] Nitesh V Chawla et al. (2002). SMOTE: Synthetic Minority Over-sampling Technique. *Journal of Artificial Intelligence Research, https://doi.org/10.1613/jair.953, 16*(1), 2-4.

[14] O. Faker, E. Dogdu. (2019). Intrusion Detection Using Big Data and Deep Learning Techniques. *ACM Southeast Conference – ACMSE 2019* (pp. 86-94). Kennesaw, GA, USA: Long Papers – ISBN: 978-1-4503-6251-1.

[15] Othman et al. (2018). Intrusion detection model using machine learning algorithm on Big Data environment. *Othman et al. J Big Data, https://doi.org/10.1186/s40537-018-0145-4, 5*(34), 1-12.

[16] P. Sangkatsanee et al. (2011). Practical real-time intrusion detection using machine learning approaches. *Computer Communications, https://doi.org/10.1016/j.comcom.2011.07.001, 34*(18), 2227–2235.

[16] Q. H. Vu, D. Ruta and L. Cen. (2019). Gradient boosting decision trees for cyber security threats detection based on network events logs. *2019 IEEE International Conference on Big Data (Big Data), DOI: 10.1109/BigData47090.2019.9006061* (pp. 5921-5928). Los Angeles, CA, USA: IEEE.

[17] Qiong Gu et al. (2016). An Improved SMOTE Algorithm Based on Genetic Algorithm for Imbalanced Data Collection. *Journal of Digital Information Management (JDIM), 14*(2), 4-6.

[18] Reham Amin et al. (2023). A Hybrid Extreme Gradient Boosting and Long Short-Term Memory Algorithm forCyber Threats Detection. *MENDEL— Soft Computing Journal, https://doi.org/10.13164/mendel.2023.k.307, 29*(2), 307-322.

[19] S. A. Repalle, V. R. Kolluru. (2017). Intrusion Detection System using AI and Machine Learning Algorithm. *International Research Journal of Engineering and Technology (IRJET), , 04*(12), 1709-1716.

[20] T. Arora, M. Sharma and S. K. Khatri. (2019). Detection of Cyber Crime on Social Media using Random Forest Algorithm. *2019 2nd International Conference on Power Energy, Environment and Intelligent Control (PEEIC), doi: 10.1109/PEEIC47157.2019.8976474* (pp. 47-51). Greater Noida, India: IEEE.

[21] T.Saranya et al. (2020). Performance Analysis of Machine Learning Algorithms in Intrusion. *Procedia Computer Science, https://doi.org/10.1016/j.procs.2020.04.133, 171*, 1251–1260.

[22] Y. Y. Aung and M. M. Min. (2017). An analysis of random forest algorithm based network intrusion detection system. *2017 18th IEEE/ACIS International Conference on Software Engineering, Artificial Intelligence, Networking and Parallel/Distributed Computing (SNPD), DOI: 10.1109/SNPD.2017.8022711* (pp. 127-132). Kanazawa, Japan: IEEE.

[23] Yasmeen S. Almutairi et al. (2022). Network Intrusion Detection Using Machine Learning Techniques. *Advances in Science and Technology Research Journal, 16*(3), 193–206.

EVALUATION OF YOLO MODELS FOR MILITARY AIRCRAFT DETECTION AND CLASSIFICATION

Mahmut SAĞLIYAN[a*], Sait Ali UYMAZ[b]

[a] *Cappadocia University, Faculty of Computer and Information Technologies, Department of Software Development, Ürgüp / Nevşehir, Türkiye*

[b] *Konya Technical University, Faculty of Computer and Information Sciences, Department of Computer Engineering, Konya, Türkiye*

A B S T R A C T

Object detection is one of the most important tasks in computer vision and remote sensing and is often accomplished using deep learning algorithms. It has many application areas such as object detection, autonomous vehicles, security system, medical imaging, industrial automation and defense industry. As a result of technological developments, it has increasingly more areas of use. With the wide range of these usage areas and the recent developments in deep learning algorithms, object detection studies are becoming increasingly important. Performance evaluation of rapidly developing algorithms on large data sets is also becoming an important problem. Convolutional Neural Networks (CNN) based algorithms are generally used to solve this problem. In this study, the performances of YOLOv5n, YOLOv5s, YOLOv6n, YOLOv6s, YOLOv8n and YOLOv8s models, which are versions of YOLO, a CNN-based algorithm, were analyzed using the military aircraft detection data set. According to the mAP50, mAP50-95, precision and recall values determined as performance metrics, the model that gave the best results was the YOLOv8s model. The fastest working models are YOLOv5 models.

K E Y W O R D S

- Deep learning
- Object Detection
- YOLO

* Corresponding author: Mahmut SAĞLIYAN
E-mail: mahmut.sagliyan@kapadokya.edu.tr

1. Introduction

Machine Learning (ML) is a subfield of Artificial Intelligence (AI) that focuses on the scientific study of algorithms and statistical models designed to perform specific tasks without the need for explicit instructions, and is commonly used in the field of data mining. In recent years, Machine Learning has become increasingly significant for individuals working in areas such as text mining, image classification, video recommendations, social network analysis, user-oriented recommendation systems, and object detection through images and videos, as studies in these fields continue to grow [1]. Consequently, the development of Deep Learning (DL) algorithms, which form a subset of Machine Learning, has also accelerated. There has been a rise in the number of deep learning algorithms frequently used in areas such as computer vision, speech recognition, natural language processing, and medical image analysis. Particularly due to advancements in the defense industry, object detection has become increasingly important. The accurate and effective detection of an aircraft in an image brings various challenges, such as the aircraft's color, size, aspect ratio, orientation, and complex backgrounds [2].

Object detection is an important and challenging issue. Most traditional object detection approaches use Haar-like detectors, and the use of these detectors leads to some problems such as the learning process becoming more difficult when working with larger datasets or the detection of false alarms [3]. The Gabor filter used in image feature extraction can be given as input to the Support Vector Machine (SVM) algorithm and can be used to perform operations such as recognizing complex patterns from image data. However, since the parameter selection of the Gabor filter can vary depending on the application and image type, modern deep learning-based algorithms are preferred for object detection. The optical flow method is also generally not applicable in real-time systems due to its low computational efficiency [4]. Deep learning algorithms are used to prevent this and similar problems. Features can be automatically extracted from images using deep learning models. Various studies have been conducted in this area due to the ability of CNN-based object detectors used for this purpose to automatically detect objects [5]. Deep learning models based on CNNs fall into two categories: single-stage detectors and two-stage detectors. Single-stage detectors perform detection directly using a regression method and operate faster than two-stage detectors; however, their object detection accuracy is lower compared to two-stage detectors. Models such as YOLO and RetinaNet can be given as examples of single-stage detectors. Two-stage detectors such as R-CNN and Fast R-CNN, on the other hand, offer higher object detection accuracy but operate more slowly in terms of speed [6]. Convolutional Neural Networks (CNNs) demonstrate successful performance in managing large amounts of data simultaneously, as well as providing enhanced or optimized classification by considering the textural, spatial, and spectral features of images [7]. In this way, issues encountered when using traditional algorithms, such as handling big data and determining threshold values, are also minimized.

Performance criteria such as model speed and object detection accuracy for real-time object detection are becoming increasingly important today. The YOLO algorithm [8], which has recently become popular as a research topic in the academic field, stands as an important area requiring further study to overcome the challenges encountered in traditional machine learning algorithms and achieve both fast and accurate results.

The YOLO model, which recently entered our lives, has undergone rapid development. This development has been driven by recent technological advances in various fields, such as autonomous driving [9], facial recognition [10], and target detection for military use. With the increasing importance of real-time object detection, various models of the CNN-based YOLO have emerged very quickly. In this article, I analyze the performance of different YOLO versions: YOLOv5s, YOLOv6s, YOLOv8s, YOLOv5n, YOLOv6n, and YOLOv8n, using a military aircraft dataset.

The overall contribution of the study is the performance evaluation of YOLO versions in the detection of military aircraft and the classification of detected aircraft.

2. Literature Review

2.1. Traditional Methods

Traditional methods used for object detection in the past frequently included approaches such as histogram-based methods [11], feature-based methods [12], local feature-based methods [13], thresholding and region labeling [14], template matching [15], and object detection based on the geometric information of target objects [16]. These methods do not possess an algorithm as well-developed as the deep learning algorithms used in object detection today to define prior knowledge. Algorithms created using these methods may lead to an unacceptable number of false positives, especially in complex images. Machine learning algorithms such as SVM, K-Nearest Neighbors (KNN), and AdaBoost can also be given as examples of traditional methods.

2.2. Deep Learning Based Methods

In recent years, due to the rapidly increasing number of object detection studies, the number of deep learning algorithms has also grown in parallel. Some deep learning algorithms that yield more successful results in object detection compared to traditional methods are as follows: R-CNN, Fast R-CNN, and Faster R-CNN. These techniques, which use two-stage detectors, provide highly successful results in object detection [17]. Methods such as SSD, RetinaNet, and EfficientNet can also be given as examples of deep learning-based approaches. Single-stage methods transform the object detection task into a simpler process by modeling detection as a regression problem. Since single-stage detectors consider object detection as a regression problem, they are referred to as regression-based methods [18]. Two-stage detectors, on the other hand, perform region-based object detection [19].

Since YOLO is a regression-based method, it treats object detection as a regression problem. It performs object detection and classification tasks by analyzing the image in a single pass. This is a feature that makes it faster than other methods and suitable for real-time applications. It divides the image into a grid, and each grid cell predicts the probabilities of belonging to specific classes as well as the coordinates of the bounding boxes of the objects [20].

3. Materials and Methods

3.1 Methods Used İn Object Detection

In this study, transfer learning was used to enable the model to learn more quickly and effectively, and the s and n versions of the YOLOv5, YOLOv6, and YOLOv8 series were compared with one another for object detection. The YOLO series is a single-stage object detector that uses independent logistic classifiers and generates multi-label bounding boxes. The first YOLO model written in PyTorch was YOLOv5. PyTorch is a Python-based open-source deep learning framework that provides a set of functions and tools for defining, training, and deploying models. YOLOv5 and YOLOv8 offer users different model options such as n, s, m, l, and x. In YOLOv6, however, the x model is not available. Each of these models offers different detection sensitivity levels and performance.

3.2. Dataset

The dataset used for training was obtained from Kaggle, a public platform where people interested in data science and machine learning come together. Our dataset is a military aircraft recognition dataset [21]. It contains 3842 images annotated with horizontal and oriented bounding boxes, 20 types of remote sensing imagery, and 22341 examples. Before being used for training the YOLO algorithms, the dataset underwent preprocessing. Twenty-one images were removed from the dataset because they did not contain any object labels. A total of 3821 images were studied. The xml files in the original dataset were converted to txt files for use in YOLO algorithms. During this conversion, the center coordinates (x, y), width, and height of the bounding box were normalized between 0 and 1. The content of the txt file is as follows: (object class label, x point, y point, width, height). Each object in the file consists of five parameters. These parameters correspond to an object in the image. Following these operations, the dataset was split into 80% training and 20% test data. 3056 images were used as the training set, and 765 images were used as the test set.

3.3 Education Process

Training was conducted in the Google Colab environment using a T4 GPU. The images contained a total of 20 different class types. The training process was performed using a transfer learning approach using pre-trained weights provided by the YOLO developers. The parameters for all training sessions were as follows:

- Size (Pixels): 640
- Batch Size: 16
- Epoch: 30

3.4. Evaluation Parameters

To compare the performance of the YOLO series versions, metrics such as mAP, precision and recall were used.

Precision is calculated by dividing the number of true positives (TP) by the total number of predicted positives. A high precision value indicates that most of the objects predicted as positive by the model are indeed correct.

Recall is calculated by dividing the number of true positives (TP) by the number of actual positives (TP + FN). A high recall value indicates that the model correctly identifies a large portion of the actual objects.

mAP represents the average of the average precision values of all classes. It is the mean Area Under the Precision-Recall Curve (AUC). Higher mAP values indicate better overall performance.

mAP50 (with an IoU threshold of 0.5) and mAP50-95 (with IoU thresholds ranging from 0.5 to 0.95) are used to evaluate the feasibility and accuracy of YOLO series models. In previously published studies, the definitions of these parameters have been explained in more detail [22].

4. Research Results and Discussion

4.1. Performance Evaluation

To evaluate the performance of the training process, 30 epochs of training were conducted for each model. Because the dataset contained 3821 images and more than 22,000 aircraft objects belonging to 20 types, successful results were achieved for each model within 30 epochs. The values obtained from the training results for the different YOLO models are shown in Table 1.

Table 1. Performance evaluation of all models

Model	*mAP50*	*mAP50-95*	*Precision*	*Recall*	*Training duration*
YOLOv5n	0.8626	0.6495	0.803	0.8536	30 min
YOLOv5s	0.9818	0.7691	0.9529	0.9586	34 min 13 sec
YOLOv6n	0.8773	0.6567	-	-	1h 30 min 18 sec
YOLOv6s	0.9735	0.7558	-	-	1 h 32 min 8 sec
YOLOv8n	0.9819	0.7882	0.9529	0.956	54 min 24 sec
YOLOV8s	0.9906	0.8164	0.9767	0.9757	56 min 51 sec

When we examine the results in Table 1, the YOLO model with the highest detection capability after training was the YOLOv8s model. Its mAP50 value was found to be 0.9906 and its mAP50-95 value was 0.8164. When evaluating the model's success rate based on the mAP50 value, a high accuracy rate of 99.06% was achieved. Based on the mAP50 value, the performance ranking of the models after YOLOv8s is as follows: YOLOv8n 98.19%, YOLOv5s 98.18%, YOLOv6s 97.35%, YOLOv6n 87.73%, and YOLOv5n 86.26. These results indicate that the YOLOv8 series provides a higher detection sensitivity rate compared to other YOLO versions. Although the success percentages of all models decrease when considering the mAP50-95 values, the ranking between the algorithm versions remains the same as the ranking based on mAP50 values.

When we look at the completion times of the model trainings, the fastest models were the YOLOv5n and YOLOv5s series, which completed training in 30 minutes and 34 minutes 13 seconds, respectively. The slowest models were YOLOv6s and YOLOv6n from the YOLOv6 series. The YOLOv8 series completed training in approximately 55 minutes. Although the YOLOv8 series provided a better detection accuracy rate than the YOLOv5 series, its training time performance was lower compared to YOLOv5 models. The YOLOv6 series, when compared to the other models based on both mAP values and training time, showed the lowest performance.

Models are being compared through an elimination-based evaluation according to their performance. So far, when considering object detection sensitivity rate and speed, the YOLOv6 model falls behind the other models. Therefore, the next evaluations will be conducted between the YOLOv5 and YOLOv8 models. The confidence curves of the YOLOv5s, YOLOv5n, YOLOv8s, and YOLOv8n models are shown in Figures (1–4).

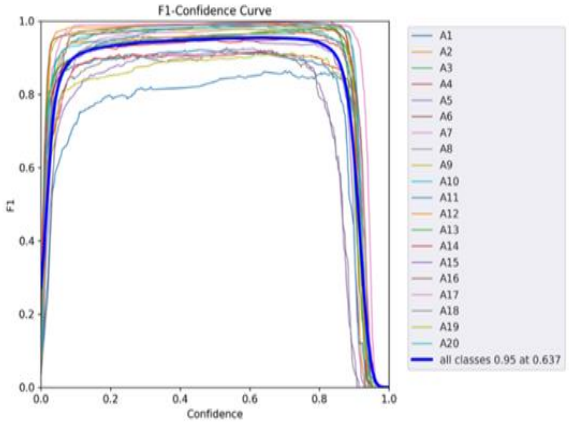

Fig. 1. YOLOv5s Confidence Curve

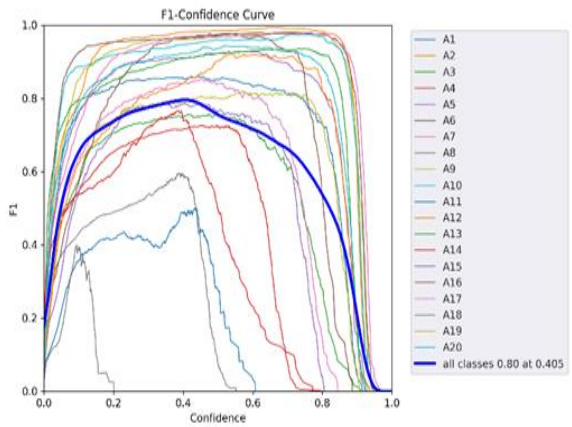

Fig. 2. YOLOv5n Confidence Curve

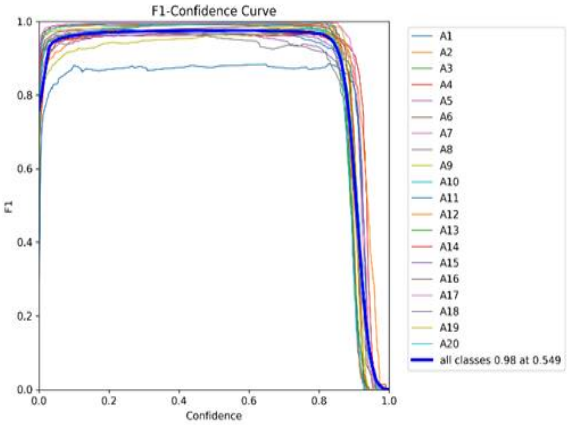

Fig. 3. YOLOv8s Confidence Curve

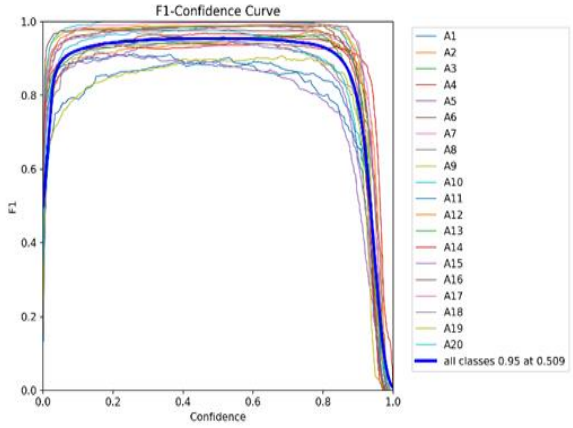

Fig. 4. YOLOv8n Confidence Curve

The confidence curve graph is a visualization that shows the confidence levels of the objects detected by YOLO. YOLO uses a window to scan an image and divides this window into subregions. Each subregion focuses on a specific object class. YOLO attempts to detect one or more objects in each subregion and generates a confidence score for each detected object.The confidence score represents the likelihood that an object has been correctly detected. It has a value between 0 and 1; the closer it is to 1, the higher the reliability of the detection.

According to the results of this graph, the confidence curve of YOLOv5n showed high variability across classes and exhibited poor performance. YOLOv8s outperformed the other models in terms of confidence score. YOLOv8n and YOLOv5s demonstrated similar confidence scores, as observed from the graph. The model with the lowest confidence score was YOLOv5n. Based on these results, among the models compared using the military aircraft detection dataset, the YOLOv8 series is ahead of the others in terms of performance. The results of the

performance metrics for YOLOv8n and YOLOv8s are given in Figures 5 and 6. Table 2 presents the loss values belonging to the training set.

Table 2. YOLOv8n and YOLOv8s loss values

Model	*box_loss*	*cls_loss*	*df1_loss*
YOLOv8n	0.768	0.5033	0.9499
YOLOv8s	0.6704	0.3236	0.9196

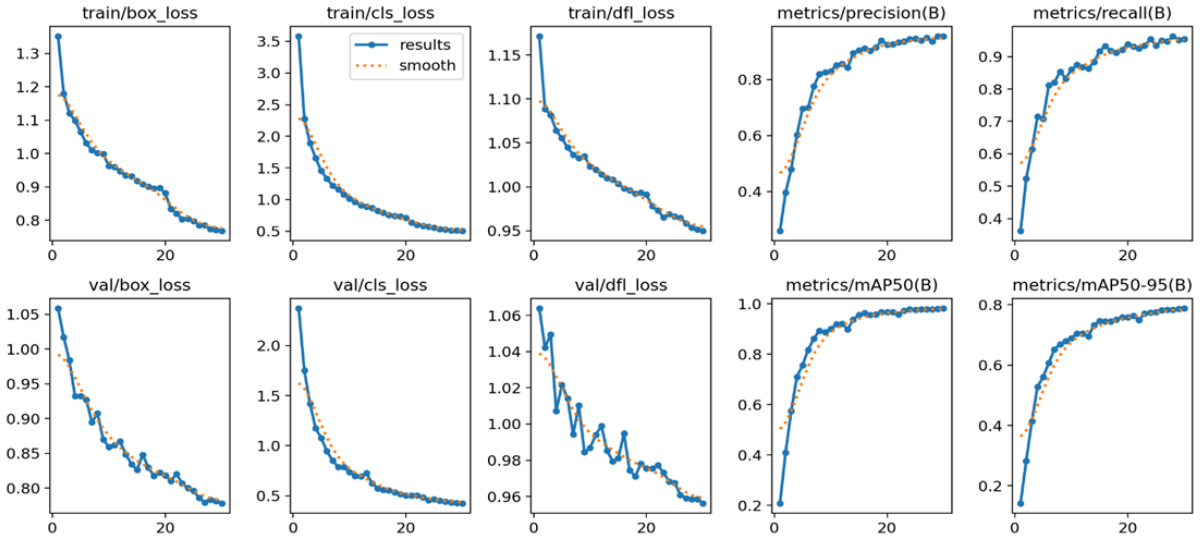

Fig. 5. Performance metrics resulting from YOLOv8n aircraft detection

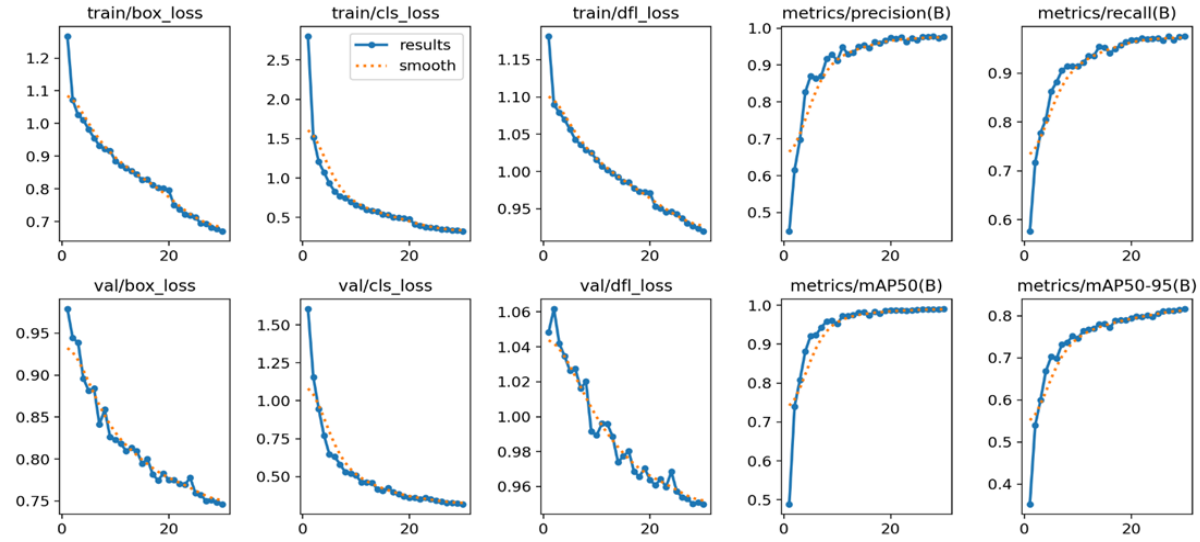

Fig. 6. Performance metrics resulting from YOLOv8s aircraft detection

Comparison of the box_loss, cls_loss, and dfl_loss parameters shown in Table 2 reveals that YOLOv8s has lower loss values than YOLOv8n for all compared loss parameters. A lower loss value indicates that it learned the object detection task better during training and has a better generalization ability.

4.2. Object Detection Results from Images

After the training process, the results of the prediction process using the test data set for all object classes of the YOLOv8s model are shown in Table 3.

Table 3. YOLOv8s model summary

Class	*Image*	*Instance*	*Precision*	*Recall*	*mAP50*	*mAP50-95*
All	765	4482	0.977	0.976	0.991	0.816
A1	765	245	0.983	0.955	0.992	0.826
A2	765	308	0.993	0.997	0.993	0.808
A3	765	228	0.958	0.998	0.991	0.798
A4	765	155	0.984	0.968	0.987	0.864
A5	765	244	0.979	0.952	0.992	0.752
A6	765	85	0.981	0.988	0.995	0.818
A7	765	181	0.988	1	0.995	0.833
A8	765	213	0.993	1	0.995	0.848
A9	765	230	0.988	1	0.995	0.817
A10	765	222	0.996	0.995	0.995	0.821
A11	765	93	0.901	0.86	0.953	0.816
A12	765	127	0.992	0.991	0.993	0.826
A13	765	449	0.967	0.982	0.993	0.787
A14	765	391	0.965	0.962	0.991	0.821
A15	765	138	0.97	0.964	0.989	0.717
A16	765	466	0.993	0.989	0.994	0.832
A17	765	225	0.994	1	0.995	0.901
A18	765	76	0.96	0.945	0.989	0.828
A19	765	192	0.949	0.978	0.992	0.808
A20	765	214	0.998	0.991	0.995	0.806

According to the results in Table 3, 765 test image data and 4482 object samples were used in the evaluation of the YOLOv8s model. According to the object classification results, the best predicted class according to mAP50 and mAP50-95 values is A17. The lowest predicted class according to mAP50 is A11. According to mAP50-95 values, it is class A15.

Images of the aircraft detected in the image as a result of training using the YOLOv8s model are shown in Figure 7a, Figure 7b, and Figure 7c. The images were taken from the test set.

Fig. 7a. Test Image

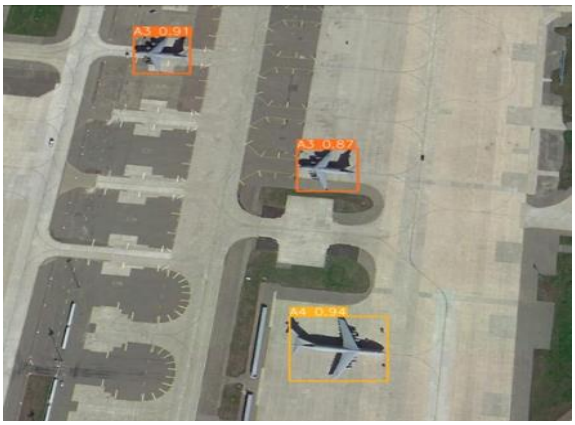

Fig. 7b. Test Image

Fig. 7c. Test Image

5. Conclusion

This study evaluated six different YOLO models—YOLOv5n, YOLOv5s, YOLOv6n, YOLOv6s, YOLOv8n, and YOLOv8s—for classifying 20 different aircraft types. The comparison results revealed that YOLOv8s outperformed the other YOLO models in performance metrics such as mAP50, mAP50-95, precision, and recall. YOLOv5n and YOLOv5s demonstrated good performance in terms of speed. The YOLOv6 models, however, were both slower and—despite their longer training time—failed to deliver the level of performance expected from such lengthy training.

When the goal is to shorten training time while still achieving an acceptable level of performance, the YOLOv5s model stands out as a suitable choice. However, if the objective is to obtain higher accuracy in object detection and more precise classification results, the YOLOv8s model becomes the more appropriate option. Therefore, the key determining factor in model selection is the nature of the expected outcomes of the study and the performance metrics corresponding to those outcomes. In other words, the model should be selected based on the metrics that align with the intended purpose of the training process.

References

[1] Antwi-Boasiako, E., Zhou, S., Liao, Y., Liu, Q., Wang, Y., & Owusu-Agyemang, K. (2021). Privacy preservation in Distributed Deep Learning: A survey on Distributed Deep Learning, privacy preservation techniques used and interesting research directions. Journal of Information Security and Applications, 61, 102949.

[2] Azam, B., Khan, M. J., Bhatti, F. A., Maud, A. R. M., Hussain, S. F., Hashmi, A. J., & Khurshid, K. (2022). Aircraft detection in satellite imagery using deep learning-based object detectors. Microprocessors and Microsystems, 94, 104630.

[3] LIENHART, Rainer; MAYDT, Jochen. An extended set of haar-like features for rapid object detection. In: Proceedings. international conference on image processing. IEEE, 2002. p. I-I.

[4] Wei, Y., Tian, Q., Guo, J., Huang, W., & Cao, J. (2019). Multi-vehicle detection algorithm through combining Harr and HOG features. Mathematics and Computers in Simulation, 155, 130-145.

[5] GIRSHICK, Ross, et al. Rich feature hierarchies for accurate object detection and semantic segmentation. In: Proceedings of the IEEE conference on computer vision and pattern recognition. 2014. p. 580-587.

[6] Qi, W. (2022). Object detection in high resolution optical image based on deep learning technique. Natural Hazards Research, 2(4), 384-392.

[7] Ajayi, O. G., Ashi, J., & Guda, B. (2023). Performance evaluation of YOLO v5 model for automatic crop and weed classification on UAV images. Smart Agricultural Technology, 5, 100231.

[8] REDMON, Joseph, et al. You only look once: Unified, real-time object detection. In: *Proceedings of the IEEE conference on computer vision and pattern recognition*. 2016. p. 779-788.

[9] AL-QIZWINI, Mohammed, et al. Deep learning algorithm for autonomous driving using googlenet. In: 2017 IEEE intelligent vehicles symposium (IV). IEEE, 2017. p. 89-96.

[10] BALABAN, Stephen. Deep learning and face recognition: the state of the art. Biometric and surveillance technology for human and activity identification XII, 2015, 9457: 68-75.

[11] Huang, C. R., Chen, C. S., & Chung, P. C. (2008). Contrast context histogram—An efficient discriminating local descriptor for object recognition and image matching. Pattern Recognition, 41(10), 3071-3077.

[12] Pavani, S. K., Delgado, D., & Frangi, A. F. (2010). Haar-like features with optimally weighted rectangles for rapid object detection. Pattern Recognition, 43(1), 160-172.

[13] Zhou, H., Yuan, Y., & Shi, C. (2009). Object tracking using SIFT features and mean shift. Computer vision and image understanding, 113(3), 345-352.

[14] Lu, C., Adluru, N., Ling, H., Zhu, G., & Latecki, L. J. (2010). Contour based object detection using part bundles. Computer Vision and Image Understanding, 114(7), 827-834.

[15] Weber, J., & Lefèvre, S. (2012). Spatial and spectral morphological template matching. Image and Vision Computing, 30(12), 934-945.

[16] Huertas, A., & Nevatia, R. (1988). Detecting buildings in aerial images. Computer vision, graphics, and image processing, 41(2), 131-152.

[17] Tong, Z., Hedayatrasa, S., Cheng, L., Pei, C., Chen, Z., Xie, S., & Kersemans, M. (2023). An efficient parametrized optical infrared thermography 3D finite element framework for computer vision applications. NDT & E International, 135, 102787.

[18] YI, Jingru; WU, Pengxiang; METAXAS, Dimitris N. ASSD: Attentive single shot multibox detector. *Computer Vision and Image Understanding*, 2019, 189: 102827.

[19] ZHAO, Zhong-Qiu, et al. Object detection with deep learning: A review. *IEEE transactions on neural networks and learning systems*, 2019, 30.11: 3212-3232.

[20] TERVEN, Juan; CÓRDOVA-ESPARZA, Diana-Margarita; ROMERO-GONZÁLEZ, Julio-Alejandro. A comprehensive review of yolo architectures in computer vision: From yolov1 to yolov8 and yolo-nas. *Machine learning and knowledge extraction*, 2023, 5.4: 1680-1716.

[21] Khlaifia Bilel. (2022). Military Aircraft Recognition dataset [Dataset].Kaggle.https://doi.org/10.34740/KAGGLE/DS/2495046

[22] Sokolova, M., & Lapalme, G. (2009). A systematic analysis of performance measures for classification tasks. Information processing & management, 45(4), 427-437.

ERP-INTEGRATED IOT FRAMEWORK: REAL-TIME PROCESS TRACKING, QUALITY ASSURANCE, AND QR-BASED TRACEABILITY FOR SMART MANUFACTURING

Erkan BEKDEMİR[a*], Sinem SELÇUK[a*], Onur İlyas YAVUZ[a], Hakkı SOY[b]

[a] *Demsay Elektronik A.Ş., R&D Center, 34520, Beylikdüzü, İstanbul*

[b] *N. Erbakan University, Electrical and Electronics Engineering Department, 42090, Konya*

A B S T R A C T

The transition to Industry 5.0 demands production systems that ensure efficiency, resilience, and human-centric traceability. This study presents an IoT-enabled smart manufacturing framework integrated with ERP systems for the real-time collection and analysis of data from production devices. Continuous acquisition of machine and sensor data supports process optimization and compliance with international standards. The framework tracks each production stage, identifies inefficiencies, and automatically halts operations when required approvals are missing, preventing defective products from advancing. A QR-code-based traceability layer links each product to its ERP record, enabling end-to-end monitoring of production history, quality control, and documentation. By combining device-level data acquisition, ERP integration, and automated quality assurance with human oversight, the proposed system provides a scalable and practical pathway for SMEs to digitalize their manufacturing lines in line with Industry 5.0 principles.

K E Y W O R D S

- Digital Transformation
- ERP Integration
- IoT
- Industry 4.0
- Digital Twin

1. Introduction

With the transition from Industry 4.0 to Industry 5.0, the manufacturing sector has adopted new paradigms that emphasize not only automation and efficiency but also human-centricity, resilience, and sustainability [1,2]. In this transformation, digital technologies such as the Internet of Things (IoT), Cyber-Physical Systems (CPS), and data analytics form the foundation of intelligent and adaptive production environments. Within this context, enabling Enterprise Resource Planning (ERP) systems to acquire real-time data from production devices has become essential for transparent and traceable manufacturing [3,4]. Although IoT and Manufacturing Execution Systems (MES) are widely adopted, small and medium-sized enterprises still face challenges such as fragmented data architectures and limited visibility across production lines. Because most systems operate independently, achieving a unified view of production performance, quality metrics, and compliance remains difficult [3].

Existing research on IoT-based monitoring and ERP–MES integration primarily focuses on data collection or visualization [3, 5, 6]. However, studies achieving full ERP–IoT integration with automated quality control and QR-based traceability are still limited [7,8]. This gap restricts the scalability of smart manufacturing, particularly in environments requiring compliance and human oversight. This study proposes an integrated ERP–IoT framework to address these challenges. The developed structure enables direct communication between production devices and enterprise systems, ensuring continuous data collection, automated process verification, and event-driven control. The architecture also incorporates quality checkpoints and traceability data throughout the product life cycle [7,8]. The main contributions of this study include the design and implementation of a scalable ERP–IoT integration architecture for real-time production monitoring, the incorporation of a QR-based traceability mechanism linking physical products with ERP records, and the demonstration of automated quality control processes aligned with Industry 5.0 principles [1, 2].

2. Materials and Methods

The proposed ERP–IoT framework enables the collection of real-time data from electronic production devices and the automatic synchronization with the ERP system. Designed with a modular and layered architecture, it ensures continuous data flow between IoT hardware, communication protocols, and enterprise software. This structure supports effective production management through traceability, quality control, and data-driven decision support.

At the device layer, ESP32-based IoT modules were integrated into pick-and-place, SPI, AOI, and reflow oven to collect parameters such as processing time, error rate, and downtime. Designed for industrial use, the modules provide stable wireless communication and long-term reliability.

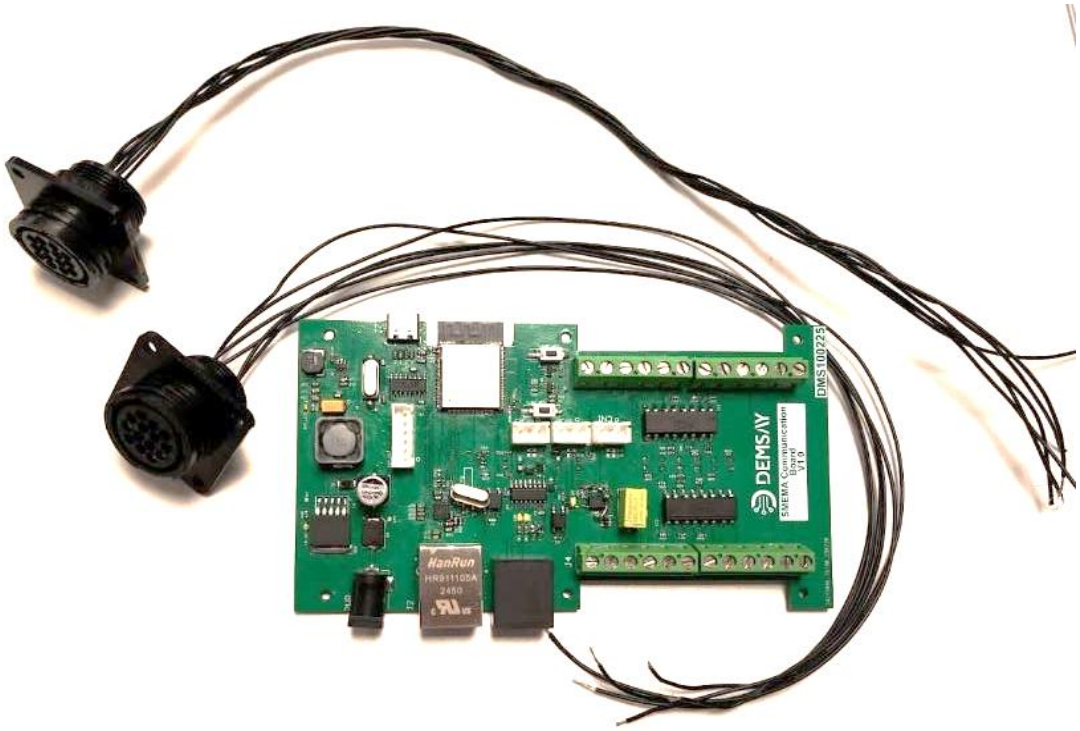

Figure 1. Hardware structure of the ESP32-based IoT module and industrial SMEMA interface.

Collected data are transmitted to a central server via the MQTT protocol with encryption, then preprocessed and transferred to the ERP through a REST API. Within our ERP application, a Real-Time Monitoring Module automatically records operations, halts processes when quality approval is missing, and notifies supervisors. This configuration enhances system visibility and minimizes manual intervention, consolidating production and quality data into a single, integrated platform.

Each IoT module is built around an ESP32-WROOM-32 microcontroller featuring a dual-core 240 MHz CPU, integrated Wi-Fi (802.11 b/g/n), Bluetooth BLE, and an optional Ethernet interface for wired network connectivity. The hardware includes 512 kB SRAM, 4 MB Flash memory, optically isolated SMEMA-compatible digital I/O, and onboard EEPROM for configuration storage. The modules operate from a 5 V DC industrial-grade supply with surge protection and support OTA firmware updates, ensuring maintainability and reliability under factory conditions.

Each product or PCB is assigned a unique QR code at the start of production, containing essential details such as materials, test results, and quality approvals. After each stage, the code is scanned or automatically recorded in the ERP, enabling end-to-end product tracking. This mechanism ensures process-level quality assurance and supply chain transparency, allowing direct verification of product history during audits and early detection of manufacturing-related quality issues.

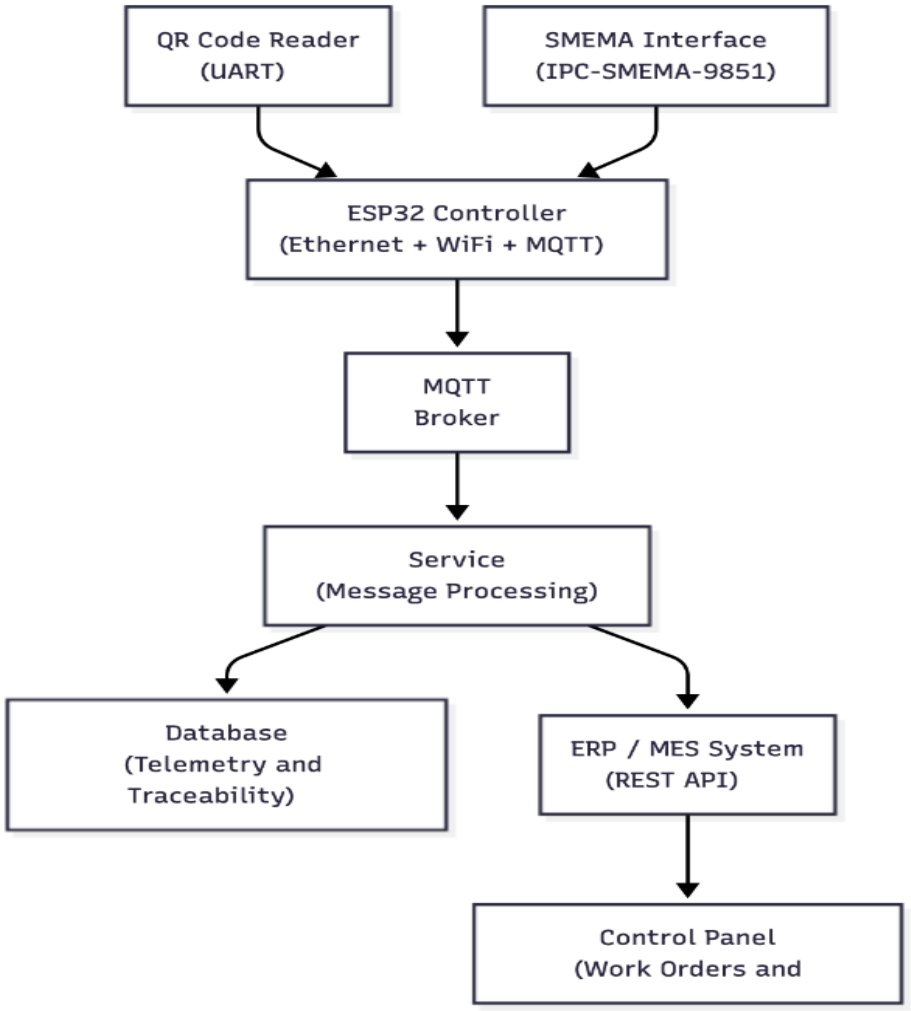

Figure 2. ERP–IoT system architecture.

The system was tested on the SMT-2 production line at Demsay Elektronik. The production process includes solder paste printing, SPI, pick-and-place, reflow soldering, and AOI stages (Figure 3). In the test setup, ESP32-based IoT modules were integrated into each machine to record process times, error rates, and operational states in real time.

Figure 3. Process sequence of the SMT-2 production line.

Figure 4. Demsay Elektronik SMT-2 production line.

Devices communicated via SMEMA connectors, where digital signals indicated machine and board status. The overall system configuration, connection layout, and hardware integration are shown in Figures 1–5. Data were transmitted via MQTT and synchronized with the ERP through REST API, providing real-time monitoring of production performance. Tests confirmed stable operation under industrial conditions. No data loss was observed during multiple test cycles, and latency measurements remained within acceptable limits, validating the compatibility and reliability of the ERP–IoT framework. A typical production cycle was completed in about seven and a half minutes.

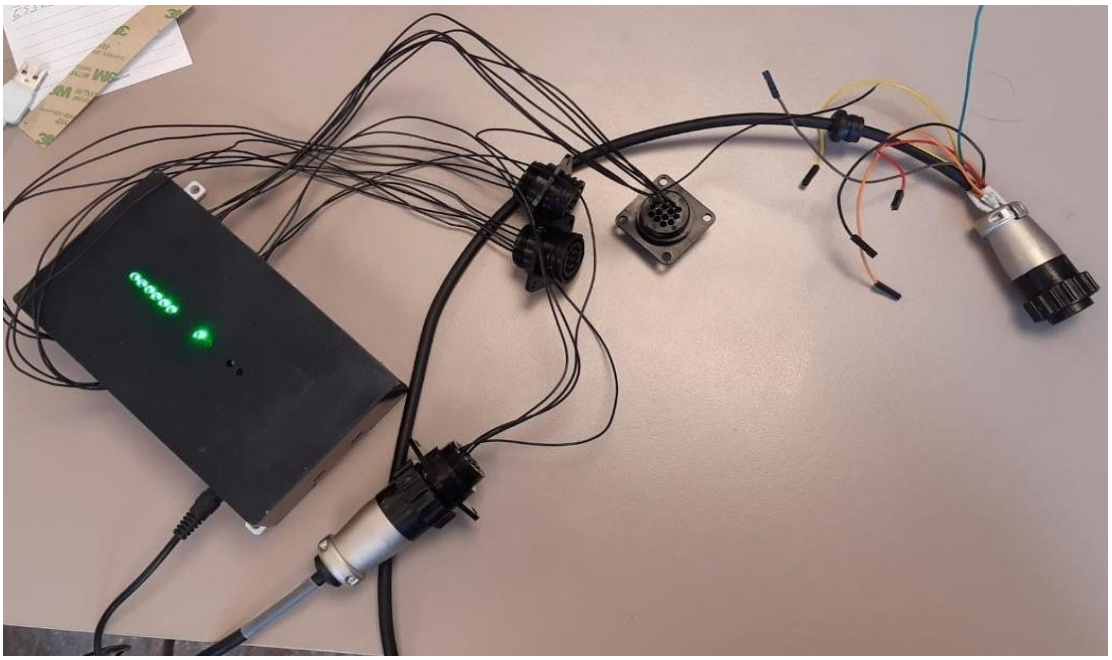

Figure 5. Test configuration: Connection layout of the IoT module, SMEMA connectors, and signal cables.

Figure 6. Physical integration of the IoT module into SMT machines and SMEMA signal lines.

3. Research Findings and Discussion

The developed ERP–IoT system was tested under real production conditions to evaluate data accuracy, communication stability, and integration performance. Analysis of timestamped machine data confirmed that the system operated reliably on the SMT production line, continuously recording downtime events, their duration, and transmitting them to the ERP in real-time. The average network transmission latency was 420 ms, and the ERP data synchronization time was 2.3 s, which is adequate for near real-time monitoring needs. During initial trials, a delay was detected at the SPI stage, resulting in idle periods in the pick-and-place units. After optimizing panel configuration and alignment parameters, the total production cycle time improved by approximately 3%. These results, summarized in Table 1, demonstrate that the system not only records production data but also actively supports efficiency improvements through real-time feedback. Overall, the ERP–IoT integration enabled the objective identification of bottlenecks and the immediate verification of corrective actions, providing a scalable, traceable, and decision-support-oriented framework in alignment with Industry 5.0 principles. These measurements are summarized in Table 1.

Table 1. Comparison of SMT-2 production line processing times before and after improvement.

Process Stage	*Before Improvement (Seconds)*	*After Improvement (Seconds)*
Loader (Input)	5	5
Printer	12	9
SPI	5	4
Pick And Place (1)	18	20
Pick And Place (2)	22	20
Reflow Oven	300	300
AOI	33	25
Loader (Output)	5	6
Total Time	400	389

4. Conclusion

This study presented an ERP–IoT integration system that enables real-time collection and synchronization of production data across electronic manufacturing lines. The integrated approach enhanced process visibility, traceability, and decision support, establishing a validated foundation for digital transformation in the electronics production industry. Field tests under industrial conditions demonstrated stable operation and a 3% improvement in production cycle

time, confirming the system's capability to support process optimization and efficiency. Direct ERP integration eliminated manual entry errors and automated quality approvals, while the QR-based traceability structure unified production history and quality data, simplifying audits and compliance. The proposed framework offers a scalable and practical solution for small and medium-sized manufacturers, aligning with Industry 5.0 principles by strengthening human–machine collaboration and fostering data-driven, adaptive production environments. Future work will focus on AI-based analytics and predictive maintenance to enhance operational efficiency and promote sustainable manufacturing practices.

Acknowledgment

This study was supported by the Demsay Elektronik R&D Center.

References

[1] Hein-Pensel, F., Winkler, H., Brückner, A., Wölke, M., Jabs, I., Mayan, I. J., Kirschenbaum, A., Friedrich, J., & Zinke-Wehlmann, C. (2023). *Maturity assessment for Industry 5.0: A review of existing maturity models. Journal of Manufacturing Systems,* 66, 200–210. https://doi.org/10.1016/j.jmsy.2022.09.013

[2] European Commission. (2021). *Industry 5.0: Towards a sustainable, human-centric and resilient European industry.* Publications Office of the European Union. https://doi.org/10.2777/308407

[3] Kunkulagunta, M. (2024). *IoT-based enterprise resource planning: Challenges, open issues, applications, and architecture analysis. International Journal of Artificial Intelligence & Machine Learning,* 3(1), 91–101. https://doi.org/10.11648/j.ijaial.20240301.16

[4] Kim, J., Seo, D., Moon, J., Kim, J., Kim, H., & Jeong, J. (2022). *Design and implementation of an HCPS-based PCB smart factory system for next-generation intelligent manufacturing. Applied Sciences,* 12(15), 7645. https://doi.org/10.3390/app12157645

[5] Wicaksono, A. A., Ningsih, Y. K., & Surjati, I. (2024). *Implementation of MQTT protocol on ESP32-based OEE analysis development board. MITOR: Jurnal Teknik Elektro,* 24(2), 169–175. https://doi.org/10.25077/mitor.24.2.169-175.2024

[6] Maroșan, A., Constantin, G., Gîrjob, C. E., Chicea, A. L., Crenganiș, M., & Morariu, F. (2024). *Real-time data acquisition with ESP32 for IoT applications using open-source MQTT brokers. Proceedings in Manufacturing Systems,* 19(2), 61–68.

[7] Benatia, K., Remadna, A., Baudry, D., Delalin, L., & Halftermeyer, F. (2018). *QR-code enabled product traceability system: A big data perspective.* In *Proceedings of the 8th International Conference on Manufacturing Engineering and Processes* (pp. 122–128). IOS Press. https://doi.org/10.3233/978-1-61499-898-3-122

[8] Schuitemaker, R., & Xu, X. (2020). *Product traceability in manufacturing: A technical review. Procedia CIRP,* 93, 700–705. https://doi.org/10.1016/j.procir.2020.04.101

SELECTION OF BATTERY COOLING SYSTEM FOR ELECTRIC VEHICLES USING MULTI CRITERIA DECISION MAKING

Mehmet ARIKAN[a*], İnci SARIÇİÇEK[b,a] , Sinem BOZKURT KESER[c], Silvia DELBONO[d], Ali KAFALI[e], Ahmet YAZICI[c,a]

[a] *Center of Intelligent Systems Applications Research, Eskişehir Osmangazi University, Address: Prof. Dr. Nabi Avcı Bul., 26480, Eskişehir, Turkiye*

[b] *Industrial Engineering, Faculty of Engineering and Architecture, Eskişehir Osmangazi University, Address: Prof. Dr. Nabi Avcı Bul., 26480, Eskişehir, Turkiye*

[c] *Computer Engineering, Faculty of Engineering and Architecture, Eskişehir Osmangazi University, Address: Prof. Dr. Nabi Avcı Bul., 26040, Eskişehir, Turkiye*

[d] *Flash Battery Srl, Address: Via XXV Aprile Ovest, 23/A, 42049, Sant'Ilario d'Enza (RE), Italy*

[e] *ACD Veri Mühendisliği, Address: Prof. Dr. Nabi Avcı Bul., 26480, Eskişehir, Turkiye*

ABSTRACT

The Battery Management System (BMS) is critical for the safe and efficient operation of electric vehicles (EVs). Insufficient cooling at elevated battery temperatures can lead to capacity loss, performance degradation, and serious safety risks. For this reason, decision makers need to select suitable battery cooling systems. This study proposes multi criteria decision making model to select a battery cooling system for BMS. Based on criteria such as technical adequacy, economic feasibility, and operational suitability battery cooling alternatives such as air cooling, direct liquid cooling, indirect liquid cooling, phase change material (PCM) cooling, and heat pipe systems are ranked using the Analytical Hierarchy Process. In this study, commonly employed battery cooling alternatives are compared with each other using AHP's pairwise comparisons. The results indicated that direct liquid cooling emerged as the most suitable alternative with its technical superiority. Indirect liquid cooling is ranked second, primarily for its balance of applicability and performance. Heat pipe systems are identified as a promising option in terms of technical efficiency. PCM and air-cooling systems, when applied independently, are identified as low-cost alternatives suitable for applications with light cooling requirements.

KEYWORDS

- Analytical hierarchy process
- Battery cooling
- BTMS
- Electric vehicles

* Corresponding author:
E-mail:

1. Introduction

Thermal stability in battery systems has become an important subject with the increasing use of electric vehicles (EVs). The effect of temperature is critical for battery performance, lifespan, and safety [1]. In situations where effective cooling performance is not achieved, overheating may lead to capacity loss, performance degradation, and even safety risks such as thermal runaway [2], [3]. For this reason, selecting the right battery cooling system is crucial and should be evaluated based on multiple criteria to ensure appropriate decision-making.

Studies on decision-making for Battery Thermal Management Systems (BTMS) have presented various approaches. In the study of Dwivedi et al., (2022), an approach was proposed to determine the most suitable nanoparticle to improve battery cooling system performance by using a hybrid Multi Criteria Decision Making (MCDM) method [4]. The authors also developed a decision-making method using multiple decision-making techniques for nanoparticle selection, while incorporating designer preferences [5]. In the study of Xu et al., (2023), a comprehensive evaluation of direct and indirect liquid cooling battery cooling systems was conducted [6]. Each system was evaluated based on multiple criteria such as thermal performance, cost, and safety, using the Analytical Hierarchy Process (AHP), an MCDM method.

Upon reviewing the literature, only a limited number of studies addressed the multi-criteria evaluation of battery thermal systems, and no comprehensive evaluation of battery cooling systems has been observed. This study provides EV manufacturers and battery designers with a methodological and holistic roadmap for their decision-making processes by enabling the systematic analysis of different cooling technologies using a multi-criteria approach, AHP. Using the AHP, criteria were selected based on technical adequacy, economic feasibility, and operational suitability, and pairwise comparisons were made between air cooling, direct liquid cooling, indirect liquid cooling, phase change material (PCM) cooling, and heat pipe system alternatives. In this regard, the most prominent alternatives for battery cooling systems were evaluated.

The structure of this paper is as follows. Section 2 provides explanations about the different cooling methods used in BTMS, the criteria to be evaluated and the AHP method. Section 3 presents the results and discussion. Finally, Section 4 concludes the study.

2. Material and Methods

2.1 Battery Thermal Management Systems

The Battery Management System (BMS) is a critical component responsible for the safety and performance of EV battery packs. The BMS performs multiple functions, including thermal management, cell balancing, power management, charge and discharge control, state estimation, data acquisition, battery prediction, fault detection, and diagnostics [7]. Among these functions, thermal management ensures that battery cells operate within their optimal temperature range. This subsystem, called the BTMS, maintains temperature uniformity by

preventing battery cells from overheating or becoming too cold. This avoids adverse conditions that could arise from inadequate thermal control.

The subsections that follow describe the main cooling methods used in BTMS: air cooling, indirect and direct liquid cooling, phase change material (PCM), and heat pipe systems.

a. Air Cooling

Air cooling is a method with a wide range of applications and stands out for its ease of application. It can be divided into two types: natural convection cooling and forced convection cooling. In natural convection, cooling is achieved by natural air convection. In forced convection, airflow is generated using mechanical equipment to increase heat transfer [1]. Air cooling offers advantages such as low cost, simple construction, and ease of maintenance, but it also has drawbacks such as limited cooling capacity and slow cooling rate [8]. For this reason, it is generally applied in battery packs with low cooling requirements [9].

b. Liquid Cooling

Liquid cooling removes heat from battery cells using liquids with high thermal capacity. It has been shown to be highly effective in maintaining temperature control during fast charging and high discharge conditions [10]. There are two types: direct and indirect. Direct liquid cooling uses dielectric fluids that come into direct contact with the cells. Indirect liquid cooling involves the circulation of coolant through plates surrounding the cells without direct contact. The direct method provides higher thermal performance due to its low thermal resistance, but it can be complex and costly because of sealing and insulation requirements [11]. The indirect method is widely adopted in industrial EV applications owing to its ease of implementation and lower cost [12]. Overall, liquid cooling is regarded as one of the most effective technologies for high-energy-density battery packs.

c. Phase Change Material

Phase Change Materials (PCMs) operate by absorbing heat and undergoing a phase transition. Their advantages include low cost, easy installation, simple structure, high cooling capacity, and the ability to provide uniform temperature distribution [13]. However, low thermal conductivity and the risk of leakage are regarded as their main disadvantages [14]. PCMs that provide passive cooling experience a significant reduction in effectiveness once the material is fully melted. For this reason, they are often used in combination with active cooling systems in most studies [15].

d. Heat Pipe

Heat pipe systems transport heat from one location to another by means of an operating fluid through a cycle of evaporation and condensation. Their advantages include high efficiency, thermal conductivity, and flexible design; however, they also have disadvantages such as complex structure, leakage risk, and high cost [16]. Studies have shown that passive heat pipe systems can be effective in battery modules [13], [17].

2.2 Criteria for Selecting Battery Cooling Systems

The evaluation battery cooling systems should consider not only technical performance but also factors such as economic feasibility and operational suitability. In the literature, thermal factors are reported as the most prominent criteria from a technical perspective, and their effects on safety and performance have been emphasized [6]. Economic factors have also been identified as key elements determining the applicability of these systems [4]. In addition, operational factors are considered important in terms of applicability and ease of maintenance [18].

The aim of this study is to select the most suitable battery cooling system for EVs from among the available alternatives. The set of criteria established for this selection, covering technical, economic, and operational factors, is presented in Table 1.

Table 1. Criteria set

Criteria Code	*Criteria*	*Criteria Categorization*
C1	Annual Cost	Economic
C2	Ease of integration	Operational
C3	Heat transfer rate	Technical
C4	Initial cost of setup	Economic
C5	Life	Operational
C6	Maintenance of system	Operational
C7	Simplicity of use	Operational
C8	Temperature distribution	Technical
C9	Temperature drop	Technical

By considering technical, economic, and operational factors, alternatives such as air cooling, indirect liquid cooling, direct liquid cooling, PCM, and heat pipe are evaluated.

2.3 Analytical Hierarchy Process

Studies on engineering design and energy systems optimisation demonstrate that the selection of a technical solution is rarely dependent on a single criterion; rather, it requires balancing multiple objectives that may conflict with one another [19], [20], [21]. This situation also applies to the selection of battery cooling systems, requiring multiple criteria to be considered in the decision-making process. Various methods have been proposed in the literature for multi-criteria decision-making [22], [23]. In this study, the AHP is applied, which can evaluate different criteria together and systematically advance the decision-making process [24].

AHP is a method that makes multi-criteria decisions in terms of relative importance. The decision-maker defines the problem in terms of objectives, criteria, and alternatives, and compares the elements pairwise on a 1–9 scale, as shown in Table 2.

Table 2. Relative importance scale

Relative Importance	*Scale*
Equally important	1
Slightly more important	3

Important	5
Very Important	7
Extremely Important	9
Intermediate values	2,4,6,8

Using the values provided in Table 2, pairwise comparison matrices defining the relative importance of the criteria are created. The column totals of these matrices are calculated, and each cell is normalised by dividing it by its column total. The row averages of the normalized matrix provide the priority vectors for the criteria and alternatives. The local priority score of each alternative under the relevant criterion is multiplied by the weight of that criterion and summed across criteria to obtain the overall score. The alternatives are ranked according to scores, and the option with the highest score is selected. Consistency is subsequently checked using a Consistency Ratio (CR) calculation to assess whether the judgements are reasonable. For acceptable consistency, the CR threshold should be below 0.10. The AHP pairwise comparison matrices are constructed for the criteria and alternatives, and the entries are scored based on expert opinions.

3. Experimental Results

This section presents the AHP results obtained for the selection problem of EV battery cooling systems. Criterion weights are derived from pairwise comparisons based on expert opinions for the nine identified criteria. Pairwise comparisons are made by a group of decision makers that included an expert from a battery manufacturer and an electrical and electronics engineer. The cooling alternatives are then evaluated using AHP with respect to the selected criteria. The criterion priority scores determined from this evaluation are presented in Table 3. The consistency ratio (CR < 0.1) confirmed that the pairwise comparisons are within the acceptable consistency threshold.

Table 3. Priority scores and rankings for criteria

Rank	*Criteria Code*	*Criteria*	*Priority scores*
1	C8	Temperature distribution	0.25667
2	C3	Heat transfer rate	0.21494
3	C5	Life	0.17074
4	C9	Temperature drop	0.10516
5	C2	Ease of integration	0.07853
6	C6	Maintenance of system	0.06655
7	C7	Simplicity of use	0.03871
8	C1	Annual cost	0.03435
9	C4	Initial cost of setup	0.03435

Table 3 shows that temperature distribution emerged as the most critical factor among the criteria. Heat transfer rate and life followed in second and third place, respectively. This order

of priority indicates that technical and operational criteria carry greater importance in the selection of a battery cooling system.

The cooling system alternatives are compared through pairwise comparisons for each criterion. The radar charts in Fig 1 illustrate the impact of each criterion on the alternatives. The percentage value of each battery cooling system for a specific criterion represents the relative strength of its performance compared to the other alternatives for the criterion.

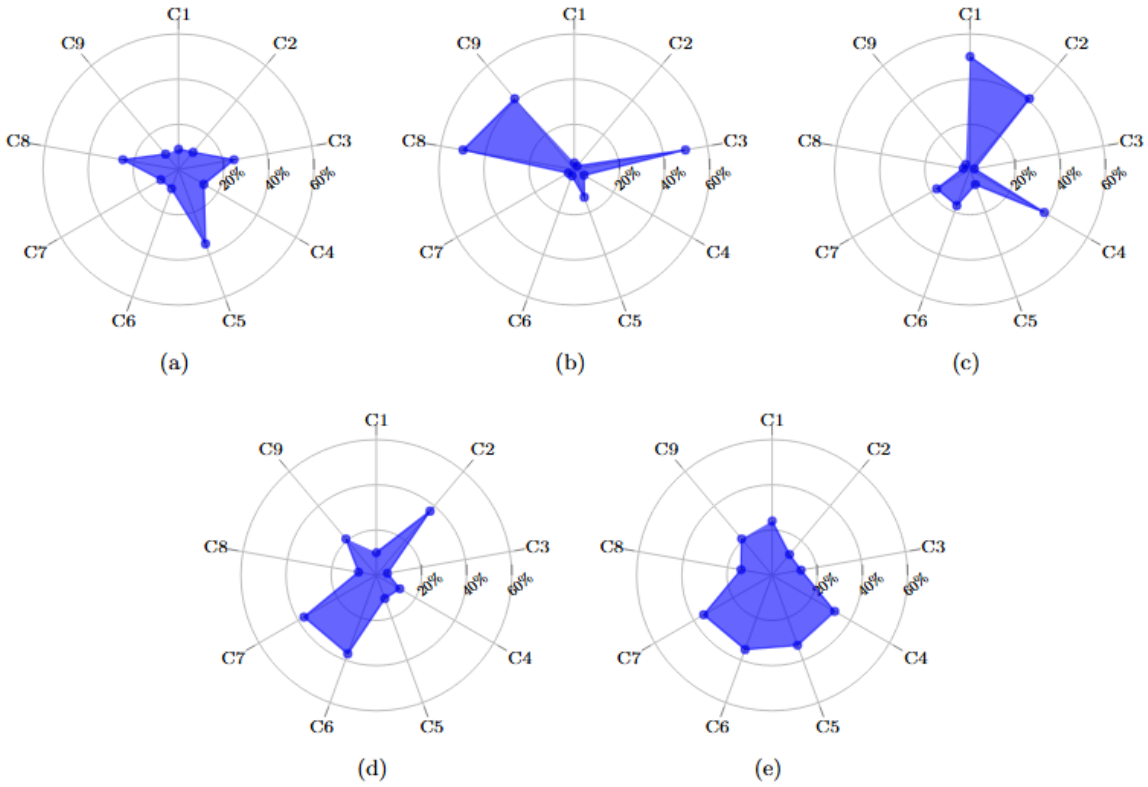

Fig. 1. The impact of criteria on alternatives: (a) Indirect liquid cooling; (b) Direct liquid cooling; (c) Air cooling; (d) PCM; (e) Heat pipe.

Radar chart for battery cooling systems shown in Figure 1 (a) indicates that indirect liquid cooling stands out in criteria including temperature distribution, life and heat transfer rate. In Figure 1 (b), temperature distribution, heat transfer rate, and temperature drop effects the selection of direct liquid cooling alternatives. In Figure 1 (c), significative criteria are initial cost of setup, annual cost, and ease of integration for air cooling systems. In Figure 1 (d), simplicity of use, maintenance of the system and ease of integration are important for PCM. In Figure 1 (e), initial cost of setup, life, maintenance of system, annual cost, and simplicity of use are the prominent criteria for heat pipe systems. This analysis revealed the criteria that influence the selection of each cooling technology. The priority of these criteria may vary from the perspective of the decision-maker.

The AHP results are summarised in Table 4, where the priority scores of all battery cooling system alternatives are presented. Based on the pairwise comparison judgements of the

decision-makers, the most suitable cooling system among the alternatives is determined in the AHP results (Table 4).

Table 4. Priority scores and rankings for alternatives

Alternative	*Priority Score*	*Rank*
Direct liquid cooling	0.31806	1
Indirect liquid cooling	0.21275	2
Heat Pipe	0.20899	3
PCM	0.14976	4
Air cooling	0.11044	5

As shown in Table 4, direct liquid cooling is determined to be the most suitable cooling system among all alternatives, achieving the highest overall score. The primary reason for this result is that the system demonstrates superior performance in the most heavily weighted criteria. High-scoring criteria such as heat transfer rate, temperature distribution, and temperature drop demonstrate that this system delivers strong technical performance. When economic and operational criteria are also taken into account, direct liquid cooling emerges as the most strategically advantageous solution for battery cooling systems.

The consistency of all pairwise comparison matrices are verified using the CR calculation. All matrices exhibited acceptable consistency ratios below the 0.10 threshold. This confirms both the reliability of the judgements and the validity of the AHP results.

The results largely correspond with the literature and actual EV applications. Studies in this field mention indirect liquid cooling as having high potential due to its strong thermal control and efficiency, particularly under increasing performance requirements, while also noting that it remains the industry standard because of its applicability and reliable performance [25], [26]. Direct liquid cooling is employed in the 2016 BMW i3, whereas indirect liquid cooling is used in the Chevrolet Volt, Tesla Model S, Tesla Model 3, and several BMW models [11], [27], [16]. Air cooling is preferred in applications with low cooling requirements because of its low cost and simple structure; however, it is reported that it cannot meet the cooling needs of high-power batteries [26]. Its efficiency is significantly lower compared to liquid cooling [11], [16], and it is mainly applied in EVs with modest cooling requirements, such as the Nissan Leaf and Toyota Prius Prime [16]. PCMs are reported to be mainly in the experimental stage, and although they offer advantages such as low cost and passive cooling, their performance may decrease at high temperatures; thus, they are typically used in combination with supporting systems [16], [26]. Heat pipes, on the other hand, have been highlighted as providing effective cooling by directly contacting the battery surface, owing to their high thermal conductivity and flexible structure [16].

4. Conclusion

In this study, five cooling alternatives for EV battery cooling systems are compared using the AHP method, by considering criteria from technical, economic, and operational perspectives. The direct liquid cooling system outperforms other alternatives for criteria such as heat transfer

rate, temperature distribution, and temperature drop. This result highlights the efficiency advantage provided by direct liquid cooling in high-power applications. However, the indirect liquid cooling system, ranked second, stands out as an important alternative due to its reliable performance and widespread use in the industry. Although heat pipe systems exhibit a strong profile in terms of operational and technical performance, they are suitable for supporting or hybrid solutions. PCM and air cooling, despite their low cost and structural simplicity advantages, are insufficient in applications requiring strict temperature control. The findings reveal that multiple factors should be considered together when selecting a battery cooling system, providing a scientifically grounded decision-making tool. Future studies may also evaluate hybrid cooling systems, and the accuracy and practical validity of the results can be strengthened through studies supported by experimental data.

Acknowledgment

Funding: This study is supported by the OPEVA project, which has received funding within the Chips Joint Undertaking (Chips JU) from the European Union's Horizon Europe Programme and the National Authorities (France, Belgium, Czechia, Italy, Portugal, Turkey, Switzerland), under grant agreement 101097267. The views and opinions expressed are, however, those of the author(s) only, and do not necessarily reflect those of the European Union or the Chips JU. Neither the European Union nor the granting authority can be held responsible for them. This work is supported by the Scientific and Technical Research Council of Turkey (TUBITAK), Contract No 222N269, project title: "OPtimization of Electric Vehicle Autonomy (OPEVA)".

References

[1] Wang, X., et al. (2022). A review of the power battery thermal management system with different cooling, heating and coupling system. *Energies*, 15(6), 1963. MDPI.

[2] Karthik, C. A., Kalita, P., Cui, X., & Peng, X. (2020). Thermal management for prevention of failures of lithium ion battery packs in electric vehicles: A review and critical future aspects. *Energy Storage*, 2(3), e137.

[3] Liu, H., Wei, Z., He, W., & Zhao, J. (2017). Thermal issues about Li-ion batteries and recent progress in battery thermal management systems: A review. *Energy Conversion and Management*, 150, 304–330.

[4] Dwivedi, A., Kumar, A., & Goel, V. (2022). Selection of nanoparticles for battery thermal management system using integrated multiple criteria decision-making approach. *International Journal of Energy Research*, 46(15), 22558–22584.

[5] Dwivedi, A., Kumar, A., & Goel, V. (2023). A consolidated decision-making framework for nano-additives selection in battery thermal management applications. *Journal of Energy Storage*, 59, 106565.

[6] Xu, J., Guo, Z., Xu, Z., Zhou, X., & Mei, X. (2023). A systematic review and comparison of liquid-based cooling system for lithium-ion batteries. *eTransportation*, 15, 100242.

[7] Waseem, M., Ahmad, M., Parveen, A., & Suhaib, M. (2023). Battery technologies and functionality of battery management system for EVs: Current status, key challenges, and future prospectives. *Journal of Power Sources*, 580, 233349.

[8] Al-Zareer, M., Dincer, I., & Rosen, M. A. (2018). A review of novel thermal management systems for batteries. *International Journal of Energy Research*, 42(12), 4095–4115.

[9] Olabi, A. G., et al. (2022). Battery thermal management systems: Recent progress and challenges. *International Journal of Thermofluids*, 15, 100171.

[10] Chen, S., et al. (2022). Multi-objective optimization design and experimental investigation for a parallel liquid cooling-based lithium-ion battery module under fast charging. *Applied Thermal Engineering*, 211, 118503.

[11] Anisha, & Kumar, A. (2023). Identification and mitigation of shortcomings in direct and indirect liquid cooling-based battery thermal management system. *Energies*, 16(9), 3857. MDPI.

[12] Rahman, M. A., et al. (2025). Energy sources and thermal management technologies for electric vehicle batteries: A technical review. *Global Challenges*, 9(1), e00083.

[13] Yu, Z., Zhang, J., & Pan, W. (2023). A review of battery thermal management systems about heat pipe and phase change materials. *Journal of Energy Storage*, 62, 106827.

[14] Kim, J., Oh, J., & Lee, H. (2019). Review on battery thermal management system for electric vehicles. *Applied Thermal Engineering*, 149, 192–212.

[15] Ling, Z., et al. (2014). Review on thermal management systems using phase change materials for electronic components, Li-ion batteries and photovoltaic modules. *Renewable and Sustainable Energy Reviews*, 31, 427–438.

[16] Moghadasi, M., Zarnoush, M., Esmaeilion, F., Radman, G., & Soltani, M. (2025). Advancements and challenges in battery thermal management technologies for electric vehicles: A systematic navigation on the latest trends. *Results in Engineering*, 19, 105830.

[17] Zhang, Z., & Wei, K. (2020). Experimental and numerical study of a passive thermal management system using flat heat pipes for lithium-ion batteries. *Applied Thermal Engineering*, 166, 114660.

[18] Abdelkareem, M. A., et al. (2022). Battery thermal management systems based on nanofluids for electric vehicles. *Journal of Energy Storage*, 50, 104385.

[19] Mardani, A., et al. (2017). A review of multi-criteria decision-making applications to solve energy management problems: Two decades from 1995 to 2015. *Renewable and Sustainable Energy Reviews*, 71, 216–256.

[20] Taherdoost, H., & Madanchian, M. (2023). Multi-criteria decision making (MCDM) methods and concepts. *Encyclopedia*, 3(1), 77–87.

[21] Sahoo, S. K., Pamucar, D., & Goswami, S. S. (2025). A review of multi-criteria decision-making (MCDM) applications to solve energy management problems from 2010–2025: Current state and future research. *Spectrum of Decision Making and Applications*, 2(1), 219–241.

[22] Tzeng, G.-H., & Huang, J.-J. (2011). Multiple attribute decision making: Methods and applications. *CRC Press*.

[23] Opricovic, S., & Tzeng, G.-H. (2004). Compromise solution by MCDM methods: A comparative analysis of VIKOR and TOPSIS. *European Journal of Operational Research*, 156(2), 445–455.

[24] Saaty, T. L. (2013). Analytic hierarchy process. In S. I. Gass & M. C. Fu (Eds.), *Encyclopedia of operations research and management science* (pp. 52–64). Springer.

[25] Tong, B., et al. (2025). Comprehensive comparison study on battery thermal management modules with indirect and direct liquid cooling. *Applied Thermal Engineering*, 268, 125945.

[26] Garud, K. S., Tai, L. D., Hwang, S. G., Nguyen, N. H., & Lee, M. Y. (2023). A review of advanced cooling strategies for battery thermal management systems in electric vehicles. *Symmetry*, 15(7), 1322. MDPI.

[27] Yang, S., et al. (2021). Essential technologies on the direct cooling thermal management system for electric vehicles. *International Journal of Energy Research*, 45(15), 6775–6795.

FUNCTIONAL IOT BOARD DESIGN USING WIRED AND WIRELESS COMMUNICATION INFRASTRUCTURE

Samet AYDIN[a*], Onur İlyas YAVUZ[a] , Hakkı SOY[b]

a Demsay Elektronik, R&D Center, 34000, İstanbul, Türkiye

b Necmettin Erbakan University, Electrical and Electronics Engineering Department, 42090, Konya, Türkiye

ABSTRACT

This study presents a functional IoT design that integrates wired and wireless communication infrastructures on the same board. The designed board serves as a flexible platform for data collection, processing, and transfer to different networks from field devices. The architecture emphasizes reliability, multi-protocol support, and compatibility with different power sources for industrial applications. The wired side supports Ethernet and serial-based industrial protocols, while the wireless side covers Wi-Fi, Bluetooth, cellular networks, and low-power wide-area networks. The input/output layer handles both analog and digital signals and is compatible with industry-standard 4–20 mA sensors. The power architecture operates with external supplies as well as PoE and USB, making the system easily adaptable to diverse scenarios. As a result, the developed IoT board provides reliable, fast, and flexible integration opportunities in fields such as agriculture, healthcare, smart homes, logistics, and industry.

KEYWORDS

- IoT
- Wired Communication
- Wireless Communication
- Industrial Applications
- Multi-Protocol
- Smart Systems.

* Corresponding author:
E-mail: **s.aydin@demsay.com**

1. Introduction

The Internet of Things (IoT) is the collection of technologies that enable devices to communicate with each other and with central systems to share data. Today, it is widely used in fields such as industry, healthcare, agriculture, smart cities, and logistics. The most important advantage of IoT devices is their ability to support different protocols and communication standards simultaneously, providing users with freedom in scenario design.

IoT technologies contribute significantly to digital transformation by enabling real-time data collection, monitoring, and control in diverse environments. In industrial applications, IoT platforms are used for predictive maintenance and machine-to-machine communication, minimizing downtime and improving production efficiency. In agriculture, IoT-based irrigation and soil monitoring systems optimize water consumption and increase crop yield. In healthcare, wearable and remote monitoring devices help track vital parameters, while in logistics, smart sensors ensure asset tracking and environmental monitoring of transported goods. These applications demonstrate that IoT systems not only provide automation but also offer data-driven decision-making support that enhances operational reliability and sustainability.

In particular, low-power wide-area networks such as LoRaWAN stand out for their energy efficiency [1]. Studies in the literature show that multi-protocol communication infrastructures increase the scalability and reliability of systems [3,6].
In this study, a functional IoT board that combines wired and wireless communication infrastructures on a single board has been designed. The board offers users a modular structure for different scenarios, and its compatibility with industrial protocols creates a wide range of applications in the market.

2. MATERIALS AND METHODS

In this section, the general system architecture of the IoT board developed is explained, consisting of hardware and software components. The system is built on a modular architecture and designed to be scalable according to different application requirements. The board consists of a central control unit surrounded by wired and wireless communication modules, sensor input/output layers, power management circuits, and service and maintenance infrastructure. With this structure, the system offers a flexible platform that can be used in various fields such as industrial automation, agricultural monitoring, environmental data collection, and healthcare technologies. During the design process, reliable communication, low power consumption, and a high level of integration were determined as primary objectives. While wired communication units provide long-distance and high data rate transmission, wireless technologies offer wide coverage and mobility. The sensor layer enhances the versatility of the system by supporting the measurement of various physical parameters. The power management and service/maintenance components ensure that the system is long-lasting, sustainable, and easily updatable.

2.1 System General Architecture

The IoT board consists of a central controller, wired communication, wireless communication, sensor input/output layer, power management, and service and maintenance blocks. The design is modular and can be configured according to user requirements. The virtual image of the card's hardware is shown by Figure 1.

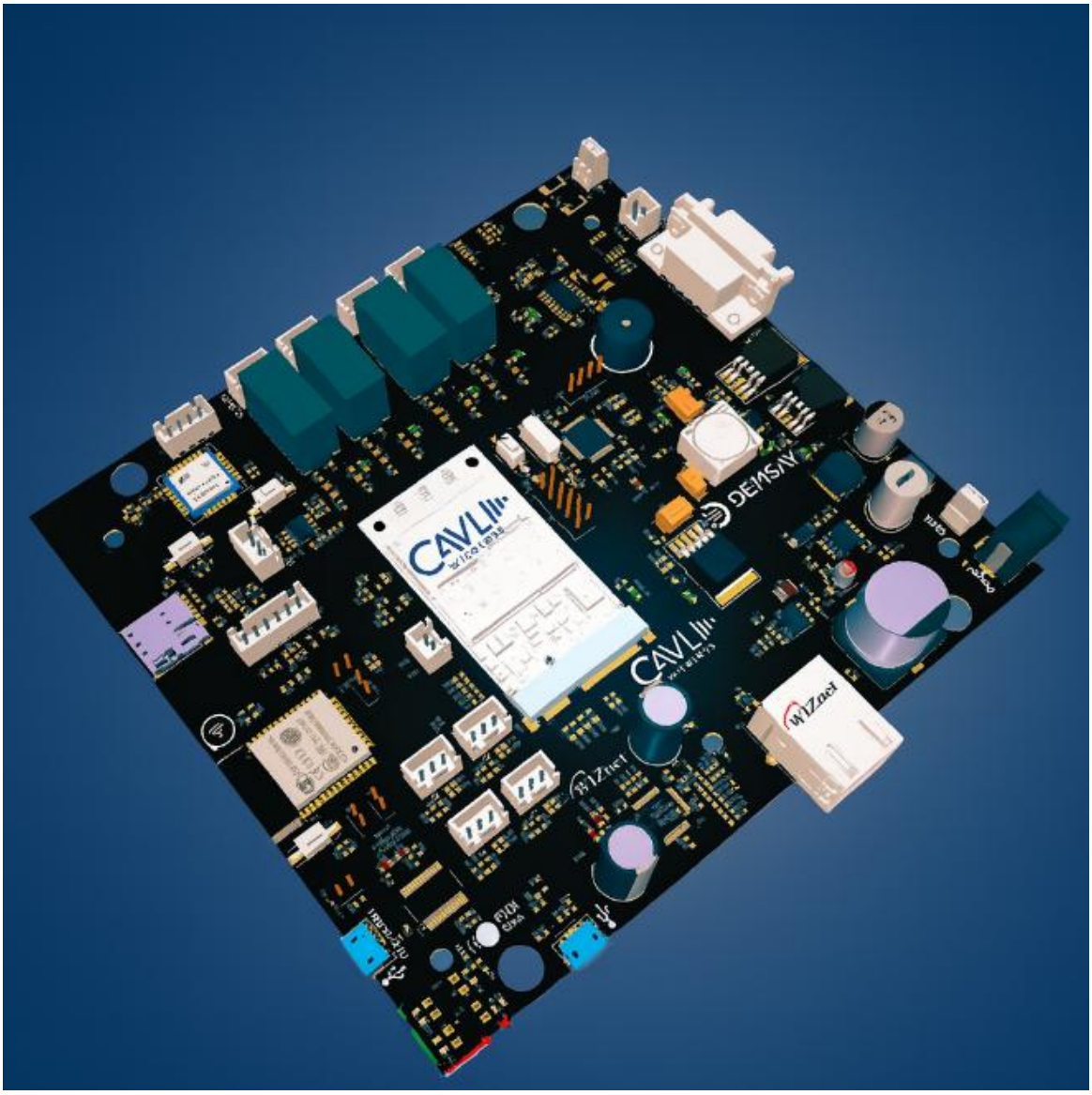

Fig. 1. Virtual view

2.2 Wireless Communication

Wi-Fi and Bluetooth are used for short-range applications, while cellular connectivity and LoRaWAN are utilized for wide-area applications. According to the literature, LoRaWAN technology provides low power consumption and long-range communication but presents certain challenges in scalability [1, 2]

2.3 Wired Communication

High-bandwidth data transmission is provided via Ethernet, long-distance industrial communication is supported through RS-485/Modbus, simple device connections are enabled via RS-232, and CAN bus communication is available for vehicle and automation systems. As stated in the literature, this allows the board to be adapted for a wide range of applications, from industrial facilities to agricultural irrigation stations [3,6].

2.4 Sensor Utilization

The system is developed to support the integration of a wide variety of sensors. Parameters such as temperature, humidity, and pressure are read through voltage-based inputs. Motion detectors, magnetic contacts, or buttons can be connected directly. It can be used in applications such as soil moisture measurement in agriculture, pressure/flow monitoring in industry, and medical pressure sensors in healthcare. Loads such as motors, pumps, and valves can be driven directly. This structure enables the system to be directly applicable across different sectors.

2.5 Power Management

A wide input range of 12–40 V is supported, along with 5V/2A through PoE and 5V via USB. The system's multiple power input options provide ease of power utilization. As stated in the literature, the device can be used both in field environments and in laboratory conditions [4].

3. RESEARCH FINDINGS AND DISCUSSION

In this section, the functionality, communication performance, sensor compatibility, and power management efficiency of the developed IoT board were experimentally evaluated. The tests confirmed stable operation under both wired and wireless communication scenarios, reliable data transmission from various sensors, and uninterrupted performance during power source transitions. The obtained results align with existing studies on multi-protocol IoT architectures, demonstrating the board's adaptability and potential for future mobile IoT applications.

3.1 Test Scenarios

The functionality of the board was tested under various communication scenarios in laboratory conditions. First, on the wired communication side, Ethernet and RS-485 lines were operated simultaneously, and it was observed that data packets were transmitted successfully without loss. On the wireless side, data transmission via Wi-Fi and long-distance sensor communication via LoRa were tested concurrently. These scenarios demonstrated that the board's multi-protocol architecture operates stably in practice.

3.2 Evaluation of Sensor Data

Data obtained from temperature and pressure sensors connected to analog inputs and from soil moisture sensors with 4–20 mA outputs were successfully transmitted through wireless channels. At the same time, motion sensors connected to digital inputs were integrated into the

system. These tests confirm the board's compatibility with different types of sensors and the reliability of its multi-protocol data transmission.

3.3 Power Management Performance

Power transitions were tested, and it was observed that the device continued to operate without interruption during transitions from a 24 V external supply to PoE and from PoE to USB. No degradation in power stability was observed during the operation of loads connected to relay outputs.

3.4 Comparison with Literature

The findings are consistent with multi-protocol IoT architectures reported in the literature. Furthermore, it is anticipated that routing protocols will become critical in mobile IoT applications [5]. The modular design of our board allows flexible protocol allocation and firmware-level scalability, enabling seamless adaptation to such developments in future IoT ecosystems. Recent studies have also proposed hybrid architectures that combine LoRaWAN and NB-IoT to leverage the advantages of both low-power and wide-area connectivity technologies. Their results demonstrate that such architectures enhance system scalability, flexibility, and reliability in distributed IoT environments. Compared to this approach, our proposed board achieves similar interoperability at the hardware level, providing simultaneous wired and wireless communication interfaces within a single modular platform. This integration eliminates the need for separate gateway units while maintaining compatibility with hybrid IoT infrastructures [7].

4. Conclusion

In this study, a modular and multi-protocol IoT board was designed, developed, and tested under various communication, sensing, and power management scenarios. The results demonstrated that the board operates stably in both wired and wireless communication modes, successfully transmits data from a wide range of sensors, and maintains continuous operation during power transitions. These findings verify the reliability and adaptability of the system for diverse applications such as industrial automation, agriculture, and smart infrastructure.

Compared to existing solutions on the market, the proposed design offers a more flexible and scalable architecture. Its modular structure allows users to configure communication interfaces, sensor types, and power sources based on specific application requirements without additional hardware modifications. Furthermore, the integration of both high-bandwidth (Ethernet) and long-range, low-power (LoRaWAN) communication options provide an advantage in hybrid systems where real-time control and remote monitoring are equally important. This versatility enhances overall system efficiency while reducing installation and maintenance costs.

The motivation behind this design stems from the need for a universal IoT platform capable of adapting to different sectors and operating environments. Many commercial IoT boards are optimized for specific use cases and lack modularity, which limits their scalability. In contrast, the developed system bridges this gap by providing a flexible foundation that can evolve alongside technological advancements, including mobile IoT and edge computing. Thus, this study not only presents a technically superior prototype but also contributes to the vision of a more accessible, adaptable, and sustainable IoT ecosystem.

References

[1] Jouhari, M., Saeed, N., Alouini, M.-S., & Amhoud, E. (2022). A Survey on scalable LoRaWAN for massive IoT. arXiv preprint. https://arxiv.org/abs/2202.11082

[2] Almuhaya, M. A. M., et al. (2022). A Survey on LoRaWAN Technology: Recent Trends. Electronics, 11(1), 164. MDPI. https://doi.org/10.3390/electronics11010164

[3] Arun, P., et al. (2021). Design and development of an IoT based intelligent multi-protocol platform. Sensors and Materials, 33(7), 2479–2495. PMC. https://doi.org/10.18494/SAM.2021.3310

[4] B. L. -H. Nguyen, H. Cha, T. -T. Nguyen and H. -G. Kim, "Family of Integrated Multi-Input Multi-Output DC-DC Power Converters," 2018 International Power Electronics Conference (IPEC-Niigata 2018 -ECCE Asia), Niigata, Japan, 2018, pp. 3134-3139, https://ieeexplore.ieee.org/document/8507791

[5] Buang, I. N., Zen, K., & Junaini, S. N. (2025). The Future of LoRaWAN Routing Protocols for Mobile IoT. Advances in Mobile Sciences Journal,5(2). ARQII Publ. https://ir.unimas.my/id/eprint/47930/1/815-2571-10%20(1).pdf

[6] Gayo-Abeleira et al. Design and implementation of multiprotocol framework… (Elsevier Internet of Things, 2023) https://www.sciencedirect.com/science/article/pii/S2542660523002202

[7] Peruzzi, G.; Pozzebon, A. Combining LoRaWAN and NB-IoT for Edge-to-Cloud Low Power Connectivity Leveraging on Fog Computing. Appl. Sci. 2022, 12, 1497. https://doi.org/10.3390/app12031497

DEVELOPMENT OF A NEXT-GENERATION CONTROL AND PLACEMENT SYSTEM: AN INTELLIGENT INTERMEDIATE CONTROL AND ASSEMBLY DEVICE FOR MASS PRODUCTION OF THERMOELECTRIC MODULES

Abdurrahman Enes ÜNSAL[a*], Hüseyin Cenk KARATOPCU[a*], Onur İlyas YAVUZ[a]

[a]Demsay Elektronik A.Ş. R&D Center, 34520, Beylikdüzü, İstanbul

A B S T R A C T

With the miniaturization of electronic devices, the precise and rapid placement of micro-scale semiconductor components has become a critical challenge. Thermoelectric modules, composed of semiconductor legs as small as 1×1×1.2 mm³, are still assembled manually, leading to high labor costs, low throughput, and frequent placement errors. This study introduces the Next-Generation Control and Placement System, which automates the assembly of thermoelectric modules through intelligent control and vision-based verification. The desktop-type system integrates an STM32-based control board, a Raspberry Pi-supported image processing unit, and precision sensors to handle positioning, sorting, and safety checks. Equipped with a vibration-assisted mechanism, magnetic sensors, and camera algorithms, the device detects empty slots and separates defective materials autonomously. IoT-based communication via GSM, Wi-Fi, and Bluetooth enables remote monitoring and data exchange. Experimental results show that the system reduces manual production time by over 80%, allowing the fabrication of hundreds of modules per hour. The developed prototype significantly enhances process efficiency, minimizes human error, and supports Türkiye's transition toward smart, digitally integrated semiconductor manufacturing.

K E Y W O R D S

- Semiconductor Assembly
- Thermoelectric Modules
- Image Processing
- IOT
- Electronic Design
- Smart Systems

* Corresponding author:
E-mail: e.unsal@demsay.com

1. Introduction

The continuous miniaturization of electronic components and the increasing demand for high-efficiency thermal management systems have led to the widespread use of thermoelectric modules in both industrial and consumer applications [1,2]. These modules consist of thermocouple structures formed by p-type and n-type semiconductor legs, and their precise alignment is critical for optimal performance.

In modern production environments, the manufacturing challenges associated with micro-scale thermoelectric modules have become increasingly evident. These modules are still largely assembled manually, which results in high labor costs, low production rates, and frequent placement errors. In recent years, such processes have been redefined through the concepts of cyber-physical systems and robotic automation [3,4].

The integration of computer vision and deep learning methods into production lines has brought significant improvements in quality control and defect detection. Studies [5,6] have shown that automated visual inspection produces results that are far more consistent and repeatable than manual inspections. Moreover, recent research emphasizes the growing importance of approaches in smart manufacturing. This method enables data to be processed locally on edge devices without relying on cloud connectivity, thereby allowing real-time decision-making within the production line [7]. Consequently, the use of vision-based position verification and locally deployed AI-driven decision systems in thermoelectric module production represents an innovative approach for improving efficiency and standardization.

The effectiveness of vibration-assisted feeding systems for the accurate alignment of micro-components has also been extensively investigated in the literature [8,9]. Such mechanisms provide substantial advantages in orienting and stabilizing parts in the correct position.

This study introduces the Next-Generation Control and Placement System, developed under the TÜBİTAK 1507 SME R&D Startup Support Program. The system integrates thermoelectric module production with standard SMD manufacturing lines, enabling automatic and high-speed assembly. This approach reduces production costs and enhances the accessibility of thermoelectric module technology for domestic manufacturers.

Designed as a desktop-type system, it consists of an STM32-based control board, a Raspberry Pi-based image-processing unit, and a set of precision sensors. Using a vibration-assisted alignment mechanism, magnetic sensors, and camera-based algorithms, the device can detect empty slots and separate defective parts. Furthermore, IoT-based communication via GSM, Wi-Fi, and Bluetooth enables remote monitoring and data exchange.

Experimental results show that the system reduces manual production time by more than 80% and allows the production of hundreds of modules per hour. The developed prototype

improves manufacturing efficiency, minimizes human error, and contributes to Türkiye's transition toward a digital, smart manufacturing infrastructure.

2. Material and Method

The control electronics are based on an STM32 microcontroller chosen for its peripheral versatility and robust real-time behavior. The board exposes SPI, UART, and I²C interfaces for peripheral integration and deterministic actuation. Upon operator command from the Raspberry Pi HMI, the STM32 generates PWM signals that drive the DC motor and execute precisely timed vibration cycles, while the Raspberry Pi coordinates execution and manages vision and user interaction. A high-resolution camera, positioned above the workspace, captures a single 1080p still image after each cycle. This image is used to compute the filling ratio and assess component alignment before deciding whether to continue or stop.

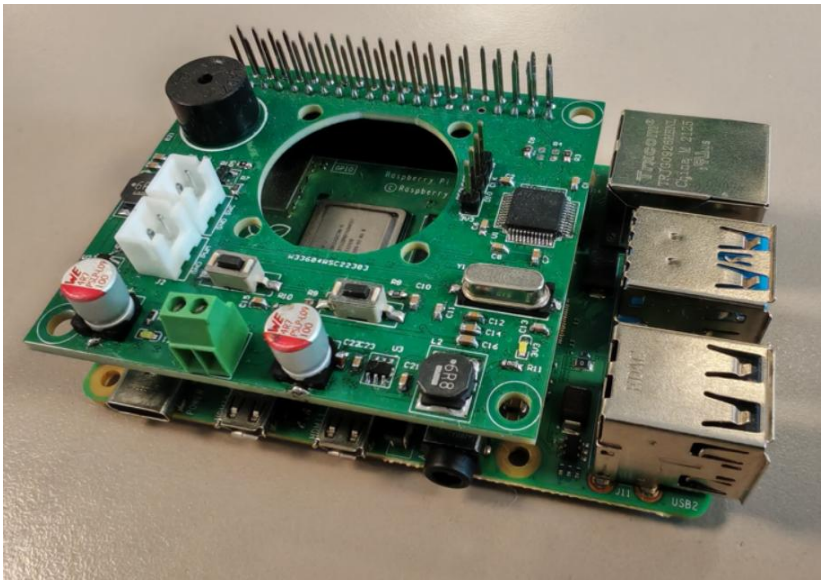

Figure 1: Physical implementation of the next-generation control and placement board.

The mechanical subsystem comprises a vibration-assisted alignment tray and a DC-motor-driven linear mechanism. The alignment tray promotes proper orientation of the semiconductor legs within their cavities prior to placement. The DC motor receives PWM commands from the STM32, enabling tightly bounded vibration durations and amplitudes that maintain stable motion profiles and repeatable positioning accuracy, this preserves determinism across cycles. Safety interlocks and limit sensors bound travel and provide calibration reference points. Coordinated timing between the STM32 and the mechanical stage supports consistent behavior under varying loads and environmental conditions.

Figure 2: Physical implementation of the next-generation control and placement board.

The STM32 firmware manages real-time PWM actuation and safety monitoring. The Raspberry Pi runs the Python-based HMI, orchestrates cycle commands, and executes the vision pipeline. After each vibration cycle, the Pi camera acquires one 1080p still image of the tray. A custom-trained YOLOv5n model processes this image to compute the filling ratio and evaluate alignment quality against a predefined threshold. If the ratio is below the threshold, the system triggers another vibration cycle and re-evaluates. The loop continues until the threshold is met or a maximum number of attempts is reached, at which point the process stops automatically and the result is presented on the HMI. The 7-inch capacitive touchscreen (Python/Tkinter) provides live status, parameter access, and direct start/stop control. The communication framework employs UART for controller interaction and Wi-Fi for local connectivity and remote data access, with cloud dashboards and MQTT-based analytics planned as future enhancements.

3. Experimental Tests

The prototype of the Next-Generation Control and Placement System was assembled and tested under laboratory conditions to validate its functionality, precision, and operational stability. The test setup consisted of the complete control unit, the mechanical placement module, the vibration alignment tray, and the camera-based vision system. The experiments aimed to evaluate motor control accuracy, visual detection reliability, filling ratio calculation performance, and user interface responsiveness.

3.1 Motor Control and Mechanical Performance

The DC motor is actuated via STM32-generated PWM, providing low-latency, stable control and predictable cycle timing. Start/stop commands issued from the HMI are executed with sub-second responsiveness. PWM duty and frequency parameters are experimentally tuned to yield consistent orientation performance within predefined cycle times. Tests with 1×1 mm and 1×1.2

mm legs confirmed stable behavior across varying loads and surface conditions. This deterministic control path HMI command → STM32 PWM → vibration simplifies commissioning and facilitates rapid refinement of motion parameters during setup.

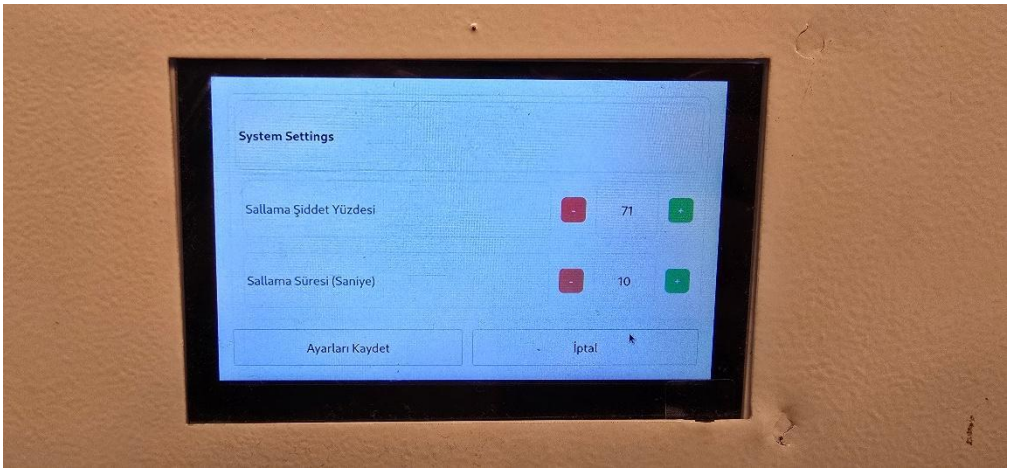

Figure 3: Control panel interface for vibration and positioning parameters.

3.2 Vision-Based Detection and Filling Ratio Analysis

The high-resolution camera supplies imagery to the Raspberry Pi, where the YOLOv5n model processes a single 1080p still image per cycle. The model identifies occupied versus empty slots and computes the filling ratio, which is visualized on the HMI to guide operator awareness. To increase robustness, an iterative procedure re-runs the vibration–settling cycle whenever the filling ratio falls below the operator-defined threshold. The loop terminates when the threshold is satisfied or the maximum retry count is reached, in which case the HMI reports the outcome. During validation, filling ratios were operator-verified by manual counts. A comprehensive statistical study (e.g., confusion matrices across part types and lighting conditions) is planned as future work.

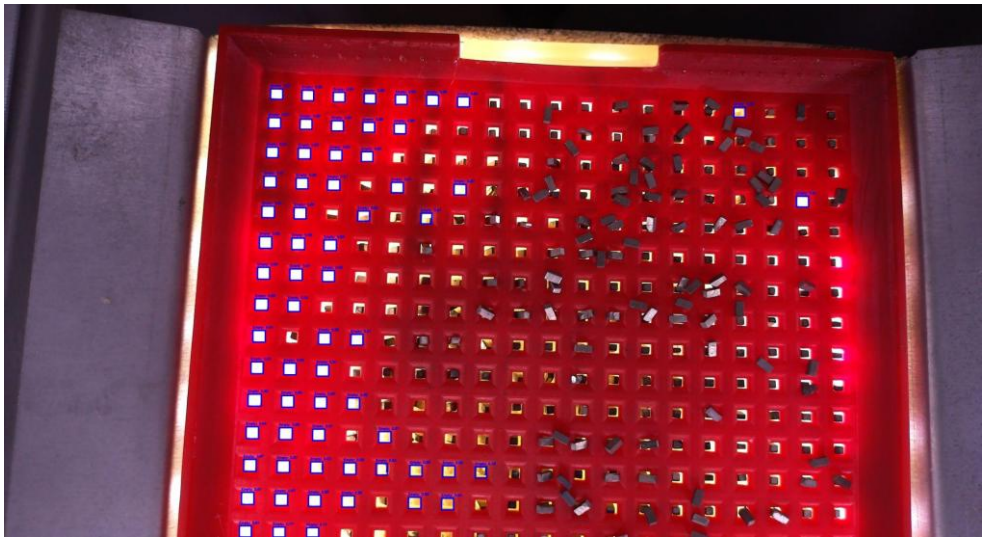

Figure 4: YOLOv5 model detection results on component tray, showing identified empty slots (blue boxes).

3.3 User Interface and System Integration

Integration tests demonstrated reliable coordination between the Raspberry Pi HMI, the STM32 controller, and the PWM-driven motor stage over extended operation. Cycle execution, image acquisition, and user feedback remained consistent and timely, indicating suitability for continuous use in small- and medium-scale production lines.

Figure 5: Visual output of the camera-based detection and filling ratio analysis.

4. Conclusion

This study presented the design and validation of a modular control and placement system for thermoelectric module assembly. The system combines a vision-guided monitoring subsystem, a vibration-assisted alignment mechanism, PWM-controlled DC drive, and a 7-inch touchscreen HMI. Experiments showed 85% correct orientation within 12 seconds under the identified operating conditions. To avoid overclaiming performance, we intentionally refrain from stating a single global accuracy for filling-ratio detection. Instead, we introduced an iterative re-inspection loop that repeats alignment and vision checks until the operator-defined threshold is met or operator intervention is requested, thereby increasing practical success without relying on a single static metric. Future work will include a formal statistical evaluation (confusion matrices across part types, lighting, and tray geometries), automated parameter tuning for the iterative loop, and cloud-connected analytics for traceability and predictive maintenance.

Although the proposed system improves repeatability and reduces operator dependency compared to manual placement, several practical limitations were observed during testing. When thermoelectric modules of inconsistent material quality were used, the vibration-assisted alignment process occasionally caused micro-damage or mechanical stress on the module surfaces, especially when the solder interface was not uniformly bonded. To minimize this effect, the vibration amplitude and duration were later optimized through iterative testing, but full elimination of this risk requires tighter control of incoming component quality.

Additionally, while the automated placement and inspection workflow significantly accelerates the process, the system cannot yet achieve 100% filling ratio in every cycle. Small misalignments or irregularly shaped elements may remain unseated after multiple vibration–

settling loops. In such cases, manual operator intervention is required to complete the tray before the next process stage. These findings indicate that human oversight remains valuable in ensuring complete assembly when component tolerances or mechanical uniformity vary across batches.

The developed system provides a practical and cost-effective solution for industrial environments where precise placement and alignment of small components are required. Initially designed for thermoelectric module assembly, the same control and inspection architecture can be adapted to sensor packaging, micro-module manufacturing, and precision part sorting applications.

Its modular structure, touchscreen interface, and vision-assisted verification enable semi-automated workflows that bridge the gap between manual labor and fully automated production. This approach is particularly valuable for small- and medium-sized enterprises (SMEs) seeking to enhance production quality and throughput without major capital investment.

By reducing operator fatigue, standardizing motion parameters, and introducing traceable digital feedback, the system supports Industry 4.0 and smart manufacturing principles. In the long term, its scalability and software flexibility allow integration into broader digital production ecosystems involving cloud monitoring, predictive analytics, and adaptive process optimization.

References

[1] Rowe, D. M. (Ed.). (2018). Thermoelectrics Handbook: Macro to Nano. CRC Press.
[2]] He, W., Zhang, G., Zhang, X., Ji, J., Li, G., & Zhao, X. (2015). Recent development and application of thermoelectric generator and cooler. Applied Energy, 143, 1–25.
[3]] Monostori, L., Kádár, B., Bauernhansl, T., Kondoh, S., Kumara, S., Reinhart, G., & Ueda, K. (2016). Cyber-physical systems in manufacturing. CIRP Annals, 65(2), 621–641.
[4] Siciliano, B., & Khatib, O. (Eds.). (2016). Springer Handbook of Robotics. Springer - Endüstriyel otomasyon, görüntü işleme ve kontrol sistemlerinin temeli.
[5]] Hütten, N., Gomes, M. A., Hölken, F., Andricevic, K., Meyes, R., & Meisen, T. (2024). Deep learning for automated visual inspection in manufacturing and maintenance: A survey of open-access papers. Applied System Innovation, 7(1), 11.
[6] Li, Z., et al. (2025). A survey of deep learning for industrial visual anomaly detection. Artificial Intelligence Review.
[7] Deng, R., Wang, J., & Li, B. (2024). Edge AI for intelligent manufacturing: deployment strategies and challenges. IEEE Transactions on Industrial Informatics, 20(3), 4210–4223.
[8] Balaji, B., & Burela, R. G. (2022). Dynamics of part motion on a linear vibratory feeder. Proceedings of the IMechE, Part C: Journal of Mechanical Engineering Science.
[9] Le, V.-M., & Nguyen, G.-N. (2019). A method to design vibratory bowl feeder by using FEM modal analysis. Vietnam Journal of Science and Technology, 57(1), 102–111.*

BASED IMAGE PROCESSING TECHNIQUE FOR ICE DETECTION IN INDUSTRIAL REFRIGERATION CABINETS

Ali DEMİR*, Kadir ERDOĞAN

Çağlayan Soğutma A.Ş., Büyükkayacıkosb Dist. 13.St. Nu:23/1,42250 KONYA TÜRKİYE

ABSTRACT

Industrial refrigeration cabinets are used as cold chain display cabinets in various areas such as hotels, supermarkets and gas stations. These cabinets are produced with doors, without doors or as freezers. Icing occurs due to the humidity of the air passing over the evaporator in the industrial refrigeration cabinets and the low evaporator operating temperature. This icing causes the air flow to slow down and the products cannot be stored at the desired temperatures. Various methods have been developed to prevent icing or to melt the ice. Some of these have become widespread as closed cycle method, closed cycle method with hot gas and resistance defrosting. The application of these methods is determined according to the type of cabinet. The ambient conditions during the tests were set at 25°C and 60% humidity as per ISO 23953 standard. However, these ambient conditions cannot be achieved in every region where the cabinet operates, and the cabinet can be used in environments with higher humidity and temperature. In this study, image processing techniques were used to investigate the feasibility of detecting icing on the evaporator for cabinets operating in different regions.

KEYWORDS

- Based Image Processing
- Defrosting
- Icing
- Industrial Refrigeration Cabinet

1. Introduction

Industrial refrigeration cabinets are widely used around the world. Freezer units, in particular, are commonly used for the storage and display of frozen products and frozen ready-to-eat foods. These units come in plug-in (plug-and-play) and remote (external refrigeration unit) types. In freezers, closed-loop, hot gas circulation, and resistance defrost methods are used to remove frost that forms on the evaporator.

Image processing is used in many different fields in the literature, such as medical imaging, satellite and drone image processing, autonomous devices, and robotics [1-5]. In the study presented in [6], the authors developed a multi-stage image processing-based method for detecting icing on power transmission lines. The proposed method achieved higher success compared to existing methods under low light and complex background conditions. In the study conducted in [7], an OpenCV-based image processing algorithm was developed to calculate sea ice density for studies aimed at determining the optimal route in the Arctic Ocean. The developed method was tested with accuracy improved by color spaces, k-means clustering, and random forest models. In another study using hyperspectral imaging and machine learning techniques to detect icing on critical infrastructure, ice types were classified with high accuracy on different surface coatings. Multiclass analyses performed with Random Forest and SVM algorithms, in particular, yielded successful results in distinguishing between glaze and rime ice [8]. In a study using hyperspectral imaging technology to detect blade icing on wind turbines, more accurate and faster results were obtained compared to traditional methods. The study shows that icing can be detected with high accuracy even in its early stages [9]. Jakonczuk et al. [10] detected icing on the evaporator using image processing techniques and investigated its effect on cooling performance. They noted that icing reduced evaporator capacity by 0.2 kW and caused a capacity loss of up to 40% in the long term. They observed that the applied methods had a positive effect on the defrost process.

In this study, the dimensions of the region where frosting occurs on the evaporator were determined using image segmentation features obtained by applying image processing techniques, and compared to the situation where no frosting occurs.

2. Maths

In this study, an image processing technique was used to detect frost on the evaporator inside the refrigerator. Within this technique, image segmentation was used to detect the frosted area and the size of the frost. The formulas and explanations for these techniques are provided below.

The thresholding equation is a common approach to binary classification of pixels, where the decision is based solely on the value of pixel I. This approach is called thresholding, and t is called the threshold value.

$$\mathrm{c[u,v]} = \begin{cases} 0, if\ I[u.v] < t \\ 1, if\ I[u.v] \geq t \end{cases} \forall (u,v) \in I \qquad (1)$$

Many modern industrial visual inspection systems use this simple approach because it allows the use of embedded computers, and it works very well if objects are silhouetted on a conveyor belt or at an inspection station in a suitable contrasting color.

The shape-from-perimeter method is used to uniquely define the shape of a region based on its boundary or surrounding pixels. In the case of a chain code with 4 direction shown in Figure 1.a), consecutive

pixels must be adjacent, and the orientation of the surrounding segments must be k × 90°, where k ∈ {0…3}. Freeman chain code with 8 direction shown in Figure 1.b has boundary segments oriented at k × 45°, where k ∈ {0…7}. The crack code shown in Figure 1.c) has segments in the cracks between the pixels on the edge of the region and the pixels outside the region. These have k × 90° orientations, where k ∈ {0…3}.

3. Figures & Tables

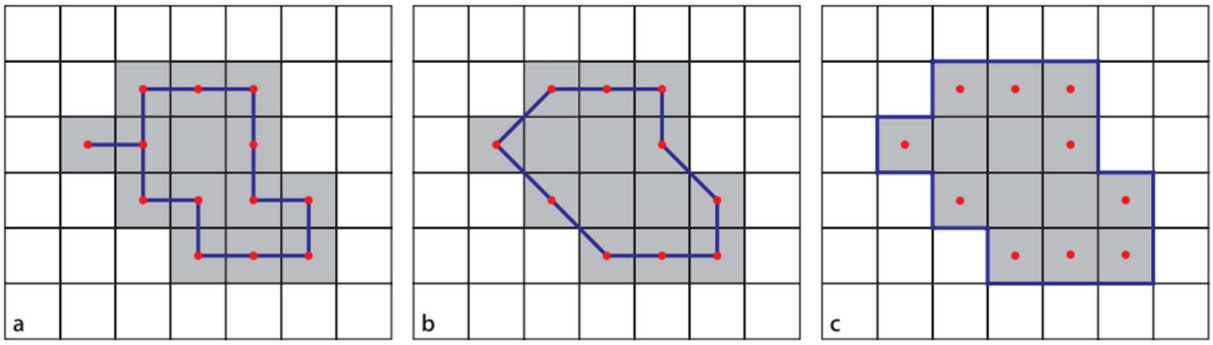

Fig. 1. a) chain code with 4 direction representation, b) Freeman chain code with 8 direction representation, c) Crack code representation.

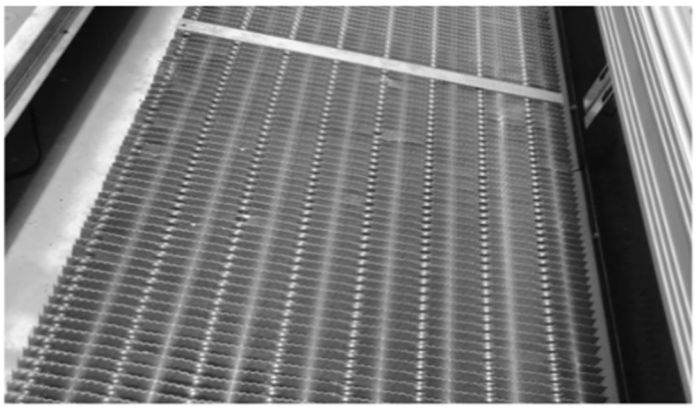

Fig. 2. Reference image (No frosting)

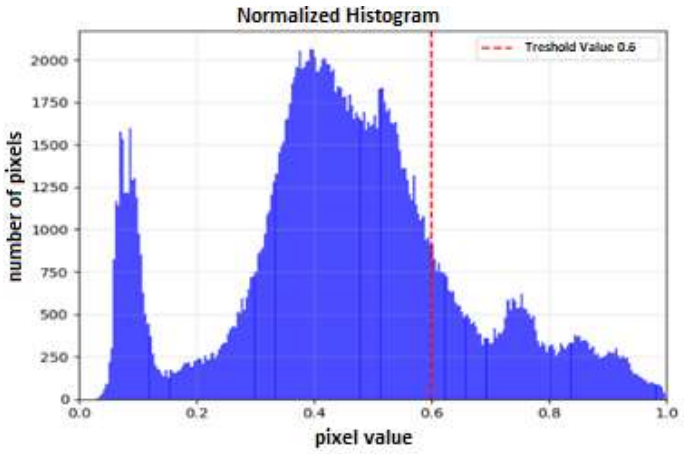

Fig. 3. Two-dimensional image histogram (No frost condition)

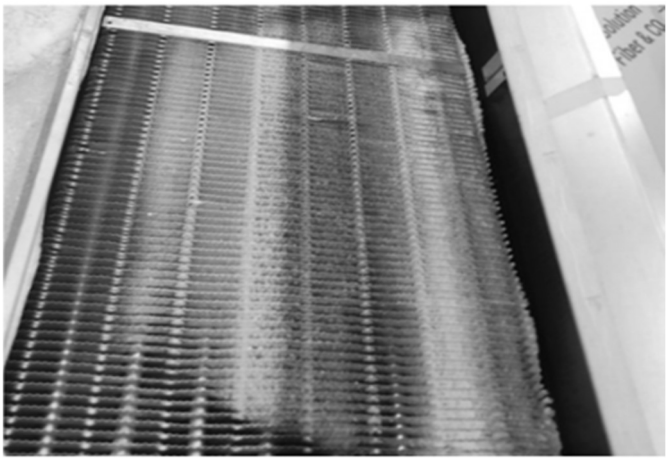

Fig.4. Frozen Evaporator

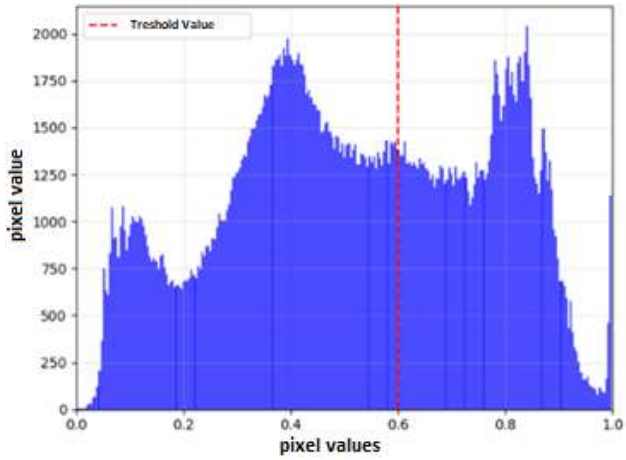

Fig 5. Two-dimensional histogram of the frosted evaporator

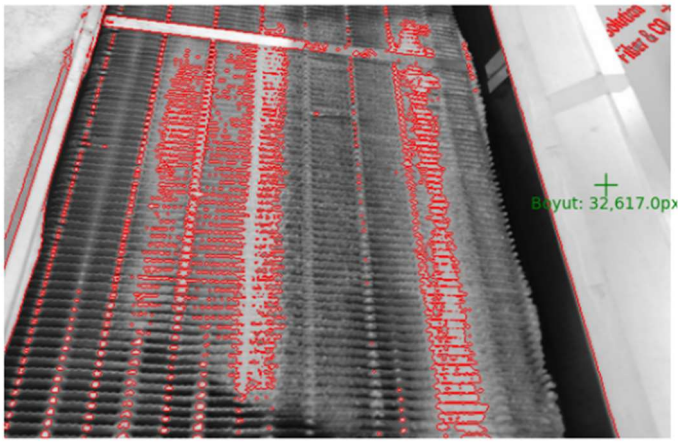

Fig. 6. Boundary lines of the frosted area

4. Results

Ice detection was performed using image processing techniques to reduce the effect of frost formation on industrial refrigeration cabinet evaporators. In the first stage, a reference image was taken when there was no frost on the evaporator, as shown in Figure 2. Then, a two-dimensional image histogram was created, as shown in Figure 3.

In the second stage, a two-dimensional image histogram was created from the frozen evaporator shown in Figure 4 and displayed in Figure 5. When examining the histograms of the images given in Figure 5, it was determined that the number of pixels at threshold values of 0.67 and above was lower, while in the frozen image, the number of pixels at threshold values above 0.67 was higher. Taking advantage of this finding, the threshold value to be used in the comparison between the two images was set at 0.67. The boundaries of the objects (ice) above the threshold value determined in the frozen image were also detected, as shown in Figure 6.

Reference image (non-frosted condition) showed 26,941 pixels at a threshold value of 0.67, while the frosted image showed 59,619 pixels at a threshold value of 0.67.

Frosting on the evaporator in industrial freezers was determined using image processing techniques. Image segmentation was used to detect frosting. The following results were obtained in this study.

- The reference image (Figure 3) and frozen image (Figure 5) histograms were examined, and the threshold value was determined to be 0.67.
- The boundaries of objects (ice formation) above the threshold value of 0.67 were determined. (Figure 6)
- It was determined that there were 26,941 pixels above the threshold value of 0.67 in the reference image and 59,619 pixels above the threshold value of 0.67 in the frozen image.
- A difference of 32,678 pixels was determined between the reference image and the frozen image.

It has been observed that frost formation on the evaporator can be detected by comparing pixel differences using basic image processing techniques. More accurate data can be obtained using detailed image processing techniques. The software developed can detect frost and be adapted to the cabinet's automation management unit using the designed commands. Thus, parameters such as when the cabinet will enter defrost mode and the defrost duration can be managed independently of the region where it will be used. This enables the optimization of parameters such as defrost time and duration, thereby achieving energy savings in the cabinet.

Acknowledgments

The authors would like to thank Çağlayan Soğutma A.Ş. for their support throughout the study.

References

[1] Soomro T. A. et al. (2023). Image Segmentation for MR Brain Tumor Detection Using Machine Learning: A Review, IEEE Reviews in Biomedical Engineering, vol. 16, pp. 70-90,.

[2] Alsawy A., Hicks A., Moss D. and Mckeever S.. (2022). An Image Processing Based Classifier to Support Safe Dropping for Delivery-by-Drone, 2022 IEEE 5th International Conference on Image Processing Applications and Systems (IPAS), Genova, Italy, pp. 1-5,

[3] Fonseca L. M. G., Namikawa L. M. and Castejon E. F.. (2009). Digital Image Processing in Remote Sensing, 2009 Tutorials of the XXII Brazilian Symposium on Computer Graphics and Image Processing, Rio de Janeiro, Brazil, , pp. 59-71

[4] Kapadnis J., Lahare P., Bhadane S., Patil C., Joshi A. and Borase J. (2025). Implementation of Autonomous Vehicle using Real-Time Image processing and Computer Vision Algorithm,2025 International Conference on Emerging Smart Computing and Informatics (ESCI), Pune, India, pp. 1-5,

[5] Byambasuren B.E., Baasanjav T., Myagmarjav T. and Baatar B. (2020). Application of Image Processing and Industrial Robot Arm for Quality Assurance Process of Production, 2020 IEEE Region 10 Symposium (TENSYMP), Dhaka, Bangladesh, pp. 526-530,

[6] Kim, H., Park, S., & Jeong, S.Y. (2023). Machine Learning-Based Image Processing for Ice Concentration during Chukchi and Beaufort Sea Trials. Journal of Marine Science and Engineering, 11(12), 2281.

[7] Nusantika, N. R., Xiao, J., & Hu, X. (2024). Precision Ice Detection on Power Transmission Lines: A Novel Approach with Multi-Scale Retinex and Advanced Morphological Edge Detection Monitoring. Journal of Imaging, 10(11), 287.

[8] Vanlanduit, S., De Vooght, A., & De Kerf, T. (2025). Surface Ice Detection Using Hyperspectral Imaging and Machine Learning. Sensors, 25(14), 4322.

[9] Rizk, P., Younes, R., Ilinca, A., & Khoder, J. (2022). Wind turbine ice detection using hyperspectral imaging. Remote Sensing Applications: Society and Environment, 26, 100711.

[10] Jakończuk, P., Śmierciew, K., Gagan, J., & Butrymowicz, D. (2022). Image-Analysis-Based Approach for Identification of Air Cooler Heat Transfer Degradation during Frosting Process. Sustainability, 14(21), 13731.

FORECASTING IN THE FIELD OF ELECTROMOBILITY USING UNIVARIATE AND MULTIVARIATE TIME SERIES MODEL

Rana Bedir URFALI[a*], Ersin KAYA[b]

[a] *Department of Computer Engineering, Faculty of Computer and Information Sciences, Konya Technical University, Rauf Orbay Street, 42250, Konya, Turkey*

[b] *Department of Computer Engineering, Faculty of Computer and Information Sciences, Konya Technical University, Rauf Orbay Street, 42250, Konya, Turkey*

ABSTRACT

This study aims to predict future usage trends by analyzing e-bike usage in a province using time-series models. E-bikes, as an important component of sustainable transportation, increase urban mobility and reduce traffic congestion. In this context, accurate demand forecasting plays a critical role in the effective management and operational planning of bike-sharing systems. In this study, forecasts were first made using the univariate time-series model ARIMA using only bicycle usage data. Then, the multivariate model SARIMAX was applied by incorporating exogenous factors such as weather. The dataset included daily bicycle usage information and meteorological variables such as temperature, precipitation, and wind speed. Model performance was evaluated using RMSE and MAE metrics. The results revealed that model performance varied across regions. While the univariate model ARIMA performed best in four regions, the multivariate model SARIMAX yielded superior results in most regions. It was observed that incorporating exogenous factors such as weather into the model increased forecast accuracy. The findings contribute to optimizing field operations of bike-sharing systems and improving urban transportation planning. Thus, it becomes possible to use resources more efficiently and increase user satisfaction.

KEYWORDS

- Electric Bicycle
- Time Series Forecasting
- Univariate Model
- Multivariate Model
- Comparative Analysis
- Performance Metrics

[*] Corresponding author: Rana Bedir Urfali
E-mail: ranabedirr@gmail.com

1. Introduction

Global climate change and increasing urbanization rates are driving a growing need for sustainable transportation solutions. In this context, electric bicycles (e-bikes) are emerging as a prominent alternative to traditional transportation systems and are undertaking a critical role in the transformation of urban mobility [1]. With zero emissions, low operating costs, and the potential to reduce traffic congestion, e-bikes have become a cornerstone of sustainable urban transport [2]. Over the past decade, bicycle-sharing systems have shown exponential growth on a global scale and have become an integral part of sustainable urban transportation ecosystems [3]. The operational success of these systems is fundamentally based on accurate demand forecasting and effective resource allocation strategies. Critical decisions such as optimizing bicycle distribution, planning station capacities, and scheduling maintenance operations all require a precise prediction of future usage patterns.

Time series analysis offers a powerful statistical methodology for forecasting future values based on past data patterns. This approach has proven particularly effective in bicycle-sharing demand forecasting. In such studies, both univariate and multivariate time series models are used to predict e-bike usage. For univariate approaches, models like Autoregressive Integrated Moving Average (ARIMA) [4] are preferred. However, bicycle usage demand is also influenced by external factors beyond past usage patterns, such as temperature, precipitation, and wind speed. For this reason, multivariate models like Seasonal Autoregressive Integrated Moving Average with Exogenous Variables (SARIMAX) [5], which incorporate these external variables to enhance forecasting capabilities, also hold a significant place.

The primary objective of this study is to conduct a comparative analysis of univariate and multivariate time-series forecasting models for e-bike usage forecasting in a specific city. The study analyzes bicycle usage data from different regions and evaluates the effects of weather variables on forecast performance. Performance evaluation was conducted using Root Mean Square Error (RMSE) and Mean Absolute Error (MAE) metrics to ensure robust model comparison [6]. The results are expected to significantly contribute to improving the operational efficiency of bike-sharing systems and urban transportation planning.

The paper is organized as follows: Section II presents related work in univariate and multivariate time series forecasting. Section III presents experimental results and discussion, and Section IV presents the paper's conclusion.

2. Materials and Methods

This section details the methods used to analyze urban electric bicycle usage and forecast future usage trends. In this paper, time series analysis and statistical models were used to create forecasting models from both univariate and multivariate datasets. By comparing the performance of these models, the approach that produced the most accurate forecasts was determined.

2.1. Dataset Description

In this paper, two different datasets were used, which consist of electric bicycle usage data. The first dataset is a univariate time series containing daily usage values, covering a period of approximately 14 months from December 31, 2022, to February 28, 2024. This dataset includes three features: date, region name (name), and the daily number of bicycles ridden (count). The second dataset, to be used with multivariate models, includes bicycle usage data along with weather information. This dataset contains environmental factors such as average temperature (tavg), precipitation amount (prcp), and wind speed (wspd). Both datasets cover the same time period and were prepared for different analyses.

The datasets consist of observations representing different regions within a specific province. Figure 1 displays a Geographic Information Systems (GIS)-based approach that was adopted to define the regions, and the GeoPandas library was used to identify 14 different regions within the provincial boundaries [7]. This regional division is critical for analyzing the impact of spatial differences on demand. The region boundaries were created and visualized using geographic data in shapefile format.

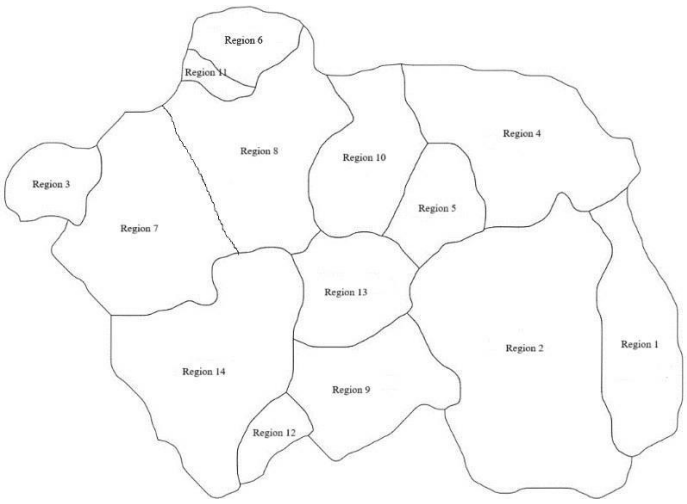

Fig. 1. Regional segmentation of the study area using GIS-based approach

Additionally, time series components were analyzed across the entire dataset. This analysis involved decomposing the observed values into their constituent elements (trend, seasonal, and residual). Figure 2 illustrates this analysis, which reveals long-term trends, seasonal cycles, and random fluctuations, providing a better understanding of the data structure [8].

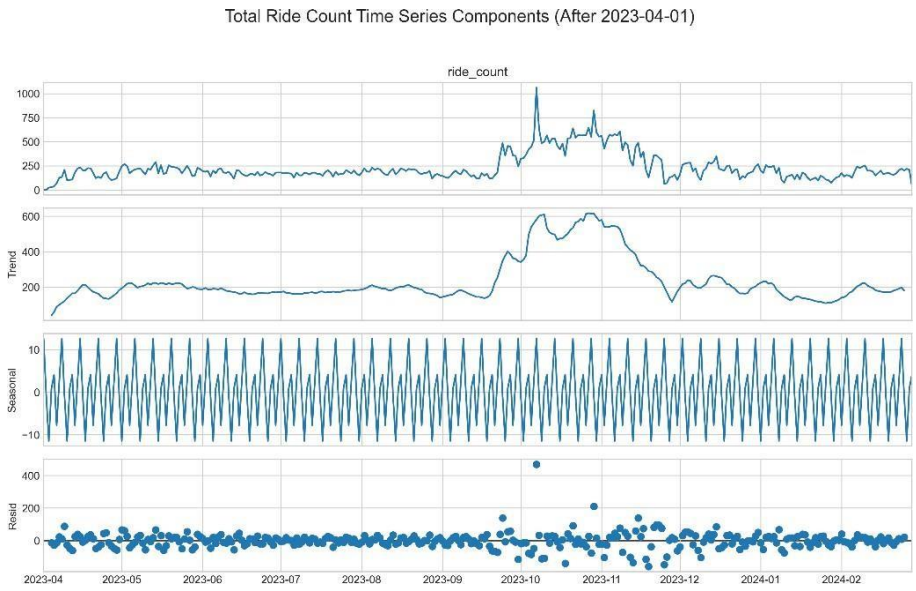

Fig. 2. Time series decomposition of electric bicycle usage (April 2023 – February 2024)

2.2. Time Series Forecasting Models

Time series forecasting is a field of analysis that uses historical data to predict future values. Models in this field are divided into two main groups: univariate and multivariate, based on the structure of the data and the goal of the forecast.

2.2.1. Univariate Time Series Forecasting Model

Univariate models predict future values using past values of a single time series.

2.2.1.1. ARIMA Model

The ARIMA (Autoregressive Integrated Moving Average) model is one of the most widely used statistical models for time series forecasting. The AR component represents past observations; the MA component represents past error terms; and the I component represents the differencing process necessary to make the series stationary [9, 10]. The basic ARIMA model can be expressed as follows:

$$y'_t = c + \phi_1 y'_{t-1} + \cdots + \phi_p y'_{t-p} + \theta_1 \epsilon_{t-1} + \cdots + \theta_q \epsilon_{t-q} + \epsilon_t \quad (1)$$

It can be seen from Equation (1) that the differenced series is represented by y'_t, while ϕ and θ are the model parameters, and ϵ_t denotes the error term.

2.2.2. Multivariate Time Series Forecasting Model

Multivariate models improve forecast accuracy by using the relationships between multiple variables.

2.2.2.1. SARIMAX Model

SARIMAX (Seasonal Autoregressive Integrated Moving Average with Exogenous Regressors) is an extended version of the ARIMA model that includes exogenous variables (x_t) and seasonal components (p_s, d_s, q_s). The general form of the SARIMAX model can be expressed as follows:

$$\Phi(B)\Phi_S(B^S)(1-B)^d(1-B^S)^{ds}\,y_t = c + \Theta(B)\Theta_S(B^S)\epsilon_t + \beta X_t \quad (2)$$

It can be seen from Equation (2) that, Φ and Θ represent the autoregressive and moving average parameters, B is the backshift operator, s is the seasonal period, and X_t denotes the exogenous variables [5].

2.3. Performance Metrics

In time series forecasting, two main evaluation metrics are used to assess the performance of the models: Root Mean Squared Error (RMSE) and Mean Absolute Error (MAE). These metrics provide a quantitative evaluation of the model's performance by measuring how much the model's predictions deviate from the actual values.

2.3.1. MAE

Mean Absolute Error (MAE) is computed as the average of the absolute differences between the predicted values and the actual values. This metric provides the average magnitude of error in a group of forecasts without considering direction. Because it assigns equal weight to the magnitude of each error, it presents a more resilient structure against outliers. The following formula is used to calculate MAE:

$$MAE = \frac{1}{n}\sum_{i=1}^{n}|y_i - y_\iota| \quad (3)$$

In this equation, n represents the number of predictions, y_i is the actual value, and $y\hat{}_\iota$ represents the model's prediction. It can be seen from Equation (3), equal weight is given to the magnitude of each error, which makes MAE more resilient to outliers.

2.3.2. RMSE

Root Mean Squared Error (RMSE) is the square root of the average of the squared differences between the predicted and actual values. The squaring of errors amplifies the effect of large errors, penalizing them more heavily. This makes RMSE a more useful metric in cases where large prediction errors are particularly important. The calculation of RMSE is performed with the formula in Equation (4).

$$RMSE = \sqrt{\frac{1}{n}\sum_{i=1}^{n}(y_i - \hat{y}_i)^2} \quad (4)$$

It can be seen from Equation (4) that n represents the number of predictions, y_i is the actual value, and $\hat{y}_i$ indicates the model's prediction.

3. Results and Discussions

This section presents a comprehensive analysis of the forecasting performance of six time series models across 14 different regions for electric bike-sharing demand prediction. The models were evaluated using Root Mean Square Error (RMSE) and Mean Absolute Error (MAE) metrics to provide a robust comparison of their predictive capabilities.

Table 1 presents the comparative performance between ARIMA and SARIMAX models across all regions. The results reveal that the effectiveness of the models varies according to regional characteristics and data patterns.

Table 1. ARIMA and SARIMAX Model Performance Comparison

Regions	*ARIMA RMSE*	*ARIMA MAE*	*SARIMAX RMSE*	*SARIMAX MAE*
Region 1	1.97	1.11	2.92	2.67
Region 2	3.25	2.44	6.92	5.65
Region 3	10.37	8.32	8.87	6.78
Region 4	3.44	2.81	2.96	2.50
Region 5	5.25	4.27	4.25	3.19
Region 6	6.26	5.85	5.44	4.97
Region 7	10.04	8.76	8.07	5.68
Region 8	8.35	6.69	7.57	6.16
Region 9	1.15	0.81	0.99	0.67
Region 10	10.33	7.94	9.69	6.64
Region 11	8.21	6.78	7.79	6.33
Region 12	1.71	1.45	1.86	1.60
Region 13	3.89	2.56	4.75	3.25
Region 14	0.90	0.77	0.77	0.69

The analysis demonstrates the significant contribution of meteorological variables to forecast accuracy, with the SARIMAX model outperforming ARIMA in 10 out of 14 regions (71.4%). The SARIMAX model, which includes weather data, achieved lower error rates in most regions. This suggests that exogenous factors such as temperature, precipitation, and wind speed have a significant impact on bicycle demand. ARIMA, however, outperformed only four regions (Regions 1, 2, 12, and 13). These regions may be less affected by exogenous weather factors and have more predictable internal patterns. This finding highlights the need to determine the most appropriate model for each region.

When the results are evaluated from the perspective of e-bike sharing system management, the consistently superior performance of the multivariate model clearly demonstrates the significant impact of weather conditions on user behavior. This demonstrates the fundamental need to consider meteorological data in demand forecasting systems. The performance differences across regions demonstrate that demand patterns are influenced by local factors such as population density, infrastructure status, and geographic characteristics, highlighting the need for customized approaches for each region.

From a model selection perspective, the SARIMAX model demonstrates the most consistent improvement compared to its univariate counterpart, proving to be a reliable option for regions with complex demand patterns. The improved accuracy of the multivariate model can directly contribute to more efficient operational resource allocation, reduced operating costs, and increased user satisfaction through improved bike availability. These findings support the need to implement weather-aware forecasting systems in electric bike-sharing operations and provide an important foundation for sustainable urban transportation planning strategies.

4. Conclusion

This study presents a comparative analysis of univariate ARIMA and multivariate SARIMAX models for demand forecasting in electric bicycle-sharing systems. The findings clearly demonstrate the critical role of external meteorological factors in demand prediction. The SARIMAX model, by incorporating weather data, was proven to provide a higher level of accuracy than ARIMA in most regions.

This result indicates that, unlike models based solely on historical usage data, multivariate approaches produce more robust and reliable forecasts. The main contribution of this study is to provide a practical pathway for optimizing resource allocation, reducing costs, and enhancing overall user satisfaction by advocating for the use of weather data in bicycle-sharing operations.

Future research could expand on these analyses by comparing the performance of these models in different geographical regions or by integrating more exogenous variables, such as social events and local infrastructure changes.

References

[1] Vishnu, G., Kaliyaperumal, D., Pati, P. B., Karthick, A., Subbanna, N., & Ghosh, A. (2023). Short-term forecasting of electric vehicle load using time series, machine learning, and deep learning techniques. World Electric Vehicle Journal, 14(9), 266.

[2] Litman, T., & Burwell, D. (2006). Issues in sustainable transportation. International Journal of Global Environmental Issues, 6(4), 331-347.

[3] İnaç, H. (2024). PREDICTION OF DRIVING TIME OF ELECTRIC SCOOTER (E-SCOOTER) DRIVERS BY MACHINE LEARNING. Elektronik Sosyal Bilimler Dergisi, 23(91), 1041-1057.

[4] Fattah, J., Ezzine, L., Aman, Z., El Moussami, H., & Lachhab, A. (2018). Forecasting of demand using ARIMA model. International Journal of Engineering Business Management, 10, 1847979018808673.

[5] Alharbi, F. R., & Csala, D. (2022). A seasonal autoregressive integrated moving average with exogenous factors (SARIMAX) forecasting model-based time series approach. Inventions, 7(4), 94.

[6] Iftikhar, H., Khan, F., Rodrigues, P. C., Alharbi, A. A., & Allohibi, J. (2025). Forecasting of Inflation Based on Univariate and Multivariate Time Series Models: An Empirical Application. Mathematics, 13(7), 1121.

[7] Taoussi, B., Boudia, S. M., & Mazouni, F. S. (2025). Wind speed forecasting using univariate and multivariate time series models. Stochastic Environmental Research and Risk Assessment, 39(2), 547-579.

[8] Kwarteng, S., & Andreevich, P. (2024). Comparative Analysis of ARIMA, SARIMA and Prophet Model in Forecasting. Research & Development, 5(4), 110-120.

[9] Cocca, M., Teixeira, D., Vassio, L., Mellia, M., Almeida, J. M., & Couto da Silva, A. P. (2020). On car-sharing usage prediction with open socio-demographic data. Electronics, 9(1), 72.

[10] Alencar, V. A., Pessamilio, L. R., Rooke, F., Bernardino, H. S., & Borges Vieira, A. (2021). Forecasting the carsharing service demand using uni and multivariable models. Journal of Internet Services and Applications, 12(1), 4.

4th International Conference on Digital Industry and Engineering Applications 2025

ICODIA 25'

InnoPark
KONYA TECHNOLOGY DEVELOPMENT ZONE